Identification and Characterisation of Microbial Effectors Interfering with the Plant Circadian Rhythm

Olivia Margaret Nippe

Thesis submitted to the University of Warwick, Department of Life Sciences for the degree of Doctor of Philosophy in Life Sciences

September 2019

Table of Contents

List of Tables

List of Figures

Acknowledgements

I would like to thank my supervisor, Dr. Vardis Ntoukakis as well as all past and present members of the Ntoukakis lab group for their extensive help, guidance, and encouragement over the last four years. I would particularly like to thank Arsheed Sheikh for his patient instruction during my first year, Ana Domingues-Ferreras for the vast amount of time she spent helping me plan the Golden Gate transgenic constructs, and Anna Gonzalez Gil for preserving so much of my sanity as we went through this process together. Finally, I would like to thank all members of the C030/046 lab groups and the 2015 MIBTP cohort for their support- I wouldn't have got far without them.

Declaration

I declare that this thesis is submitted to the University of Warwick in support of my application for the degree of Doctor of Philosophy. It has been composed by me and has not been submitted in any previous application for any degree.

The work presented (including data generated and data analysis) was carried out by me except in the cases outlined below:

Dr. Gerben van Ooijen (Institute for Molecular Plant Sciences, University of Edinburgh, UK) together with the assistance of Dr. Louise Lipczak Hansen (Novo Nordisk, Denmark and formerly of the Institute for Molecular Plant Sciences, University of Edinburgh, UK) performed the bioluminescence effector screen in protoplasts presented in Chapter 3 as well as the corresponding rhythm analysis.

Dr. Ana Domingues-Ferreras (University of Warwick, UK) performed the large-scale Y2H screen and scoring of interactors for the effector HopAO1 versus the full *A. thaliana* transcription factor library in liquid media presented in Chapter 4. She also generated the level 0 HopAO1 and N-terminal tag Golden Gate cloning modules.

Several of the confocal images of the transgenic HopAO1 *A. thaliana* lines presented in Chapter 5 (including other images representative of each line that were not included) were produced by and/or with the assistance of Iosif Zacharia (University of Warwick, UK).

The library preparation and all subsequent steps of the RNA-seq analysis presented in Chapter 5 including bioinformatic analysis was performed by the BGI sequencing group (BGI, Hong Kong).

Abstract

Infection of economically important crops by rapidly evolving pathogenic bacteria poses an on-going threat to food security, often causing substantial loss to crop yields. Such aggressive pathogens rely on the delivery of virulence factors, known as effectors, for the suppression of plant immunity and to ensure successful infection of the host (Büttner et al., 2016). One posited mediator of *Arabidopsis thaliana* defence is the circadian clock, which regulates susceptibility to invading pathogens, and the expression levels of immune receptors in a temporal fashion (Bhardwaj et al., 2011; Wang et al., 2011b). While this rhythmicity enables the plant to maximise efficiency of its immune system through synchronisation with the environment, it also makes the circadian oscillator a likely target for manipulation by bacterial effectors. This project aimed to identify effectors in the *Pseudomonas syringae* repertoire capable of disrupting circadian rhythmicity and characterise their mechanism of action. Our use of bioluminescence detection assays indicates that secretion of specific effectors by *P. syringae* significantly influences the rhythmic expression of *A. thaliana* core clock genes. Through the large-scale transcriptomic analysis of stable transgenic lines expressing the *Pst* effector HopAO1 with targeted sub-cellular localisation we present evidence that HopAO1 significantly reduces clock gene expression in a way that is dependent on its previously uncharacterised function in the nucleus. Assessment of HopAO1's interaction partners by Y2H reveals it is able to interact with two closely related NAC transcription factors and enhance their binding of the *LHY* promoter. We propose that HopAO1 alters the clock and enhances *Pst* virulence by interacting with the two NAC transcription factors in order to repress core clock gene expression. It is hoped that the characterisation of the molecular mechanisms employed by effectors such as these will permit the engineering of more disease resistant crops.

List of Abbreviations

3AT: 3-amino 1,2,4 triazole

AD: Activation Domain

ANOVA: Analysis of Variance

BAK1: BRI1-Associated Receptor Kinase 1

BD: Binding Domain

BIK1: Botrytis-Induced Kinase 1

BLAST: Basic Local Alignment Search Tool

bp: Base Pair

BRASS: Biological Rhythms Analysis Software System

CC: Coiled Coil

CCA1: Circadian Clock Associated 1

cDNA: Complementary DNA

CDPK/CPK: Calcium-Dependent Protein Kinase

CFU: Colony Forming Unit

CHE: CCA1 Hiking Expedition

Col-0: Columbia ecotype *A. thaliana*

CT: Circadian Time

DAMP: Damage-Associated Molecular Pattern

DD: Constant Dark

DEG: Differentially Expressed Gene

Dpi: Days Post Infection

EC: Evening Complex

EE: Evening Element

EF-Tu: Elongation Factor Tu

EFR: EF-Tu Receptor

ELF: Early Flowering

est: β-estradiol

ET: Ethylene

ETS: Effector-Triggered Susceptibility

EV: Empty Vector

FFT: Fast Fourier Transform

FLS2: Flagellin Sensing 2

GA: Gibberellin

GFP: Green Fluorescent Protein

GI: Gigantea

GO: Gene Ontology

Hpi: Hours Post Infection

HR: Hypersensitive Cell Death Response

IP: Immunoprecipitation

JA: Jasmonate

kDA: kilo Daltons

KEGG: Kyoto Encyclopedia of Genes and Genomes

LB: Lysogeny Broth

LD: Light:Dark

LHY: Late Elongated Hypocotyl

LL: Constant Light

LOV: Light-Oxygen-Voltage

LPS: Lipopolysaccharide

LRR: Leucine-Rich Repeat

LTAH: Leucine, Tryptophan, Alanine, Histidine

LUC: Luciferase

MAMP: Microbe-Associated Molecular Pattern

MAPK/MPK: Mitogen-Activated Protein Kinase, or MAP Kinase

MAPKK: MAP Kinase Kinase

MAPKKK: MAP Kinase Kinase Kinase

mRNA: Messenger RNA

MS: Murashige and Skoog Media

MTI: MAMP-Triggered Immunity

NB-LRR: Nucleotide-Binding Leucine-Rich Repeat

NB: Nucleotide-Binding

NES: Nuclear Exclusion Sequence

NLS: Nuclear Localisation Sequence

OD: Optical Density

PAMP: Pathogen-Associated Molecular Pattern

PCA: Principle Component Analysis

PRR: Pattern Recognition Receptor

PRR: Pseudo-Response Regulator

Pst: *Pseudomonas syringae pv. (pathovar) tomato*

PTI: PAMP-Triggered Immunity

R gene/protein/allele: Resistance gene/protein/allele

RBOH (D): Respiratory Burst Oxidase Homolog (D)

RLCK: Receptor-Like Cytoplasmic Kinase

RLK: Receptor-Like Kinase

RNA-seq: RNA Sequencing

ROI: Region of Interest

ROS: Reactive Oxygen Species

RPK: Receptor Protein Kinase

RPM: Revolutions Per Minute

RT-qPCR: Real Time- Quantitative Polymerase Chain Reaction

RVE: Reveille

SA: Salicylic Acid

SAR: Systemic Acquired Resistance

SDS-PAGE: Sodium-Dodecyl Sulphate- Polyacrylamide Gel Electrophoresis

SEM: Standard Error of the Mean

SNP: Single Nucleotide Polymorphism

t-DNA: Transfer DNA

T3SE: Type III Secreted Effector

T3SS: Type III Secretion System

TF: Transcription Factor

TIR: Toll and Interleukin-1 Receptor

TOC1: Timing of CAB Expression 1

TTFL: Transcription-Translation Feedback Loop

UTR: Untranslated Region

WT: Wild Type

Y2H: Yeast 2-Hybrid

YFP: Yellow Fluorescent Protein

ZT: Zeitgeber Time

ZTL: Zeitlupe

Chapter 1: Introduction

1.1 Phytopathogens: increasing pressure on agricultural sustainability

According to the most recent estimates, the global population is likely to increase from the current 7.7 billion people, to between 8.5 and 8.6 billion by 2030, and between 9.4 and 10.1 billion by 2050 (United Nations, 2019). Although the rate of population growth has considerably slowed, and there is a chance that it could stabilise before 2100, the most likely scenario remains that our numbers will continue to increase. It is therefore of paramount importance that we find new ways to augment agricultural productivity in order to meet the demands exerted by this additional pressure. A new study into crop yield losses conducted over a 3-month period and over 67 countries in varying geographical regions found pathogens and pests to be responsible for enormous losses to five of the most produced crops worldwide; The average yield losses recorded for wheat were 21.5%, rice 30%, maize 22.5%, potato 17.2%, and soybean 21.4% (Savary et al., 2019). These results far exceed predictions previously made by Oerke in 2006, and demonstrate a growing need to take more heed of plant pathogens and pests when addressing the matter of food security.

Phytopathogens account for much of these losses, with rapid rates of evolution expediting their adaptation to crop resistance in our increasingly monocultural agro-ecosystems (McDonald and Stukenbrock, 2016). Examples of such crop infecting pathogens can be found among both fungi and prokaryotes. The vascular bacterial pathogen *Ralstonia solanacearum* for instance targets a broad range of host crop species including potato and banana, causing bacterial wilt by secreting large amounts of extracellular polysaccharides that block plant vasculature (Prior et al.). The pathogen was reported to have caused yield losses of over 14% in Bangladesh potato crops (Elphinstone et al., 2005), and remains one of the most destructive pathogens identified due to its rapid induction of wilting symptoms (Yuliar et al., 2015). The citrus canker causing bacterium *Xanthomonas axonopodis pv. citri* is a biotroph that causes great economic losses to the citrus industry (CABI, ISC 2019). It secretes a natriuretic peptide-like protein (controlling ion flux and fluid circulation) to regulate

host homeostasis and maintain healthy host tissues during its colonisation within the apoplast, resulting in characteristic raised lesions (Wang et al., 2011d; Gottig et al., 2010). During later stages of infection, the induced hyperplasia, or increased cellular reproduction, causes the leaf epidermis to rupture, facilitating bacterial dispersal by the wind to new hosts. The fungal pathogen *Mycosphaerella graminicola* causes Septoria tritici blotch (STB) and is the most prevalent disease of wheat globally (Suffert et al., 2011). It relies on its ability to feed on decaying organic matter (saprotrophy) which enables it to build up inoculum on plant material over subsequent seasons living in seeds, stubble and debris. STB is estimated to account for 5-10% of losses to wheat amounting to harvest losses valuing 120-140 million Euros in the UK alone (Fones and Gurr, 2015).

It is within our power, however, to tip the balance of these pathosystems in favour of host plant success (Dangl et al., 2013). High levels of resistance to the powdery mildew causing fungus *Botrytis cinerea* were achieved in strawberry plants by *Agrobacterium tumefaciens* mediated transformation of a chitinase encoding gene *ch5b* in order to prevent degradation of the cell wall in host tissues (Vellicce et al., 2006; Olivier et al., 2018). In another instance, a method of disease resistance has been developed in rice through the overexpression of the *WRKY45* transcription factor. *WRKY45* regulates the signalling of Salicylic Acid (SA, a phytohormone involved in pathogenic defence, Kumar, 2014), and its overexpression was shown by the author to confer enhanced resistance against the rice blast pathogen *Xanthomonas oryzae* (Takatsuji, 2014). A single gene identified as conferring resistance to bacterial spot disease (caused by a complex of the *Xanthamonas* species) in pepper, *Bs2* was transgenically expressed with great success in tomato, producing yields approximately 2.5 times greater than the non-transformed parent line over an 8 year field study, even with no bacteriocidal treatment (Horvath et al., 2012). It is therefore clear that continuously improving our understanding of virulence mechanisms employed by phytopathogens is crucial as we endeavour to inform the development of disease-resistant crops.

1.2 Disease resistance in plants: an overview

For vertebrates, the immune system relies on a complex system of both highly specialised cells and molecules. These guard the organism against foreign substances suspected of being agents of disease by migrating through the circulatory system. Immunity in plants, however, represents quite a different state of affairs. Although both plants and animals recognise an overlapping set of conserved microbe-associated molecular patterns (MAMPs) (Haney, 2014), since plants lack these specialised immune cells capable of circulating the organism, every cell in a plant must be capable of recognising potential threats and contributing to their elimination. They must also each be ready to transmit signals to more distal tissues to warn of the need to induce transcriptional changes and limit the extent of pathogenic spread, as well as distinguish foreign from self-peptides to prevent autoimmune responses (Spoel and Dong, 2012). Bacterial pathogens, meanwhile, have evolved a plethora of ways to regulate the plant immune system, such that it benefits their own growth and development. This one-upmanship between invader and host has led to what many describe as an arms race- an ongoing state of co-evolution, with each facing constant evolutionary pressure to acquire new mechanisms that would give them the advantage at the plant-pathogen interface. Even as a single pathogenic cell infects a single plant cell in real time, however, there exists a back and forth between pathways inducing resistance and those inducing susceptibility. Just as bacteria attack plants using a multifaceted approach in the form of assorted secreted proteins with diverse virulent functions (known as effectors), plant defence can also be described as layered, with multiple tiers dedicated to specific defensive reactions.

These tiers of plant immunity are well explained by the "zigzag" model, introduced by Jones and Dangl (2006). Illustrating the first principles of plant defence outputs, and the interplay between host and pathogen, the zigzag model has become a cornerstone of our understanding of plant immunity since its publication (Figure 1.1). In the model, the degree of plant defence achieved is said to be determined the contribution of three separate phases during infection. A plant's first line of defence relies on transmembrane pattern-recognition receptors (PRRs) that transmit signals upon the perception of conserved microbe or pathogen-associated molecular patterns (MAMPs or PAMPs) (Couto and Zipfel, 2016; Bigeard et al., 2015). In this first phase, known

as MAMP-triggered immunity (MTI) PRRs interact specifically with elicitors such as elongation factor Tu (EF-Tu) and bacterial flagellin to prevent further pathogenic invasion, initiating early resistance pathways. These include but are not limited to stomatal closure, production of reactive oxygen species (ROS), callose deposition in cell walls, activation of the mitogen-activated protein kinase (MAPK) signalling cascades and transcriptional activation of resistance related genes (Hou et al., 2011; Bigeard et al., 2015; Couto and Zipfel, 2016). Next, the earliest attempts are made by the pathogen to induce susceptibility in the host. In the case of most Gram-negative phytopathogenic bacteria this means the employment of a type III secretion system (T3SS) to inject host cells with effector proteins, whose job it is to manipulate plant cellular processes, enhancing virulence and growth (Lee et al., 2013). When successful, this is known as effector-triggered susceptibility (ETS) and reduces the amplitude of disease resistance.

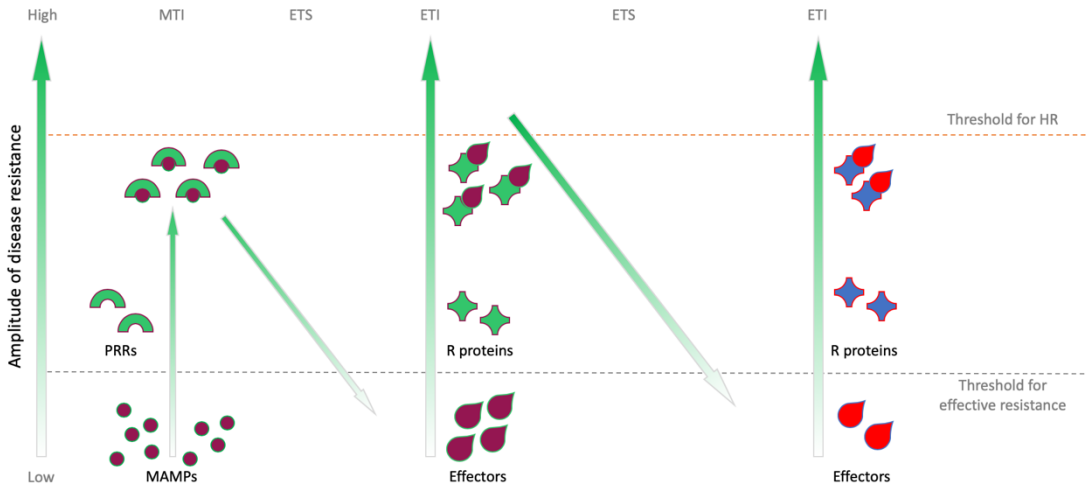

Figure 1.1: The zigzag model demonstrates core principles in plant immunity (figure and legend adapted from Jones and Dangl, 2006). In this model, the amplitude of susceptibility or resistance to pathogenic infection is proportional to [MTI – ETS + ETI]. Plants detect microbial-associated molecular patterns (MAMPs, purple circles) via pattern-recognition receptors (PRRs, green semicircles) bringing about MAMP-triggered immunity (MTI). Successful pathogens deliver effector proteins (purple teardrops) that interfere with MTI progression, or otherwise enhance pathogen nutrition and dispersal, resulting in effector-triggered susceptibility (ETS). Effectors are recognized by Nucleotide-binding, Leucine Rich Repeat receptor proteins (NB-LRRs, green crosses), which are encoded by resistance (*R)* genes. This activates effector-triggered immunity (ETI), an amplified version of MTI that may pass a threshold for induction of the hypersensitive response (HR), triggering local cell death and limiting pathogenic spread. Pathogen isolates that have lost the purple effector or that have gained new effectors through horizontal gene transfer (in red) are able to suppress ETI. Finally, selection favours new plant R alleles (in blue) that can recognize the pathogen's newly acquired effectors, resulting again in ETI.

The second phase of immunity comes into play when effector proteins are directly or indirectly detected by a class of cytoplasmic receptors known as Nucleotide Binding Leucine Rich Repeat proteins (NB-LRRs). This induces a more intense immune response than that of MTI, and often results in the triggering of a hypersensitive cell death response (HR) (Jones and Dangl, 2006). This second phase, named effector-triggered immunity (ETI) works on the premise of limiting the advancement of pathogenic invasion at the cost of a few cells at the site of infection (Bigeard et al., 2015). By inducing these defence mechanisms, plants are able to restrict the damage done by invading pathogens. Of course, HR is most effective against pathogens that are biotrophic, that is to say pathogens that can grow in healthy living host tissue, but not those that are necrotrophic, and have evolved to feed on the remains of dead cells (Kennedy and Beattie, 1982; Govrin and Levine, 2000). This makes the identification of an invading pathogen's preferred source of nutrition an important part of plant defence signalling (Glazebrook, 2005).

Finally, there remains the possibility that following these two phases of immunity, the advantage continues to alternately be conferred between the host and invading pathogen, in accordance with the zigzag model, through cycles of ETS and ETI on the basis of effector and *R* gene frequency (Jones and Dangl, 2006). If within the invading population exists an individual pathogen that either lacks or contains a mutated version of an effector that the host plant can recognise, it may be passed around a colony by horizontal gene transfer in order to bypass ETI if its cognate NB-LRR has not sufficiently been selected for within the plant population. Similarly, NB-LRRs and decoy proteins that act as effector target mimics experience selective pressure to evolve and recognise new effectors (Van der Hoorn et al., 2002; van der Hoorn and Kamoun, 2008).

The zigzag model has its limitations, however, as all models inherently do (Pritchard and Birch, 2014). Firstly, it does not necessarily take into account other causes for disease susceptibility (such as in necrotrophic pathogens that can exploit HR to benefit their own nutrient supply) (Keller et al., 2016). It does not account for the priming of plant immunity by systemic acquired resistance (SAR) in which a local infection can cause accumulation of SA and subsequent upregulation of antimicrobial proteins in distal tissues protecting the host for up to months in the future (Fu and Dong, 2013).

It also does not describe the dynamics of pathogenic infection of plants in real time or scale, as it considers both long-term evolutionary adaptation of whole populations, as well as molecular processes that occur at the single cell level during one incidence of infection. This has led to the recommendation by some that it should not be used as a fully accurate basis for the quantification of infection dynamics, as well as to the development of more complex models (Pritchard and Birch, 2014). All this being said, these caveats do not negate the usefulness of the zigzag model in defining the fundamentals of plant immunity, and in the case of environmentally controlled studies of largely uniform populations, and bio- or hemi-biotrophic pathogens, it still represents a highly relevant narrative; a starting point for elucidating the subtleties of individual pathosystems.

1.3 MAMP-triggered immunity (MTI)

The detection of foreign peptides by PRRs in the first phase of plant defence has the potential to activate a diverse set of pathways to counter infection (Bigeard et al., 2015). Once termed PAMP-triggered immunity (PTI), on the basis that receptors perceive pathogen-associated molecular patterns (PAMPs), it is now increasingly referred to as MAMP-triggered immunity (MTI), or immunity triggered by microbe-associated molecular patterns (MAMPs, Ausubel, 2005). This is because the elicitors that are able to trigger downstream immune responses are not always pathogen derived, but can also include chemicals and peptides from non-pathogenic microbes, or even endogenous plant-derived signals secreted in response to pathogenic action known as damage-associate molecular patterns (DAMPs) (Guillaume et al., 2012).

PRRs are plasma membrane spanning receptor-like kinases (RLKs) that specifically recognise MAMP and DAMP epitopes using an extracellular domain, and possess intracellular kinase domains, phosphorylation of which can transduce signals that bring about immune responses (Böhm et al., 2014) (Figure 1.2). Among the more extensively studied MAMP/PRR interactions are those involving the *A. thaliana* PRRs Flagellin Sensing 2 (FLS2) and the EF-Tu receptor (EFR). FLS2 and EFR respond to the presence of the MAMPs flagellin and elongation factor Tu (Ef-Tu) respectively,

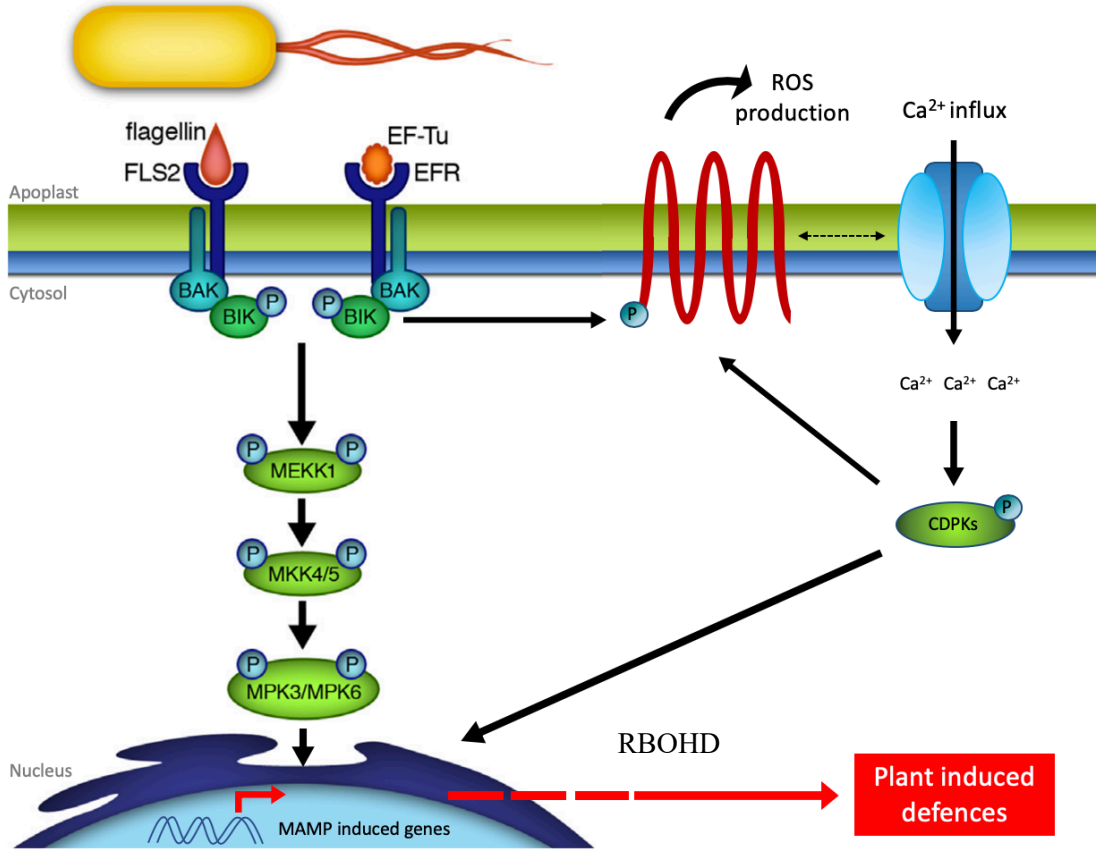

Figure 1.2: Pattern recognition receptors (PRRs) recognize MAMPs and trigger downstream immune responses (figure adapted primarily from Lee et al., 2013, also drawing from other sources referenced throughout the main text). PRRs including FLS2 and EFR allow the plant host to recognize MAMPs at the plasma membrane, such as bacterial flagellin and EF-Tu respectively. This MAMP recognition leads to the activation of signaling cascades via a series of phosphorylation events, notably the activation of MAPKs and RBOHs by BIK1. RBOHD phosphorylation triggers extracellular ROS bursts which induce calcium influx to the cytosol, and so activates signaling by calcium-dependent protein kinases (CDPKs). CDPKs also feedback to positively regulate further ROS production. The phosphorylation of these protein kinases subsequently enables them to mediate transcriptional reprogramming of defence-related genes in the nucleus.

as well as their synthetic peptide derivatives flg22 and elf18 (Chinchilla et al., 2006; Gómez-Gómez and Boller, 2000; Kunze et al., 2004; Zipfel et al., 2006). FLS2 forms a heterodimer with BRI1-associated receptor kinase 1 (BAK1) which then becomes phosphorylated, all within 15 seconds of perceiving flg22 (Chinchilla et al., 2007; Schulze et et al., 2010), demonstrating the speed at which MTI can be triggered. The transphosphorylation of BAK1 and a receptor-like cytoplasmic kinase (RLCK) named Botrytis-induced kinase 1 (BIK1, Lu et al., 2010) activates downstream signalling responses via Mitogen-activated protein Kinase (MAPK) signalling cascades (Hou et al., 2011) and the generation of highly toxic reactive oxygen species (ROS) (Smith and Heese, 2014). Loss of FLS2 such as in the *A. thaliana fls2* mutant results in an

increased susceptibility to wild type *Pseudomonas syringae* when spray treated (Zipfel et al., 2004). The receptor EFR is also known to associate with BAK1 at the plasma membrane in a way that is dependent on the perception of a different MAMP, EF-Tu. Just as with FLS2, the two form a heterodimer that recruits the cytoplasmic kinase BIK1 resulting in downstream phosphorylation events involved in instigating ROS bursts and MAPK signalling (Lee et al., 2013). Transient expression of EFR in *Nicotiana benthamiana* increases susceptibility to infection by *Agrobacterium tumefaciens,* and loss of the *efr* gene in *A. thaliana* results in increased susceptibility (Zipfel et al., 2006).

One of the processes downstream of PRR activation, the generation of ROS during MTI is of great importance, both for their role as signalling molecules and due to the detrimental effects they are able to exert (Marino et al., 2012). The NADPH oxidase respiratory burst oxidase homolog (D) (RBOHD) is able to associate with FLS2 and ERF in a BIK1 dependent manner, and is subsequently phosphorylated by BIK1, becoming activated in the process (Kadota et al., 2014). RBOHD can then produce O_2^- superoxide in the apoplast, which is converted into the membrane permeable species hydrogen peroxide H_2O_2 (Bigeard et al., 2015). Locally, ROS can mediate the strengthening of the cell wall via oxidative cross linking within 10 minutes of treatment with an immune elicitor, trigger increases in $Ca2^+$ and act as a threshold promotor of HR, substantially contributing to disease resistance (Bradley et al., 1992; Torres et al., 2005; Levine et al., 1994; Lamb and Dixon, 1997). Reduced detection of a T3SS injection marker during early MTI in tobacco cells has also led to the speculation that ROS may inhibit the injection of effectors by altering bacterial transcription and translation, thereby inhibiting the assembly of the T3SS (Crabill et al., 2010). In cells further away from the site of infection however, RBOH triggered ROS bursts can supress SA-dependent cell death, permitting spatial limitations on the induction of HR within the host and establishing SAR (Torres et al., 2005). Additionally, the calcium influx brought on by ROS burst is of great importance in MTI, contributing to extracellular alkalinisation, and potentiating multiple downstream calcium dependent protein kinases (CDPKs), a subgroup of which are known to differentially regulate flg22 responsive genes during early MTI (Seybold et al., 2017; Boudsocq et al., 2010). CPK1,2,4 and 11 are known to phosphorylate RBOHs at the membrane, further activating ROS production, whereas CPK4, 5, 6 and

11 translocate to the nucleus and phosphorylate WRKY transcription factors (TFs) to mediate expression of defence genes during ETI (Gao et al., 2013). CPK5 also phosphorylates RBOHD, and *cpk5* mutants are compromised in their ability to mount an immune response in distal tissues (Dubiella et al., 2013).

Protein kinases such as CDPKs and MAPKs are crucial in conveying signals elicited by receptor protein kinases (RPKs) like EFR and FLS2 at the plasma membrane to other subcellular locations. In response to immune elicitors such as flg22, consecutive phosphorylation events occur amongst the MAPKs, such that phosphate groups are transferred firstly from MAP kinase kinase kinases (MAPKKKs, including MEKK1), to MAP kinase kinases (MAPKKs, including MKK4 and 5), and finally to MAP kinases (MAPKs, including MPK3 and 6) (Asai et al., 2002; Tena et al., 2011). The activation of these kinases enables transcriptional reprogramming of defence genes via phosphorylation of proteins in various families of transcription factors with both repressor and promotor activity, including WRKYs and ethylene responsive factors (Tena et al., 2011; Eulgem, 2005; Hake and Romeis, 2019; Li et al., 2016). As such, MAPK cascades have been shown at length to contribute to plant defence. The disruption of MAPK signalling enables increased levels of *P. syringae* growth in *A. thaliana* (He et al., 2006). Mutation to the *mpk4* gene initially revealed a negative role for the kinase in immune regulation, with mutants exhibiting autoimmune phenotypes and elevated SA levels (Petersen et al., 2000), although it was later shown that this MAPK module is in fact a positive element in defence during ETI, and is indirectly guarded by the NB-LRR protein SUMM2 such that late immunity is activated by SUMM2 when MPK4 is inhibited by the action of secreted effectors (Zhang et al., 2012). Accumulation of inactive MAPK proteins MPK3 and MPK6, as well as their mRNA transcripts has also been detected in defence primed *A. thaliana*, indicating that MAPKs are important for priming of induced resistance pathways (Beckers et al., 2009).

Another of the pathways initiated by MAMP perception is stomatal closure. While it was once thought that pathogens were freely granted entry to inner leaf tissue through open stomata, it is now known that the plant immune system gates stomatal aperture to limit invasion upon the perception of various MAMPs. The fungal wall component chitosan, bacterial flagellin-derived flg22 peptide, and Gram-negative bacterial

membrane-derived lipopolysaccharide (LPS) have all been shown to elicit stomatal closure in the model plant *Arabidopsis thaliana* (Melotto et al., 2006; Lee et al., 1999). FLS2 is necessary for the inhibition of K^+ ion influx in guard cells induced by flg22 (Zhang et al., 2008), and downstream signalling is known to be mediated by MAPKs and secondary signalling messengers, with oscillations in ROS, calcium, and nitric oxide having previously been detected in MAMP elicited guard cells (Arnaud and Hwang, 2015; Desclos-Theveniau et al., 2012; Melotto et al., 2017).

Finally, the deposition of callose, a high molecular weight polysaccharide is elicited during MTI in order to generate a matrix into which antimicrobial compounds can be deposited at the site of infection (Büttner et al., 2016). Both flg22 and chitosan elicit increases in callose deposits, with flg22 elicitation being dependent on *rbohD* expression (Luna et al., 2011).

1.4 Effector-triggered susceptibility (ETS)

As shown in Figure 1.1, the overall level of disease resistance achieved by plants during infection can be greatly augmented through the induction of MTI responses, however pathogens evolve their own mechanisms in turn to sabotage these intracellular pathways in order for them to become established within the host. For many Gram-negative bacteria this is made possible through the secretion of proteins that aid virulence and pathogenic survival, known as effectors (Macho and Zipfel, 2015). They do this by using a type III-secretion system (T3SS), a multi-domain structure anchored in the Gram-negative double membrane with a needle-like appendage or "injectisome" that spans the host plasma membrane connected by a central tube (Cornelis, 2006). When contact is made with a eukaryotic cell membrane, the secretion of effectors through this central tube is initiated, allowing them to enter the host cytosol. Effectors secreted in this way are often termed type III secreted effectors (T3SEs) (O'Brien et al., 2011). In the foliar phytopathogen *P. syringae*, the *hrp-hrc* cluster of genes encode the structural components of the T3SS, and are located within a tripartite pathogenicity island (T-PAI), where they are flanked by loci for T3SEs that are both conserved and variable in the *P. syringae* phylogroups (Alfano et

al., 2000; Yuan and He, 1996; Xin et al., 2018). Loss or mutation of multiple genes within the *hrp-hrc* cluster results in significant losses to pathogenicity, reportedly due to a reduced capability to induce callose deposition, HR, actin bundling, and decreased apoplastic osmolarity amongst other avirulence phenotypes that have been well characterised across numerous studies (Kennedy and Beattie, 1982; Roine et al., 1997; Zhao et al., 2003; Luna et al., 2011; Shimono et al., 2016).

A working secretion system alone is not sufficient for pathogenicity, however, and along with the components of the T3SS, effectors are required to instigate virulence in host cells. To this end, *hrp-hrc* mutant strains have been developed enabling the study of individual effectors within pathogenic repertoires. By comparing the elicited immune phenotypes of T3SS mutants and virulent wild type bacteria to knockouts of individual T3SEs, or effector polymutant strains, the contribution of an effector to overall virulence may be ascertained. It was notably in this way that Cunnac et al. (2011) discovered the minimal repertoire of 8 effector proteins needed by wild type *P. syringae pv. tomato* to recover the virulence lost in the effector polymutant DC3000Δ28E. The distinct mechanisms and targets of many effectors' induction of host susceptibility have now been discovered (Xin et al., 2018).

Perhaps one of the best characterised effectors capable of altering MTI mechanisms to induce susceptibility is AvrPto (Büttner et al., 2016). AvrPto is a general kinase inhibitor known to target the PRRs FLS2 and EFR inhibiting their autophosphorylation and downstream signalling, although discrepancies have been reported regarding whether or not it interacts with BAK1 or is able to dissociate the FLS2/BAK1 complex (Xiang et al., 2008; Shan et al., 2008; Xiang et al., 2011). The effector is able to block early MAPK signalling associated with MTI, and was found to be able to regulate ~80% of T3SS regulated genes known to be differentially expressed during infections of *A. thaliana* with *P. syringae* (He et al., 2006; Hauck et al., 2003). *Arabidopsis* plants in which AvrPto is transgenically expressed have massively compromised ability to form callose deposits in response to challenge by avirulent *hrcC* mutant of *P. syringae*. The promotion of bacterial growth by AvrPto in the pathogen's host tomato has also been reported to produce disease symptoms of increasing severity in a way that is dependent on its undergoing *in vivo*

phosphorylation within a cluster of three serine residues (Hauck et al., 2003; Anderson et al., 2006).

Another enactor of effector triggered susceptibility, HopN1 prevents ROS production and callose deposition in *A. thaliana*, as well as the onset of HR in tomato in a way that is dependent on its function as a cysteine protease (Rodríguez-Herva et al., 2012; López-Solanilla et al., 2004). Its enzymatic activity also permits the binding and disruption of tomato protein PsbQ, a component of photosystem II, presumably acting to diminish photosynthetic activity, and consequently ROS production in the chloroplast. Interestingly, HopN1 was shown to not significantly enhance the bacterial growth of the effector polymutant DC3000Δ28E 6 days after infection, although given this mutant also expresses a minimal repertoire of 5 effector proteins that promote bacterial growth (AvrPtoB, HopM1, HopE1, HopG1 and HopAM1), this could be due to functional redundancy shared with one or more of the retained effectors (Rodríguez-Herva et al., 2012). HopQ1 meanwhile is a T3SE that inhibits MTI at the source, by preventing the expression of PRRs themselves. Transgenic expression of HopQ1 in 6-week old *A. thaliana* suppressed ROS production and MAPK phosphorylation, both early MTI events, but also reduced the accumulation of *FLS2* transcripts by activating the synthesis of the plant signalling hormone cytokinin (Hann et al., 2014).

1.5: Effector-triggered immunity (ETI)

Through the secretion of effectors by the T3SS machinery, pathogens may reduce the amplitude of disease resistance, and become better established within host cells over the course of an infection. However, for a pathogen to be successful it must not only attack a plant's immune system and tissues, it must also evade detection by its host. Plants are able to detect pathogenic presence both directly and indirectly using proteins that confer resistance, or R proteins, which are encoded by *R* genes. The majority of these so-called R proteins are NB-LRRs, of which there are 126 in *A. thaliana* (Jones and Dangl, 2006). These NB-LRRs possess a C-terminal leucine-rich repeat (LRR) domain often used for ligand perception, which can be highly diverse enabling the NB-LRR repertoire to target a wide variety of pathogenic effectors, a central nucleotide binding pocket, and an N-terminal Toll and Interleukin-1 Receptor homology (TIR) or

Coiled Coil (CC) domain (Collier and Moffett, 2009). Differences have been found in the structures of CC-NB-LRRs that indicate that the receptors can shift between an intermediate and an activated conformation. This activation involves the formation of a wheel-like pentameric structure called the "resistosome" from α-helices in the NB and CC domains upon ligand perception and is required for immune responsiveness and localisation at the plasma membrane (Wang et al., 2019a, 2019b). TIR domains on the other hand have recently been identified as having self-association dependent NADase activity, forming an octameric structure that allows cell death signalling during ETI (Horsefield et al., 2019; Wan et al., 2019). The rate of evolution amongst NB-LRRs has the potential to be rapid, but is largely variable, as it is thought that fluctuating levels of selective pressure are exerted on their encoding genes according to the frequency by which pathogens present new and cognate effectors (Michelmore and Meyers, 1998; McHale et al., 2006). Following the specific recognition of effectors, the central NB region undergoes a conformational change from an ADP to and ATP-bound state, thereby activating the protein for participation in downstream signalling pathways, particularly by triggering ROS production in order to induce HR, the definitive output of ETI (Andersen et al., 2018).

The recognition of effectors by NB-LRRs is often categorised as being direct or indirect, and may further conform to a "Guard", "Decoy", or "Integrated-decoy" mechanistic model (Dodds and Rathjen, 2010; Adachi et al., 2019). Directly interacting pairs of receptors and effectors have been reported, such as the rice CC-NB-LRR Pi-ta which binds effector AvrPita from fungal rice blast pathogen *Magnaporthe grisea* (Jia et al., 2000). As pathogen and host evolve over time to evade and enact such interactions respectively there is a strong selection for sequence diversification, with variants of receptors and effectors exhibiting different recognition specificities (Dodds and Rathjen, 2010). Indirect recognition meanwhile involves the plant making use of accessory proteins that interact with the effector and undergo a conformational change perceived by the NB-LRR (Dodds and Rathjen, 2010).

The specific targeting of MTI pathway components by effectors has enabled plants to develop a final tier of resistance using R proteins with the potential to outsmart their invaders. In the decoy models, mimics of effectors' functional targets have evolved within the host that rather than enhancing susceptibility, initiate pathways associated

with resistance (McHale et al., 2006; van der Hoorn and Kamoun, 2008; Sarris et al., 2015). In the case of PopP2 from *R. solanacearum*, the acetyltransferase effector specifically targets the *R* protein and NB-LRR RRS1-R, directly interacting with it in the nucleus such that the effector acetylates RRS1-R's DNA binding WRKY domain (Deslandes et al., 2003; Sarris et al., 2015). The WRKY domain is an uncommon NB-LRR feature possessed by WRKY transcription factors, which function in defence gene regulation, and its acetylation results in the inhibition of RRS1's DNA binding capacity (Le Roux et al., 2015; Sarris et al., 2015). This WRKY domain acts as an integrated-decoy within RRS1-R, since PopP2 targets multiple WRKY transcription factors, presumably to inhibit their immune regulatory capacity, however the interaction with RRS1-R has been shown to confer resistance to *R. solanacearum* (Büttner et al., 2016; Deslandes et al., 2003). A further NB-LRR R protein, RPS4 is also involved in this detection system. RPS4 has a TIR domain which activates cell death independently of effector detection within the cell, but is usually sequestered through heterodimerisation with the TIR domain of RRS1-R (Swiderski et al., 2009; Williams et al., 2014). The heterodimerisation of RRS1-R and RPS4 is required for the recognition of PopP2 (Williams et al., 2014). It is therefore thought that RRS1-R acts as a sensor, directly binding PopP2, while RPS4 indirectly perceives the effector, acting as an "executioner" *R* protein triggering ETI in response to molecular rearrangements within the complex (Büttner et al., 2016; Delga et al., 2015). Non-integrated decoys have also been described such as RIN4, an *A. thaliana* protein degraded by *P. syringae* effector AvrRpt2, which once cleaved abolishes its interaction with RPS2 and thus activates RPS2-dependent ETI (Mackey et al., 2003, 2002).

This Decoy Model, of which RRS1-R and RPS4 form an excellent example, represents a revised form of the Guard Model, or Gene for Gene concept, in which specific host targets of pathogenic effectors rather than structural mimics are "guarded" by R proteins ready to trigger immune responses (van der Hoorn and Kamoun, 2008; Van der Biezen and Jones, 1998). The decoy system however accounts for the fact that the intended effector targets are less evolutionarily stable, with important functions that cannot easily be gone without. By adopting mimics of these immune components whose sole purpose is effector perception, the mimics can safely evolve over time to match the diversification of effector repertoires (van der Hoorn and Kamoun, 2008).

1.6 Pseudomonas syringae as a model bacterial phytopathogen

Recently named the top pathogenic bacteria in plant pathology on account of its broad importance to science, and its environmental and agricultural impact, *Pseudomonas syringae* and its respective pathovars represent a giant amongst model organisms (Mansfield et al., 2012). With over 60 identified pathovars each affecting a specific group of host plants spanning from chestnut and cherry trees, to soybean and rice, and new isolates still being reported, *P. syringae* is of vast economic importance (Xin et al., 2018; Società italiana di patologia vegetale. et al., 1997; Webber et al., 2008; KAMIUNTEN et al., 2000; Budde and Ullrich, 2000; Reinhardt et al., 2009; O'Brien et al., 2011). *P. syringae pv. tomato* (*Pst*) was first recorded in 1933 as a rod-shaped Gram-negative bacterium that induced symptoms of disease in the tomato host, manifesting as sunken brown spots on the leaf (Okabe, 1933). Since then much has been discovered about the tomato-infecting strain regarding its life cycle and molecular mechanisms of virulence. As a hemibiotroph, *Pst* is able to survive as a saprophyte on decaying organic matter, and is dispersed by rain splashes, but must transition to an endophytic lifestyle entering plant tissue in order to cause disease (Xin et al., 2018; Preston, 2000). It does this by first entering the leaf through open wounds or stomata, then by multiplying in the apoplast.

Pst delivers effectors to host cells using a T3SS, and a number of its effectors have been characterised as having virulence promoting function (Xin et al., 2018). The *Pst* effector HopW1 disrupts the actin cytoskeleton, and subsequently limits endocytosis and the vesicular trafficking of proteins required for immune signalling (Kang et al., 2014). Similarly, effector HopE1 enhances pathogenic virulence by using the plant host calcium sensor calmodulin as a cofactor to target the microtubule-associated protein 65 (MAP65) and dissociate it from microtubules, inhibiting the secretion of immunity related proteins (Guo et al., 2016). HopD1 targets the *A. thaliana* NAC transcription factor NTL9 in the endoplasmic reticulum (ER) to inhibit its induction of immune-related genes during ETI (Block et al., 2014). Many of the effectors that have been identified however have yet to be attributed to specific host targets and mechanisms (Xin et al., 2018; Lindeberg et al., 2012; Block and Alfano, 2011).

The effector HopM1 has many functions including inhibition of ROS bursts, callose deposition, proteasomal function and stomatal closure, but was also discovered to be able to enhance the accumulation of water in the apoplast, presumably to dilute antimicrobial compounds, and facilitate nutrient uptake by the pathogen (Lozano-Durán et al., 2014; Nomura et al., 2006; Üstün et al., 2016; Xin et al., 2016). This study of *Pst* HopM1 elucidated the molecular basis of the humidity effect in bacterial pathogenesis (Xin et al., 2016). Analysis of the kinase inhibitor AvrPto enabled the discovery of the first gene-for-gene pair with the plant *R* gene *Pto*, and their participation in a guard pathogen recognition system with host NB-LRR protein Prf led to the synthesis of the Guard Hypothesis, initiating a field-wide search for host targets of pathogenic effectors as a way of identifying novel immune system components (Ronald et al., 1992; Scofield et al., 1996; Van der Biezen and Jones, 1998). Analysis of T3SEs in the *Pst* repertoire has enabled a vast number of discoveries such as these relating to plant pathology, however new virulent functions and targets amongst them have to be revealed, and so *Pst* with the model plant organism *Arabidopsis thaliana* are the primary pathosystem used in this study.

1.7 The plant circadian clock

One posited mediator of the Arabidopsis defence response is the circadian clock (Zhang et al., 2013). Circadian rhythms are endogenous oscillations in biological processes that occur with a period of approximately 24 hours when entrained by fluctuations in the organism's environment, persisting under constant conditions over a range of physiological temperatures. In this way the clock can coordinate a wide range of physiological outputs including not only biotic and abiotic stress, but also hormone signalling, flowering time, growth and metabolism (Michael et al., 2008; Covington et al., 2008; Greenham and McClung, 2015). Circadian oscillators generally rely on an interconnected network of transcription-translation feedback loops (TTFLs), in which positive and negative elements respectively activate and repress each other's activity, leading to their regulating each other in a cyclical way. While the kinetics and delays introduced by reciprocal regulation of these elements by

their nature tend to maintain a constant rate oscillating approximately every 24 hours, the clock can also keep pace by resynchronizing its phase with entraining signals such as light and temperature (Hubbard & Dodd 2016).

Although the circadian clock varies between organisms with respect to specific clock components, this general TTFL structure is conserved (Andreani et al., 2015). Still, notable differences have been found between the classic clock architecture, consisting of positive and negative elements, and that of plants. Our understanding of the plant molecular clock has recently been revised in light of the discovery that in place of a positive arm of the TTFL, additional repressor elements exist such that increased activity of certain genes is achieved indirectly through the repression of that gene's repressors. Plant's rhythms in clock gene transcription thus appear to be regulated instead by reciprocal repressive feedback loops, and while summarised below, have also been described at length in several excellent reviews (See Figure 1.3) (Hubbard and Dodd, 2016; Nohales and Kay, 2016; Lu et al., 2017; Millar, 2016). Importantly, the architecture of the plant circadian clock has been found to be largely conserved between the model organism *A. thaliana* and multiple agriculturally significant crops including rice and barley, making the results of studying circadian rhythms in *A. thaliana* highly relevant in identifying potential means of crop improvement (Song et al., 2010; Hubbard and Dodd, 2016).

The first characterised components of the plant circadian clock (dawn-phased components that fittingly receive first mention in most descriptions of the clock) are the MYB-like transcription factors CIRCADIAN CLOCK ASSOCIATED 1 (CCA1) and LATE ELONGATED HYPOCOTYL (LHY) (Wang et al., 1998; Schaffer et al., 1998). CCA1 and LHY form a heterodimer, and once activated at dawn directly repress the expression of several other clock components assisted by the corepressor DE-ETIOLATED1 (DET1) by binding to a motif known as the evening element (EE) (Lau et al., 2011; Michael and McClung, 2002). In addition to negatively regulating their own expression, CCA1 and LHY repress morning-phased *PSEUDO-RESPONSE REGULATOR* (PRR)-encoding genes *PRR9*, *PRR7*, and *PRR5*, evening phased *TIMING OF CAB EXPRESSION 1* (*TOC1*) and *GIGANTEA* (*GI*) and members of the so-called evening complex (Kamioka et al., 2016; Adams et al., 2015; Alabadi et al., 2001; Lu et al., 2012; Huang et al., 2012). The evening complex (EC) is comprised of

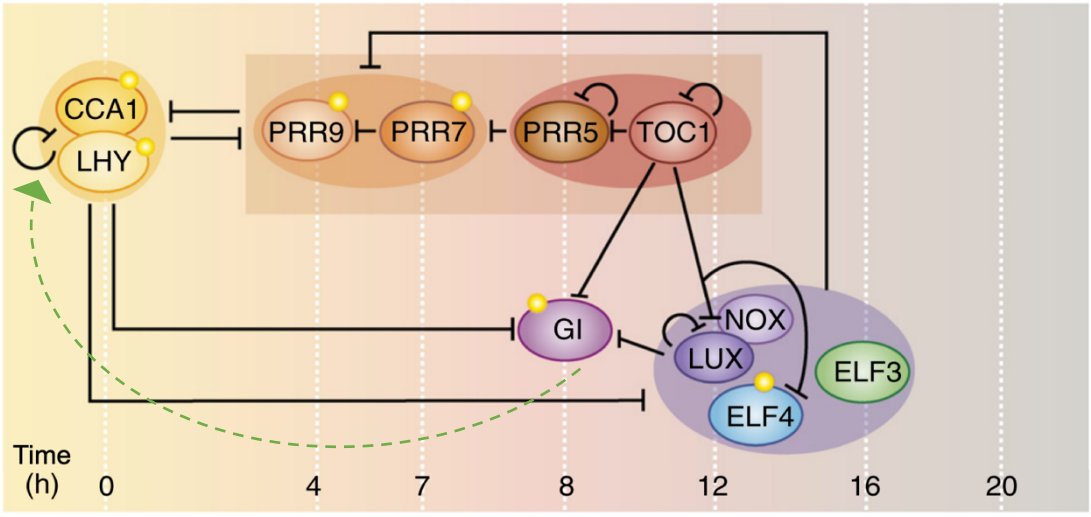

Figure 1.3: A schematic of transcriptional feedback loops at the core of the *A. thaliana* circadian clock (figure and legend adapted from Nohales & Kay 2016). Chronological expression of genes over a 24-hour period is depicted from left to right, starting at dawn (where time = 0 hours). Black bars indicate repression of transcription, and green, activation. Dashed lines designate interactions that may only apply under certain conditions, or that have not yet been proven to be direct. Ovals enclose functional groups, and yellow suns show genes whose transcription is promoted by light. The CCA1/LHY heterodimer activates at dawn, repressing the morning phased *PRR*-encoding genes along with *TOC1, GI,* and the Evening Complex (EC, purple oval). As the day progresses, *PRR9,7* and *5* are expressed, and repress each other, as well as *CCA1/LHY*. As CCA1 and LHY levels fall due to transcriptional repression, the EC components become derepressed, and repress *PRR9* and *7,* thus relieving the repression of dawn phased *CCA1* and *LHY*, permitting their transcription once more at dawn, and recommencing the daily cycle. *GI* may also be required for the upregulation of *CCA1* and *LHY*.

another MYB-like transcription factor, LUX ARRYTHMO (LUX), the LUX homolog NOX (also called BROTHER OF LUX ARRYTHMO, or BOA) and two proteins EARLY FLOWERING 3 (ELF3) and EARLY FLOWERING 4 (ELF4). Between the morning and afternoon, *PRR9*, *PRR7* and *PRR5* are gradually expressed 4, 7 and 8 hours after dawn respectively, and successively work to repress each other's transcription, as well as that of *CCA1* and *LHY* (Liu et al., 2016).

In the afternoon (approximately between 4 and 12 hours after dawn), EE regulated clock genes including *PRR9*, *PRR5*, *TOC1*, *LUX* and *ELF4* are induced by REVEILLE 8 (in addition to RVE4 and RVE6 in a partially redundant manner) and in turn repress *CCA1* and *LHY* expression (Hsu et al., 2013; Huang and Nusinow, 2016). Finally, as CCA1 and LHY levels fall resulting in EC components being derepressed, activity of the evening-phased EC begins. TOC1, previously assumed to activate the dawn components, is now thought to repress *CCA1* and *LHY* by interacting with the

transcription factor CCA1 HIKING EXPEDITION (CHE) in an uncharacterised manner, further limiting the window of activity for the heterodimer (Pruneda-Paz et al., 2009). TOC1 is also a negative regulator of *GI*, *PRR5*, and EC component genes *LUX* and *ELF4* (Huang et al., 2012). The evening complex itself represses *PRR9, PRR7, TOC1, GI* and *LUX* (Kiba et al., 2007; Herrero et al., 2012). The repression of *PRR9, PRR7* and *TOC1*, which are themselves repressors of CCA1/LHY heterodimer levels is suggested to relieve the repression on *CCA1* and *LHY*, thus permitting expression levels of the morning genes to increase, and the daily cycle to recommence. The short period phenotype of GI loss of function mutants would indicate that GI is an activator of *CCA1* and *LHY* too, however the nature of this induction has not yet been ascertained (Martin-Tryon et al., 2006).

The feedback loops involved in the circadian clock create rhythms in expression levels of the core clock components, which consequently result in the temporal regulation of many pathways downstream on account of approximately one third of *A. thaliana* genes' transcripts exhibiting circadian rhythmicity in expression (Covington et al., 2008). Oscillations in clock gene transcripts continue over time thanks to this on-going feedback, but constantly resynchronise with any sufficiently perceptible entraining cues. Light inputs are incorporated into the regulation mechanisms of the clock in several ways to keep it in phase with the environment, influencing transcription, messenger RNA stability, and rate of clock gene translation (as reviewed by Hsu and Harmer, 2014, and Oakenfull and Davis, 2017)). The protein ZEITLUPE (ZTL), which contains a blue light sensing LIGHT, OXYGEN OR VOLTAGE (LOV) domain, stabilises GI by forming a complex with it once light-activated, and together they target TOC1 for ubiquitination (Kim et al., 2007). In this way light cues gate the proteolysis of TOC1. LIGHT-REGULATED WD 1 (LWD1), which has both blue and red light sensitivity, appears to facilitate light input to the clock due to *CCA1*, *PRR9*, *PRR5* and *TOC1* expression being dependant on its binding their promoters (Wu et al., 2008; Wang et al., 2011c). Another mechanism of the clock's light entrainment involves cryptochromes and phytochromes, blue/UV sensitive flavoproteins and red/far red sensitive photoreceptors respectively, which mediate light signals and impact period length in plants, however the signalling pathways underlying this entrainment are not well understood (Somers et al., 1998; Fankhauser and Staiger, 2002; Oakenfull and Davis, 2017).

1.8 Regulation of plant immunity by the circadian clock

All in all, the rhythmicity achieved by the clock enables an organism to maximise its efficiency through synchronisation with its environment, permitting precise temporal regulation of physiology in response to biotic stimuli (Harmer, 2009). As such, a functioning clock has been shown at length to be advantageous to plant fitness, conferring benefits such as increases in chlorophyll, carbon fixing, growth and survival rate (Dodd et al., 2005; Green et al., 2002). Furthermore, orthologues of central clock components are thought to impact key crop phenotypes in oilseed rape after being detected in genome regions affecting these traits. Genotyping and SNP analysis of 158 accessions of homozygous inbred *B. napus* lines found several clock genes including *CCA1* and *GI* in regions associated with height and yield, inciting interest in the value of circadian genes in plant adaptation for important crop species (Schiessl et al., 2015). Regulation of immune receptor expression levels too in a temporal fashion would no doubt enable plants to fine-tune the efficacy of pathogen detection and elimination at times of greater risk of invasion while minimising the metabolic cost that would otherwise be required to support constantly elevated immune function. Over the past 15 years there has been a growing body of experimental evidence in support of this crosstalk between the circadian clock and plant defence (Figure 1.4). Many of the mechanisms of defence associated with the MTI response in particular have been linked to the clock. The extent of callose deposition in cell walls is seen to vary according to time of inoculation, while circadian control of stomatal aperture has been implicated as an active way for the innate immune system to physically limit bacterial entry at night (Bhardwaj et al., 2011). Arrhythmic lines overexpressing core clock components CCA1 and LHY exhibit significantly increased stomatal aperture during the light phase, coinciding with the plant's increased susceptibility to infection by infiltrated *Pseudomonas syringae* at that time of day (Zhang et al. 2013). This would indicate that through circadian control, the plant relies on physical restriction of pathogen invasion offered by closed stomata during the dark phase, lowering the efficacy of stomata-independent defence in a compensatory trade-off. Disruption of CCA1 or LHY function appears to facilitate invasion of the leaf interior by preventing

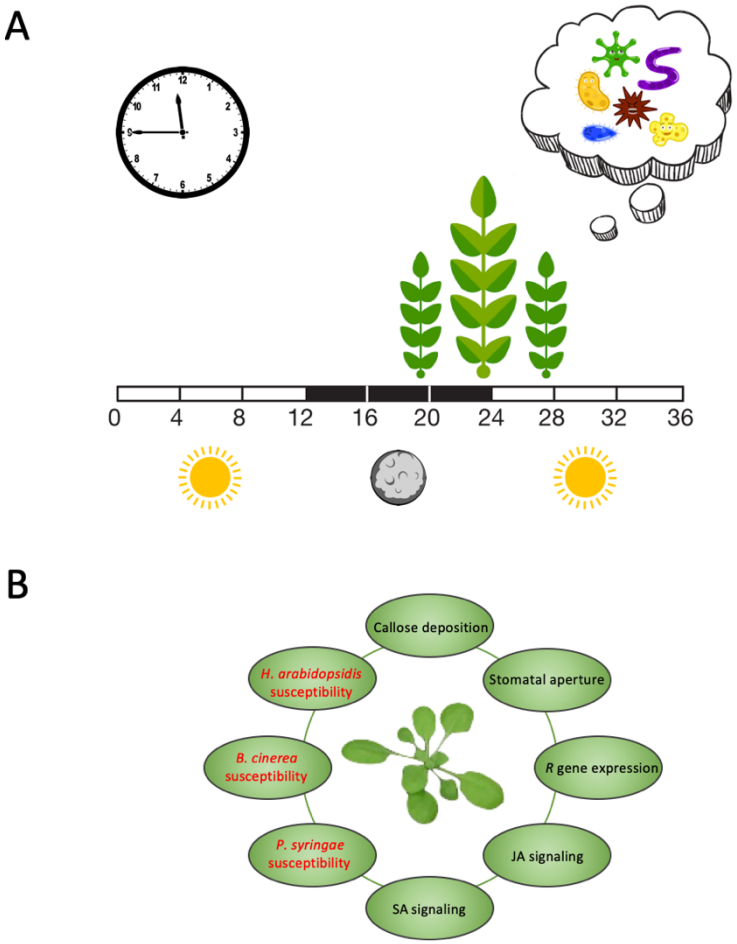

Figure 1.4: Pathogenic defence mechanisms in plants are regulated by the circadian clock (figure adapted from Wang et al., 2011 and Lu et al., 2017). A) By using the circadian oscillator to regulate immune-associated pathways, plants may "anticipate" pathogenic infection and employ defence mechanisms at specific times of day when they would be most effective. B) The *A. thaliana* circadian clock has been shown to regulate many biological processes related to the immune response (black) such as callose deposition, stomatal aperture, *R* gene expression, and phytohormone signaling, as well as the plant's susceptibility to infection by certain pathogens (red) including *H. arabidopsidis*, *B. cinerea*, and *P. syringae* (see main text for details).

stomatal closure during the day when stomata-independent defence is dampened. Another study describes an *R* gene *Arabidopsis* mutant with 106 genes expressed differentially to the wild type, 22 of which influenced susceptibility to *Hyaloperonospora arabidopsidis* pathogenesis; 14 of this subset were found to possess either CCA1-binding sites and/or Evening elements (EE), motifs bound by CCA1 and LHY, and/or have rhythmic expression patterns (Wang et al., 2011b). Other genes known to be associated with reduced susceptibility to pathogenic infection have also been found to be rhythmically expressed, suggesting a level of circadian regulation, and reinforcing the link between immunity and the clock in more general terms

(Sauerbrunn and Schlaich, 2004; Wang et al., 2011a; Zhang et al., 2013; Xu et al., 2017).

The evidence in support of the clock's role in plant innate immunity when paired with the rapid rate at which pathogens evolve to disrupt the key components of the plant immune system makes it seem highly likely that the plant's circadian oscillator is a target for disruption by pathogens. One group has reported a link between stress response-related *C-REPEAT-BINDING FACTOR (CBFs)* transcript levels and diurnal variations in *Arabidopsis* susceptibility to WT strain *P. syringae* DC3000*,* with *CBF* knockdown line amiR-1 almost completely losing rhythmicity in susceptibility to *P. syringae* seen in WT strains. This CBF knockdown line is only able to attain approximately 20% *CCA1* expression, thus indicating that CBFs may play a role in clock control of immunity, through the regulation of *CCA1* (Shi et al., 2016). Certain phytohormones have also been suggested to facilitate feedback between the immune system and the clock. In one such study, the investigation of the mechanism behind circadian-driven susceptibility of *A. thaliana* to *B. cinerea* using a transcriptomic approach led to the discovery that jasmonic acid and ethylene-mediated defence gene expression is more rapid when plants are infected at dawn (when the fungus exhibits the least pathogenicity) (Ingle et al., 2015). Furthermore, this temporal variation in susceptibility is dependent on the expression of *JAZ6,* a circadian regulated JAZ protein whose role is characterised as a transcriptional repressor of JA and ET-mediated defence (Ingle et al., 2015; Covington et al., 2008; Pauwels and Goossens, 2011). Another group has postulated that perturbations in immune response-stimulating hormone SA alter rhythms in the metabolic pacemaker, which likely feeds back through the master immune and SA regulator NON-EXPRESSOR OF PATHOGENESIS-RELATED GENE 1 (NPR1) to reinforce the transcriptional clock in its stead to maintain cellular rhythmicity (Zhou et al., 2015). NPR1, which was confirmed in the same study to have circadian oscillations in monomer protein levels, is shuttled from the cytoplasm to the nucleus as part of its role in SA signalling. SA biosynthesis is also under circadian control (Zheng et al. 2015). However, a dual or combined function in regulating the clock and inducing the SA-response seems probable given that NPR1 has also been confirmed as interacting directly with key clock components. NPR1 physically binds TOC1, and *PRR7*, *CCA1* and *TOC1* all demonstrate upregulation by NPR1 under stress conditions, indicating that NPR1 has

the capacity to bolster the clock through both morning and evening loops as part of its immune regulator function (Zhou et al., 2015). Yet another point of crosstalk between the immune system and the clock is CHE. This aforementioned chaperone of TOC1 required for repression of the CCA1/LHY complex is a temporally expressed transcription factor that is needed for the induction of SA biosynthesis gene *isochorismate synthase 1* (*ics1*). CHE binds to the promoter of *ICS1*, and mirrors its rhythms in expression levels, indicating that may be involved in the temporal regulation of *ICS1*. Additionally, CHE is seen to partake in the immune response, as *CHE* mutants triggered by infection (with virulent *Pseudomonas syringae pv. Maculicola* carrying the effector *avrRpt2*) have abolished systemic induction of *ICS1* normally observed during the onset of systemic acquired resistance (Zheng et al., 2015). Interestingly, the proposed role for the involvement of SA in the circadian clock has been linked to rhythmic cycling of bacterial community structure of the root microbiome. The microbial community of the rhizosphere responds to changes both in circadian clock gene expression and SA levels, suggesting that clock regulation of immunity may even modulate downstream changes in the rhizosphere (Hubbard et al., 2018; Staley et al., 2017; Lebeis et al., 2015). The recent discovery of genes with novel functions linking the clock and the immune system suggest that feedback from the clock may form a substantial part of immune regulation, thus making it a presumable target for invading pathogen effectors.

1.9 Aims

In spite of the strong recent substantiation of clock and immunity interconnectivity, there is still a distinct lack of knowledge concerning the up- and downstream pathways of circadian clock-mediated defence. We hypothesised that plant's circadian oscillator would be a target for disruption by bacterial effectors and sought to investigate the subversion of circadian rhythms in plants by *P. syringae pv. tomato* effectors in order to elucidate the mechanistic link between the clock and the immune system. The primary aims of this project was therefore firstly, to assess the requirement of functioning Type 3 Secretion Systems (T3SS) in the conjectured pathogenic interference of rhythmicity, and secondly, to identify *Pst* effectors that target the *A.*

thaliana circadian clock, and characterise the molecular mechanisms underlying their virulent function.

Chapter 2: Materials and methods

2.1 Plant materials and growth conditions

The *Nicotiana benthamiana* and *Arabidopsis thaliana* plants used in this project were (unless stated otherwise) grown in 12-hour photoperiods at 22°C, relative humidity 60%, light irradiance 100 μmol $m^{-2}s^{-1}$ in Aralab plant growth chambers. Seeds were sown on soil, covered with cling film and stratified in the dark at 4°C for 3 days before being moved to a growth chamber to germinate. After 7 days seedlings were pricked out with forceps and put into individual modules, with trays covered with a vented, translucent plastic lid for a further week. At 14 days this lid was removed, and plants were left uncovered until plants had reached 4-5 weeks of age. In experiments where specific leaves from the *A. thaliana* rosette were used in order to maintain a consistent developmental stage between biological replicates, leaf numbering was performed as has been described in Farmer et al., 2013. For the RNAseq assay, plants were grown to 10 days old on solid Murashige and Skoog (MS) media [2.15g/L MS salts (Murashige and Skoog, 1962), 10g/L sucrose, 5g/L phytagel, pH 5.8] then transferred to liquid MS (lacking phytagel) for β-estradiol/mock treatment (see section 2.21 for further details).

Nicotiana benthamiana plants used were either wild type (WT) or *dcl4* mutants. WT *Arabidopsis thaliana* plants were of the ecotype Columbia (Col-0). The *A. thaliana* luciferase fusion lines *CCA1::LUC* and *TOC1::LUC* used in the bioluminescence study were kindly donated by Prof. Murray Grant (University of Warwick, UK). T-DNA insertion lines of the genes AT3G12910 (SALK_016619C) and AT4G28530 (SALK_104622C and SALK_094441C) were produced by the Nottingham Arabidopsis Seed Centre (NASC). The former of these, SALK_016619C was kindly donated by Dr. Isabelle Carré (University of Warwick, UK), while the remaining two were obtained directly from the NASC. The generation of transgenic *A. thaliana* lines *est::NLS-HopAO1-GFP*, *est::NES-HopAO1-GFP* and *est::3HA-HopAO1-GFP* is described in full elsewhere (see section 2.6.2 for vector creation, and section 2.11 for stable transformation of plants).

2.2 Bacterial strains and media

Bacterial cultures of *Pseudomonas syringae pv. tomato* (*Pst*) were grown in King's B (KB) medium (King et al., 1954) at 28°C in a shaker. *Agrobacterium tumefaciens* strain GV3101 used for transient protein expression in *Nicotiana benthamiana* was grown in Lysogeny Broth (LB) medium (Bertani, 1951) also at 28°C in a shaker. *Escherichia coli* cultures used for molecular cloning were grown also in LB medium at 37°C in a shaker. All bacterial strains were revived from 60% glycerol stocks by streaking on solid media plates prior to inoculation of liquid media with single colonies. Antibiotics used were at the following working concentrations unless otherwise stated: Rifampicin 100µg/mL, Gentamycin 20µg/mL, Kanamycin 25µg/mL, Ampicillin 100µg/mL, Spectinomycin 50µg/mL, Zeocin 50µg/mL.

2.3 Bioluminescence image analysis in planta

Arabidopsis thaliana lines *CCA1:LUC* and *TOC1:LUC* were grown to 4 weeks of age in standard 12:12 LD (12 hours in the light, 12 hours in the dark) conditions at 22°C. 24 hours prior to image analysis, plants were sprayed on the adaxial leaf surface with a solution of luciferin (5mM beetle D-luciferin, 0.02% Silwet L-77, 0.01% Triton-X-100) where approximately 5ml of solution was used for every 6 plants. On the day of image analysis, plants were kept in constant darkness (DD) starting from subjective dawn (circadian time or CT0). Plants were pressure infiltrated in adult leaves 7, 8 and 9, four hours before dusk (CT7) with a suspension of either *Pst* DC3000 or *Pst hrcC* in infiltration media (10mM MES, 10mM $MgCl_2$, pH 5.5), or a mock solution (infiltration media only). Bacteria were grown and made up in the suspension to a final OD_{600} of 0.001. Infiltration was performed in a dark room under a green safety light. Infiltrated leaves were gently secured in place using bent toothpicks in order to mark the infected leaves for later identification in image analysis as well to limit the movement of leaves while being imaged.

Image capture was undertaken using the Micromanager 1.4 software, with pre-exposure clearing, hot pixel correction, 2x2 binning, and the acquisition of 432 images

each with an exposure time of 10 minutes (i.e. a 3 day long time-lapse). Image stacks were analysed in ImageJ, and average luminescence was calculated by measuring average pixel intensity for each time point within manually determined Regions of Interest (ROIs), chosen by specifying only an area occupied by an infected leaf throughout the entire time course.

2.4 Bioluminescence image analysis of protoplasts

The analysis of circadian phenotypes in protoplasts transfected with a luminescent clock reporter was performed as has been previously described in Hansen & van Ooijen, 2016 where further details regarding methods and buffers can be found. *Arabidopsis thaliana* lines were grown to 4 weeks of age in long day conditions (16h:8h LD) at 21°C. Protoplasts were harvested from lower epidermal leaf tissue using magic tape and resuspended to a concentration of 7×10^5 protoplasts/ml in MMg solution.

Cells were transfected with both a circadian reporter (one of CCA1pro::LUC or GIpro::LUC) and either the pEG201 plasmid encoding one of a collection of 23 *Pst* effectors (HopO1-1, HopM1, HopN1, HopAD1, HopY1, HopT1-1, HopAB2, HopX1, HopP1, HopC1, HopF2, HopAF1, HopA1, HopB1, HopH1, HopG1, HopAO1, HopAI-1, HopK1, AvrPto, HopQ1-1, HopV1 and HopD1) or the empty vector in a solution of PEG before being collected and resuspended in W5 imaging solution and aliquoted into three replicate wells of a 96-well plate sealed with a clear adhesive lid. The plate was read approximately every 35 minutes (5 seconds per well) for 5 days at room temperature, and exposed to blue (wavelength) only, at light intensity of 5µmol m^{-2} s^{-1}. Luminescence results were analysed by Fast Fourier Transform (FFT) using Biological Rhythms Analysis Software System (BRASS).

2.5 Bacterial growth in Arabidopsis thaliana

For the assessment of susceptibility of *A. thaliana* plants to pathogens, bacterial suspensions were generated by adjusting overnight cultures of *P. syringae* to an

Optical Density at 600nm (OD_{600}) of 0.001 and resuspending in 10mM $MgCl_2$. Leaves 7 and 8 of adult (4-week old) plants were pressure-infiltrated using a needless syringe with this bacterial suspension or where specified a mock solution of solely 10mM $MgCl_2$ infiltration buffer. The time at which leaves were harvested is cited throughout in days post infection (dpi). Unless stated otherwise, infiltrations were performed in the morning, and samples were harvested at the same time of day following a set time of bacterial incubation *in planta*. A disc was taken from each infiltrated leaf using a #4 cork borer (8.75mm diameter) such that a pair of leaf discs, one from leaf 7 and one from leaf 8, represented each individual plant as one biological sample. Between 4 and 6 biological replicates were used per genotype. Samples were lysed in a 2ml eppendorf tube containing 200µl of 10mM $MgCl_2$ and two metal beads using a Mixer Mill TissueLyser (Qiagen) for 60 seconds at 17.8 Hz. Pathogen growth was quantified by dispensing serial dilutions of the lysed tissue suspension onto solid growth media. Plates were incubated for 48 hours at 28°C prior to the counting of colonies and calculation of Colony Forming Units (CFU)/ml.

In the case of the bacterial susceptibility time series using Col-0, upon reaching 4 weeks of age plants were moved to constant darkness (DD) for 48 hours prior to starting infiltrations. These infiltrations were performed on previously untreated individual plants every 4 hours over a period of 48 hours, and as such samples were harvested at the same time of day as the plants were infiltrated, either at the time of infiltration itself (0dpi), or 48 hours later (2dpi).

Statistical analysis of results was performed using a 2-way Analysis of Variance (ANOVA), followed by either Tukey's or Bonferroni's post hoc test for multiple comparisons (given that Tukey's test is more conservative but works best with equal sample sizes, occasional elimination of outlier values in sample sets made Bonferroni a more appropriate choice). A P value of less than 0.05 was considered to be significant (*). The Prism 8 software package (Graphpad, U.S.A) was used for all statistical analysis.

2.6 Molecular cloning

2.6.1 Cloning using the Gateway system

All of the plasmid constructs used in this study were produced by subcloning sequences from in-house generated vectors with the Gateway cloning system (Invitrogen, U.S.A), by way of performing standard BP/LR reactions according to the specifications of the manufacturer. The exceptions to this are the CCA1pro:LUC and GIpro:LUC bioluminescent reporter plasmids which were provided by Dr. Gerben van Ooijen (University of Edinburgh, UK) and have been described previously by Kim and Somers (2010), the pLHY in pHis3Leu2 vector which was kindly given by Dr. Isabelle Carré (University of Warwick, UK) and has been described previously by Davies (2013), and the estradiol-inducible HopAO1 constructs which were made by Golden Gate assembly, the details of which can be found in full in 2.6.2.

2.6.2 Cloning using Golden Gate assembly

The *est::NLS-HopAO1-GFP*, *est::NES-HopAO1-GFP* and *est::3HA-HopAO1-GFP* constructs were generated by performing a Golden Gate assembly using the enzymatic reactions, primer design principles, and numerous standard module parts described in the MoClo Plant Parts Kit (Engler et al., 2014).

Several custom modules were also created as part of this assembly. The estradiol inducible promoter system (kindly donated by Dr. Nicola Patron, The Sainsbury Laboratory, UK) originally including the estradiol inducible promoter paired with a 5' UTR within the pICSL120005 vector had its sequence altered using primers to swap the 3' AATG 4 base pair (bp) overhang for the sequence CCAT such that the level 0 module could be assembled in frame with an N-terminal tag module in level 1. The sequence for the XVE receptor protein which binds the estradiol inducible promoter in the presence of β-estradiol (Zuo et al., 2000) contained within the pICSL80003 vector was assembled along with the standard MoClo level 0 modules encoding a 35S promoter and 5'UTR (pICSL13001) and a 3'UTR and terminator (pICH44300) into

the level 1 position 3 (L1P3) vector pICH47751. The FAST-R seed selection cassette (Shimada et al., 2010, standard MoClo level 0 module pICSL70008) was assembled into the level 1 position 3 (L1P2) vector pICH47742 with the same promoter and terminator modules as the XVE L1P3 construct.

The nuclear localisation sequence (NLS) and nuclear exclusion sequence (NES) level 0 modules were created using primers encoding the NLS and NES with the 5' CCAT and 3' AATG overhangs (see Table 2.1). The 3HA-FLAG N-terminal tag module was kindly donated by Dr. Weijie Huang (John Innes Centre, UK).

The sequence encoding the *P. syringae* effector HopAO1 contained an internal Bpi1restriction enzyme recognition site which was incompatible with the level 0/1 Golden Gate assembly reaction, and so the primers HopAO1domF and HopAO1domR (see Table 2.1) were used to domesticate the gene. The primers HopAO1 4bpF 4bpR (see also Table 2.1) were then used to confer the 5' AATG and 3' TTCG overhangs respectively. All custom level 0 modules, including the 3HA-FLAG N-terminal tag, were assembled within the level 0 acceptor plasmid pAGM9121.

The complete coding sequences for N and C-terminal tagged HopAO1 under the estradiol inducible promoter were assembled in the level 1 position 1 (L1P1) vector pICH47732, such that the inducible promoter and 5' UTR was followed by the N terminal signal peptide or 3HA-FLAG tag, the domesticated HopAO1 CDS, a C terminal GFP tag (standard MoClo level 0 part pICH50008) and finally a 3'UTR and terminator (standard MoCLo part pICH44300) by way of a one-pot Bsa1 reaction according to manufacturer instructions.

The aforementioned level 1 constructs were assembled such that position 1 was occupied by the inducible HopAO1 sequence, position 2 by the FAST-R seed selection cassette, and position 3 by the XVE estradiol receptor, along with the position 3 end-linker pICH41766, into the level 2 backbone pAGM4723 using a one-pot Bpi1 reaction according to manufacturer instructions. The final product was a vector in which the effector HopAO1 had either an NLS, NES or 3HA-FLAG N terminal tag, a GFP C-terminal tag, would only be expressed in the presence of the β-estradiol

hormone, and resided within a construct that could be selected for *in planta* by selecting red fluorescing seeds using stereomicroscopy.

Table 2.1: Primers for use in Golden Gate assembly.

Primer Name	Sequence
NES F	TTGAAGACAACTCACCATGGGTGGAAATGAACTTGCTC TCAAGCTTGCAGGACTT
NES R	TTGAAGACAACTCGCATTGTCTTATTAATATCAAGTCCT GCAAGCTTGAGAGC
NLS F	TTGAAGACAACTCACCATGGCTTCTAGCCCACCGAAGA AGAAGCGG
NLS R	TTGAAGACAACTCGCATTTTCCAGCTGACCTTCCGCTTC TTCTTCG
HopAO1 dom F	TTGAAGACAAGGACCAATGTGTTATGGTGATCGACA
HopAO1 dom R	TTGAAGACAAGTCCTCGGTTTCCCGAGGGG
HopAO1 4bp F	TTGAAGACAACTCAAATGAATCCCCTGCAACCTATTCA
HopAO1 4bp R	TTGAAGACAACTCGCGAACCTTCTAACGCTATTTTTGC GCGC

2.6.3 Generation of Escherichia coli chemically competent cells

A 100ml culture of bacterial *Escherichia coli* strain TOP10 cells were grown to an OD_{600} of 0.3, chilled on ice for 15 minutes, and then pelleted at 4000 rpm for 10 minutes at 4°C before being resuspended in 80ml of ice cold 0.1M $CaCl_{2.}$. Following a further 30-minute incubation on ice, cells were pelleted once again and resuspended in a total volume of 10ml ice cold 0.1M $CaCl_2$ containing 15% glycerol. Prior to general use, competency of cells was tested by transformation with previously successfully transformed plasmids and incubation on selective LB solid media, along with untransformed competent cells as a negative control. Cells were stored at -80°C.

2.6.4 Transformation of E. coli

Chemically competent *E. coli* TOP10 cells were transformed by incubating a 50µl aliquot of cells on ice for 30 minutes with 1µl of either miniprepped plasmid a completed BP/LR reaction mix in the case of newly generated constructs. Cells were subject to heat shock for 30 seconds in a 42°C water bath, then immediately returned to ice before being used to inoculate 250µl of LB media and incubated for 1 hour at 37°C with shaking. Successfully transformed cultures were selected by plating on solid LB agar plates containing appropriate selective antibiotics.

2.6.5 Plasmid preparation

Plasmid preparations were preformed using the NucleoSpin® Plasmid kit (Macherey-Nagel) according to the manufacturer's protocol, where the final elutions were done in 50µl of warmed RNAse-free water. Where greater yield of plasmid was required, namely in the bioluminescent imaging of protoplasts, preps were instead performed using the ZymoPURE II midiprep kits (Zymo Research) according to manufacturer instructions.

2.6.6 Plasmid sequencing

Plasmids were quantified using a Nanodrop ND 1000 spectrophotometer (Thermo Fisher Scientific, U.S.A) and samples were prepared in a 10µl volume made up with ddH_20 such that it contained plasmid at a final concentration of 100ng/µl, and forward/ reverse primer at a final concentration of 10µM. Samples were sequenced by Eurofins-GATC. Where plasmids had been constructed using Gateway cloning, primers specific for attB1/B2 minisites in the case of expression clones, and M13 in the case of entry clones generated in the pDONRzeo vector (Invitrogen, U.S.A), were used.

AttB1: GGGGACAAGTTTGTACAAAAAAGCAGGCT
AttB2 GGGGACCACTTTGTACAAGAAAGCTGGGT

M13 Forward: GTTGTAAAACGACGGCCAGT
M13 Reverse: CACAGGAAACAGCTATGACC

2.6.7 Generation of electrocompetent Agrobacterium tumefaciens

A 500ml culture of bacterial *Agrobacterium tumefaciens* strain GV3101 was grown to an OD_{600} of 0.5, chilled on ice for 30 minutes, and then pelleted at 4000G for 15 minutes at 4°C. The resultant pellet was resuspended in ice cold water and spun down again twice in volumes of 500ml and 250ml respectively, then resuspended and spun again under the same conditions in ice cold 10% glycerol in 10ml and 3ml respectively. Cells were tested for competency as previously described in 2.6.2, and stored at -80°C.

2.6.8 Transformation of A. tumefaciens

Electrocompetent *A. tumefaciens* GV3101 cells were transformed by adding to a 50µl aliquot of cells, already thawed on ice for 20 minutes, 1.5µl of plasmid. Electroporation was performed using a MicroPulser Electroporator (Bio-Rad Laboratories) according to manufacturer instructions, after which cells were incubated in 250µl of LB media and incubated for 1 hour at 28°C with shaking. Successfully transformed cultures were selected by plating on solid LB agar plates containing appropriate selective antibiotics.

2.7 Effector localisation analysis

2.7.1 Nuclear isolation and immunoprecipitation

Agrobacterium tumefaciens GV3101 expressing the constructs of interest (here *Pst* effector HopAO1-YFP in pEG104, free YFP in the empty vector pEG104, HA-HopAO1 in pEG201, HA-GFP in pEG201, or GFP-H2B in pGFP-Nbin, where YFP and GFP are yellow and green fluorescent proteins, respectively) were grown for 2 days in the presence of appropriate antibiotics, collected, and resuspended in agroinfiltration media (10mM MES, 10mM $MgCl_2$, pH 5.5) at an OD_{600} of 0.4. Cultures were pressure infiltrated using a needless syringe into fully expanded leaves of adult wild type *Nicotiana benthamiana* plants, fully saturating the entire leaf. Two days after transformation, plant tissue was harvested and vacuum infiltrated in a desiccator with 1% formaldehyde to cross link protein complexes by way of 3 repetitions of 5 minutes under vacuum, then quenched with 0.125M Glycine and held under vacuum for a further 5 minutes. Tissue was frozen in liquid nitrogen and ground to a fine powder using a pre-chilled mortar and pestle.

Nuclei isolation was achieved by incubation of tissue in HONDA buffer [Hepes KOH pH 7.4 20mM, $MgCl_2$ 10mM, Sucrose 440mM, Ficoll 1%, Dextran T40 2.5%, Triton X-100 0.5%, Dithiothreitol (DTT) 5mM, Phenylmethylsulfonyl fluoride (PMSF) 1mM, Plant Protease Inhibitor Cocktail 1%] with rotation at 4°C until homogenous, filtration through miracloth, and fractionation by centrifuging at 2000 x g for 17 mins at 4°C. A 50µl aliquot of the upper supernatant was retained as a cytoplasmic fraction. The pellet was resuspended in HONDA buffer using a paintbrush to undergo a minimum of 5 washes at 1500 x g for 15 mins at 4°C (or until pellet had no trace of green colour that would indicate the presence of chloroplasts).

Isolated nuclei were lysed using nuclear lysis buffer [Tris-HCl pH 8.0 50mM, ethylenediaminetetraacetic acid (EDTA) pH 8.0, Triton X-100 1% PMSF 1mM, Plant Protease Inhibitor Cocktail 1%] and sonication for 4 repetitions on low power for 30 seconds in a prechilled water bath (Diagenode Bioruptor), then pelleted at 16100 x g for 15 mins at 4°C. A 50µl aliquot of the supernatant was here taken to be used as a nuclear fraction. The remaining supernatant was diluted by a factor of 10 in immunoprecipitation (IP) buffer (Tris-HCL pH 8.0 16.7mM, EDTA pH 8.0 1.2mM, NaCl 167 mM, Triton X-100 1.1%, Plant Protease Inhibitor Cocktail 1%), before addition of either anti-GFP agarose beads (Chromotek GFP-Trap) or anti-HA agarose

beads (Sigma-Aldrich) that had been cleaned 3 times in detergent-free bead washing buffer (Tris-HCL pH 8.0 20mM, EDTA pH 8.0 2mM, NaCl 150 mM, PMSF 1mM, Plant Protease Inhibitor Cocktail 1%), to be incubated for 2 hours at 4°C with rotation. Beads were pelleted at 141 x g for 3 mins at 4°C and subsequently washed five times in bead washing buffer, centrifuging at 400 x g for 2 mins at 4°C between washes. Excess buffer was removed with the biased edge of a needle syringe leaving only the protein bound agarose beads.

2.7.2 Visualisation of sub-cellular protein extracts by western blot

Following immunoprecipitation washed beads, along with the nuclear input, and cytoplasmic fractions were heated to 95°C for 10 minutes in sodium dodecyl sulphate (SDS) loading buffer (SDS 2%, Bromophenol blue 0.01%, Glycerol 7.8%, Tris HCl pH 6.8 10mM, DTT 50mM) before being loaded onto an SDS polyacrylamide gel electrophoresis (SDS-PAGE) gel. 6µl of PageRuler prestained protein ladder (Thermo Fisher Scientific, U.S.A) was also loaded, and empty wells were filled with 1X SDS loading dye. Gels were run for 15 minutes at 110V, and then at 150V for a further hour, or until the dye front was approaching the end of the 10cm gel and bands of the protein ladder were well separated. Proteins were transferred from the gel to a nitrocellulose membrane (preactivated in methanol for 3 minutes) by wet transfer for 30V overnight at 4°C.

For the detection of YFP and GFP-tagged proteins, membranes were blocked for 1 hour at room temperature with gentle agitation in a solution of 5% milk in Tris-buffered Saline (TBS, 24.2g Tris, 80g NaCl, adjusted to 1L with ddH_2O, pH 7.6) with 0.1% Tween-20 (TBS-T). This blocking buffer was discarded and the primary antibody (either α-GFP-HRP, 1:10000 Santa Cruz or α-HA-HRP, 1:2000 Sigma-Aldrich) diluted in 5% milk TBS-T was applied, again with shaking for a further hour at room temperature. Given that the primary antibody was conjugated, no secondary antibody was needed, and following primary incubation the membrane was washed with shaking 3 times for 10 minutes in TBS-T, and twice for 10 minutes in TBS. The

membrane was finally incubated in ECL detection reagent for 5 minutes protein side down on an acetate film and imaged using an X-ray developer.

2.7.3 Mass spectrometry

Proteins were extracted and purified as described in section 2.7.1 and run on an SDS PAGE gel as described in section 2.7.2. Protein digestion was performed using an in-gel trypsin enzyme incubation as has previously been described in Piquerez et al., 2014. An aliquot containing 20µl of digested peptides (total sample volume 50µl) per sample was submitted for analysis by Mass Spectrometry to the University of Warwick Proteomics Facility (University of Warwick, U.K). Samples were analysed by means of nanoLC-ESI-MS/MS using the Ultimate 3000/Orbitrap Fusion instrumentation (Thermo Fisher Scientific, U.S.A) and a 60-minute LC separation on a 50 cm column.

Raw data was searched using MaxQuant against the *A. thaliana* TAIR10, *N. benthamiana* and *P. syringae* databases (www.uniprot.org/proteomes), as well as the MaxQuant common contaminant database. The Scaffold software package was used for data analysis and visualisation of the results.

2.8 Working with yeast

2.8.1 Transformation of yeast

Cultures of *Saccharomyces cerevisiae* were grown overnight at 28°C with shaking in 3ml of rich Yeast Extract Peptide Dextrose (YEPD) media (Dreze et al., 2010). Cultures were pelleted and resuspended in 0.1M LiAc in a 1.5ml eppendorf tube, spinning at 2500RPM for 5 mins at room temperature, then resuspending again in 20µl 0.1M LiAc. To this was added 30 µl 1M LiAc, 40µl 2mg/ml ssDNA, 10µl sterile ddH_2O and ~200ng of miniprepped plasmid. The tube contents were inverted following addition of 200µl of PEG 4000 (made fresh and filter sterilised) then incubated for 1 hour at 42°C in a water bath. Transformed yeast were isolated using

Synthetic Complete (SC) media (6.8g Yeast Nitrogen Base, 20g ammonium sulphate, 40g glucose, 5.2g amino acid drop out mix, 15g agarose, ddH_2O to 1L, adjusted to pH 5.9 with NaOH) lacking the appropriate amino acids for the selection of transformed constructs, with incubation for 2 days at 28°C.

2.8.2 Yeast Two-Hybrid (Y2H)

The yeast two-hybrid (Y2H) assay was performed using the pDEST-DB/pDEST-AD Y2H system previously described (Dreze et al. 2010), where bait constructs HopAO1 (sub-cloned into the yeast 2-hybrid vector pDEST-DB) and empty vector control pDEST-DB were transformed into the haploid *S. cerevisiae* strain Y8930, while *Pst* transcription factors were transformed into haploid strain Y8800 as prey constructs in pDEST-AD (also known as pDEST22). Prey constructs were +Leucine, while bait constructs were +Tryptophan, with interactions permitting the synthesis of Histidine, such that successfully mated yeast containing both a bait and prey construct might grow on -LeuTrp but would only grow on -LeuTrpHis if the proteins encoded by bait and prey constructs interacted in yeast. The competitive inhibitor of the HIS3 enzyme 3-amino 1,2,4 triazole (3AT) was also used as a supplement to test the strength of interaction.

All yeast cultures were grown in SC media lacking the appropriate amino acids to select for constructs of interest at 28°C for 2 days at constant shaking and brought to an OD_{600} of 2.0. Mated strains containing the bait and prey interaction pair to be tested were grown in -Leu-Trp then spotted onto selective solid media plates. Plates were incubated at 28°C for a minimum of 3 days, and digitally photographed daily. Growth was compared between the various selection plates, as well as to the Y2H controls C1, C3, C5 and C4 which demonstrate negative, moderate, strong and very strong interactions respectively, and used to suggest the strength of interactions between transcription factors and the effector.

2.8.3 Yeast One-Hybrid (Y1H)

As has been described in section 2.9 the +Tryptophan (Trp) vector pDEST-AD was used as a backbone for the *A. thaliana* transcription factors *NAM* and *NAC074* (AT3G12910 and AT4G28530 respectively) and *GFP* in order to create the prey constructs, which were transformed into haploid Y8800 *S. cerevisiae*. In some instances, haploid Y8800 yeast that had been transformed with one of these prey constructs was sequentially transformed with a second construct. This second construct contained *HopAO1* or *GFP* within the pARC352 vector, a vector that confers the ability to synthesis Adenine, but neither a binding nor an activation domain. The bait construct for the yeast one-hybrid assay was kindly given by Isabelle Carré (University of Warwick, UK) and encoded the full sequence of the *LHY* promoter within the pHis3Leu2 vector. This vector confers the ability to synthesise Leucine constitutively, as well as Histidine in the event that the binding and activation domains of the two appropriate yeast vectors are able to interact with one another.

Haploid Y8930 yeast were transformed with the *pLHY* bait construct, and then mated with the Y8800 containing prey only, or prey and pARC352 vectors, to generate diploid yeast expressing 2 or 3 vectors. Cell cultures of mated yeast were grown in SC media lacking Leucine and Tryptophan (-LT) if they contained two vectors, or Leucine, Tryptophan and Adenine (-LTA) if they contained three vectors at 28°C for 2 days at constant shaking and brought to an OD_{600} of 2.0. Each cell culture was spotted onto various mixes of selective SC media in order to test firstly whether the constructs of interest had been successfully taken up by the mated yeast (-T, -A, -L, -LT, -LTA), secondly whether the bait and prey constructs were able to interact (-LTH), and finally whether HopAO1 was able to alter the strength of binding between bait and prey constructs (-LTAH). The competitive inhibitor of the HIS3 enzyme 3-amino 1,2,4 triazole (3AT) was also used as a supplement to test the strength of interactions.

Yeast were grown at 28°C for a minimum of 3 days, and digitally photographed daily. Growth was compared between the various selection plates and used to suggest the strength of interactions between transcription factors and the *LHY* promotor, as well as the capability of HopAO1 to influence the strength of binding in said interactions.

Constructs containing *GFP* were used as negative controls, forming the baseline of growth considered to be non-significant in terms of indicating the capability of constructs to interact.

2.11 Agrobacterium mediated stable transformation of Golden Gate lines

For the generation of *A. thaliana* lines that had been stably transformed with the *est::NLS-HopAO1-GFP*, *est::NES-HopAO1-GFP* and *est::3HA-HopAO1-GFP* vectors described in detail in section 2.6.2, the vectors were first transformed into *A. tumefaciens* as described in 2.6.8, and made into a glycerol stock. Stable transformation of these cultures was performed using the floral dip method described in Zhang et al., 2006. Seeds produced by the transformed plants were selected for uptake of construct using the seed-specific selectable FAST-R marker, by which only transformed seeds appear red under a fluorescence stereomicroscope (Shimada et al., 2010). Constructs were transgenically transformed into *LHY:LUC* plants of the Col-0 ecotype background.

2. 12 Confocal microscopy

All confocal microscopy was performed either on discs of tissue taken from adult leaves 7 and 8, or 10-day old seedlings using a Zeiss Laser Scanning Microscope (LSM) 880 (Zeiss). GFP and chlorophyll autofluorescence were detected using lasers at 488nm and 633nm, respectively. Images were processed using both Zeiss 2011 and ImageJ software.

2.13 Chlorophyll quantification

The extraction of chlorophyll from was performed as has been previously described in (Song et al., 2014). Briefly, detached leaves 7 and 8 from adult *A. thaliana* rosettes were used to represent one biological replicate and were first weighed to record fresh

weight in grams. They were then incubated in a 95% acetone/ethanol (v/v = 2:1, 5% ddH_2O) solution inside a 2ml eppendorf tube for 12 hours in constant darkness and centrifuged at 4000 x g for 5 minutes.

Concentrations of chlorophyll A and chlorophyll B per gram of fresh weight were quantified by measuring absorbance at 645 and 663 nm, and by using the formulae below, as formulated by Arnon (1949).

$$C_A = (12.7A_{663} - 2.69A_{645})\ g^{-1}$$
$$C_B = (22.9A_{645} - 4.68A_{645})\ g^{-1}$$
$$C_{A+B} = (20.23A_{645} + 8.023A_{663})\ g^{-1}$$

Statistical analysis of results was performed using multiple paired t-tests comparing genotypes on each day, where a P value of less than 0.05 was considered to be significant (*). The Prism 8 software package (Graphpad, U.S.A) was used for all statistical analysis.

2.14 Dark-induced senescence

The induction of senescence in *A. thaliana* plants was performed according to Song et al., 2014, whereby leaves 7 and 8 were detached from the adult rosette and placed in a petri dish. Dishes were sealed using micropore medical tape (Bunzl Healthcare, U.K), wrapped in aluminium foil and kept at 22°C. Leaves were later imaged using a digital camera.

2.15 Induction of hypersensitive response in N. benthamiana and A. thaliana

The *N. benthamiana* and *A. thaliana* plants used for analysis of the Hypersensitive Response (HR) were 5 and 4 weeks old, respectively. In the case of *N. benthamiana*, the first fully expanded leaf, and the two immediately younger leaves were used, while

in *A. thaliana,* leaves 7 and 8 were used. Leaves were infiltrated using a needless syringe with bacterial suspensions made up to an OD_{600} of 0.1.

For *N. benthamiana* assays, the suspensions were of *A. tumefaciens* transformed with HopAO1-YFP in pEG104, empty pEG104 vector (negative control), NAM-FLAG in pEG202, NAC074-FLAG in pEG202, or the empty pEG202 vector. Each leaf was first infiltrated with one construct expressing bacterial suspension, left to dry for approximately 30 minutes, and then infiltrated with another such that there were two overlapping circles which had been infiltrated, one of which containing a pEG104 construct, and one containing a pEG202 construct. Leaves were imaged with a digital camera 3 and 4 days following bacterial infiltration.

For *A. thaliana* assays, leaves were fully infiltrated with a suspension of either *P. syringae* wild type strain DC3000*,* the Type III secretion system (T3SS) mutant *Pst hrcC,* or a mock solution of solely infiltration buffer. Leaf pairs were detached and imaged with a digital camera on the day of infiltration as a baseline for leaf appearance, and four days after infiltration. Different individual plants were used for 0dpi (days post infection) and 4dpi images.

2.16 Ion leakage

For measuring ion leakage, leaves 7 and 8 of adult *A. thaliana* plants were pressure infiltrated using a needless syringe with either mock infiltration media, or one of three bacterial suspensions: The *P. syringae* wild type strain DC3000, the *hrcC* mutant which has been shown to provoke only a very small release of electrolytes from leaf discs (Johansson et al., 2015), or DC3000 *(AvrRpm1)*, which expresses an effector capable of recognising the CC-NB-LRR protein RPM1 and subsequently causing HR and increased electrical conductance (Mackey et al., 2002; Boyes et al., 1998). All bacterial suspensions were made up to an OD_{600} of 0.1.

The surface of infiltrated leaves was blotted dry with a paper towel, and a disc was taken from the middle of each leaf using a #3 borer (7.55mm diameter) and avoiding

the thick central vein. Each biological replicate consisted of a two leaf discs, one from leaf 7 and one from leaf 8. Leaf discs were quickly rinsed in sterile water, then placed in the well of a 24-well cell culture plate filled with 1ml of sterile water. Readings of electrical conductance were taken at regular intervals by applying 60µl of solution from each well to a conductivity meter (Thermo Fisher Scientific, U.S.A). Conductivity was measured in μScm^{-1}.

2.17 Working with RNA

2.17.1 RNA extraction and DNase treatment

RNA was extracted either from leaves 7 and 8 where both leaves together would represent a biological replicate (*nam-1* analysis of circadian gene expression assay) or in the case of testing HopAO1 expression levels in the transgenic golden gate lines, from 10-day old seedlings, where three seedlings represent a biological replicate.

Extractions of RNA for use in RT-qPCR assays was performed using TRIzol™ Reagent (Thermo Fisher Scientific, U.S.A) according to manufacturer instructions. RNA extractions for RNAseq analysis were performed using the RNeasy Plant Minikit (Qiagen, Germany) according to manufacturer instructions. For both assays, RNA total RNA was eluted in a final volume of 30µl RNase free water.

The removal of DNA contaminants using the TURBO DNA-free™ kit (Thermo Fisher Scientific, U.S.A) was performed on all RNA samples according to manufacturer instructions. Resultant RNA concentrations were assessed spectrophotometrically, and their integrity was assessed by agarose gel electrophoresis.

2.17.2 cDNA synthesis

All synthesis of cDNA was performed using SuperScript II Reverse transcriptase according to manufacturer instructions (Invitrogen, U.S.A), and primed using oligo(dT)12-18.

2.17.3 Real-Time Quantitative Polymerase Chain Reaction (RT-qPCR)

In order to quantify the cDNA synthesised from extracted RNA, real-time quantitative Polymerase Chain Reactions (RT-qPCRs) were employed. Reactions were run on either an Mx3005P qPCR system (Agilent Technologies, U.S.A) in the case of testing HopAO1 expression in the newly generated transgenic lines, or a CFX384 Touch Real-Time PCR (Bio-Rad, U.S.A) detection system in the case of assessing circadian gene expression patterns in the *nam-1* mutant which required a greater number of wells to be run simultaneously. All qPCR's were performed using SYBR® Green JumpStart™ Taq ReadyMix™ (Sigma Aldrich, U.S.A) according to the manufacturer's instructions. Expression levels were calculated relative to the expression of the housekeeping gene UBOX (AT5G15400). Each reaction was prepared in both technical and biological triplicate, using specific primers as detailed below (Table 2.2).

Statistical analysis of results was performed using a 2-way Analysis of Variance (ANOVA), followed by Bonferroni's post hoc test for multiple comparisons, where a P value of less than 0.05 was considered to be significant (*). The Prism 8 software package (Graphpad, U.S.A) was used for all statistical analysis.

Table 2.2: Primers for use in qPCR.

Primer Name	**Sequence**
Circadian gene primers	
CCA1 F	TCCAATGCACGCCGCAGTAGAA
CCA1 R	AGGCAA TTCGACCCTCGTCAGACA

LHY F LHY R	TGCCTCAAAGCTTTTCGCCTCCT GTCTGCAGCACAAGAATCCTGGCT
TOC1 F TOC1 R	TGATGGATCGGGTTTCTCTGCACCA TGAGGCATCATGGCTGCTGATTGC
HopAO1 primers	
HopAO1 #1 F HopAO1 #1 R HopAO1 #2 F HopAO1 #2 F	GCAGAAACCCTCATCACGCG GGTTGTTGCGGGCATAGTCG AACAGGCCTAGTCCGGAAGC GCGTGATGAGGGTTTCTGCG
Housekeeping gene primers	
UBOX F UBOX R	TGCGCTGCCAGATAATACACTATT TGCTGCCCAACATCAGGTT

2.17.4 RNASeq analysis

2.17.4.1 Sample preparation and sequencing

Seedlings were grown on solid MS plates (See section 2.1) until 10 days old, then removed with a pair of forceps into a falcon tube containing either liquid MS media (mock) or 20μM β-estradiol in media to incubate for 24 hours. Seedlings were then transferred into eppendorfs containing either sterile water (mock) or 1μM flg22 and vacuum infiltrated for 3 repetitions of 5 minutes at ZT23 (one hour before dawn). At ZT0 (dawn) seedlings were flash frozen in liquid nitrogen, and RNA was extracted and contaminating genomic DNA removed as described in section 2.18. The integrity of the RNA was assessed using the Agilent 2100 Bioanalyzer System (Agilent. U.S.A).

All subsequent steps in the RNA-Seq assay were performed by the BGI sequencing group (BGI, Hong Kong) according to their BGISEQ-500 RNA-Seq library preparation protocol. Firstly, mRNA molecules were using oligo(dT)-attached magnetic beads, then broken into small fragments (~200bp) using fragmentation reagent. First-strand cDNA was generated using random hexamer-primer, followed by a second-strand cDNA synthesis. Synthesised cDNA was subjected to end-repair and then was 3' adenylated, and sequencing paired-end adapters were ligated to the ends of these 3' fragments (Illumina, U.S.A). PCR was performed to amplify the cDNA fragments, which were then purified with Ampure XP Beads (Agencourt Biosciences, U.S.A). The library was again validated using an Agilent 2100 Bioanalyzer System (Agilent. U.S.A). The double stranded PCR products were heat-denatured and circularized into single strand circle DNA (ssCir DNA) to form the final library. Finally, the library was amplified with phi29 to make DNA nanoballs (DNB) (>300 copies), which were loaded into a patterned nanoarray, and single end 50 base reads were generated. The library was sequenced using the BGISEQ-500 sequencer.

2.17.4.2 Bioinformatics

Reads were filtered using the SOAPnuke software (v1.5.2, paramters: -l 15 -q 0.5 -n 0.1, Chen et al., 2018) so as to remove reads with adaptors, more than 10% unknown (N) bases, and low quality reads (where low quality is defined as the percentage of bases with a quality of less than 15 being greater than 50% within a read). Genome mapping was performed using Hierarchical Indexing for Spliced Alignment of Transcripts (HISAT2) software (v2.0.4, parameters: -p 8 --phred64 --sensitive -I 1 -X 1000 , Kim et al., 2015). Clean reads were mapped to the TAIR10 reference *A. thaliana* genome (Berardini et al., 2015), using Bowtie2 (v2.2.5, parameters: -q --phred64 --sensitive --dpad 0 --gbar 99999999 --mp 1,1 --np 1 --score-min L,0,-0.1 -p 16 -k 200, Langmead and Salzberg, 2012).

Gene expression levels were calculated with RSEM using default parameters (v1.2.12, , Li and Dewey, 2011). Clustering results were presented using javaTreeview (Saldanha, 2004) using cluster software to analyse the expression genes and sample

scheme at the same time by using the Euclidean distance matrix as the matrix formula (v3.0, parameters: -g 7 -e 7 -m a, Eisen et al., 1998; de Hoon et al., 2004). Differentially expressed genes (DEGs) were detected using DESeq2 (parameters: fold change ≥ 2.00 and Adjusted p value ≤ 0.05), based on binomial distribution as has previously been described (Love et al., 2014). Hierarchical clustering was performed for DEGs using pheatmap, a function of R. For clustering of more than two groups, the intersection and union DEGs between them were performed, respectively.

Regarding the gene ontology (GO) annotation result, DEGs were classified according to official classification. GO functional enrichment was also performed using phyper, a function of R where the p value calculating formula for the hypergeometric test is as follows:

$$P = 1 - \sum_{i=0}^{m-1} \frac{\binom{M}{i}\binom{N-M}{n-i}}{\binom{N}{n}}$$

False discovery rate (FDR) was then calculated for each p value. The terms for which FDR was not larger than 0.01 were defined as being significantly enriched. For the KEGG annotation, DEGs were categorised according to official classification, and pathway functional enrichment was done using phyper, a function of R. Calculation for p values and FDR was done as above.

Chapter 3: Identifying bacterial effectors that influence rhythmicity in *Arabidopsis thaliana*

3.1 Introduction

As has been reviewed in the introduction (section 1.8), the regulation of immune responses in *Arabidopsis thaliana* by the circadian clock is a long-established concept. It appears that this first began with a study on the characterisation of a rice blast resistance (*R*) gene *Pib* which led the authors to tentatively consider the fact that *Pib* exhibits a diurnal rhythm in gene expression (Wang et al., 2001). Since then, the notion of feedback between the circadian and immune systems in plants has gained considerably more traction. A notably high proportion of *R*-genes associated with resistance against powdery mildew, as well as numerous components of MAMP detection and MTI signalling (including the PRR FLS2 and the downstream MKK4/5-MAPK3/6-WRKY22 module) have been found to be either rhythmically expressed, or to possess motifs commonly bound by core clock regulators, strongly suggesting that the clock has a role in the balancing of defence responses (Wang et al., 2011b; Bhardwaj et al., 2011). *A. thaliana* has been shown to exhibit clock gene dependent temporal variation in its susceptibility to *Pseudomonas syringae pv. tomato (Pst)* DC3000 (Bhardwaj et al., 2011). Furthermore, a number of studies have uncovered genes postulated to be specific points of feedback between plant defence and the clock, beginning to build up a picture of the interconnecting framework of these two systems (Shi et al., 2016; Zhou et al., 2015; Zheng et al., 2015; Xu et al., 2017; Ingle et al., 2015; Zhang et al., 2013).

Although the picture is certainly only just coming into focus, this ever increasing amount of evidence has led to the suggestion that in the ongoing arms-race between pathogens and their plant hosts, it might benefit a pathogen to try and manipulate the output of the circadian clock (Lu et al., 2017; Zhang et al., 2013). It has also been suggested that some plant pathogens have their own circadian clock that influences the course of infection, though this school of thought has not largely been addressed so far (Hevia et al., 2015; Lu et al., 2017). By making use of microbial-associated molecular patterns (MAMPs) such as flagellin, or secreted effector proteins, pathogens might

subvert the host circadian oscillator in order to dysregulate downstream mechanisms of defence. Indeed it has been seen that treating wild-type *A. thaliana* with flg22 is sufficient to shorten period length in the rhythmic expression of the *CCA1* promoter (Zhang et al., 2013). The *Pst* type III secreted effector (T3SE) HopU1 is known to bind to the GRP7 protein, a regulator of stomatal aperture whose expression is regulated by the clock (Kim et al., 2008; Fu et al., 2007; Green et al., 2002). While Nicaise et al. (2013), attribute the virulent function of HopU1 to its blocking the interaction of GRP7 with the transcripts of key pattern recognition receptors (PRRs) FLS2 and EFR, it has also been suggested that it binds GRP7 in order to facilitate pathogen access to the inner leaf tissue during the light phase (Lu et al., 2017). This theory is supported by the fact that the *grp7-1* mutant has significantly enhanced susceptibility to virulent *P. syringae pv. maculicola DG3* (*PmaDG3*) when compared to wild-type plants, but only if infected at dusk when stomata would typically be closed (Zhang et al., 2013). It seems likely that through its interaction with GRP7 HopU1 has dual virulent function quelling MAMP-triggered immunity (MTI) as well as interfering with clock-mediated outputs.

Despite the substantiation that at least one effector manipulates clock-gated pathways as a way to enhance host susceptibility, there has been a distinct lack of new studies investigating the impact of T3SE's on rhythms in plants. Many studies of plant immunity make use of *P. syringae* strains carrying mutations in the type III secretion system (T3SS) machinery (and thus cannot deliver effectors into the host) to demonstrate the value of the secreted effector repertoire to pathogenic virulence, such as the use of the *Pst hrcC* mutant in elucidating the role of effectors on actin remodelling, callose deposition and bacterial growth during infection (Shimono et al., 2016; Hauck et al., 2003). Others have used such mutants as negative controls for elicitation of the hypersensitive response (HR) when investigating the role of clock genes in basal immunity (Zhang et al., 2019). The use of these mutants in order to ascertain the role of T3SEs in the disruption of circadian rhythmicity however has not yet been described, and with only one effector being even incidentally linked to circadian dysfunction, there is great scope to uncover further effectors targeting the clock.

The experimental aims of this chapter were therefore as follows:

i) To test whether the priming of effector-responsive pathways contributes to the *Arabidopsis* rhythm in susceptibility to *Pst* (section 3.2.1).

ii) To investigate whether virulent wild-type *Pst* can induce changes in core clock gene expression rhythms, and the dependence of such changes on the secretion of T3SEs (section 3.2.2).

iii) To test whether individual T3SEs within the *Pst* repertoire are able to induce changes in core clock gene expression rhythms (section 3.2.3).

3.2 Results

3.2.1 Temporal variation in the susceptibility of A. thaliana to P. syringae, and its relationship with type III secreted effectors (TTSEs)

The temporal variation in the susceptibility of *A thaliana* to being challenged by the wild-type pathogen *Pst* DC3000 has previously been identified by Bhardwaj et al. (2011). While this variation cannot strictly be described as rhythmic, or oscillatory in nature without further statistical analysis, it has nonetheless been shown to persist under constant light conditions and be dependent on the expression of core clock genes, as it is lost in the *CCA1*-overexpressor, and *elf3-1* mutant line. Furthermore, the times at which they found susceptibility to be highest coincided with the times at which the T3SS mutant *Pst hrpA* elicited reduced callose deposition [a MAMP-triggered response known to limit microbial spread (Luna et al., 2011)]. This led the authors to surmise that the varying susceptibility was brought on by the priming of MTI responses by the circadian clock.

While the evidence that the circadian priming of MTI contributes to temporal variation in susceptibility is convincing, it cannot be ruled out from this study alone that the variation is also caused in part by the contribution of effector-responsive pathways. We therefore first ascertained the extent to which the efficacy of effector-responsive mechanisms of host defence was impacted by the time of infection. For this, a direct

comparison of the bacterial titres of both *Pst* DC3000 and a T3SS mutant within a time series was needed.

Adult wild-type *A. thaliana* plants of the ecotype Columbia (Col-0) were infected with either *Pst* DC3000, or the *hrcC* mutant (which, like *hrpA* carries a mutation in the *hrp-hrc* gene cluster that encodes the T3SS and thus cannot secrete effectors) at 13 time points over 2 days. Plants were raised in a 12:12 LD photoperiod until 4 weeks of age, then moved into constant light (LL), starting at dawn, or circadian time 0 (CT0). Infiltrations were performed starting at CT24, or subjective dawn, 24 hours after being moved into LL, and thereafter at regular intervals for a period of 48 hours, or until CT71. Two days after infiltration samples were taken from infiltrated leaf tissue, and bacterial titres were calculated as described in section 2.3. Comparisons between the effects of infiltration time and pathogen genotype on bacterial growth were compared using a two-way Analysis of Variance (ANOVA). Multiple comparisons were made using Tukey's post-hoc test.

As has previously been described by Bhardwaj et al. (2011), a significant variation in the susceptibility of *A. thaliana* to DC3000 with respect to time of infection was evident (Figure 3.1, A). On the first day of infiltrations, the highest titres were recorded at CT24 and CT39 (at and approaching subjective midnight, respectively), in agreement with the previous study. It was found however that on the second day of infiltrations susceptibility to DC3000 was consistently high, with plants at all timepoints except CT59 harbouring significantly more colony forming units (CFU) than those infiltrated at any time on the first day. Similarly, while the temporal variation detected could not be described as rhythmic, multiple comparisons analysis of the highest and lowest bacterial titres for DC3000-infiltrated plants found a significant difference between what could be called the "peak" and "trough" values on day 1 (CT24 and CT47 respectively, $p<0.05$), but not on day 2 (CT63 and CT59 respectively). Analysis of data points on each day of infiltrations separately (i.e. day 1 CT24-CT47, day 2 CT51-71) found that the significant temporal variation in susceptibility to DC3000 was lost on the second day of infiltrations, with no significant difference between those time points. It is worth noting that the damping of this temporal regulation of susceptibility by the clock may occur at a decreased rate in plants grown in long (16:8 LD) rather than standard (12:12 LD) days, accounting for

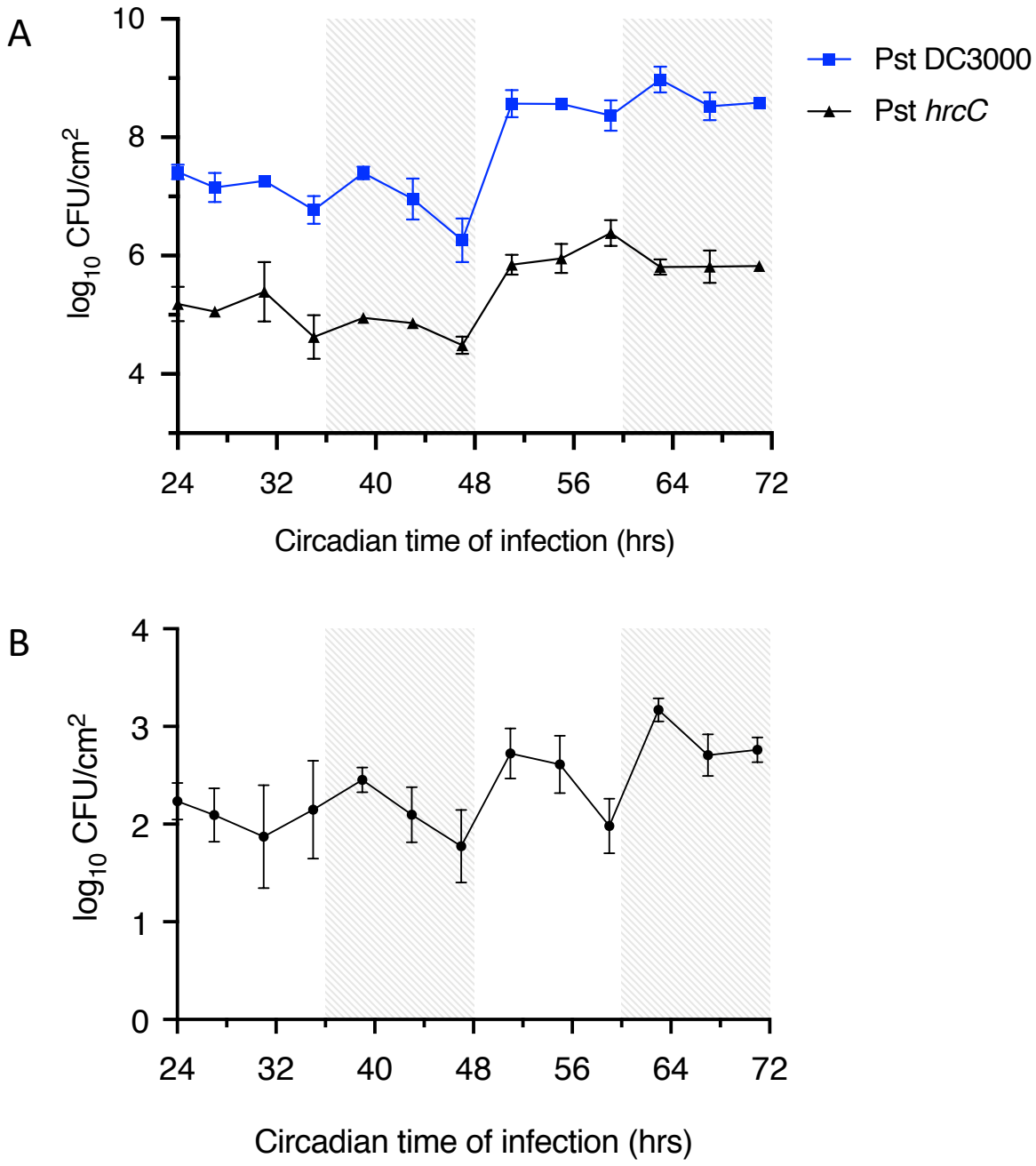

Figure 3.1: *Arabidopsis thaliana* exhibits temporal variation in its susceptibility to infection by both virulent and avirulent *P. syringae pv. tomato*. A) 4-week-old wild-type Columbia (Col-0) *Arabidopsis* plants were grown at 22°C in 12:12 LD conditions, then moved to LL for 24 hours. Leaves were pressure infiltrated at the times indicated with *Pst* DC3000 (blue squares) or *hrcC* (black triangles) at OD_{600} 0.001. Bacterial counts were recorded (CFU/cm^2 ± SEM, n = 4) in leaves at 48 hours post infection (hpi). Two-way Analysis of Variance (ANOVA) revealed a significant effect of time of infection on bacterial growth, as well as on pathogen genotype ($p<0.0001$), but not on the interaction between time of infection and genotype. B) Difference in bacterial titre between *Pst* DC3000 and *hrcC* infected wild-type Columbia (Col-0) *Arabidopsis* at different times of day (± SEM, n = 4). Two-way Analysis of Variance (ANOVA) revealed a marginally significant effect of time of infection on the difference in bacterial growth between genotypes ($p = 0.0469$). Grey shaded areas indicate subjective night.

the discrepancy in bacterial growth seen on the second day of infiltrations between the results here and in the preceding investigation. These data suggest that while *A. thaliana* susceptibility to *Pst* DC3000 does vary with respect to time of infection when grown under standard 12:12 LD conditions, and are consistent with a role for the circadian clock priming innate defence mechanisms, the regulation of these processes by the clock is not strong enough to persist under constant conditions for over 48 hours.

The mutant *hrcC* had significantly reduced bacterial growth in comparison to DC3000 at all time points, in agreement with its established characterisation as an avirulent bacterial strain (Figure 3.1, A). While this vast difference in virulence makes comparison of bacterial growth between the two genotypes easiest to see on a logarithmic scale, the results were additionally plotted on a linear scale to facilitate the evaluation of rhythmicity in susceptibility (Supplementary Figure S3.1). These linear representations of bacterial growth were further split between the first and second day on account of the disparity between the bacterial titres on day 1 and 2, particularly for DC3000-infiltrated plants (Supplementary Figure S3.2). As with DC3000, the *hrcC* mutant demonstrated greatest potential for bacterial growth when infiltrated on the second day, and susceptibility to *hrcC* was only significantly dependent on time of infection on the first day. The plotted bacterial counts reveal a discernible pattern mirroring the temporal susceptibility of both bacterial strains, although no significant peaks in susceptibility were determined for *hrcC* treated plants between CT24 and CT47. Multiple comparisons testing of the highest and lowest bacterial titres as an approximation of peak to trough ratio also found no significant difference between peak and trough on day 1 (CT31 and CT47 respectively) or on day 2 (CT59 and CT63 respectively) for the *hrcC* mutant.

In order to further scrutinise the contribution of effector mediated pathways, the difference in CFU counts between DC3000 and *hrcC* throughout the time series was also plotted and subject to ANOVA and post-hoc testing (Figure 3.1, B). When looking at the contribution of effector mediated pathways to susceptibility in this slightly more conservative way it is interesting to note that although the spread of data amongst the raw CFU values masks it to the point of insignificance (Figure 3.1, A), there is a marginally significant ($p = 0.0469$) effect of T3SEs on the outcome of the plant-pathogen interface according to the time of infection, with an apparent rhythm in the

advantage conferred by effector secretion. While it is plausible that the efficacy of T3SEs themselves may vary throughout the day due to rhythmic expression of resistance (*R*) genes, these data on the whole suggest that the advantage conferred to the extent of DC3000 growth by the T3SS does not significantly vary with infection time. Note; It is also not likely that perceived temporal variation in the contribution of T3SEs could be caused by any hypothetical clock mechanism in the pathogen, given that from initial growth to infiltration *in planta,* bacterial cultures were kept under constant conditions.

Taken together, these results demonstrate that *A. thaliana* exhibits temporal variability in its susceptibility to both the virulent pathogen *Pst* DC3000 and the avirulent pathogen *hrcC*. The lack of a significant interaction between time of infection and bacterial strain indicates that the plant circadian clock regulates basal immunity in a way that is independent of pathways that respond to secreted effectors.

3.2.2 P. syringae uses a repertoire of T3SEs during in planta infection to induce changes in the amplitude of core clock genes' expression rhythms

Before looking at the roles of individual T3SEs, our foremost interest was to investigate whether *P. syringae pv. tomato*'s ability to secrete a full repertoire of effectors into host *A. thaliana* cells would allow it to induce changes in the expression of genes at the core of the circadian clock. After all, the impact of one solo effector on circadian rhythmicity would be of no true biological relevance if it was masked by the effects of another pathway when secreted alongside all other *Pst* effectors, as would be the case during a typical infection. To do this, we used the virulent and avirulent *Pst* strains DC3000 and *hrcC* respectively. The latter of these, as has previously been described in section 3.2.1 is unable to secrete effectors using the T3SS, while the former can, and uses effectors to suppress immune responses by the host, generating effector triggered susceptibility (ETS). In this manner the *hrcC* mutant acts as a control for pathways dependent on secretion of type III effectors.

We chose to look at rhythms in the expression of two genes at the core of the plant transcriptional-translational feedback loop (TTFL) network responsible for driving circadian rhythmicity; *CIRCADIAN CLOCK-ASSOCIATED 1* (*CCA1*) is a morning phased gene that peaks at dawn (ZT0), while the expression of *TIMING OF CAB EXPRESSION 1* (*TOC1*) peaks in the evening at dusk (ZT12) (Hsu and Harmer, 2014). It was our hope that by using two clock genes with opposing phases it would be possible to see any changes to host rhythmicity in a way that would be less limited by whichever arm(s) of the TTFL might first be visibly affected.

In a study by Li et al. (2018) it was shown that when *CCA1* expression is visualised using a *CCA1::luc+* system (whereby the luciferase reporter gene is under the control of the CCA1 promoter), leaves submerged in a high level of *Pst* DC3000 inoculum (OD_{600} 0.2) and kept in constant light (LL) become arrhythmic after 24 hours while mock treated leaves maintain visible circadian rhythmicity for the full five days assayed. The involvement of effectors in this induced arrhythmicity however has not yet been explored and represents a current gap in the field.

In order to investigate the role of a complete effector repertoire in altering rhythms in core TTFL gene expression, adult *A. thaliana* plants of the luciferase fusion genotypes *CCA1::LUC* and *TOC1::LUC* were grown in 12:12 LD conditions, and sprayed with 5mM luciferin 24 hours prior to infection. The following day plants were moved into constant darkness at dawn (CT0) and rosette leaves 7, 8 and 9 were pressure infiltrated with either mock infiltration media or a bacterial suspension of *Pst* DC3000 or *hrcC* five hours before dusk (CT7) under a green safety light. Varying optical densities of inoculum were used in this study and are detailed in the respective figures. Images of the plants were taken every 10 minutes until CT72, and mean pixel intensity of the infected leaves was quantified from the resultant pseudo-coloured images such that pixel colour/intensity corresponded to expression level of the circadian constructs (Figure 3.2, C-E). The traces for mean bioluminescence over time were also fit by a non-damping sine wave using prism over the course of the first two expression peaks for each reporter line in order to speculate on changes to the overall expression rhythm's waveform. The only constraint for this curve fitting was that the wavelength, or period, must be greater than or equal to 18 hours. This was to minimise the fitting

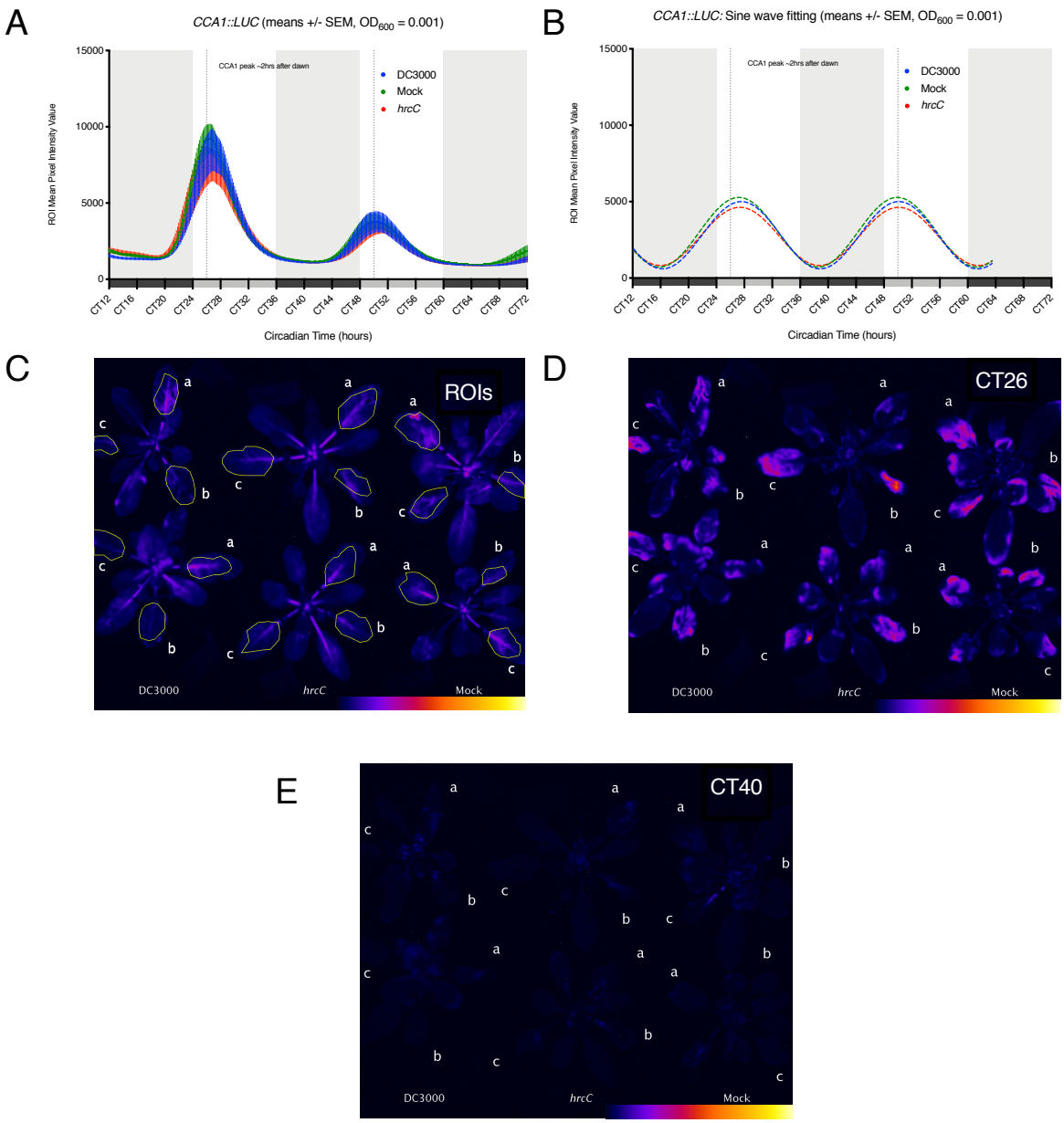

Figure 3.2: Bioluminescence time course of *CCA1:LUC A. thaliana* following infection with *Pst* DC3000 or *hrcC* (OD600 0.001), or mock infiltration media. *CCA1:LUC* plants grown in 12:12LD were sprayed with 5mM luciferin 24 hours before imaging. On the day of imaging plants were kept in constant darkness (DD) starting from subjective dawn (CT0). Plants were infiltrated with an OD_{600} 0.001 suspension of either *Pst* DC3000 (blue) or *hrcC* (red), or mock infiltration media (green). Images were taken every 10 minutes. A) Mean *CCA1::LUC* expression (± SEM, n = 6). Dark grey regions denote subjective night. Dotted vertical lines denote reporter gene expression peaks. B) Curves (dashed lines) were fitted to the first two expression peaks for each mean data set (constraint of period ≥18 hrs). Note: fit curves do not account for damping rhythmicity. C) Images of plants were pseudocoloured and regions of interest (ROIs) were used to determine mean pixel intensity within infiltrated leaves (labelled a, b and c, yellow outlines). D-E) Pseudocoloured image slices from CT26 and CT40 reflect the *in planta* changes in *CCA1::LUC* expression (as indicated by bioluminescence detection) at peak and trough expression times respectively.

of nonsense waves that did not represent an appropriate fit for the data by visual inspection.

We first looked at the morning phased *CCA1* with an inoculum of OD_{600} 0.001, which corresponds to ~5 x 10^5 cfu ml^{-1}. This value is just above the threshold of epiphytic *P. syringae* populations suggested to be sufficient to induce disease symptoms in field grown bean plants (Lindemann, 1984), and so here represents a minimal concentration of bacteria able to successfully infect a host plant. It was found that in the case of *CCA1* expression, rhythmicity was maintained in plants having undergone all three treatment types (Figure 3.2), each satisfying the fit of a curve with a wavelength of approximately 23.25 hours with minimum constraints (only that requiring wavelength to be over 18 hours, to reduce the chance of "nonsense" fits). There was a significant effect of bacterial strain on this rhythm, with *hrcC* eliciting a small decrease in amplitude (about 23%) relative to the mock-treated plants only between CT25 and CT27, indicating that at low inoculum, while the induction of MAMP-triggered immunity (MTI) may cause a small amplitude decrease in *CCA1* expression after dawn, this is brief, and buffered by the secretion of effectors in DC3000.

When infiltrating plants using a moderately high inoculum of OD_{600} 0.1 (5 x 10^7 cfu ml^{-1}), the changes brought on by bacterial presence are more distinct. Again, all three treatments remain rhythmic, with peaks in *CCA1* expression two hours after dawn (CT26) and wavelength of ~24 hours, with a significant effect of genotype on expression of the reporter construct (Figure 3.3, B). Here however, DC3000 significantly reduced amplitude relative to the mock between CT21 and CT29 (or over the course of the first peak in *CCA1* expression), amounting to around a 155% decrease in expression at CT26 (Figure 3.3, A). Between CT44 and CT56 (or the second *CCA1* peak), DC3000 treated plants had significantly lower amplitude than both the mock and *hrcC*. From CT47-59 *hrcC* elicits about significant decrease in amplitude relative to the mock control (about 63%), however at no other time are the two significantly different. It is notable however that the *hrcC* traces here showed a larger degree of variability amongst themselves, making identifying possible outliers and attribution of significant effects more challenging. By CT57, there was no significant difference in amplitude between treatment types, and for all three the *CCA1* rhythm appeared largely to have diminished. These data suggest that with moderate strength inoculum,

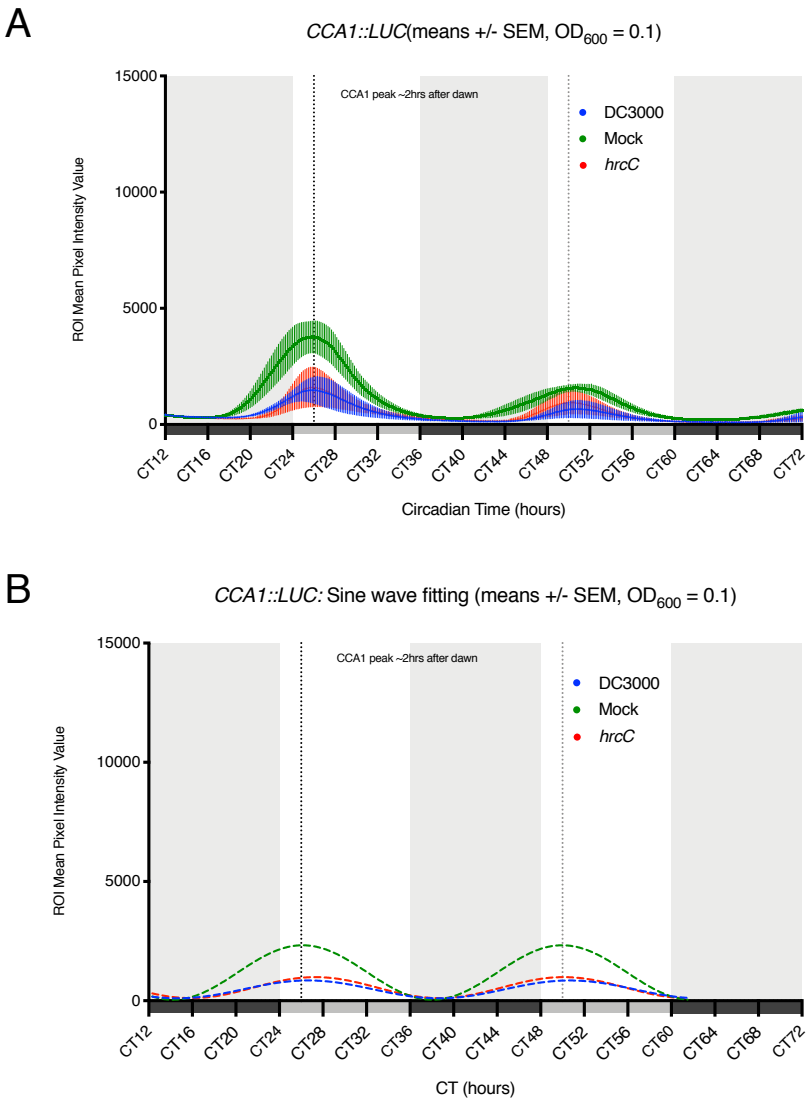

Figure 3.3: Bioluminescence time course of *CCA1:LUC A. thaliana* following infection with *Pst* DC3000 or *hrcC* (OD600 0.1), or mock infiltration media. *CCA1:LUC* plants grown in 12:12LD were sprayed with 5mM luciferin 24 hours before imaging. On the day of imaging plants were kept in constant darkness (DD) starting from subjective dawn (CT0). Plants were infiltrated with an OD_{600} 0.1 suspension of either *Pst* DC3000 (blue) or *hrcC* (red), or mock infiltration media (green). Images were taken every 10 minutes. A) Mean *CCA1::LUC* expression (± SEM, n = 6). Dark grey regions denote subjective night. Dotted vertical lines denote reporter gene expression peaks. B) Curves (dashed lines) were fitted to the first two expression peaks for each mean data set (constraint of period ≥18 hrs). Note: fit curves do not account for damping rhythmicity.

the secretion of effectors triggers a significant reduction in the amplitude of *CCA1* expression that is most distinct 2 hours after dawn when expression peaks, and that by the third day of constant darkness rhythmicity is mostly lost regardless of treatment type.

We next looked at effector-induced changes to the expression profile of evening phased *TOC1*. For all inoculum concentrations used the *TOC1* gene peaked at around CT16, or 4 hours after dusk (Figure 3.4). It is worth noting that although the genes *CCA1* and *TOC1* are referred to throughout the literature as morning and evening phased genes that peak at CT0/24 and CT12 respectively (Hsu and Harmer, 2014), there exist slight shifts in the expression peaks presented here. These likely differ from previous studies on the basis of variations in light intensity, photoperiod length, and ecotype, all of which have been linked to circadian phase shift (Ohara et al., 2015; Perales and Más, 2007; Kubota et al., 2015). This is also supported by the wide array of phases for *CCA1* and *TOC1* across different experimental datasets that are available on the genome-wide time-series expression data mining resource DIURNAL (Mockler et al., 2007). Any changes to the phase of the rhythm induced by treatment type in this study should therefore be identified by difference in peak expression relative to the mock-treated plants. Strikingly, even at minimal inoculum levels (OD_{600} 0.001), both DC3000 and *hrcC* infiltration elicited significant effects on *TOC1* rhythmicity. Treatment of plants with *hrcC* caused a significant increase in *TOC1* amplitude between CT12 and CT21 (or over the course of the first *TOC1* peak) in comparison to the mock (Figure 3.4, A-B). The *hrcC* plant's peak in TOC1 levels was roughly 14% greater than that of DC3000 at its peak, and 15% greater than the mock. During the second peak (CT33-CT44) *TOC1* amplitude in response to *hrcC* was significantly increased relative to both other treatments. DC3000 induced very few significant changes compared to the control at any time at this concentration (only one time point at approximately CT15), although visual inspection of mean pixel intensity traces suggest that it may have slightly increased amplitude on the first day of infection and slightly advanced the onset of arrhythmicity (Figure 3.4, A). At minimal inoculum it would appear as though in the absence of effectors to suppress MTI responses by the host, pathogen perception leads to an increase in TOC1 levels. When these effectors are secreted however, the boost in expression is circumvented.

Increasing the optical density of bacterial suspensions to moderately high levels (OD_{600} 0.1) exacerbated the changes brought on at lower bacterial concentrations. Again, *hrcC* has greatly increased amplitude compared to both mock and DC3000

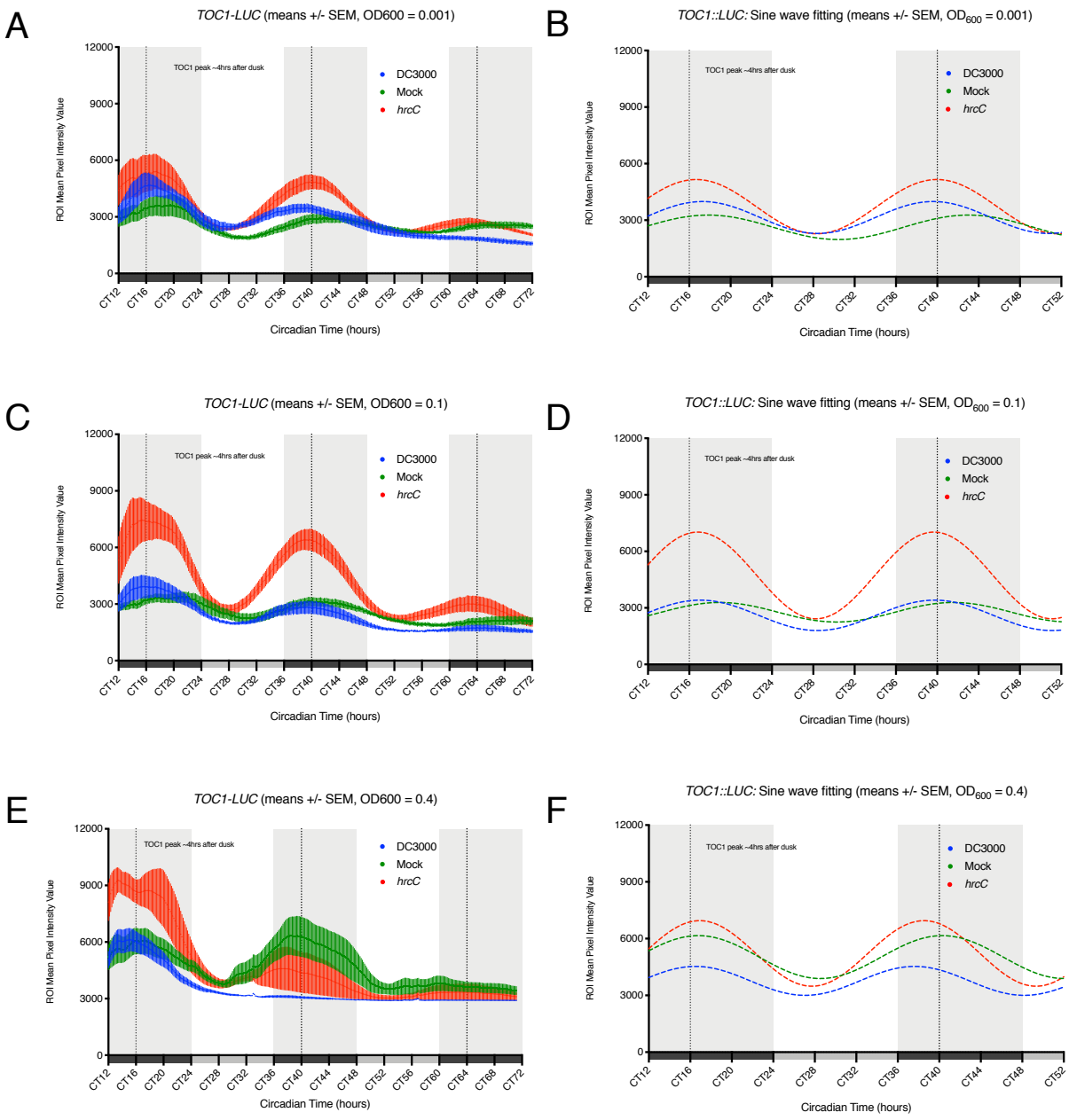

Figure 3.4: Bioluminescence time course of *TOC1:LUC A. thaliana* following infection with *Pst* DC3000 or *hrcC*, or mock infiltration media *TOC1:LUC* plants grown in 12:12LD were sprayed with 5mM luciferin 24 hours before imaging. On the day of imaging plants were kept in constant darkness (DD) starting from subjective dawn (CT0). Plants were infiltrated with either *Pst* DC3000 (blue), *hrcC* (red), or mock infiltration media (green). OD_{600} of bacterial suspensions were 0.001 (A-B), 0.1 (C-D), and 0.4 (E-F). Images were taken every 10 minutes. Dark grey regions denote subjective night. Dotted vertical lines denote approximate reporter gene expression peaks. A, C and E) Mean *TOC1::LUC* expression (± SEM, n ≥ 3). B, D and F) Curves were fitted to the first two expression peaks for each mean data set (constraint of period ≥18 hrs). Results are representative of two repeat experiments. Note: curves do not account for damping rhythmicity.

during the first rise in *TOC1* expression (CT13-CT26), with mean pixel intensity at the peak being roughly 129% and 89% greater than those of mock and DC3000 treated plants respectively (Figure 3.4, C). The same is seen on the second day of constant darkness between CT35 and CT49, where the *hrcC* induced peak is about 105% greater than that of the mock, and 127% greater than with DC3000. For plants treated with the avirulent strain, this boost to the *TOC1* amplitude appears to confer extended robustness in the rhythm overall, with a distinct peak on the third day of constant darkness (~CT64), while rhythmicity in DC3000 and mock infiltrated plants is mostly diminished by this time. These results indicate that the increase in *TOC1* amplitude brought on in response to pathogen perception may be dose-dependent, becoming more extreme at higher bacterial concentrations, and that the secretion of T3SEs is still able to counter this effect at high OD.

As has previously been mentioned, in Li et al. (2018) it was found that a high level of inoculum was sufficient for DC3000 to induce total arrhythmicity in *A. thaliana* seedlings as early as 24 hours after infection in three different circadian reporter constructs. In light of the findings presented here, this would suggest that effectors not only work to rebuff the changes to clock gene expression rhythms brought on by MTI, but may actively bring about an opposing influence, negating the rhythmic expression of clock genes entirely. In order to test the agreement of this past work with the present study therefore, we next examined changes to the *TOC1* rhythm with the use of a very rich inoculum (OD_{600} = 0.4, or 2 x 10^8 cfu ml^{-1}). Once more, *hrcC* drastically increased expression levels during the first *TOC1* peak, producing an approximately 56% increase in mean pixel intensity compared to both other treatments, although after CT22 the *hrcC* treated plants decrease in amplitude to the point of no longer being significantly different from the mock for the remainder of the time course (Figure 3.4, E). By CT34 DC3000 causes a sufficient reduction in amplitude to be significantly different to the mock, by which time expression values appear to flatline, with absolutely no visible trace of remaining rhythmicity, in perfect agreement with Li et al. (2018). Note that the sine curve fits in Figures 3.3, 3.3 and 3.4 take into account from ~CT12-CT48 to inform the approximate wavelength and phase of any detectable rhythmicity, however visual inspection of the mean pixel intensity traces in Figure 3.4, panel E reveals that no rhythmicity remains after CT34 and that the fitted curve is skewed by the values of the first day.

These data collectively support the findings of Li et al. (2018), which report the ability for the virulent *Pst* strain DC3000 to eliminate the rhythmic expression of core clock genes within 24 hours of infection when the host plant is infected at high concentration and kept under constant conditions. Further to this, we find here that this influence may be dose-dependent, with lower bacterial concentration eliciting more subtle effects. A moderate concentration of DC3000 produces a decrease in *CCA1* but not *TOC1* rhythmic amplitude within the first 24 hours, and for both genes arrhythmicity is induced between 48- and 72-hours post infection (hpi). Minimal concentrations of DC3000 elicited no significant change in either *CCA1* or *TOC1* expression levels. Avirulent *Pst* for the most part exhibits a contrasting influence on the clock in a way that is also highly dependent on the concentration of bacterial suspension. Infiltration of *hrcC* at an OD_{600} of over 0.1 provokes a massive increase in the amplitude of the *TOC1* translation rhythm (although at an optical density of 0.4 this is not sustainable and diminishes to that of the mock-treated control). At an OD_{600} of 0.001 *hrcC* also caused a significant increase in TOC1 amplitude, albeit a far smaller change than those of richer inoculums. Only a small decrease in CCA1 amplitude was recorded for both *hrcC* bacterial concentrations.

The results jointly suggest that the perception of MAMPs by the host during infection by *P. syringae* stimulates significant changes in the amplitude of core clock gene expression rhythms, drastically increasing *TOC1* amplitude, and slightly reducing that of *CCA1*. The secretion of T3SEs is able to largely buffer these effects however, aiding the significant disruption of circadian rhythmicity in a way that is dose dependent. The effectors prevent an increase in the expression of core clock genes and actively decrease their expression relative to uninfected plants when the concentration of colony forming units exceeds 5×10^5 ml^{-1}.

3.2.3 Screening individual T3SEs in the P. syringae DC3000 repertoire for their ability to alter circadian rhythmicity in protoplasts

In section 3.2.2 it was shown that the delivery of type III secreted effectors (T3SEs) with a functional secretion system, such as with the virulent pathogen *Pst* DC3000, has a significant influence on the circadian phenotype of the host plant *A. thaliana* during infection. The known virulent functions, intracellular localisation and targets of T3SEs however vary greatly (Block and Alfano, 2011), and so it would be highly unlikely that the clock-disrupting function seen following infiltration of plants with *Pst* DC3000 was due to the equal action of all effectors injected by the pathogen. In order to identify clock-disrupting effectors, we co-transfected protoplasts with a transcriptional fusion reporter construct for one of two circadian gene promoter regions (either *proCCA1:LUC* or *proGI:LUC*) along with a construct containing one of a library of 23 *Pst* T3SEs (HopO1-1, HopM1, HopN1, HopAD1, HopY1, HopT1-1, HopAB2, HopX1, HopP1, HopC1, HopF2, HopAF1, HopA1, HopB1, HopH1, HopG1, HopAO1, HopAI-1, HopK1, AvrPto, HopQ1-1, HopV1 and HopD1). These protoplasts were then kept in constant light for a minimum of 5 days, while being imaged for changes in detected luciferase activity that would correspond to expression of the clock reporters (Figure 3.5).

This screen of circadian phenotypes was performed a total of three times. The purpose of the first of these screens was to assess the clock-modulating capability of all 23 *Pst* effectors, by using the *proCCA1:LUC* expression rhythm as an output for host circadian function. The second screen was then performed (identical to the first in design) in order to test the repeatability of the results found in the first screen. While all effectors were assayed in screens 1 and 2, only effectors that presented with particularly (and reproducibly) distorted rhythms were carried forward into the third and final screen, in which impact of effector transformation was compared between two different clock gene reporters, *proCCA1:LUC* and *proGI:LUC*. The purpose of introducing a second circadian reporter to the assay was to test whether the changes induced by the transformed effectors were specific to the expression of the *CCA1* promoter or affected the clock in general. Within the translational fusion constructs

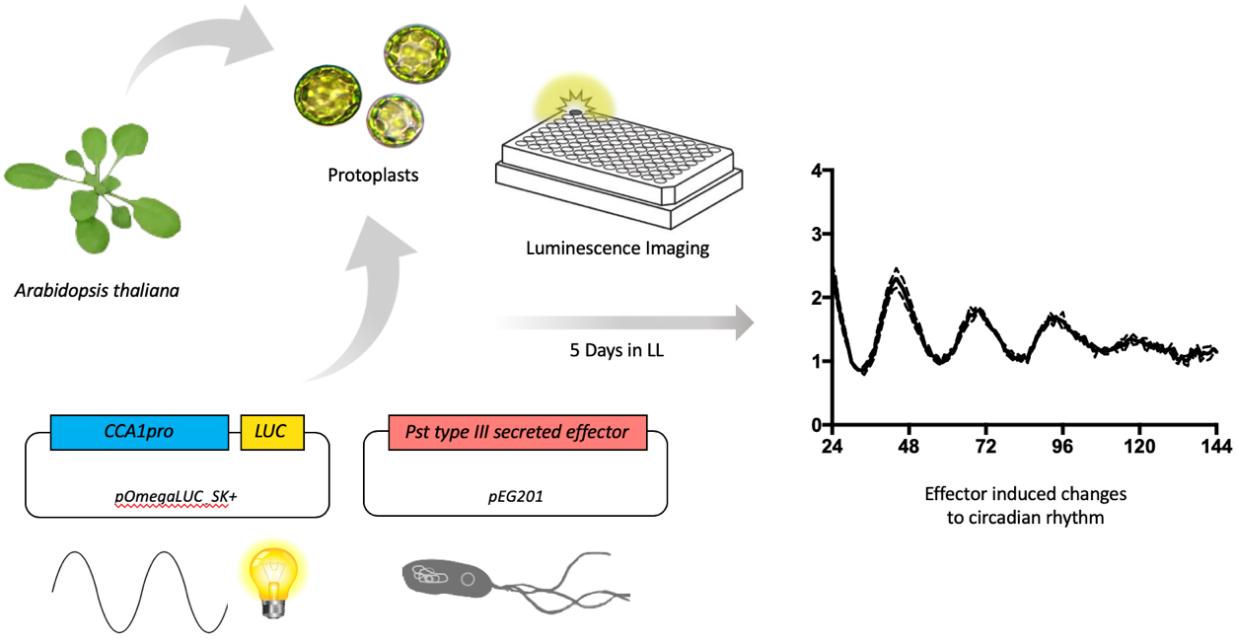

Figure 3.5: Schematic representing the workflow of the clock-modulating effector screen (for full details, see section 2.5). Mesophyll protoplasts were harvested from the lower epidermal leaf tissue of 4-week-old *A. thaliana* plants using magic tape and resuspended to a concentration of 7 x 10^5 protoplasts/ml in MMg solution. Cells were then transfected with both a transcriptional fusion circadian reporter (*proCCA1:LUC* or *proGI:LUC* within the pOmegaLUC_SK+ vector) and one of a collection of 23 *Pst* DC3000 effectors (in the pEG201 vector). Cells transformed with a reporter along with the empty pEG201 plasmid were used as a negative control. Cells were suspended in W5 imaging solution in a 96-well plate, and luminescence was measured over a period of 5 days in constant light. The resulting traces were analysed using Biological Rhythms Analysis Software System (BRASS), and rhythmicity was compared between effector transfected protoplasts and the empty vector control.

used in this study the promoter for the gene *GIGANTEA* (*GI*) is expressed in the evening at about ZT7 as opposed to the dawn (ZT0) phased *CCA1* promoter making them a good pair for testing the effectors in this way (Kim and Somers, 2010). The traces and analyses for the pilot screens 1 and 2 examining the full list of effectors are not shown, however a summary of results from all three screens are shown in Table 3.1, with details of notable changes to period length and amplitude for all tested reporter constructs and effectors. In some instances, the variability in luminescence readings was not sufficiently rhythmic to be fit by a wave in any suitably meaningful way, and so the quantification of period and amplitude estimates was not possible. In these cases, the raw luminescence traces themselves were examined, and where clear changes in expression when compared to the empty vector control were apparent, they have been described qualitatively.

Pst T3SE	Screen 1		Screen 2		Screen 3			
	CCA1pro:LUC		*CCA1pro:LUC*		*CCA1pro:LUC*		*Glpro:LUC*	
	Period	Amplitude	Period	Amplitude	Period	Amplitude	Period	Amplitude
HopO1-1	ns	No real change	ns	ns	-	-	-	-
HopM1	ns	No real change	ns	**Very low, Erratic**	-	-	-	-
HopN1	ns	No real change	ns	ns	-	-	-	-
*HopAD*1	ns	No real change	ns	**Very low, Erratic**	No real change	**Slightly low**	**Long (~ +0.5hr) ******	**Low ******
HopY1	ns	No real change	ns	ns	-	-	-	-
HopT1-1	**Long (~ +1 hr) ****	No real change	ns	ns	-	-	-	-
HopAB2	**Arrhythmic**	**Very low, Erratic**	ns	**Very low, Erratic**	**Arrhythmic**	**Very low**	**Arrhythmic**	**Very low ******
HopX1	**Arrhythmic**	**Very low, Erratic**	ns	**Very low, Erratic**	**Arrhythmic**	**Very low**	**Arrhythmic**	**Very low ******
HopP1	ns	No real change	ns	ns	-	-	-	-
HopC1	**Short (~ -0.5 hr) *****	No real change	ns	ns	No real change	No real change	No real change	**Low ******
HopF2	ns	No real change	**Long (~ +2 hrs) ***	ns	**Long (~ +1.5 hrs) ******	No real change	**Long (~ +0.5hr) ****	**Very Low ******
HopAF1	**Short (~ -0.5 hr) ******	**Erratic**	ns	ns	-	-	-	-
HopA1	ns	No real change	ns	ns	-	-	-	-
HopB1	ns	No real change	ns	ns	-	-	-	-
HopH1	ns	No real change	ns	ns	-	-	-	-
HopG1	ns	No real change	ns	ns	-	-	-	-
HopAO1	**Short (~ -0.5 hr) *****	**Low**	ns	**Low**	**Arrhythmic**	**Low**	**Arrhythmic**	**Low ******
HopAI-1	ns	No real change	ns	ns	-	-	-	-
HopK1	**Long (~ +1.5 hr) ******	No real change	ns	**Low**	**Short(~ -1hr)******	**Low**	**No real change**	**Low ******
AvrPto	ns	No real change	ns	ns	-	-	-	-
HopQ1-1	ns	No real change	ns	ns	-	-	-	-
HopV1	**Long (~ +1.5 hr) ******	No real change	ns	ns	-	-	-	-
HopD1	ns	No real change	ns	ns	-	-	-	-

Table 3.1: *P. syringae pv. tomato* DC3000 type III effectors can alter the rhythmicity of circadian clock genes in *A. thaliana*. In three independent screens where protoplasts were transfected with a *Pst* effector and either the *CCA1pro:LUC* or *Glpro:LUC* luciferase-fused circadian reporter construct, changes to clock gene expression were observed. For each screen, period and amplitude analyses were performed in Prism. Significant differences in comparison to the empty vector transfected control were determined by one-way ANOVA with Tukey's multiple comparisons test, where ≥0.05 was non-significant (ns), <0.01 (**) and <0.0001(****). In instances where meaningful rhythmic analyses were not possible (i.e. induced arrhythmicity or nonsensical analyses), changes to amplitude were inferred through visual examination of the raw luciferase detection traces and are described in the table qualitatively (i.e. Low, No Real Change). 3-6 wells were imaged for each sample. Only effectors that were suspected of causing legitimate clock defects (HopAD1, HopAB2, HopX1, HopC1, HopF2, HopAO1, and HopK1) on the basis of results from screens 1 and 2 were carried forward for analysis in Screen 3.

Of the 23 effectors examined in the first two screens, 12 were found to have no discernible impact on the expression rhythm of *proCCA1* (HopO1-1, HopN1, HopY1, HopP1, HopA1, HopB1, HopH1, HopG1, HopAI-1, AvrPto, HopQ1-1 and HopD1) (Table 3.1), and as such were not tested in the third screen. From the 11 that did impact the *proCCA1* rhythm in some way, an additional 4 were chosen not to be subjected to further analysis. These were HopM1, HopT1-1, HopAF1 and HopV1, and were eliminated from the third screen largely on the basis that the phenotype they elicited was either insignificant (HopM1) or inconsistent between the two screens (HopT1-1, HopAF1 and HopV1). HopT1-1 was excluded despite having a significantly lengthened period in screen 1 due to it having a borderline significant shortening of period in screen 2, i.e. being particularly inconsistent. Two effectors were chosen for the third screen partially regardless of these criteria, as a point of interest. HopAD1 was chosen, despite its effect not being consistent having presented a particularly severely impaired rhythm in the second screen, along with HopC1, which exhibited a minor but significant shortening of period in screen 1, and a short period that was insignificant by only a very small margin in the second screen. The third and final screen was therefore performed using the effectors HopAD1, HopAB2, HopX1, HopC1, HopF2, HopAO1, and HopK1.

HopAD1 had a significantly longer period length than the empty vector control, along with significantly lower amplitude for expression of *proGI:LUC* (Figure 3.7, A, H and I), however its *proCCA1:LUC* (Figure 3.6, A and H) period seemed largely unaffected, and amplitude only slightly diminished.

Both HopAB2 and HopX1 induced an extreme clock phenotype, with near complete arrhythmicity for all screens and reporter constructs as early as the first day of imaging and displayed the lowest recorded signal amplitudes of all effectors tested (Figure 3.6 and 3.10, B, C, H). Both effectors' luminescence traces in screen 3 show some evidence of daily expression peaks even at very low amplitude, although it is possible that this is bleed-through detected from adjacent wells during imaging. The apparent severity of these effectors' circadian phenotypes might suggest that the protoplasts had in fact undergone cell death. The lack of detectable rhythmicity is highly unlikely to be due to experimental/user error given that the effect is seen exclusively for these effectors, and in all three screens. It is of course also possible that the protoplasts were

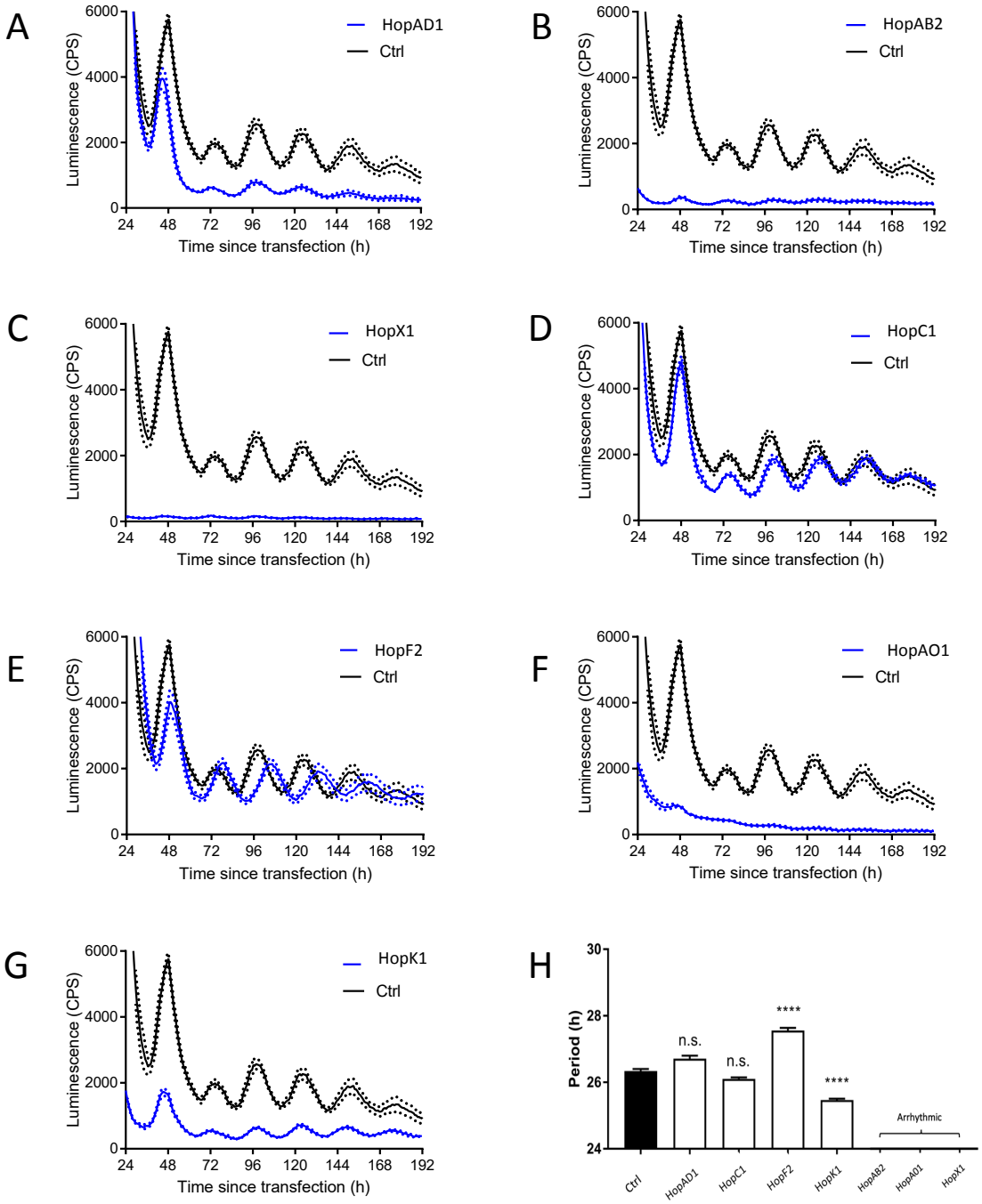

Figure 3.6: *A. thaliana* protoplasts transfected with individual *P. syringae* type III secreted effectors exhibit atypical phenotypes in *proCCA1:LUC* expression rhythm. A-G) Protoplasts were co-transfected with *proCCA1*:LUC and either effector plasmid or an empty vector (EV) control. Luminescence was recorded as counts per second and normalized by dividing by the rolling average of the subsequent 24 hours of data to remove dampening rhythmicity. Mean luminescence from the effector transfected protoplasts is plotted in blue overlaying the trace of EV-only transfected samples in black, which represent the wild type *CCA1* promoter expression profile (± SEM in dotted lines around mean luminescence values, n = 6). H) Period of *CCA1pro* linked luminescence rhythms were determined using Prism, then analysed via one-way ANOVA with Tukey's multiple comparisons test. Significance differences in comparison to the EV-transfected control, are denoted by asterisks where P values are ≥0.05 (n.s.), <0.01 (**), and <0.0001 (****).

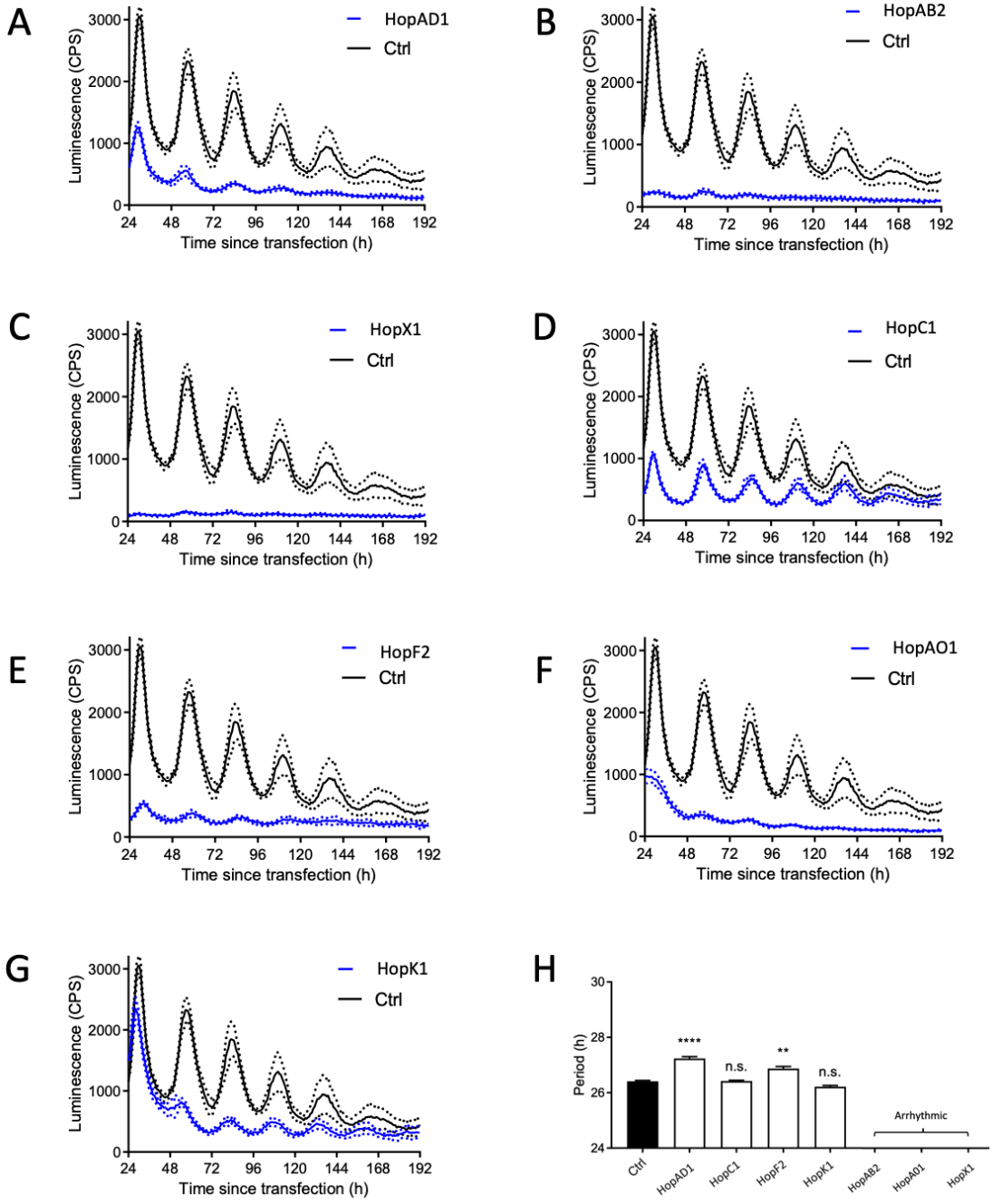

Figure 3.7: *A. thaliana* protoplasts transfected with individual *P. syringae* type III secreted effectors exhibit atypical phenotypes in *proGI:LUC* expression rhythm. A-G) Protoplasts were co-transfected with *proGI:LUC* and either effector plasmid or an empty vector (EV) control. Luminescence was recorded as counts per second and normalized by dividing by the rolling average of the subsequent 24 hours of data to remove dampening rhythmicity. Mean luminescence from the effector transfected protoplasts is plotted in blue overlaying the trace of EV-only transfected samples in black, which represent the wild type *GI* promoter expression profile (± SEM in dotted lines around mean luminescence values, n = 6). H-I) Period of *GI:pro* linked luminescence rhythms were determined using Prism, then analysed via one-way ANOVA with Tukey's multiple comparisons test. Significance differences in comparison to the EV-transfected control, are denoted by asterisks where P values are ≥0.05 (n.s.), <0.01 (**), and <0.0001 (****).

otherwise healthy, and that these effectors truly induce a severe and yet non-specific impact on the expression of clock gene promoters. This seems more plausible in the case of HopAB2 (alias AvrPtoB) which has been shown in the past to supress ETI-associated cell death in *Nicotiana benthamiana* and yeast (Wei et al., 2015; Abramovitch et al., 2003). HopX1 (alias AvrPphE) meanwhile has been previously associated with the induction of the cell death response in A. thaliana (Nimchuk et al., 2007), and arrhythmicity may simply be a symptom of this mechanism. If these effectors were of interest in the future the use of Evans Blue stain might be prudent as a way of identifying dead protoplasts at the end of an imaging run.

HopC1 elicited no significant disruption to the expression rhythm of *proCCA1:LUC* (Figure 3.6, D and H). It was able to significantly reduce *proGI:LUC* amplitude (albeit in screen 3 only) but was still very much rhythmic over the duration of the time course, with no change in period length (Figure 3.7, D, H).

HopK1 had a fairly consistent ability to diminish rhythmic amplitude of the reporter constructs in screens 2 and 3 (Table 3.1, Figures 3.6, G, and 3.7, G). Interestingly, it was also able to significantly lengthen and shorten the period of *proCCA1:LUC* in screens 1 and 3 respectively, by approximately an hour in each instance (Table X, Figure 3.6, H). This would indicate that HopK1 is able to significantly change rhythms in the transcription of core clock genes, but that the output of this function is dependent on an unknown factor that was not kept constant within this experiment.

HopF2 did not alter rhythmicity of *proCCA1* expression in the first screen, however in screens 2 and 3 it caused a lengthening of period in protoplasts transfected with both *proCCA1:LUC* and *proGI:LUC* (Table 3.1). Changes to amplitude were only evident when examining the *proGI*:*LUC* rhythm. Furthermore, its long period phenotype in screen 3 was the only period change that could objectively be seen by visual inspection of the raw traces (Figures 3.6 and 3.7, E), enforcing the notion that this is a genuine circadian phenotype, as opposed to, say HopAD1, which was reported by the waveform analysis to have a *proGI:LUC* expression period that is even longer than that of HopF2 but is not evident in the trace (Figure 3.7, A and H). This is most likely due to inaccuracies in the curve fitting process and enforces the need to always look at the data qualitatively rather than taking analyses at face value, as fit curves are not

always a meaningful representation of the actual rhythm. Overall HopF2 here appears to influence the expression rhythms of two differently-phased clock gene promoters, inducing both a significant and consistent lengthening of period, and in the case of *proGI:LUC,* a significant reduction in amplitude.

Finally, HopAO1 (alias AvrPphD2) was found to have a highly consistent effect on the clock (Table 3.1). It reduced the amplitude of expression rhythms in screens 1-3 on both *proCCA1:LUC* and *proGI:LUC* and rendered the cells largely arrhythmic in screens 2 and 3, with no quantifiable periodicity (Figure 3.6 and Figure 3.7, F, H). In screen 1, analysis determined it to have significantly shortened period length by approximately 30 minutes, however by 48 hours post transfection it appeared to be completely arrhythmic, or at least rhythmic at such a low amplitude so as to be visually indiscernible at this scale (Table 3.1). Most importantly, while HopAO1 was able to render the protoplasts assayed arrhythmic, unlike HopAB2 and HopX1 its signal levels did not start at lower amplitude, but appeared to depreciate over the course of the first day, rather than starting at an initially low level (Figures 3.6, F and 3.7, F). This lends weight to the thought that HopAB2 and HopX1 may have caused cell death, or widescale transcriptional subversion soon after they are transformed into the protoplasts, whereas HopAO1 seems to induce a gradually more severe circadian phenotype over time, as if acting to subdue the ability of the clock to remain entrained to its previous environmental cues under constant conditions.

The results of this study support our hypothesis that certain type III secreted effectors from the *Pst.* DC3000 repertoire are able to induce changes to the expression of core components of the circadian clock. While some of the T3SEs included here had no visually discernible or statistically quantifiable influence on the rhythms of *proCCA1:LUC* and *proGI:LUC* expression, others did. With regards to periodicity these changes manifested in different ways and to different degrees. HopAD1 was able to alter the period of one of the circadian reporters but not the other, signifying a possible clock gene-specific mechanism of action. HopAB2 and HopX1 both appeared to cause severe arrythmia across all experiments, and both constructs used, with no gradual damping of rhythmicity, indicative of a robust and non-specific influence on the transcription of clock genes. HopK1 had little impact on the period length of *proGI:LUC* but changed the period of the *CCA1* promoter by both lengthening and

shortening it in different iterations of the assay, suggesting an effect on the expression rhythm of the *CCA1* promoter in a way that is specific, but also highly variable considering every effort was made to maintain constant environmental conditions. HopF2 produced a highly reproducible phenotype of a longer period, and HopAO1 a gradual yet robust arrythmia for both constructs. Interestingly, in spite of the varying circadian phenotypes brought on by the transfection of *Pst* T3SEs, not a single effector caused an increase in amplitude for the circadian reporters used. Of those that induced an altered phenotype, the amplitude was in every case either not significantly different from the control or was reduced in comparison to it. These results strongly support the hypothesis that the pathogen *Pst* uses T3SEs to diminish the output of the plant circadian clock in order to subvert regulation of host defence pathways and enhance pathogenic virulence.

3.3 Discussion

At the start of this project the degree of involvement of pathways influenced by type three secreted effectors (T3SEs) in the disruption of the plant circadian rhythm by the virulent pathogen *Pst* DC3000 was not known. Although substantial links between *Pst.* DC3000 infection and the disturbance of the *A. thaliana* clock have since been uncovered (Li et al., 2018), there remained a considerable gap in the knowledge of how T3SEs contributed to these altered circadian phenotypes. The aim of this chapter was to examine the role exerted by T3SEs on the host clock in this pathosystem.

3.3.1 Temporal variation in the susceptibility of A. thaliana to Pst DC3000 is not dependent on effector mediated pathways

By using the avirulent *Pst* T3SS mutant *hrcC* alongside DC3000 in a bacterial growth time series under constant conditions we found that the temporal variation in susceptibility of *A. thaliana* is not significantly dependent on the secretion of effectors through the T3SS. It is important to clarify that it was not expected that effectors would be able to change the rhythm in host susceptibility. Susceptibility is here defined as

the extent to which the inner leaf tissue of host *A. thaliana* might be liable to colonisation by the foliar pathogen *Pst and* represents the innate condition of the host immediately prior to being presented with a pathogenic challenge. Therefore, it would not semantically be possible for the action of effector secretion into the plant to alter its susceptibility. It would, however, be possible for instance, for the plant to regulate the expression of defence genes in a rhythmic fashion, such that components of immune pathways that recognise effectors would temporally fluctuate. This would mean that the efficacy of effectors to enhance pathogenic virulence would also be rhythmic. The *A.* thaliana resistance (R) protein RPP4 for example has been shown to confer resistance to *Hyaloperonospora arabidopsidis* (*Hpa*) and to bind a cognate *Hpa* effector HaRxL103 (Asai et al., 2018), but also has two "evening elements" (a sequence subject to regulation by the core clock gene *CCA1*)(Zhang et al., 2013) and is rhythmically expressed with a daily peak at ZT8 in both Col-0 and Ler-0 ecotypes and multiple light and temperature conditions (DIURNAL online tool, Michael et al., 2008). The *hrcC* mutant was thus included in order to assess the dependence of host susceptibility over time not on effectors, but on pathways that are responsive to effectors.

The difference in bacterial growth between *hrcC* and DC3000 treated plants was not found to significantly vary according to time of infiltration by more stringent statistical methods, though slightly more conservative analysis performed in light of the apparent rhythmicity of the data found there to be a borderline significant effect. This would indicate that effector-triggered susceptibility (ETS) in the *A. thaliana-Pst* pathosystem is not subject to substantial regulation by circadian rhythms. That is to say that while susceptibility to virulent *Pst* may oscillate throughout the day, the virulence enacted by its effectors, and the ability for host R proteins to react to their secretion does not.

As mentioned in section 3.2.1 there is not sufficient evidence in the field to conclude whether or not *P. syringae* itself possesses a molecular clock mechanism. The fungal pathogen *Botrytis cinerea* possesses a homolog for the *Neurospora crassa* clock gene *frq,* mutation of which reduces virulence and eliminates time of day dependent susceptibility of the host *A. thaliana,* leading the authors to suggest that the functioning of the *B. cinerea* clock affects the outcome of the infection (Hevia et al., 2015). Harper et al. (2003) report *P. syringae pv. syringae* to be among four tested prokaryotes that

contain a light-sensing LOV (light, oxygen or voltage) flavin domain, a domain characterised within plant phototropins and thought to aid in the mediation of blue light responses such as stomatal opening and phototropism (Briggs and Christie, 2002). They also found the LOV domain to contribute to virulence in light-stimulated *Brucella abortus* (a blood-borne animal pathogen), although the domain's impact on *P. syringae* virulence was not assessed. It is possible that *Pst* might make use of entraining environmental cues such as light to regulate expression of its effectors and expend the metabolic cost of their translation/secretion only when the plant is most susceptible. It cannot, therefore, be ruled out that the efficacy of *Pst* effectors themselves is rhythmic. Given however, that the bacterial cultures used in this study were grown entirely under constant light and temperature conditions with the only possible rhythmic environment for cells to entrain to being the retained rhythmicity of the infiltrated plants, we attribute any faint oscillation in the difference between *hrcC* and DC3000 bacterial growth to the circadian regulation not of effectors by the pathogen, but of immune responsiveness by the host plant. The furthering of an understanding of a potential pathogenic clock could be achieved by replicating this assay using additional bacterial cultures raised in rhythmic photoperiods.

In agreement with the work done by Bhardwaj et al. (2011), these results indicate that the time of day *A. thaliana* is infected with *Pst* has a significant bearing on total bacterial growth. Just as in this previous study, we infiltrated bacterial cultures rather than applying them only to the outer leaf surface and found that our results also support the conclusion that this effect is not solely dependent on rhythms in stomatal opening. We have here furthered those results by proving that this susceptibility is also not caused in any significant part by effector-mediated pathways when bacterial cultures are raised without entraining cues; it is likely brought on instead by the host through the priming of MTI pathways by the circadian clock, confirming and extending the findings reported by Zhang et al. (2013).

3.3.2 A. thaliana induces changes to the amplitude of clock gene expression during MTI, while P. syringae uses T3SEs to buffer these effects

The outcome of the bacterial time course enabled us to proceed with *in planta* bioluminescence circadian analyses in a way that was more informed. The transgenic plants used in this assay expressed translational fusion reporter constructs of core clock genes that peak at different times of day (*CCA1* ~dawn, *TOC1* ~dusk) thus it was important to determine if it would be best to infiltrate plants at the same time each day between *A. thaliana* genotypes or at different times of day. There were potential caveats to either experimental approach. By infiltrating at the same time each day we would more closely mirror the methodology of Li et al. (2018), facilitating the comparison of results. We would also be preventing the masking of effector-induced changes to reporter rhythms by temporal differences in host susceptibility, i.e. if a change in *CCA1* expression amplitude appeared bigger only because the plants had been infiltrated when susceptibility was higher than in the *TOC1* line. This would, however, mean that the two reporter lines had been subjected to a pathogenic presence for different lengths of time when their reporter constructs peaked, meaning the extent of changes to the clock at each time point might not be comparable between them. On the other hand, we could infiltrate at different times of the day, for instance, always infiltrating 5 hours before the anticipated peak in expression. In this case, plants of each reporter line would have been infected for the same amount of time when reporter expression peaked, however, they would also have had to have been kept in constant conditions for different lengths of time. Infiltrating 5 hours before an expression peak for the *CCA1::LUC* line would mean either infiltrating at ZT19, before plants had even been placed in the dark, or at CT19, having spent 19 hours in the dark. For *TOC1::LUC* they would have been infiltrated at CT7, or CT31. This would constitute a large difference in the innate robustness of the circadian rhythm at the point of infection, as without entraining cues the rhythm will damp over time, which would cloud our ability to attribute rhythmic changes to the presence of effectors rather than typical damping. Having confirmed then, that the variation in susceptibility is robust when assayed under our conditions (and in the heretofore untested *hrcC* mutant), we decided that performing infiltrations for each genotype at the same time of day would least limit the interpretation of results. Instead of performing infiltrations at dawn as in the previous study, plants would be infiltrated before dusk. This would allow us to comment on whether or not observed changes in the two reporter lines were likely due to effector-mediated pathways, or length of time without entraining cues.

In light of these caveats we must be careful in our comparison of the *CCA1::LUC* and *TOC1::LUC* reporter lines, because the former was infected with *Pst* 10 hours longer at the time of reporter expression peak. In fact, the phenotype elicited on the *CCA1::LUC* rhythm was broadly less severe than that of *TOC1::LUC* even given this longer incubation time. It may be the case that a complete T3SE repertoire favours the induction of changes to the expression of evening-phased *TOC1* when orchestrating circadian disruption, and host MTI pathways focus on the boosting of *TOC1* expression over *CCA1*, or that while some effectors disrupt the *CCA1* rhythm, more disrupt that of *TOC1.* This is supported by the results of Li et al. (2018), who found that infection with DC3000 elicited a greater change in amplitude of *TOC1* promoter expression than of the *CCA1* promoter, even when plants were infiltrated at dawn, as this implies that the different phenotypes of the two reporter lines are not due to the difference in duration having been infected, or kept in constant light conditions at the time of the first expression peak.

The aim of investigating clock gene rhythms *in planta* by detecting reporter bioluminescence was to assess whether changes in core clock gene expression rhythms could be induced by *Pst* with and without a functioning T3SS. Although the impact of *Pst* DC3000 on the expression of 3 clock gene promoters had previously been addressed, the dependence of such changes on the secretion of T3SEs had not. We report that effector-mediated pathways do indeed influence circadian rhythmicity following infection by *Pst,* and that the discrepancies between the phenotypes of *CCA1::LUC* and *TOC1::LUC* suggest that these changes may be differentially exerted on different regulatory arms of the TTFL. The results of this study indicate that the detection of MAMPs by the host *A. thaliana* leads to the upregulation of the clock gene *TOC1* in order to limit bacterial growth. Secretion of a full repertoire of T3SEs seems to inhibit this effect, further lowering clock gene amplitude at high bacterial concentration. This is in line with work by Zhou et al. (2015) which showed that stress conditions result in the upregulation of TOC1 by non-expressor of pathogenesis-related gene 1 (NPR1), a mechanism suggested to gate the expression of defence genes (Lu et al., 2017). We also prove that the ability for DC3000 to disrupt circadian rhythms is independent of rhythms in stomatal aperture, reproducing the formerly published phenotypes by infiltrating rather than dipping leaves with bacterial cultures (Li et al., 2018). It is of note that the difference between DC3000 and *hrcC* treated

plants was largely dose-dependent, eliciting consistently greater changes in amplitude as the concentration of inoculum used was increased. The circadian phenotypes brought on by DC3000 and *hrcC* infection were more robust at higher concentration, but this does not necessarily represent the biological actuality during infection, as the lowest concentrations here used are also sufficient to enable bacterial growth of both strains (see section 3.2.1). The induction of total arrhythmicity in a gene's expression within 24 hours of bacterial infection is probably more than is typical in nature, while an advancement of arrhythmicity in the presence of secreted effectors may be closer to the reality.

3.3.3 The Pst T3SE repertoire collectively acts to diminish the amplitude of core clock gene expression in A. thaliana, with certain effectors contributing to the circadian phenotype

Having demonstrated that *Pst* T3SEs play a role in determining the rhythmicity of the host plant during infection, we next sought to identify which effectors were actively involved in this mechanism. In a screen of 23 effectors from the *Pst* DC3000 repertoire we were successful in finding 6 effectors that elicit significant and consistent alterations to the circadian phenotype of *A. thaliana*. These were HopAD1, HopAB2, HopX1, HopF2, HopAO1, and HopK1. Note, not all known *Pst* DC3000 effectors were tested, however a representative from the majority of its 28 most frequently occurring effector families was included (Lindeberg et al., 2012). As expected, not all assayed effectors caused a circadian phenotype, since DC3000 effectors are known to exert a wide variety of virulent mechanisms on the host, and while there is some functional redundancy within the repertoire, the effectors by all means do not have identical functions (Xin et al., 2018; DebRoy et al., 2004). Furthermore, of the effectors that did influence the clock, the elicited host phenotypes varied, suggesting that the mechanisms they employ differ from one another.

Not one of the effectors resulted in an increase in the amplitude of either clock gene reporter's expression rhythm. Considering the fact that the overexpression of core clock genes *CCA1* and *LHY* has been shown to result in an increase in susceptibility

to virulent *P. syringae pv. maculicola* (Zhang et al., 2013) one might have expected the secretion of effectors to cause an increase in clock gene expression. While decreasing amplitude also seems likely to have its benefits as far at the pathogen is concerned as discussed above in the case of *TOC1* (Zhou et al., 2015), it is interesting to see that where *Pseudomonas syringae pv.* tomato is concerned, even secreted effectors with apparently different mechanisms enact a concerted effort to diminish amplitude. This supports the notion that the impact on the clock seen by these effectors is part of a deliberate mechanism to induce arrhythmicity, rather than a random accumulation of symptoms downstream of other virulent pathways. It also suggests that when it comes to plant pathogens disrupting the clock, there is no one-mechanism-fits-all policy, and different pathogens may alter the clock in different ways to suit their developmental needs.

With regards to periodicity, however, the effectors did appear to elicit different phenotypes, even between screens, with some lengthening, and some shortening reporter gene rhythms. This indicates that altering period length is not a consistent phenotype amongst T3SEs and may not form any substantial part of *Pst* DC3000's enhanced virulence. In the case of HopF2 therefore, which generated a highly repeatable period lengthening for the expression of both reporter constructs, and only minimal changes to amplitude, we suspect that the effector's mechanism was more likely a downstream symptom of its primary virulent function. HopF2 is known to be expressed at the plasma membrane where it promotes growth of *Pst* DC3000 through its ADP-ribosylation of MKK5 and RIN4 (Wang et al., 2010; Wilton et al., 2010). Although HopF2 may not have evolved to target the clock to enhance virulence, if its clock altering phenotype was found to be independent of this virulent function it may have some use as a tool for synthetically manipulating the clock in future studies.

One might expect the effectors most suited to having a direct influence on the clock to be those localised in the nucleus or perhaps the chloroplast. In the nucleus, an effector might dysregulate the transcriptional-translational feedback loop itself to prevent regulation of defence. In the chloroplast, it could interfere with the pathogen-induced biosynthesis of immune response-stimulating salicylic acid (SA) which is a known point of feedback between the clock and the immune system (Li et al., 2018; Zheng et al., 2015). HopK1 is known to suppress the hypersensitive response (HR) (Gimenez-

Ibanez et al., 2018) and uses a cleavable transit peptide to localise to the chloroplast where it significantly contributes to DC3000 virulence, suppressing callose deposition and enhancing bacterial growth (Li et al., 2014), but its targets have not yet been identified. HopK1 has already been shown to not suppress SA signalling, but on the basis of its being able to suppress both early and late immune responses, the authors of the study suggest HopK1 may target signalling components that originate in the chloroplast but regulate the expression of genes in the nucleus (Li et al., 2014). This could also represent the mechanism by which HopK1 is able to exert negative regulation on *CCA1* and *GI* in the protoplast screen.

HopAD1 was one of the few effectors that caused inconsistent phenotypes in the two circadian reporter genes, lowering amplitude of the *GI* promoter, but eliciting no change on *CCA1*, which could indicate a specific targeting of *GI*, rather than a systemic influence on the whole clock. HopAD1 is however known to induce HR in *Nicotiana benthamiana* (Wei et al., 2015), and while this is suppressed by the effector AvrPtoB, the deletion of HopAD1 from DC3000 confers greater virulence to the pathogen in *N. benthamiana* (Wei et al., 2018). This suggests that HopAD1's influence on circadian rhythmicity does not significantly contribute to the virulence of *Pst.* Notably, although rhythm analysis indicates that HopAD1 significantly decreased amplitude in the *proGI:LUC* transfected protoplasts, this looks to have been largely skewed by the amplitude at later stages of the assay, as at 48 hours post transfection the amplitude of both constructs appears far greater than that of effectors HopAB2, HopX1, HopK1 and HopAO1. If a reduction in the amplitude of clock gene expression confers enhanced virulence to DC3000, it could be that the benefit to pathogenic spread is felt most within the first 48 hours of infection. It could also be that since multiple effectors diminish amplitude, the action of one alone is not sufficient to induce arrhythmicity that enhances bacterial growth, or merely that expression of HopAD1 is such a hindrance to DC3000 that in spite of its diminishing clock gene amplitude it still limits growth.

The remaining three effectors which caused circadian defects differ from HopAD1 in the sense that rather than exerting an effect that was specific to one of the clock reporters, they induced changes to both in equal measure. HopAB2, HopX1, and HopAO1 produced arguably the most severe phenotypes recorded throughout the

effector screen, massively reducing amplitude and rendering protoplasts largely arrhythmic in all three screens. As noted in section 3.2.3, we must be cautious in interpreting these results. Firstly, without the use of a constitutive LUC reporter, or a non-circadian gene/LUC fusion construct we cannot be sure that the phenotypes here observed are specific to the clock. Secondly, the viability of protoplasts cannot be tested throughout the assay, and while the protoplast bioluminescence method has been shown to replicate published circadian phenotypes, we cannot rule out the possibility that the transformation of certain effectors may have induced cell death in protoplasts over the course of the screen. To this end, the quantifying of viable protoplasts at the end of the run compared to EV transformed controls in the future could be informative.

HopAB2 (also known as AvrPtoB) is an E3 ubiquitin ligase identified as one of 8 effectors in a minimal functional effector repertoire needed for DC3000 to suppress host immunity (Cunnac et al., 2011). It suppresses MTI by ubiquitinating the PRRs FLS2 and CERK1 at the plasma membrane (Shan et al., 2008; Göhre et al., 2008; Gimenez-Ibanez et al., 2009), and can suppress ETI-associated cell death in *N. benthamiana* and yeast (Wei et al., 2015; Abramovitch et al., 2003). HopAB2's lack of association with the induction of cell death suggests that it does exert a genuine impact on clock gene expression, however this is non-specific, and the comparatively extensive work on HopAB2 (considered a model effector) has not yet revealed any obvious mechanistic link to the clock.

The cysteine protease HopX1 has a well-established function promoting host susceptibility through the degradation of multiple JAZ family proteins, and activation of jasmonate responsive genes (Gimenez-Ibanez et al., 2014). It is believed to degrade its target JAZ proteins in the nucleus where it has a small but detectable level of expression, but is predominantly found in the cytoplasm (Gimenez-Ibanez et al., 2014). Additionally, HopX1 has been shown to trigger cell death in *A. thaliana*, although not in *N. benthamiana* (Sarris et al., 2011). Jasmonic acid (JA) signalling and biosynthesis have been shown to be clock-regulated (Goodspeed et al., 2012), with temporal variation in *Arabidopsis* susceptibility to *B. cinerea* having been shown to be dependent on expression of the JAZ6 protein (Ingle et al., 2015), and the clock gene *TIME FOR COFFEE* (*TIC*) controlling the rhythmic expression of JA receptor

CORONATINE INSENSITIVE1 (*COI1*) (Shin et al., 2012). Furthermore, the JA pathway has an antagonistic relationship with SA signalling (Caarls et al., 2015). It seems possible, therefore, that HopX1 would be able to cause a circadian phenotype as a result of its degradation of JAZ proteins, although JAZ6 was not included amongst the proteins tested by Gimenez-Ibanez et al. (2014). This could plausibly relieve the repression of JA-mediated defence and inhibit the accumulation of SA to benefit the biotrophic phase of *P. syringae* growth, as well as potentially disrupt downstream feedback from the SA pathway to the clock (Pauwels and Goossens, 2011; Zhang et al., 2017; Zhou et al., 2015).

Another effector with non-discrete localisation, HopAO1 has previously been characterised as a tyrosine phosphatase with published activity in the cytoplasm where it prevents the phosphorylation of the *Arabidopsis* receptor kinases ERF and FLS2, which would otherwise be activated following MAMP perception and initiate downstream MTI responses (Macho et al., 2014). HopAO1 may have a further role limiting MTI by dephosphorylating MAP kinases, although studies in both *N. benthamiana* and *A. thaliana* have shown contradicting evidence for this (Espinosa et al., 2003; Underwood et al., 2007). The effector has also been detected in the nucleus after transient *Agrobacterium*-mediated expression by both western blot of nuclear protein extracts and confocal microscopy in *N. benthamiana* leaf tissue and *A. thaliana* protoplasts (Mastorakis, 2017). HopAO1 significantly enhances the virulence of the *Pst* T3SS mutant *hrpA*, although its deletion from *Pst* DC3000 does not reduce bacterial growth (Underwood et al., 2007). Its role in the induction of HR is unclear as it has been seen to elicit symptoms of the response in transgenic *A. thaliana* 3 days after induction (Underwood et al., 2007), however it also inhibits HopAD1-induced HR in tobacco (Castañeda-Ojeda et al., 2017), delays HR in *N. benthamiana*, and inhibits it in the host tomato plant *L. esculentum* cv. money-maker (Espinosa et al., 2003). Given, however, that the significant reduction in clock gene reporter amplitude caused by HopAO1 in the protoplast screen is evident within the first 72 hours, well before symptoms of HR have previously been reported in *A. thaliana*, we suspect that this effector has a genuine impact on *Pst* virulence altering the amplitude of clock gene expression, likely a result of its as-of-yet uncharacterised function in the nucleus.

3.3.4 Overview

The results of this chapter have shown that *A. thaliana* possesses a temporal variation in its susceptibility to *P. syringae pv. tomato* that is not significantly dependent on effector-mediated pathways, and so is likely constituted by the priming of MAMP-triggered immune responsiveness by the circadian clock. We have found that in response to challenge by the avirulent pathogen *hrcC*, *A. thaliana* induces substantial changes to the expression of core clock genes, the most notable of which perhaps is a drastic increase in the expression of the evening-phased *TOC1* promoter. When the infiltrated pathogen, however, is able to secrete type III effectors, these changes in amplitude are offset in a dose-dependent manner.

We have also identified a number of type III secreted effectors able to induce a circadian phenotype when individually transformed into *A. thaliana* protoplasts. We suggest that the effector HopF2 may be of use as a synthetic tool in circadian studies for inducing an increase in period length and ascertaining whether this effect is independent of its virulent function warrants further study in the future. We propose that HopX1 may produce circadian defects through its degradation of JAZ proteins in the nucleus (Gimenez-Ibanez et al., 2014). Finally we find that the effector HopAO1 also produces a robust circadian phenotype, and given its non-discrete localisation (Mastorakis, 2017, Macho et al., 2014), hypothesise that this is brought on by a novel virulent mechanism in the nucleus.

In light of the findings presented in this chapter, we found ourselves asking questions concerning the various possible mechanisms of action exerted by the effectors here found to alter the plant circadian rhythm, in particular that of HopAO1 with its demonstrable nuclear localisation that has not yet been examined with regards to its virulent function. This ultimately led us to next examine the molecular interplay between the effector HopAO1 and the clock.

Chapter 4: The binding partners and molecular mechanism of *Pst* effector HopAO1 in the nucleus

4.1 Introduction

The type III secreted effector HopAO1 was shown in the previous chapter to induce significant changes to circadian clock function in protoplasts transfected with two different circadian reporter lines, *proCCA1:LUC* and *proGI:LUC.* Transformation of the effector was able to repeatably reduce the amplitude in expression of both circadian reporter constructs in a way that became gradually more severe as the time course progressed and eliminated any quantifiable periodicity in multiple rounds of the screen. This robust circadian phenotype suggests that HopAO1 employs disruptive action on the clock in order to limit circadian regulation of immune responses and enhance pathogenic virulence. Considering that the reduction of circadian gene expression was shown in section 3.3.2 to be triggered by infection with virulent *Pst*, while the opposite was true for the avirulent *hrcC* mutant, it seems likely that a decrease in circadian gene expression during infection is beneficial to *P. syringae,* but detrimental to the host.

As has been briefly discussed previously, HopAO1 (formerly HopPtoD2) is T3SE with protein tyrosine phosphatase activity, whose enzymatic action relies on a conserved catalytic cysteine residue, Cys_{378} (Espinosa et al., 2003; Bretz et al., 2003). Catalytically active HopAO1 is thought to inhibit PRR activation by physically interacting with both the cytoplasmic and kinase domains of PRRs EFR and FLS2, and it causes a ~50% reduction in EFR phosphorylation following treatment with elf18 when its expression is induced in transgenic *A. thaliana* seedlings (Macho et al., 2014). The dephosphorylation of FLS2 by HopAO1 was marked by the authors in the same study. Expression of HopAO1 in this way has also been reported to cause a reduction in the activation of MAPKs (MPK6, MPK3, and MPK4/11) (Espinosa et al., 2003; Macho et al., 2014). Another study however contrastingly describes HopAO1 as activating rather than inhibiting MAPK3 and MAPK6 (Underwood et al., 2007). The lack of MAPK inhibition in the latter of these studies may have been due to

experimental differences such as the use of the avirulent *Pst* strain *hrpA* to induce MTI rather than 100mM elf18, or may indicate as some have suggested that the MAPKs are not direct targets of HopAO1 (Block and Alfano, 2011). Changes in their phosphorylation states may instead lie downstream of HopAO1's dephosphorylation of PRRs.

The role of HopAO1 on pathogenic virulence demonstrably involves the inhibition of immune responses on various fronts. In addition to changing the phosphorylation state of MAPKs, other MTI mechanisms subject to mediation by transgenically expressed HopAO1 include the production of Reactive Oxygen Species (ROS) and the extent of callose deposition which is reduced in *A. thaliana* in a manner that is dependent on the effector's catalytic cysteine residue (Macho et al., 2014; Underwood et al., 2007). The disruption of MTI and ETI mechanisms has also been reported *in planta* in crop species. A homolog for HopAO1 in the olive pathogen *P. savastanoi pv. savastanoi* (confirmed as a T3SE with phosphatase activity) contributes to fitness and virulence during infection of olive plants, suppressing callose deposition and ROS production, and facilitating the formation of necrotic lesions (Castañeda-Ojeda et al., 2017). The homolog was also able to suppress cell death response when transiently expressed in *N. benthamiana*. In a tomato host plant (*Lycopersicon esculentum cv. moneymaker*), *Pst*'s potential for bacterial growth and HR elicitation is reduced in HopAO1 mutant strains, with virulence restored by *in trans* complementation with the functioning effector (Espinosa et al., 2003). Furthermore, the effector represses the expression of several genes with established function in host immunity such as PR1 and PR5 (both SA-responsive genes associated with pathogenic infection, Uknes et al., 1992), although this was not in all cases dependent on its enzymatic activity (Underwood et al., 2007). This discovery, in combination with HopAO1's variable influence on HR elicitation/suppression in different plant hosts (see section 3.3.3) led to the hypothesis that the effector may possess further virulent mechanisms that are independent of PRR and MAPK de-phosphorylation (Macho et al., 2014; Underwood et al., 2007).

Transient expression of HopAO1 in *N. benthamiana* has since been shown to significantly suppress proteasomal activity in a way that is thought to enhance virulence by preventing the establishment of systemic acquired immunity (SAR). *Arabidopsis thaliana* lines carrying mutation of certain proteasome subunits were

more susceptible to infection by *P. syringae pv. maculicola* and were unable to mount typical MTI and SAR responses such as increased ROS burst, MAPK signalling, as well as the expression of WRKY transcription factors and the SA-pathway marker gene *PR1* (Üstün et al., 2016).The phosphorylation of proteasome subunits enables activation and assembly of the ubiquitin-proteasome system, thus the dephosphorylation of them by this effector is noted to plausibly be a mechanism for inhibition of host defence, although direct interaction of the effector with such subunits has not yet been confirmed (Satoh et al., 2001; Üstün et al., 2016).

These published functions for HopAO1 all corroborate it having virulent function in the host cytoplasm, a concept backed up by its verified presence in the soluble but not membranous fraction of *A. thaliana* protein extracts (Underwood et al., 2007). It has been stated, however, that HopAO1 also localises to the nucleus (Mastorakis, 2017, Figure 4.1), where it has yet to have been attributed to any specific virulent mechanism. Given that the nucleus is a hub for the transcriptional-translational feedback loop at the heart of the plant circadian oscillator, and subsequently its regulation of other genes' expression, we hypothesised that HopAO1's nuclear localisation permits its disruption of the clock.

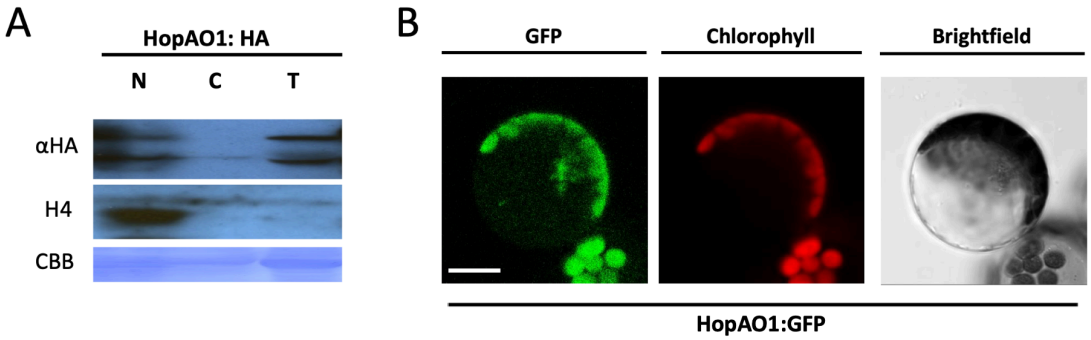

Figure 4.1: Visualisation of HopAO1 subcellular localisation by nuclear exclusion and confocal microscopy (Images and adapted legend from Mastorakis, 2017). A) Leaf samples form adult *N. benthamiana* transiently expressing N-terminal 3xHA tagged HopAO1 were subject to protein extraction and nuclear isolation. Nuclear (N), cytoplasmic (C), and total input (T) were analysed by western blot and compared to a nuclear control, the histone H4 in order to ascertain the subcellular localisation of the effector. CBB represents Coomassie Brilliant Blue staining and shows equal loading of protein between wells. B) *A. thaliana* protoplasts transfected with and N-terminal GFP fusion of HopAO1 are imaged by confocal microscopy. Scale bar represents 10μm.

There is a substantial precedent for post-translational modifications, specifically including changes in phosphorylation state, having a proven role in the regulation of clock activity (Seo and Mas, 2014). CK2, a highly conserved Ser/Thr kinase interacts with and phosphorylates the core clock proteins CCA1 and LHY (Sugano et al., 1998, 1999). This phosphorylation is necessary for CCA1 to form DNA-protein complexes, and overexpression of CK2 subunits results in increased CK2 activity and shortened periods of *CCA1* and *LHY* expression (Sugano et al., 1999; Daniel et al., 2004). The function of two other clock components, TOC1 and the PRRs is also dependent on phosphorylation (Fujiwara et al., 2008; Seo and Mas, 2014). Phosphorylation of PRR5, PRR3 and TOC1 enhances their interaction with the blue light sensing protein ZTL (a component of an E3 ubiquitin ligase, Kim et al., 2007) in a manner thought to allow PRR3 to outcompete TOC1 for binding of ZTL, protecting TOC1 from degradation and enhancing the amplitude of its expression (Fujiwara et al., 2008; Seo and Mas, 2014). The light input pathway component LWD1 interacts with a tyrosine phosphatase YET ANOTHER KINASE1 (AtYAK1) which has been proven to have functions in light responsiveness and maintaining circadian period length (Huang et al., 2017). Finally, immune and SA regulator NPR1 (which is expressed under circadian control) requires phosphorylation in order to translocate to the nucleus and activate SAR (Kinkema et al., 2000), and while none of the residues identified as mediating its phosphorylation levels were tyrosine residues, incomplete sequence coverage could potentially reveal a role for tyrosine phosphorylation in NPR1's regulatory action (Lee et al., 2015). Thus, there is ample scope for the enzymatic action exerted by tyrosine phosphatase HopAO1 to target nuclear localised clock components in order to disrupt host circadian rhythmicity and enhance the virulence of *P. syringae*.

The experimental aims for this chapter were therefore as follows:

i) To confirm the previously reported nuclear localisation of the *Pst* T3SE HopAO1 (section 4.2.1).
ii) To identify binding partners of HopAO1 in the nucleus (section 4.2.2).
iii) To elucidate the molecular basis of HopAO1's induced circadian phenotype, as informed by its interacting partners in the nucleus (section 4.2.3).

4.2 Results

4.2.1 Nuclear localisation of the P. syringae pv. tomato effector HopAO1

HopAO1 has been well characterised in the cytoplasm (see section 4.1), however it has only been reported as exhibiting nuclear localisation in one instance before now (Mastorakis, 2017, Figure 4.1). In this previous study the effector was shown to be localised in the nucleus by biochemical nuclei purification of *N. benthamiana* leaf tissue following transient expression by agroinfiltration, as well as by confocal microscopy in transfected *A. thaliana* protoplasts. The author reports that HopAO1 exhibited localisation purely in the nucleus but not the nucleolus, as well an "intermediate" recovery time after photobleaching in the nucleus suggesting that the effector is transiently associated with chromatin. Interestingly, HopAO1 was not predicted as having a nuclear localisation sequence when subject to extensive *in silico* analysis using online prediction tools. Furthermore, HopAO1 was not seen in the cytoplasm when analysed by either biochemical nuclei purification or confocal microscopy, despite numerous sources citing the effector as having function dependent on cytoplasmic localisation (Macho et al., 2014; Underwood et al., 2007). Therefore, while we posited that this effector's ability to disrupt circadian function may come as a result of its potentially being nuclear localised, we wanted to verify this localisation under our own experimental and environmental conditions before proceeding.

In order to verify the nuclear localisation of HopAO1, the effector was subcloned into the empty pEG104 N-terminal YFP fusion vector, along with the nuclear localised histone protein H2B in pGFP-Nbin C-terminal GFP fusion vector to act as a positive control for protein expression in the nucleus. The empty pEG104 vector (i.e. free YFP) was also used as a positive control for anti-YFP/GFP detection by the antibody. Note: unfused YFP is localised in both the nucleus and the cytoplasm on account of its being small enough to enter through nuclear pores and so does not act as an exclusive cytoplasmic marker, although it does act as a control for the ability to detect proteins in the cytoplasmic fraction (Hanson and Köhler, 2001). The constructs were each used to stably transform *A. tumefaciens*, which in turn was used to pressure infiltrate 4-5-week old *N. benthamiana* plants and so transiently express the protein fusions *in*

planta. Tissue was harvested 2 days following leaf infiltration and sub-cellular fractionation was achieved by suspending and centrifuging ground tissue in a high viscosity Ficoll-containing HONDA buffer. A fraction of the supernatant "upper" was retained to be the cytoplasmic fraction, while nuclei were purified from pellet and lysed by sonicating to produce the nuclear fraction. Immunoprecipitation (IP) of the nuclear fraction was performed using GFP-Trap beads. Cytoplasmic, nuclear and IP fractions were all subsequently visualised by immunoblot using α-GFP antibody to detect any GFP or YFP tagged fusion proteins.

In agreement with the previous study, our results indicate that *Pst* HopAO1 expressed in this way is localised to the nucleus, with clearly visible bands corresponding to the molecular weight of YFP-HopAO1 (~77.4 kDa) in both the nuclear and IP fractions (Figure 4.2). This is supported by the control lanes, which show free YFP in all 3 fractions, and the band corresponding to histone H2B localised only in the nuclear

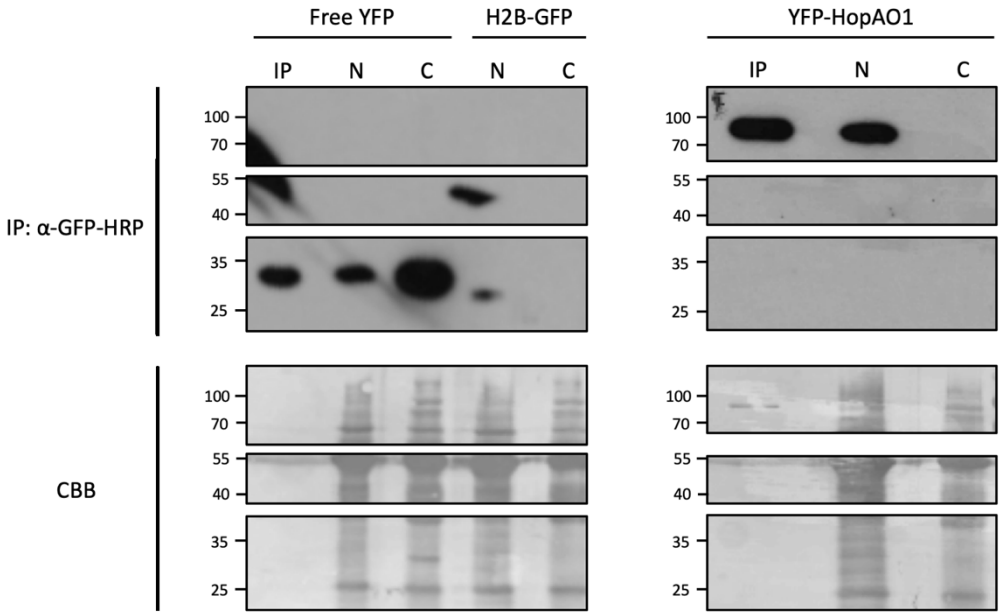

Figure 4.2: Visualisation of YFP-HopAO1 subcellular localisation by nuclear exclusion. Proteins were extracted from adult *Nicotiana benthamania* leaf tissue samples transiently expressing either free YFP (expected band ~26.4 kDa), H2B-GFP (expected band, ~42.8 kDa), or YFP-HopAO1 (expected band ~77.4 kDa). All cloned fragments were expressed under a 35S promoter and had either an N-terminal YFP tag (HopAO1 and free YFP) or a C-terminal GFP tag (H2B). Tissue was prepared for nuclear purification and subsequent immunoprecipitation using GFP-TRAP agarose beads. Cytoplasmic (C), nuclear (N) and IP fractions were assessed by immunoblot using α-GFP-HRP antibody. Successful purification of the nuclear fraction is shown by the presence of the histone protein H2B. Equal loading of subcellular input fractions is shown by Coomassie Brilliant Blue (CBB) stained membranes in lower panels. Results are representative of two repeat experiments.

fraction indicating the successful isolation of nuclei. A faint unexpected band was visible in the H2B nuclear input sample between 25 and 35 kDa, however given the molecular weight this is likely to simply be leaky GFP expression.

In order to further scrutinise the localisation status of HopAO1 the assay was also performed using a different expression vector and antibody detection system. In this way, any question of adequate nuclear purification or the efficacy the H2B detection could be dismissed. HopAO1 and GFP were subcloned into the HA tag fusion vector pEG201, with constructs again expressed *in planta* and subcellular fractions extracted and purified by IP using α-HA agarose beads prior to analysis by immunoblotting. An α-H3k27me3 antibody, which detects the methylated form of the H3 histone was used as a nuclear control. Although protein yield was lower overall, the same localisation patterns were observed (Figure 4.3). The methylated H3 histone was detected only in the nuclear fraction verifying successful nuclear purification, and HA-HopAO1

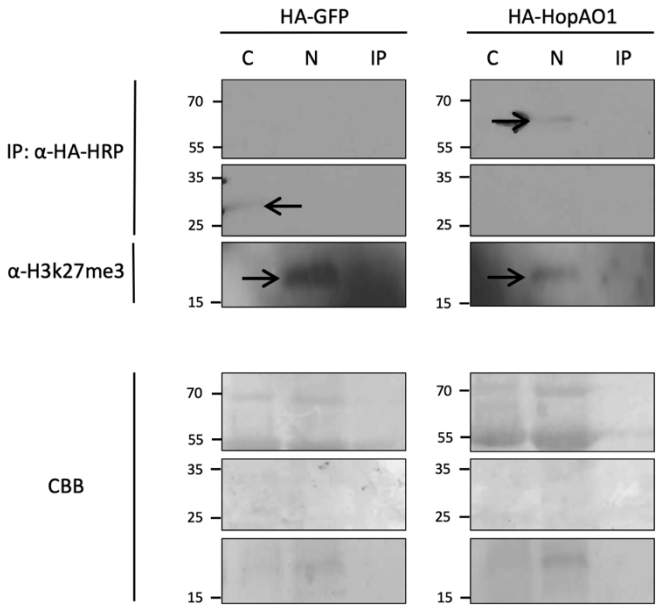

Figure 4.3: Visualisation of HA-HopAO1 subcellular localisation by nuclear exclusion. Proteins were extracted from adult *Nicotiana benthamania* leaf tissue samples transiently expressing either HA-GFP (expected band ~29 kDa) or HA-HopAO1 (expected band ~56.5 kDa). All cloned fragments were expressed under a 35S promoter and had an N-terminal HA tag. Tissue was prepared for nuclear purification and subsequent immunoprecipitation using α-HA agarose beads. Cytoplasmic (C), nuclear (N) and IP fractions were assessed by immunoblot using α-GFP-HRP antibody. Successful isolation of the nuclear fraction is shown by the presence of the methylated form of the histone protein H3, H3k27me3 (expected band ~17 kDa). Equal loading of subcellular input fractions is shown by Coomassie Brilliant Blue (CBB) stained membranes in lower panels.

produced a visible band at approximately the expected molecular weight of 56.5 kDa. HA-GFP produced a band only in the cytoplasmic fraction at ~29 kDa despite being known to also be nuclear localized, which we suggest is due to the lower overall protein yield, given that the assay shown in Figure 4.2 showed free YFP producing a stronger band in the cytoplasm than in the nuclear fraction.

Together, these results support previous findings that the *Pst* T3SE HopAO1 exhibits nuclear localisation under multiple expression systems *in planta* (Mastorakis, 2017). Furthermore, these results agree that despite as-of-yet unidentified function in the host nucleus and multiple sources supporting HopAO1 having binding partners in the cytosol (Underwood et al., 2007; Macho et al., 2014), expression of the effector in this way does not produce a detectable amount of the protein in the cytoplasmic fraction. Overall, this suggests that in *N. benthamiana* and *A. thaliana* HopAO1 is localised more strongly in the host cell nucleus and is perhaps more diffuse in the cytosol.

4.2.2 Identification of Pst HopAO1 binding partners in the plant cell nucleus

Having confirmed that the effector HopAO1 exhibits strong nuclear localisation *in planta* we next sought to identify its binding partners within the plant cell nucleus. In order to achieve this, we first set out to identify HopAO1 interacting partners *in planta* by mass spectrometry. For this, *N. benthamiana* leaves transiently expressing either YFP-HopAO1 or free YFP as a negative control were subjected to vacuum infiltration with formaldehyde. In this process, formaldehyde reacts with strong nucleophiles, such as lysine side chains or the amino groups on DNA bases to produce Schiff bases which then react with each other resulting in the covalent linking of intermolecular functional groups (Hoffman et al., 2015). This allows for the stabilisation of proteins in close proximity with each other, providing strong indications of protein-protein binding partners and can potentially permit the identification of even transiently formed complexes. An isolated nuclear fraction was obtained as previously described, and an IP was performed to purify free YFP and YFP-HopAO1, along with any interacting proteins. Peptide digestion was done overnight by in-gel trypsin enzyme incubation, and digested peptides were analysed by Liquid Chromatography

Electrospray Ionization Tandem Mass Spectrometry (LC-ESI-MS/MS). Free YFP-expressing samples were compared to those of YFP-HopAO1 such that unique peptide hits in the latter would be indicative of proteins binding specifically to HopAO1, and not to the YFP tag or the GFP-Trap beads.

It was hoped that identification of protein binding partners of HopAO1 from *in planta* nuclear protein extracts would inform us regarding its mechanism in the nucleus. Unfortunately, despite successfully identifying a significant abundance of unique peptide hits matching *Pst* HopAO1 in the test sample relative to the control, and YFP in both test and control samples, no other significant unique peptides were discovered in the test sample (Figure 4.4). This could be due to many reasons. Firstly, whenever chemical crosslinking is performed, the abundance of cross-linked peptides may represent only a very small proportion (<0.1%) of total theoretical peptide combinations within a sample (Zhang et al., 2009). This low abundance can occur as a result of too few pairs of specific residues able to be chemically crosslinked being

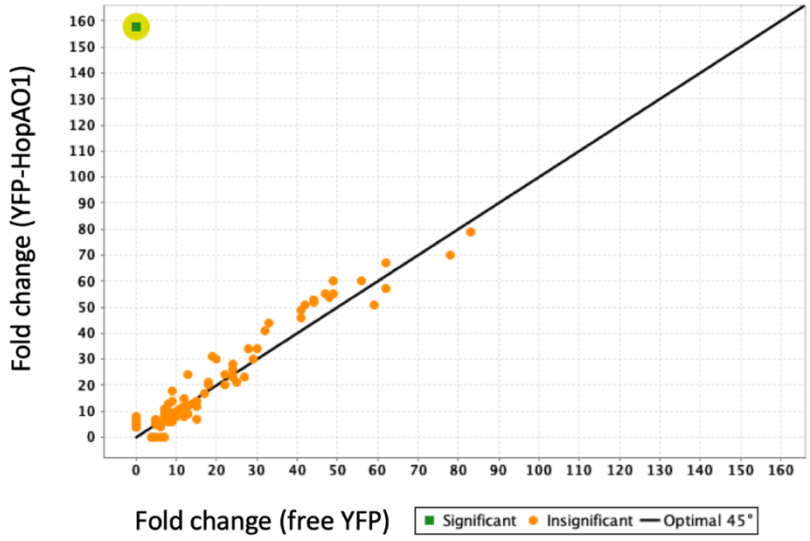

Figure 4.4: Mass spectrometric analysis of the peptide binding partners of nuclear HopAO1. Leaf tissue samples of adult N. benthamiana transiently expressing either free YFP or YFP-HopAO1 under the expression of a 35S promoter were formaldehyde crosslinked to stabilize protein-protein interactions then used to extract nuclear peptides. These peptides were subjected to immunoprecipitation using α-GFP-Trap agarose beads in order to purify HopAO1, free YFP and any associated peptides, and submitted for analysis by mass spectrometry in order to identify interacting partners. The fold change of detected proteins relative to the control (free YFP) and test (HopAO1) samples are plotted on the y and x axes, respectively, such that abundance of a detected unique peptide sequence within a sample is represented by distance from the optimal 45° line (which denotes equal abundance in both sample types). Significance of peptide fold change was calculated using Fisher's exact test ($p<0.01$, $p(Z<3.79) = 0.00022$) with multiple tests adjusted using Bonferroni's correction. HopAO1 is highlighted by the yellow circle. Results indicative of three experimental repeats.

physically close enough in the native protein structure to be cross-linked, even when in complex (Barysz and Malmström, 2018). Protein residues that are successfully cross-linked may also not in fact be linked at the same residues, creating a more complex sample in which significant unique peptide hits are fewer still, and the increased number of fragmentation combinations can further complicate their identification by producing spectra with low signal-to-noise ratios (Chen and Rappsilber, 2018; Wang and Schey, 2011). Thus, while HopAO1 and YFP may be are both highly expressed in the samples, identification of their unique protein interactions has the potential to present particular challenges depending on the orientation of cross-linkable residues in their respective complexes, or the complexity of said complexes' fragmentation patterns. It is also the case that any binding partners of HopAO1 associated with chromatin, such as histones or transcription factors, may not have been sufficiently enriched by this method.

Considering the important role of transcriptional regulation in the circadian clock, we therefore next chose to investigate the capacity of HopAO1 to bind to *A. thaliana* transcription factors. We adopted an approach in which HopAO1 interaction was tested against a library of *A. thaliana* transcription factors (Pruneda-Paz et al., 2014) by performing yeast 2-hybrid (Y2H) analysis according to the methodology published by Dreze et al. (2010). In this experiment, a library of 2016 transcription factor sequences isolated from *A. thaliana* were cloned into the prey vector pDEST-AD, containing an activation domain (AD) for the LYS2::GAL1-HIS3 reporter, and transformed into haploid Y8800 yeast. Expression of this reporter confers the ability to grow on media not supplemented with histidine, but only if the activation domain fused to the prey transcription factor protein comes into close proximity with the sequence by first binding to a bait protein. This bait protein (here HopAO1) was cloned into the pDEST-BD vector resulting in a HopAO1-binding domain (BD) fusion protein that binds to the GAL1-HIS3 reporter. When able to do so, HopAO1 additionally binds the prey transcription factor permitting reporter gene expression, and so, growth in the absence of histidine. Haploid Y8930 yeast containing the LYS2::GAL1-HIS3 reporter were transformed with this HopAO1 bait construct, and then mated with the prey TF-containing yeast before being inoculated into selective liquid media in 96 well plates. Growth of mated yeast in the absence of histidine, and in the presence of the HIS3 inhibitor, 3-amino-1,2,4-triazole (3AT) was assessed by measuring absorbance at

OD_{420} of each well using a plate reader. These absorbance readings were used to score interactions of HopAO1 across the transcription factor library, where growth above the level achieved by expression of HopAO1 and an empty prey vector negative control represented the baseline for comparison.

Of the 2016 transcription factors analysed using this Y2H system, we found HopAO1 was able to bind to 105 (Table 4.1). Those that displayed autoactivation on the basis of exhibiting growth when mated with an empty vector were omitted from analysis. Our primary focus was to identify interactors with the potential to regulate circadian rhythmicity, and so the 105 positively interacting proteins were analysed using the genome-wide time-series expression data mining resource DIURNAL (Mockler et al., 2007). This online tool encompasses the results of gene expression in common model plants including *A. thaliana* assessed by microarray time series and performed under a variety of standard light and temperature cycling conditions and assesses their expression patterns to determine rhythmicity and average phase. Genes encoding transcription factors that interacted with HopAO1 were searched for using DIURNAL, and where data was available, features of any detectable rhythmicity were noted in Table 4.1. Strength of amplitude in this DIURNAL-determined rhythmicity was determined as being "low", "mid", "high", or "very high" based on the height of each gene's peaks in normalized expression (see Supplementary Figure S4.1 for examples of these descriptions alongside representative expression profiles). Average phase for rhythmic expression profiles was quoted for genes whose expression peaks for available datasets all fell within a window of time lasting 6 hours or less (i.e. "phase ZT2-8" or "phase ZT3"). When the average phase of expression peaks was more variable than this amongst available datasets, genes are quoted as having various phases under different conditions. Similarly, when a gene was only rhythmic under one experimental condition, this is cited in the table (i.e. "ZT16, high, LD"), but if it was found to be rhythmic under multiple experimental conditions these are not listed in full for the sake of brevity (i.e. ZT2-4, mid, various conditions).

Table 4.1: *Pst* HopAO1 associates with *A. thaliana* transcription factors with rhythmic expression patterns and links to the circadian clock. (Overleaf) Binding partners of HopAO1 as determined by Y2H (see text for details) are listed, along with their TF family, expression rhythms, and publications reporting activity directly associated with the circadian clock. Transcription factors with clock-associated activity are highlighted in dark grey.

Gene name	TF family (Berardini et al., 2015)	Expression profile: phase, amplitude and experimental conditions (Mockler et al., 2007)	Circadian clock: References
AT1G68150	WRKY	-	-
AT5G26650	MADS	-	-
AT5G23260	MADS	ZT8, mid, short day	-
AT2G22760	bHLH	-	-
AT4G36900	AP2-EREBP	ZT8, mid, LL	-
AT5G08070	TCP	ZT22, mid, LD	-
AT2G44910	HB	ZT0, mid, short day	-
AT1G64380	AP2-EREBP	ZT22, mid, short day	-
AT3G14020	CCAAT/ CCAAT-HAP2/ CBFB_NFYA	-	-
AT3G30530	bZIP	-	-
AT1G06280	LOB/ AS2	-	-
AT5G15130	WRKY	-	-
AT3G27650	LOB/ AS2	ZT0, mid, long day	-
AT4G30080	ARF	ZT15, high, LD	-
AT1G69690 : TCP15	TCP	High, various phases and conditions	(Giraud et al., 2010)
AT1G08970	CCAAT/ CCAAT-HAP5	-	-
AT2G47460	MYB	Mid, various phases and conditions	-
AT3G17860	ZIM	High, various phases and conditions	-
AT4G02590	bHLH	ZT17-21, high, various conditions	-
AT1G14920 : GAI	GRAS	High, various phases and conditions	-
AT1G69170	SBP	ZT20-23, mid, various conditions	-
AT5G24110	WRKY	ZT11-16, low, various conditions	-
AT5G65790	MYB	-	-
AT2G01570 : RGA1	GRAS	Very high, various phases and conditions	(Wu et al., 2008)
AT5G60970	TCP	ZT2-4, mid, various conditions	-
AT5G16560	G2-like	ZT13, mid, LL	-
AT5G07310	AP2-EREBP	Mid, various phases and conditions	-
AT1G58100 : TCP8	TCP	ZT18-22, high, various conditions	(Wu et al., 2016)
AT3G07650	C2C2-CO-like	ZT14-17, very high, various conditions	-
AT2G23760	HB	ZT8-11, high, various conditions	-
AT2G45680	TCP	-	-
AT2G31070	TCP	ZT21-4, high, various conditions	-
AT1G03040	bHLH	ZT17-19, high, various conditions	-
AT2G20880	AP2-EREBP	-	-
AT1G31630	MADS	-	-
AT2G02540	zf-HD	-	-
AT1G48500	ZIM	low, various phases and conditions	-
AT4G27330	NOZZLE/ NZZ	ZT5, low, LL	-
AT2G28610	HB	ZT10, low, LD	-
AT4G15248	Orphans	-	-
AT5G50470	CCAAT/ CCAAT-HAP5	ZT6, low, long day	-
AT4G04450	WRKY	ZT7-8, low, various conditions	-
AT1G21970	CCAAT/ CCAAT-HAP3	-	-
AT3G02150	TCP	ZT22-1, high, various conditions	-
AT5G18560	AP2-EREBP	ZT2, low, LL	-
AT1G18400	bHLH	Mid, various phases and conditions	-
AT5G60120	AP2-EREBP	High, various phases and conditions	-
AT1G68510	LOB/ AS2	-	-
AT2G22800	HB	ZT23-1, mid, LD	-
AT5G03150	C2H2	Mid, various phases and conditions	-
AT1G15050	AUX-IAA	ZT5-7, low, LL	-
AT2G42280	bHLH	ZT16, high, LD	-
AT5G60440	MADS	-	-

Gene name	TF family (Berardini et al., 2015)	Expression profile: phase, amplitude and experimental conditions (Mockler et al., 2007)	Circadian clock: References
AT1G19270	Orphans/ LIM	ZT7-11, mid, various conditions	-
AT5G13330	AP2-EREBP	-	-
AT1G66350	GRAS	High, various phases and conditions	-
AT5G26805	REM(B3)	-	-
AT2G40970	G2-like	ZT1-7, mid, various conditions	-
AT3G51180	ND	-	-
AT5G39820	NAC	-	-
AT3G25790	G2-like	-	-
AT1G19180 : JAZ1	ZIM	High, various phases and conditions	(Grundy et al., 2015)
AT1G72210	bHLH	-	-
AT3G13960	GRF	ZT10-14, low, various conditions	-
AT5G14170	SWI/SNF-BAF60b	High, various phases and conditions	-
AT1G24260	MADS	ZT11, low, LL	-
AT2G40740	WRKY	ZT20, low, long day	-
AT2G01200	AUX-IAA	ZT11, low, DD	-
AT3G18550	TCP	-	-
AT3G12910 : NAM	NAC/ NAM	ZT10-16, low, various conditions	(Davies, 2013)
AT5G17810	HB	-	-
AT2G33880	HB	ZT15, low, LD	-
AT3G27010	TCP	Mid, various phases and conditions	-
AT1G24590	AP2-EREBP	-	-
AT1G32240	G2-like	ZT16-21, mid, various conditions	-
AT2G22840	GRF	ZT8, mid, various conditions	-
AT2G02450	NAC	ZT8, mid, LD	-
AT1G67710	ARR-B	Mid, various phases and conditions	-
AT2G27050 :EIL1	EIL	High, various phases and conditions	(Covington et al., 2008)
AT5G03220	MED7	High, various phases and conditions	-
AT5G10510	AP2-EREBP	Mid, various phases and conditions	-
AT1G43160	AP2-EREBP	ZT4, high, long day	-
AT3G49690	MYB	ZT3, low, long day	-
AT4G37180	G2-like	ZT5-8, mid/high, various conditions	-
AT5G51910	TCP	Mid, various phases and conditions	-
AT3G50510	LOB/ AS2	-	-
AT1G20696	HMG	ZT12-16, very high, various conditions	-
AT4G22070	WRKY	-	-
AT3G18650	MADS	-	-
AT4G32570	ZIM	ZT0-21, very high, various conditions	-
AT4G32010	ABI3-VP1	ZT17, mid, various conditions	-
AT3G16857	ARR-B	Mid, various phases and conditions	-
AT3G54220	GRAS	ZT22-3, high, various conditions	-
AT1G73360	HB	ZT8, low, short day	-
AT5G41410	HB	High, various phases and conditions	-
AT4G04885	C2H2	-	-
AT5G66630	Orphans/ LIM	ZT20-23, low, LD	-
AT5G64750	AP2-EREBP	-	-
AT5G23280	TCP	-	-
AT1G12980	AP2-EREBP	-	-
AT4G31920	ARR-B	-	-
AT5G08330 : CHE	TCP	Very high, various phases and conditions	(Pruneda-Paz et al., 2009)
AT4G03250	HB	-	-

Amongst those transcription factors indicated as associating with HopAO1 were several of interest within the scope of the current study. TFs with published activity relating to the circadian clock were specifically highlighted in Table 4.1 such as CHE (AT5G08330), the TOC1 chaperone required for its repression of the CCA1/LHY morning complex as well as for induction of the SA biosynthesis gene *ics1* (Zheng et al., 2015). Further identified interactors with clock associations were NAM (AT3G12910), a NAC family transcription factor with diurnal rhythmic expression patterns that is known to bind to the promoter of *LHY* (Davies, 2013), TCP15 (AT1G69690) which binds both to PRR1 and PRR5 as well as the negative immune regulator *SUPPRESSOR OF rps4-RLD1* (*SRFR1*) (Giraud et al., 2010; Kim et al., 2014), and TCP8 (AT1G58100) which binds clock proteins LWD1 and LWD2 (Wu et al., 2016).

Other interactors of note both for their shared function and links to the circadian clock are REPRESSOR OF GA1-3 1 (RGA1, AT2G01570), JASMONATE-ZIM-DOMAIN PROTEIN 1 (JAZ1, AT1G19180), and ETHYLENE-INSENSITIVE3-LIKE 1 (EIL1, AT2G27050). Transcription factor RGA1 is differentially expressed in *lwd1lwd2* double mutants (Wu et al., 2008), while JAZ1 is directly regulated by TOC1 (Grundy et al., 2015), and EIL1 transcripts are also thought to be under circadian control (Covington et al., 2008). However, the three are also heavily involved in gibberellin (GA), jasmonate (JA) and ethylene (ET) hormonal signalling pathways respectively. Along with another HopAO1-interacting TF with high rhythmic expression patterns, GIBBERELLIC ACID INSENSITIVE (GAI, AT1G14920), these transcription factors form a close network with experimentally determined interactions amongst each other (Figure 4.5). Interestingly, GAI and NAM are also known to interact with one another (Rosa et al., 2014). These results prompted us to question whether NAM is able to act as a point of feedback between the circadian clock and maintaining the balance in hormonal biosynthesis that determines host susceptibility to biotrophic versus necrotrophic pathogens, as this could account for it being targeted by *Pst* HopAO1, amongst the other aforementioned TFs in this network. Previous work has suggested that NAM may recruit other TFs to repress the *lhy* promoter, so it could be that NAM associates with GAI in order to repress *lhy* in a way that is dependent on GA levels, since DELLA proteins accumulate in the absence of GA (Davies, 2013; Silverstone et

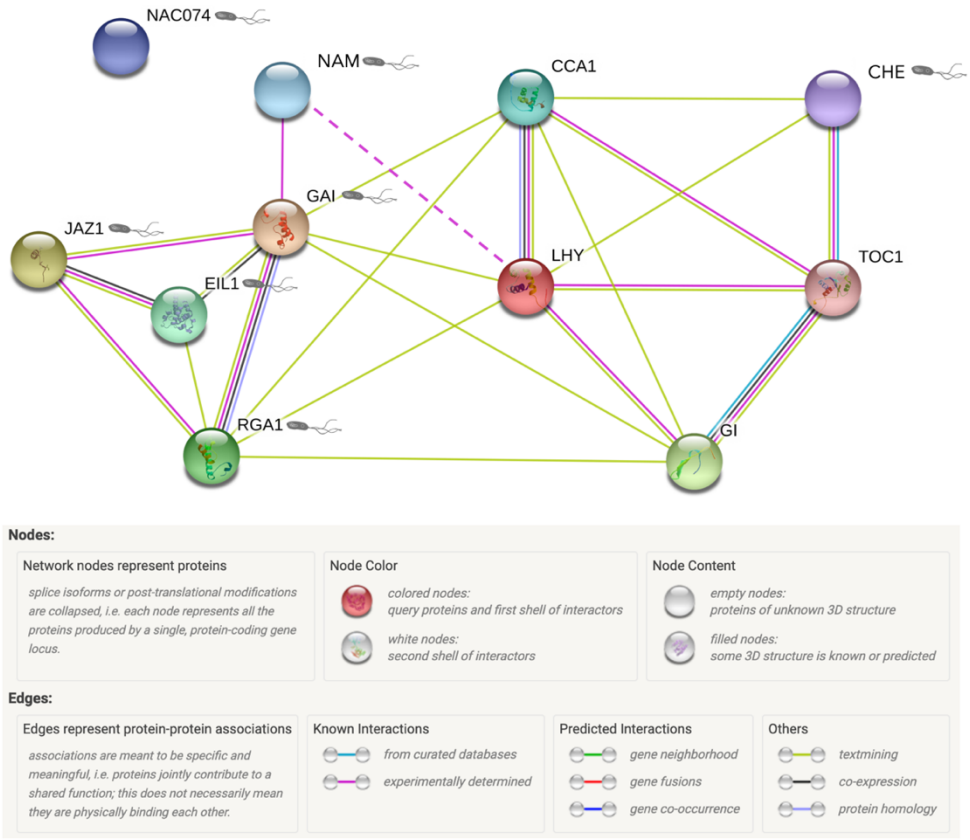

Figure 4.5: A close network of associations exists amongst HopAO1 interactors with roles in hormone signaling and the circadian clock. A STRING interaction network was constructed whereby nodes represent input proteins, and coloured edges between nodes (see key above) denote different methods of detecting known protein interactions and associations. Input proteins used were core clock components CCA1, TOC1, GI and LHY, as well as Y2H verified HopAO1-binding partners from the current study (denoted by bacterium icon) NAM, NAC074, CHE, GAI, JAZ1, EIL1 and RGA1. Solid lines represent associations made using the STRING database, while the dashed line between NAM and LHY indicates an interaction experimentally verified in an academic thesis outside of STRING textmining sources (Davies, 2013).

al., 2001). In turn, DELLA protein expression is reported to be under circadian control, with transcript levels greatly diminished in *lhy* single mutants (Arana et al., 2011).

Ensuring the repeatability of notable interactions revealed in this study was essential in order to minimise the likelihood of incorrect interpretation of false discoveries. We therefore decided to next reassess the binding of HopAO1 to NAM by Y2H, this time on solid media, also testing HopAO1 versus 3 other NAC transcription factors of different degrees of phylogenetic closeness to NAM (Figure 4.6). These were NAM's two closest relatives in the NAC TF family, AT2G43000 and AT4G28530, and one more distant member AT3G12977 (Figure 4.6, A). In this version of the Y2H assay,

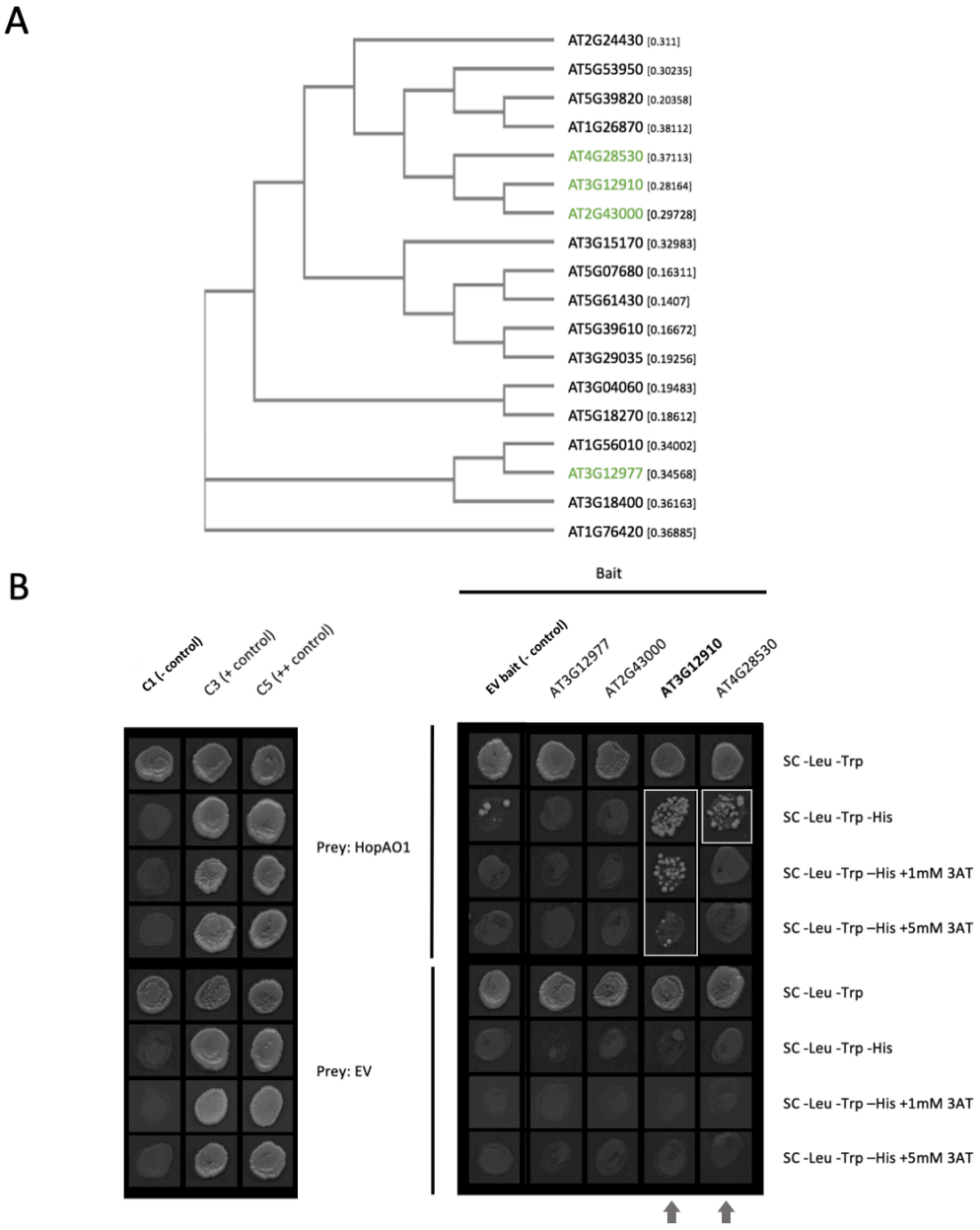

Figure 4.6: HopAO1 specifically binds to *Arabidopsis thaliana* NAC transcription factors NAM (AT3G12910) and NAC074 (AT4G28530). A) Sequences of all 18 members of an *A. thaliana* NAC domain transcriptional regulator family (PTHR31744,Mi et al., 2010) were obtained by BLAST searching using NCBI BLAST, then sequence alignments were performed with Clustal Omega and used to generate a phylogenetic tree using the EMBL-EBI Simple Phylogeny tool (Zerbino et al., 2018). Highlighted in green are those transcription factors assayed here by yeast two-hybrid (Y2H). Numbers in brackets represent branch length. B) Haploid Y8930 yeast containing the LYS2::GAL1-HIS3 reporter constructs and transformed with the vector pDEST-BD (either empty vector or containing the HopAO1 gene) were independently mated with Y8800 yeast containing a selection of NAC transcription factors in pDEST-AD vectors, and inoculated onto solid selective media. NAM (AT3G12910) is highlighted in bold. Bait constructs permit the growth of yeast on Tryptophan, and prey on Leucine. If yeast are successfully mated and contain both a prey and bait construct, they may grow without supplemented Tryptophan and Leucine. Interaction of the tested proteins will also permit growth in the absence of Histidine. Strength of interactions is indicated by growth in the presence of the HIS3 inhibitor, 3AT. Images of spotted yeast culture shown are representative of 3 technical replicates within one experiment, and of three sperate experiments run on different days.

strength of interaction was also tested by comparing the extent of growth on increasing concentrations of 3AT, where greater amounts of the HIS3 inhibitor would increasingly limit the capability of mated yeast cultures to grow making the presence of visible growth indicative of a stronger interaction between HopAO1 and the bait TFs. In agreement with the results of the high throughput Y2H screen versus HopAO1, this smaller scale assay found the effector to strongly bind to NAM (Figure 4.6, B). HopAO1 was also able to bind to NAC074, however not to either of the other two NAC TFs assayed, including its closest phylogenetic relative, NAC042 (AT2G43000). The results of this experiment indicate that the *Pst* effector HopAO1 is able to bind to NAM, and to a lesser degree NAC074 but not to a more distant member of the TF family.

Taken together the results of this section have found that HopAO1 is able to bind to a number of transcription factors in the plant cell nucleus. Among these are a notable proportion of target proteins both with roles in the biosynthesis of various hormones and experimentally verified links to the circadian clock, and that exist in a close interaction network. Of these binding partners, the NAC transcription factor NAM, which is known to interact with members of both these functional networks, is here shown to be bound by HopAO1 in a way that is robust and specific.

4.2.3 Characterising the molecular basis of the effector HopAO1's induced circadian phenotype in A. thaliana

We have shown in the present study that the *Pst* effector HopAO1 is able to specifically bind the *A. thaliana* NAC transcription factor NAM, which in turn is known to directly associate with the promoter region of core clock gene *LHY* (Davies, 2013). Given that HopAO1 has characterised enzymatic function as a tyrosine phosphatase we therefore next sought to perform *in silico* analysis of NAM, along with the other three NAC TFs assessed by Y2H in the previous section (AT2G43000, AT4G28530, and AT3G12977) to search for tyrosine residues within their structures that may be predicted to undergo phosphorylation *in planta*, and so potentially be dephosphorylated by HopAO1. This was achieved through the use of the PhosPhat 4.0

online resource (Durek et al., 2010). This protein phosphorylation site database contains information on *A. thaliana* phosphorylation sites that have been identified by mass spectrometry in large scale experiments across various research groups and incorporates a built-in phosphorylation site predictor trained on the serine, threonine and tyrosine phosphorylation experimental dataset. Amino acid sequences of the four NAC TFs were submitted to the phosphorylation site prediction software, where the output was an amino acid sequence with likely residues for phosphorylation highlighted, as well as common motifs, and phosphorylation hotspots previously identified within the *A. thaliana* proteome (Figure 4.7, A). These residues were compared to a global Multiple Sequence Alignment analysis achieved using Clustal Omega (Madeira et al., 2019) to identify any commonality of residues once conserved protein domains had been aligned (supplementary Figure S4.2). A number of tyrosine residues with predicted phosphorylation scores were identified in all four of the transcription factors assessed, however there were no tyrosine residues was found to be present only in those TF's bound by the effector and tyrosine phosphatase HopAO1. This indicates that while HopAO1 may be able to bind both NAM and NAC074 in a way that is specific, this interaction is independent of its ability to dephosphorylate a conserved tyrosine residue, and is instead grounded by other conserved residues that do not participate in an enzymatic reaction. Given however, that HopAO1 binds more strongly to NAM than to NAC074, we could reason that HopAO1 may able to genuinely dephosphorylate NAM, whereas NAC074 is simply sufficiently structurally similar to be bound, but not dephosphorylated by HopAO1, and instead acts as a competitive inhibitor of the tyrosine phosphatase as a way of limiting its virulent action, if NAM and NAC074 were found to be functionally distinct. These results suggest that when HopAO1 specifically binds NAM and NAC074 in preference to other NAC TFs, it may be able to dephosphorylate this single conserved tyrosine residue associated with potential phosphorylation status. The sequences of proteins GAI, RGA1, EIL1, JAZ1 and CHE were also submitted for phosphorylation prediction using PhosPhat, and each possessed at least one tyrosine residue with potential for phosphorylation in agreement with their being bound by HopAO1 (Supplementary Figure S4.3).

Not much is known about the function of the NAC family transcription factor NAM. NAM has a low amplitude diurnal expression pattern (Table 4.1), is highly expressed

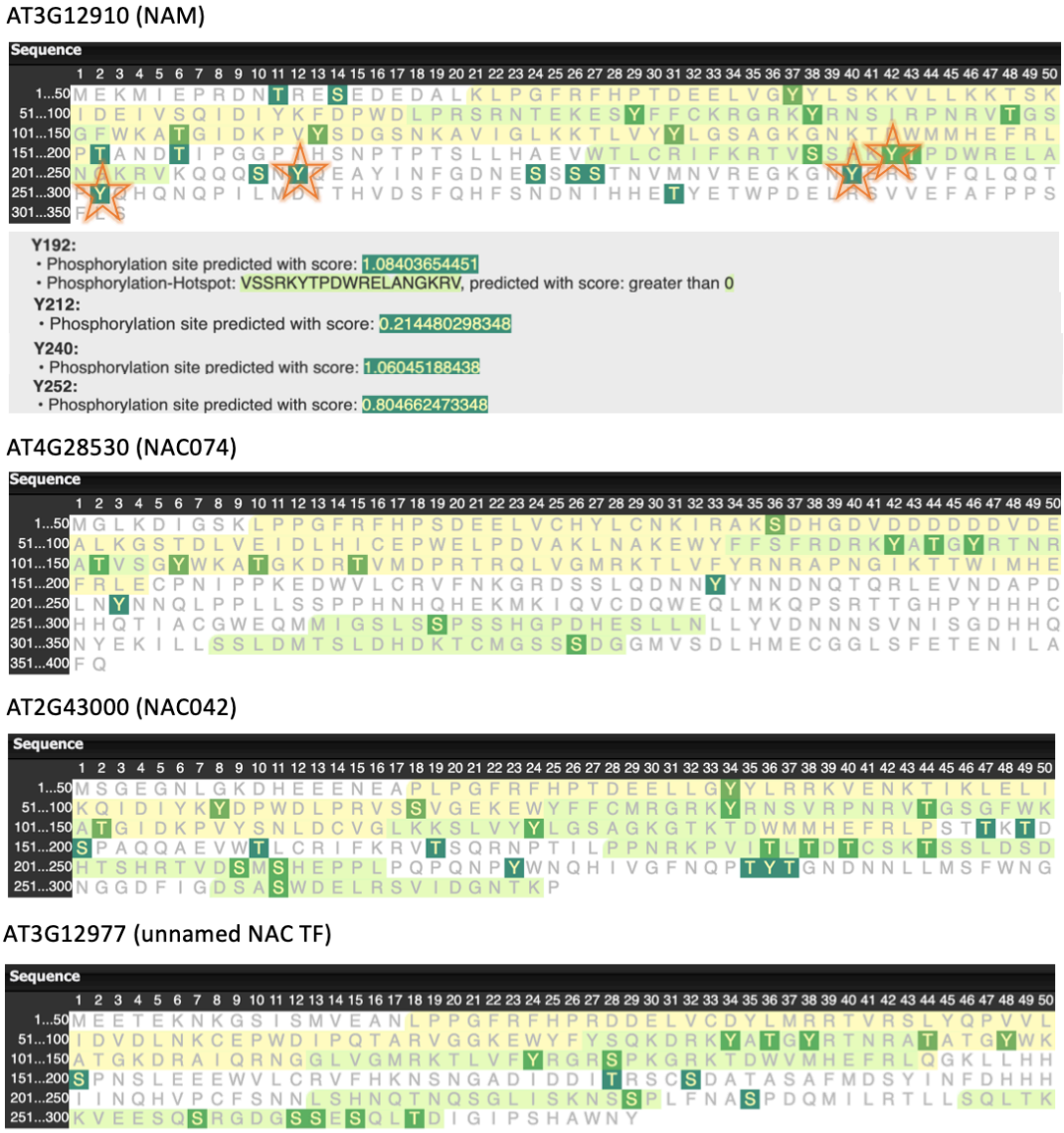

Figure 4.7: NAC transcription factors bound by HopAO1 do not share any common tyrosine residues predicted to be subject to phosphorylation. A) The four NAC transcription factors assessed by Y2H for binding to HopAO1 were analysed using the phosphorylation site database and predictor (Phosphat) to identify residues predicted to be phosphorylated. No phospho-tyrosine was shared exclusively by those NACs that were bound by HopAO1, NAM and NAC074, however four residues were found to be exclusive to NAM. These residues are highlighted with a star, with phosphorylation prediction scores reported below. Yellow highlighted regions represent the conserved NAM protein family domain. Green highlighted regions denote phosphorylation hotspots.

in the senescent leaf (Klepikova et al., 2016), and was shown to have its expression negatively regulated by a trio of NACs that repress senescence and its promoting processes including SA and ROS responses (Kim et al., 2018). NAM has also been shown to bind to the promoter of clock gene *LHY,* mutants of which are known to exhibit accelerated leaf yellowing senescent phenotype (Davies, 2013; Song et al., 2018). It therefore seems plausible that NAM would exert regulatory action on the

LHY promoter in order to induce responses associated with the onset of senescence. In consideration of this, we next chose to verify NAM's ability to bind to the *LHY* promoter, similarly assessing binding capability of NAC074, which while largely uncharacterised has been linked to the activation of PCD-related genes and senescence in stigma cells (Gao et al., 2018). We hypothesised that if HopAO1 was able to bind to two relatively conserved transcription factors with comparable functional links, the two may possess shared functionality at the *LHY* locus. In order to do this, we performed a Y1H assay in which the promoter region of the *LHY* gene was cloned upstream of a *his3* reporter (using the pHis3Leu2 vector), such that binding of the promoter by a bait protein with a fused activation domain would permit the activation of *his3*, and so growth of the mated yeast on media lacking histidine. Bait constructs used in this assay expressed fusion proteins of both NAM and NAC074, as well as HopAO1 and a GFP negative control to use as a baseline for significant growth. Mated yeast cultures were grown on increasing amounts of 3AT to test the strength of interactions.

In agreement with previously reported findings by Davies (2013), expression of NAM was able to permit growth at a higher concentration of 3AT than yeast expressing the GFP negative control, indicating the capability for NAM to bind to *pLHY* (Figure 4.8). Furthermore, HopAO1 was also able to associate with *pLHY* in yeast. NAC074 however, was not seen to permit significant growth on 3AT supplemented media above that of the GFP control, and so may not directly associate with *pLHY*, in spite of its conserved sequence with NAM and association with HopAO1. This suggests that HopAO1 is able to bind to the promoter of clock gene *LHY*, even in the absence of NAM (as *Saccharomyces cerevisiae* lack a NAM homolog). Additionally, while the NAC transcription factor NAM alone is able to bind to *pLHY*, NAC074 is not.

Next we wanted to investigate whether or not HopAO1 was able to alter the binding of NAM to the *LHY* promoter by employing a modified yeast one-hybrid assay (previously described in Davies, 2013). In this assay, a third construct containing a protein with no binding or activation domain, but that confers the ability to grow without supplemented adenine is also transformed into the Y8800 yeast along with that containing the prey transcription factor. In this way, the third protein is present, and its transformation can be tested using selective media lacking adenine. Since this

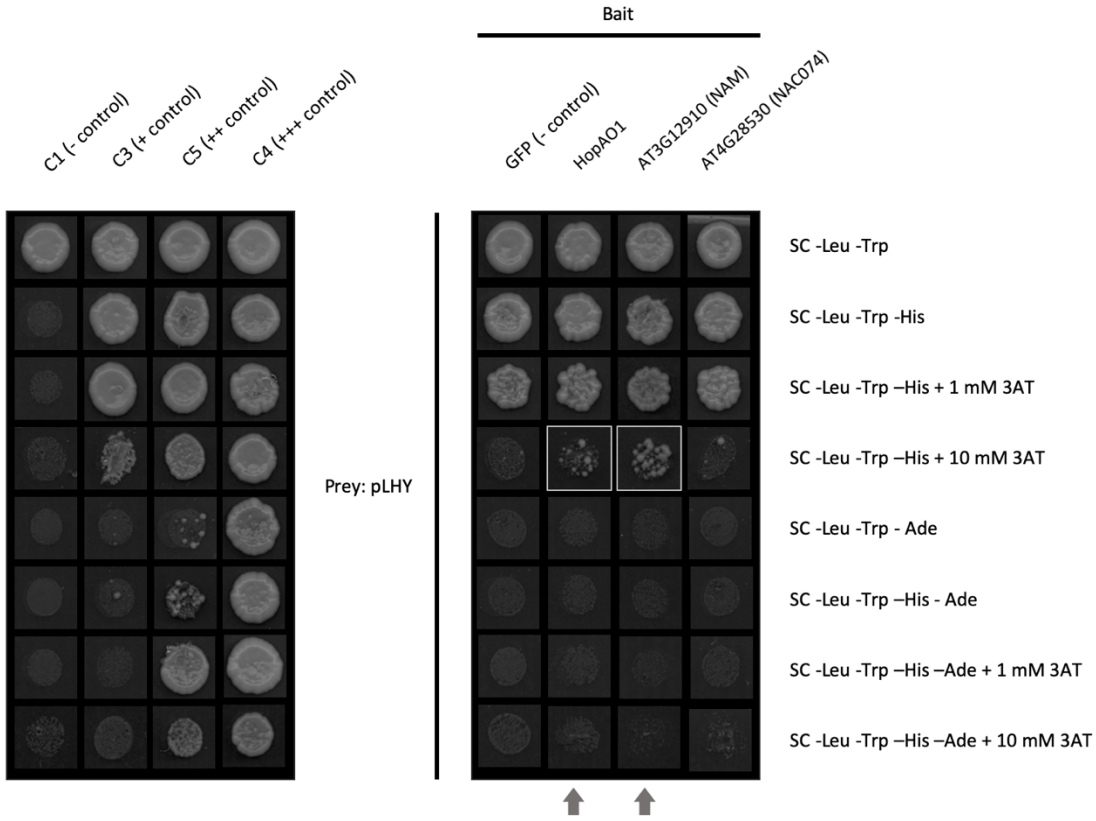

Figure 4.8: HopAO1 and NAM both associate with the LHY promoter. Haploid Y8930 yeast transformed with the reporter construct (the LHY promoter region in the pHis3Leu2 vector) were independently mated with Y8800 yeast transformed with a prey construct (HopAO1, NAM, NAC074 or GFP negative control, in pDEST-AD) and inoculated onto solid selective media. The pHis3Leu2 vector confers the ability to grow on media lacking leucine, as well as histidine provided that the prey protein associates with the bait sequence. The pDEST-AD constructs confer the ability to grow on media lacking tryptophan. Neither construct permits growth in the presence of adenine. Strength of interactions is indicated by growth in the presence of the HIS3 inhibitor, 3AT, as well as by comparison to the controls C1, C3, C5, and C4 which exhibit negative, moderate, strong, and very strong interactions respectively. The growth of negative control GFP represents a baseline, above which the level of inhibition by selective media is significant. Images of spotted yeast culture shown are representative of 3 technical replicates within one experiment, and of two sperate experiments run on different days.

third protein lacks an activation or binding domain, the only way it can impact growth of the mated yeast on media lacking histidine or containing 3AT is if its encoded protein is capable of enhancing or inhibiting the binding of the transcription factor to the bait *pLHY* sequence. To this end, Y8800 haploid yeast transformed with either NAM, NAC074 or a GFP negative control within the pDEST-AD vector was subsequently transformed with either HopAO1 or GFP within the pARC352 vector, conferring only adenine synthesis. This was then mated with Y8930 yeast containing the *pLHY* in the pHIS3LEU2 reporter vector such that mated yeast might grow on

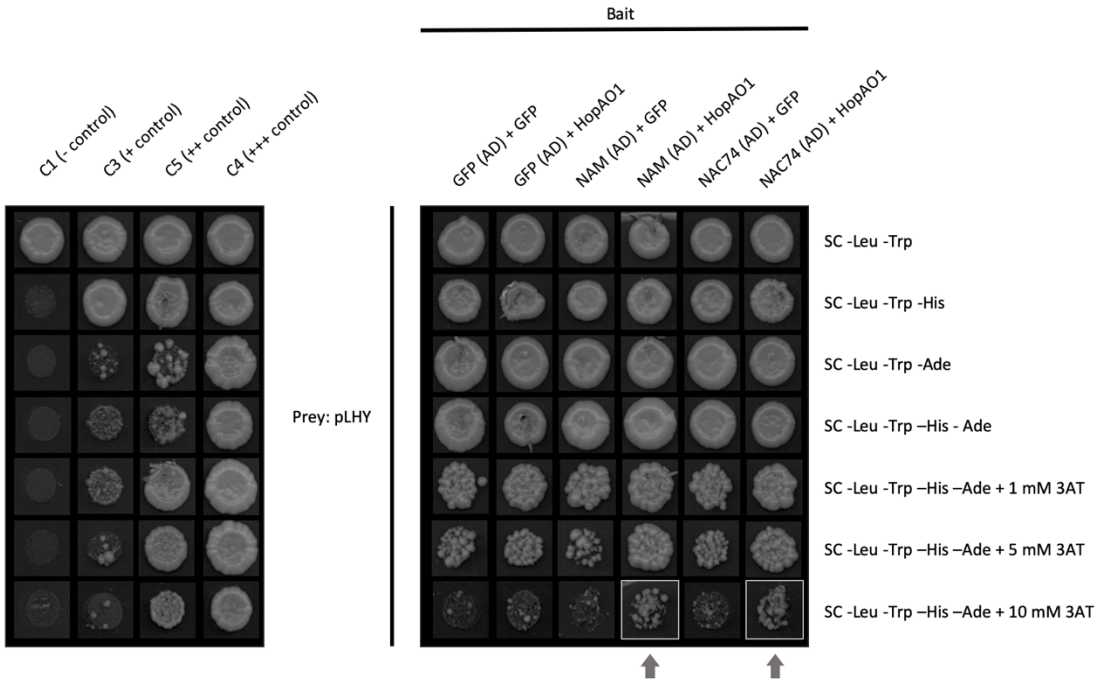

Figure 4.9: HopAO1 enhances the binding of NAM and NAC074 to the LHY promoter. Haploid Y8930 yeast transformed with the bait reporter construct (the LHY promoter region in the pHis3Leu2 vector) were independently mated with Y8800 yeast that had been sequentially transformed with both a prey (NAM, NAC074 or GFP negative control, in pDEST-AD), and an "enhancer" construct (HopAO1 or GFP control in pARC352- no AD) and inoculated onto solid selective media. The pHis3Leu2 vector confers the ability to grow on media lacking leucine, as well as histidine provided that the prey protein associates with the bait sequence. The pDEST-AD constructs confer the ability to grow on media lacking tryptophan. The pARC352 constructs permit growth in the absence of adenine. Strength of interactions is indicated by growth in the presence of the HIS3 inhibitor, 3AT, as well as by comparison to the controls C1, C3, C5, and C4 which exhibit negative, moderate, strong, and very strong interactions respectively. The growth of negative control GFP represents a baseline above which the level of inhibition by selective media is significant. Images of spotted yeast culture shown are representative of 3 technical replicates within one experiment, and of two sperate experiments run on different days.

media without leucine, tryptophan, adenine, and only histidine should the prey protein sufficiently activate expression of the HIS3 reporter.

It should be noted that the positive controls C3, C4, and C5 are able to grow on adenine (albeit often at an impaired rate), however they are expressed in yeast carrying a mutation in the *ade1* gene within the adenine biosynthesis pathway which leads to the accumulation of a red pigment in cells (Ugolini and Bruschi, 1996). This red colour was very much visible in all three of the positive controls as a halo around growing spots, but in none of the mated yeast cultures used to test *pLHY* binding, and so the controls' ability to grow on media without added adenine is not indicative of an inability to select for uptake of the pARC352 construct on adenine-lacking media,

particularly at earlier stages of growth. Colour images of the Y1H screen are not shown in order to minimise the appearance of light refraction when imaging plates.

It was found that HopAO1 was able to enhance the binding of both NAM and NAC074 to the *LHY* promoter (Figure 4.9). When the prey transcription factors were co-transformed alongside HopAO1 as opposed to the GFP in pARC352 negative control, growth of the culture was more extensive. Additionally, this enhancement effect appeared to be specific, as HopAO1 was not able to enhance the binding of GFP expressed within the pDEST-AD vector in the same way.

Taken together, the results presented in this section indicate that NAM, a NAC family transcription factor is able to bind to the promoter of core clock gene *LHY* in yeast, and that this binding is enhanced by the co-expression of *Pst* T3SE HopAO1. HopAO1 also enhances the binding of another NAC transcription factor, NAC074 to the *LHY* promoter, although NAC074 was unable to bind *pLHY* unaided by HopAO1 in the yeast system. This may simply be indicative of limitations in the yeast 1 and 2-hybrid assays, reducing the appearance of interactions within a yeast system (particularly given HopAO1's weaker interaction with NAC074 in comparison to NAM). Alternatively, this may suggest that HopAO1 is able to recruit NAC074 to the *LHY* promoter even though it does not bind there unassisted. NAM and NAC074 did not share any single conserved tyrosine residues predicted to be subject to phosphorylation in *A. thaliana* that were not also shared by two other NAC transcription factors of both close and distant phylogenetic relation that were unable to bind HopAO1. This suggests that dephosphorylation of these two TFs alone by HopAO1 is not the cause of their enhanced binding to *pLHY* in the presence of the effector, but that instead their specific binding by HopAO1 is likely due to the effector interacting with them by orienting itself on other conserved residues, and that NAC074 may even compete with NAM for its active site.

4.3 Discussion

The results of Chapter 3 presented evidence for HopAO1 possessing novel function disrupting the circadian clock. While HopAO1 has been characterised extensively in the plant cytosol, it has only once been documented as having nuclear localisation (Mastorakis, 2017). The aims of this chapter were therefore to confirm the nuclear localisation of HopAO1 and elucidate the nature of its function in the nucleus. It was hoped that identification of nuclear binding partners of the *Pst* effector would provide insight into a novel mechanism by which it directly or indirectly targets the circadian clock.

4.3.1 HopAO1 exhibits nuclear localisation, and is able to bind to a suite of functionally close A. thaliana transcription factors with links to hormone homeostasis, senescence and the clock

The localisation of HopAO1 in the plant cell nucleus verified within this study and in confirmation of the observations made by Mastorakis (2017) provides evidence for as-of-yet unidentified function for the effector within the plant host. It is interesting that in spite of functional analysis of HopAO1 supporting cytoplasmic localisation, both of these studies appear to find HopAO1 to be localised much more strongly in the nucleus than the cytoplasm. Whilst for the effector to reach the nucleus it must, of course, first migrate there from the cytoplasm following injection into the host cell by the type III secretion system (Cornelis, 2006), it is nonetheless surprising that nuclear function of HopAO1 has yet to be investigated prior to the current study. It is notable that previous analysis of subcellular localisation by confocal microscopy (Figure 4.1, B; Mastorakis, 2017) indicates that HopAO1 may also localise to the chloroplast, where circadian dysfunction could be achieved through interference with ICS1 and the pathogen-induced SA biosynthesis pathway (Strawn et al., 2007). The nuclear compartment, however, provides further scope for manipulation of host circadian rhythmicity by HopAO1, particularly through post-translational modifications of proteins involved in the regulation of clock output pathways, and the TTFL itself.

The high proportion of transcription factors found able to bind to HopAO1 does raise some questions regarding the validity of the high throughput Y2H screen (Table 4.1). Although reports on data from the Molecular INTeraction (MINT) Database suggest that 22.8% of all proteins interact with at least 5 other proteins, and hub proteins of considerably higher connectivity than this do occur (Chatr-aryamontri et al., 2007; Keskin and Nussinov, 2007), the wide array of TF families bound by HopAO1 introduces a certain degree of doubt. Y2H assays are often associated with high rates of false positive discovery. This is particularly true of high throughput analyses where coding sequences of target inserts within a large library such as in this study can unintentionally be expressed in the wrong reading frame, or untranslated regions (UTRs) resulting in the positive scoring of nonspecific interactions (Koegl and Uetz, 2008). Thus, while the interactions of NAM and NAC074 were subject to extensive repeats to provide further assurance of true interaction, the results of the original 2000+ transcription factor screen may include some false positives. However, among the extensive list of interacting partners is a notable enrichment of certain transcription factor families, particularly of TCPs (11 bound), AP2-EREBPs (12 bound), and to a lesser extent, GRASs (4 bound). Additionally, the associative network of several of the transcription factors bound by HopAO1 (Figure 4.6), which contains two GRAS and two TCP family TFs, supports a genuine role for the effector targetting proteins potentially linking the clock and hormone biosynthesis.

Of these, the GRAS family members RGA, GAI, and a third HopAO1 interactor without clock association, RGL1 (AT1G66350) all belong to a subgroup of GRAS protein homologs known as DELLA proteins, so called for their D-E-L-L-A amino acid N-terminal sequence, which is highly conserved across many plant species including rice, barley and maize (Locascio et al., 2013; Sun and Gubler, 2004). The DELLA proteins are often called “pseudo-transcription factors” on account of the fact that they are not known to target any particular DNA motif or possess a clear DNA-binding domain themselves, but instead regulate gene expression by interacting with other transcription factors as co-activators or corepressors (Sun and Gubler, 2004). One such example is the recruitment of RGA by type-B ARABIDOPSIS RESPONSE REGULATORS (ARRs), also associating with GAI, where they act as a coactivators of cytokinin-regulated genes (Marín-de la Rosa et al., 2015). DELLA proteins are known as repressors of GA signalling in plants (Hussain and Peng, 2003), making

them capable of regulating a wide variety of physiological processes including cell proliferation and expansion, ROS accumulation, and salinity stress response (Achard et al., 2009, 2008, 2006). Their stability has been shown to be controlled by phosphorylation and dephosphorylation, whereby DELLAs are targetted for degradation, subsequently lifting their repression on GA pathways (Qin et al., 2014). Loss of function DELLA mutants produce phenotypes akin to that of continuous GA application, with massive increases in stem growth, early flowering and leaf expansion (Locascio et al., 2013; Dill and Sun, 2001).

In defense *A. thaliana* DELLA mutants exhibit higher levels of SA-dependent resistance to *P. syringae*, but enhanced susceptibility to a necrotrophic fungal pathogen, *Alternaria brassicola* (Navarro et al., 2008). This has led to the idea that DELLAs may modulate the balance between SA and JA signalling, which causes a trade off in levels of susceptibility and resistance to biotrophs and necrotrophs, respectively (Navarro et al., 2008; De Bruyne et al., 2014). It therefore seems plausible that HopAO1 might dephosphorylate the DELLA homolog proteins GAI, RGA and RGL1 in order to prevent their being targetted for degradation, resulting in repression of GA signalling and so preventing biotrophic pathogen responses by the host. This is consistent with HopAO1's binding of JAZ1, which associates with the DELLA proteins (Figure 4.6), and functions as a point of feedback between GA and JA signalling pathways, (Hou et al., 2010). This idea is further supported by previous reports of HopAO1 inducing differential expression of genes induced by JA after inoculation with *Pst hrpA* (Underwood et al., 2007).

How the DELLA proteins might relate to the induction of circadian phenotypes is less clear. As mentioned above, Y2H analysis has indicated the ability for GAI and NAM to interact (Rosa et al., 2014). It has also been reported that DELLA quintuple mutants (for there is a large amount of functional redundancy within the DELLA subfamily) have attenuated upregulation of senescence-associated genes, and dark induced chlorophyll degradation (Zhang et al., 2018). NAM is highly expressed in the senescing leaf, and is a negative regulator of *LHY* (loss of function mutants of which have accelerated senescence) (Klepikova et al., 2016; Davies, 2013; Song et al., 2018). Together these reflect the possibility that DELLAs may act as corepressors of *lhy*

together with NAM, potentially accelerating the onset of senescence and inducing changes in clock gene expression.

Although the transcription factor CHE (also found to associate with HopAO1) has well characterised function linking defense and circadian rhythmicity (see section 1.7), it has not been directly linked to NAM or the DELLA proteins, and therefore seems unlikely to participate in a shared pathway. Given that CHE is a TCP family transcription factor there is sufficient evidence to suppose that it is involved in a genuine interaction with HopAO1, and so verification and functional assessment of their interaction certainly warrants further study in the future.

4.3.2 HopAO1 enhances the binding of two NAC transcription factors at the LHY promoter

A mechanism for NAM in plant responses to biotic stress has not yet been well studied. Microarray and large scale data presented in the *Arabidopsis* eFP Browser (Winter et al., 2007) reveal that NAM expression has some association with biotic stress-related stimuli. Expression of the TF is not largely affected by infection with *Botrytis cinerea* or *Pseudomonas syringae*, nor the oomycete pathogen *Hyaloperonospora arabidopsidis* or the aphid species *Myzuz persicaere*, although expression was not recorded later than 48 hours post infection for any of these systems. It is however, upregulated 5 days following infection by the fungal biotrophic pathogen *Golovinomyces orontii*, the causing agent of powdery mildew and is reported to produce symptoms of early senescence in the common poppy (Choi et al., 2018). Additionally, it is upregulated 4 hours after treatment with immune elicitors HrpZ (bacterial derived) and NPP1 (oomycete derived), but not flg22 or lipopolysaccharide (LPS). This could point to a role for NAM in regulating late immune responses. The negative regulation by NAM on *lhy* expression might also negatively contribute towards pathogenic resistance on account of *lhy* loss of function mutants exhibiting reduced capability to close stomata in response to infection (Davies, 2013; Zhang et al., 2013). Further examination of NAM and its interaction with HopAO1 may provide insight into novel function for the NAC transcription factor in immunity.

The results of this chapter raise a number of intriguing questions regarding the unknown immunological consequences of HopAO1's association with the NAC transcription factors. Although on the face of it, the generation of circadian defects through repression of *lhy* might be considered beneficial to *Pst*, the possible role for NAM as a positive regulator of late immune responses makes it less obvious how enhancement of NAM's binding to *pLHY* would cause a net benefit to *Pst* virulence. While NAM has been reported to be expressed in response to challenge by two different pathogens as discussed above as might be expected of a positive regulator of host immunity, the enhancement of its binding to *pLHY* by HopAO1 suggests that the more likely hypothesis is that NAM is a negative regulator of immune responses, and that HopAO1 targets NAM as a way of suppressing immune function. Nonetheless, if NAM was in fact found to be a positive regulator of immunity, it may be the case that HopAO1's binding of DELLA proteins could result in reduced accumulation of ROS, promoting virulence of *Pst* in spite of its association with NAM, which could induce circadian disruption and reduced stomatal closure at the cost of accelerated senescence. It is unlikely that HopAO1's interaction with NAM is purely as a result of its being recruited by DELLA proteins as *Saccharomyces cerevisiae* lacks homologs of the DELLA proteins to facilitate the interaction in a Y2H assay, however *in planta* the action exerted by HopAO1 on NAM could perhaps be enhanced by its first associating with the DELLA proteins. It could also be argued that the disrupted rhythmicity and inhibition of stomatal closure potentially generated by NAM-mediated repression of *lhy* would sufficiently benefit bacterial spread to be worth the induction of senescence pathways for the hemibiotrophic *Pst.* Assessment of the immunity phenotype of NAM loss of function mutants was therefore determined as being crucial moving forward in order to ascertain the TF's role in host immunity and is explored in Chapter 5. Additionally, analysis of any ability by NAM to actually induce senescence in *A. thaliana* such as in studies using common poppy (Choi et al., 2018) might elucidate the potential benefit of HopAO1 acting upon it. This would fit with reports of *lhy* single mutants displaying advanced senescence (Song et al., 2018) since NAM has been suggested to negatively regulate *LHY* through the activation of day-specific repressors (Davies, 2013), potentially indicating a model by which NAM represses *LHY* and so allows for the onset of senescence. The study of circadian phenotypes of DELLA quintuple loss of function mutants (particularly in comparison

to those also crossed with NAM mutants) would also no doubt be informative in the future to confirm the link between them, NAM, and the clock.

Another interesting question following on from the results of this chapter is the interaction of HopAO1 with NAC074. A scarcity of mentions of NAC074 throughout the literature makes drawing comparisons in function between it and its phylogenetically close relative NAM difficult. NAC074 has however, in contrast to NAM, been shown to induce a strong PCD phenotype in *A. thaliana* (Gao et al., 2018), and undergo rapid upregulation of expression in response to a broad range of pathogens and immune elicitors including *P. syringae,* but also following mock treatment (Winter et al., 2007). Additionally, NAC074 was not found to bind the promoter of *lhy* alone, only when in the presence of HopAO1. While this would indicate that the regulation of *LHY* is not a function shared by NAM and NAC074, there are of course always limitations to the study of these interactions in a non-host environment such as yeast. Tyrosine kinases for instances are toxic to yeast when highly expressed, and so if tyrosine phosphorylation plays a crucial part of the association of these TFs to *pLHY in planta*, their strength of binding in yeast may appear lower than they would in a plant cell nucleus (Koegl and Uetz, 2008).

It was also found that these, the only NAC TFs bound by HopAO1 in the small scale Y1H screen, did not share any conserved tyrosine residues predicted to potentially undergo phosphorylation *in planta* , although NAM possessed four that were exclusive to it alone. It should be noted that the phosphorylation prediction scores generated by PhosPhat are all based on site prediction, since experimental data and MASCOT mass spectrometry scores were not available for the TFs analysed. While the z-scores associated with the predicted sites of the NAC TFs were not always sufficiently high to be associated with an assurance of a significant likelihood of phosphorylation, numerous phosphorylation sites have been experimentally verified that were not predicted high phosphorylation scores by the same prediction software, and so these values certainly do not rule out the possibility of phosphorylation. For instance, EFR has been shown to undergo phosphorylation by HopAO1 on the Y836 residue (Macho et al., 2014), despite no phosphorylation score being predicted for the residue. Similarly BIK1 was recently shown to be phosphorylated at sites S233, S236, and

T242 by MAP4K4 (Jiang et al., 2019), with none of these residues producing significant scores within PhosPhat.

The finding that HopAO1 may be able to bind to a wide variety of transcription factors in the nucleus suggests that nuclear localised HopAO1 may contribute to virulence independent of its interaction with PRRs at the plasma membrane by influencing transcriptional regulation. While downstream transcriptional changes in response to HopAO1 expression during infection by *Pst hrpA* have previously been reported (Underwood et al., 2007), these have not been distinguished between what is induced by action of HopAO1 in the nucleus as opposed to the cytosol. In order to better our understanding of nuclear HopAO1 mechanistic action, assessment of transcriptional changes dependent on its expression solely in the nucleus was posited to be informative, and so is also investigated in the next chapter. This may also reveal further evidence of HopAO1's interference with the clock should differential expression be observed for genes under circadian control, particularly in the case of clock-controlled genes involved in defence.

A final and important consideration is that HopAO1 could theoretically be acting as a general binder of DNA, given that it is able to associate with the *LHY* promoter unassisted according to the results of the Y1H assay. This would open up huge mechanistic potential for the effector to regulate transcription on a large scale, in line with the activity of transcription activator-like (TAL) effectors that have been characterised in the phytopathogen species *Ralstonia* and *Xanthamonas*, respectively (Schornack et al., 2006; Heuer et al., 2007). Reported strategies by which T3SEs might regulate transcription are the direct targeting of host transcription factors, the induction of chromatin remodelling, and the mimicking of transcriptional activators (Canonne and Rivas, 2012; Tasset et al., 2010). If HopAO1 was not in fact targeting transcription factors, but rather the host DNA or histones such as *P. syringae* effector HopAI1 is suggested to do (Canonne and Rivas, 2012), regulation of the clock could occur entirely independently of interaction with the NAC transcription factors. In the future it would therefore be prudent to rule out this possibility by testing HopAO1 against other DNA regions using a Y1H approach to prove that its association at the *LHY* promoter is indeed a specific interaction.

4.3.3 Overview

The results of this chapter have revealed an abundance of evidence for novel HopAO1 function in the plant cell nucleus. The *Pst* effector was verified as having nuclear localisation and was found to be capable of binding a number of transcription factors, particularly within the TCP, AP2-EREBP and GRAS families. Amongst these were several transcription factors with links to both the clock and hormone homeostasis, including CHE, NAM, JAZ1, EIL1, and the DELLA proteins RGA, GAI, and RGL1. These transcription factors share a highly connected network of function which suggests a role for HopAO1 as a repressor of GA signalling in the nucleus, with what may be associated effects leading to circadian dysfunction and early-onset senescence.

HopAO1 is able to enhance the binding of both NAM and NAC074 (transcription factors within the NAC family) to the promoter of core clock gene *LHY*, even in the absence of DELLA proteins in a yeast system, in a way that is independent of any conserved tyrosine residues predicted to be phosphorylated *in planta*. It is unknown whether the two NACs share functional redundancy, or if they contribute to resistance/susceptibility against *Pst* infection.

The findings presented in this chapter led us next to particularly consider the role of NAM in *A. thaliana* immune responses and rate of senescence, causing us to next examine the immune and senescent phenotype of the *nam-1* loss of function mutant. Additionally, having revealed likely novel function for HopAO1 impacting transcriptional changes in the nucleus through interactions with *A. thaliana* transcription factors, we sought to investigate the differential expression of genes in response to solely nuclear-localised HopAO1, and thus discriminate its transcriptional impact from its function dephosphorylating PRRs at the plasma membrane.

Chapter 5: Phenotype and transcriptome analysis of pathways affected by nuclear HopAO1 expression

5.1 Introduction

In Chapters 3 and 4 the type III secreted *Pst* effector HopAO1 has been shown to influence the expression of core clock genes in *A. thaliana* (Section 3.2.3), most probably by binding to a host of transcription factors with links to the regulation of plant hormone signalling and the circadian clock (Section 4.2.2). Among these, a NAC transcription factor (NAM) was noted as a link between these two functional groups. NAM has been suggested to bind to the promoter of clock gene *LHY* to negatively regulate its expression under normal 12-hour photoperiods (12:12 LD, Davies, 2013), and was found to exhibit enhanced binding to the *pLHY* in the presence of HopAO1 when expressed in yeast (Section 4.2.3). As has been discussed in section 4.3.2, NAM has some documented association with response to biotic stress in plants, however whether or not it has a specific role in plant immunity has not yet been studied. In order to better understand the mechanism enacted by the binding of HopAO1 to NAM, and the subsequent enhancement of NAM's binding to *pLHY*, it was therefore determined that a phenotypic analysis of the NAM t-DNA insertion knockout mutant line, *nam-1*, was required. While this analysis would naturally include assessment of the mutant's immunity phenotype as well as general characterisation of developmental traits, we also theorised that it might be possible for NAM to act upon the *lhy* gene to accelerate the onset of senescence in *A. thaliana*, and so assessment of the senescent phenotype of *nam-1* was also deemed necessary.

In Chapter 4 we proposed a model for a new HopAO1 function in the *A. thaliana* nucleus whereby its interaction with NAM, enhancing its binding of *pLHY,* might result in an increase in NAM's capability to negatively regulate *LHY*, and so induce a disrupted circadian phenotype such as those seen in Chapter 3. Since HopAO1 was previously shown to supress immunity through its function at the plasma membrane/in the cytosol, we hypothesise that the effector has a dual function. We therefore sought to perform transcriptomic analysis of HopAO1 expression in transgenic *A. thaliana*

lines in which the effector was localised to different sub-cellular compartments. While analysis of the transcriptomic changes brought on by HopAO1 expression have previously been performed, this was presented largely within the context of HopAO1 functioning in the plant cytosol/at the plasma membrane to repress downstream MTI signalling pathways (Underwood et al., 2007). We aimed to employ transcriptomics to verify our model by comparing RNA transcripts in plants where HopAO1 was localised in the cytosol and nucleus, or had targeted localisation conferred by a nuclear exclusion or localisation signal (NES/NLS respectively) at its N-terminus, and observing any subsequent changes to the expression of core clock genes (particularly *LHY*). In this way, our hypothesis regarding novel function for HopAO1 targeting the circadian clock in the nucleus might be supported if such transcriptional changes were found to be reliant on the nuclear localisation of HopAO1, as opposed to an effect downstream of HopAO1's action elsewhere in the cell.

The experimental aims of this chapter were therefore as follows:

i) To verify the negative regulation of *LHY* expression by NAM previously reported by Davies (2013) and so validate the use of the *nam-1* mutant line in other phenotype analyses (section 5.2.1).
ii) To elucidate the role of NAM in plant immunity, as informed by the immunity phenotype of the *nam-1* mutant (section 5.2.1).
iii) To identify any prominent developmental traits of the *nam-1* mutant (section 5.2.1).
iv) To elucidate the role of NAM in senescence, as informed by the senescence onset phenotype of the *nam-1* mutant (section 5.2.1).
v) To generate and test a series of inducible transgenic *A. thaliana* lines expressing HopAO1 under different sub-cellular localisations (section 5.2.2).
vi) To assess the transcriptomic changes induced by expression of HopAO1 under different subcellular locations in the aforementioned transgenic lines, and thus determine the likelihood of clock disrupting function being enacted by the effector in the nucleus (section 5.2.2).

5.2 Results

5.2.1 Phenotype analysis of the NAM transcription factor A. thaliana knockout mutant, nam-1

In order to investigate the various physiological effects enacted by the *A. thaliana* NAC transcription factor, NAM (AT3G12910), we employed the use of a t-DNA insertion line of a wild type *A. thaliana* Columbia (Col-0) ecotype background (SALK_016619C). This *A. thaliana* line was previously confirmed as being null for the transcription factor NAM through PCR amplification (Davies, 2013), and is homozygous for the insertion. Past work on this *nam-1* line revealed that it has altered expression levels of the morning-phased core clock gene *LHY* relative to a wild type control, Col-0 (Davies, 2013). Under normal 12:12 LD photoperiodic conditions *nam-1* exhibited far greater levels of *LHY* transcripts at actual dusk (ZT12, dark onset). Under constant light conditions, *LHY* transcripts were slightly lower at subjective dusk (CT0, anticipated light onset) in the *nam-1* mutant relative to the control. *LHY* transcript levels at dawn were not obviously different in *nam-1* plants under either light conditions. These results suggest that NAM acts as a negative regulator of *LHY* expression at dusk under normal light:dark conditions. Before investigating the immune phenotype of the *nam-1* mutant, we therefore first sought to replicate this previously reported effect to validate the reliability of the mutant's phenotypes. This was done by assessing *LHY* expression by RT-qPCR, as well as the expression of two other core clock genes, CCA1 and TOC1, to further characterise its circadian phenotype.

Rosette leaves 7 and 8 were gathered at actual dawn and dusk (ZT0 and ZT12, respectively) from individual 4-week old *nam-1* and Col-0 control *A. thaliana* plants that had been grown under 12:12 LD photoperiods such that one pair of leaves from an individual represented a biological replicate. RNA was extracted and used to synthesise cDNA which could then be used for RT-qPCR analysis. Primers specific for the genes *LHY, CCA1 and TOC1* were used to amplify transcripts and enable comparison of the clock genes' expression levels between *nam-1* and the wild type control (Figure 5.1).

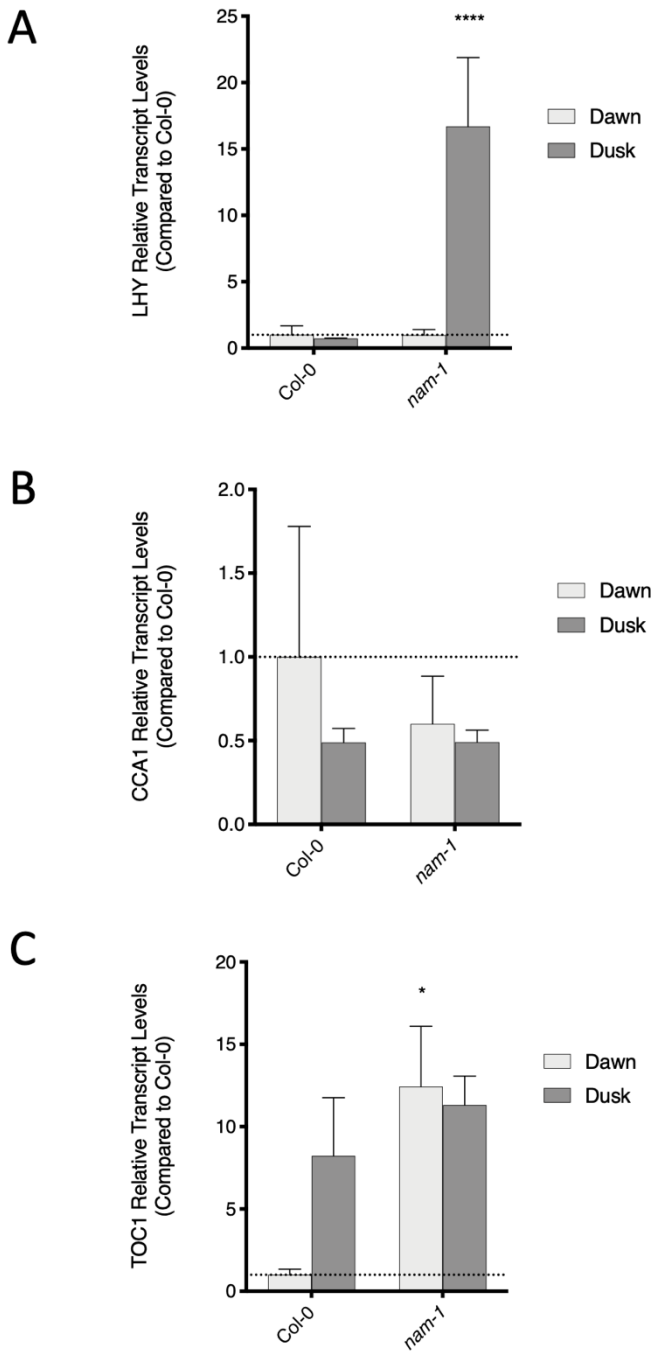

Figure 5.1: Expression levels of *A. thaliana* core clock genes are affected in NAM mutant plants. Rosette leaves 7 and 8 from 4 week-old Col-0 and nam-1 *A. thaliana* plants were excised at dawn (ZT0, light onset, light grey) and dusk (ZT12, dark onset, dark grey), and used to extract RNA which was used for analysis of clock gene transcripts A) LHY, B) CCA1, and C) TOC1 by RT-qPCR. 3 biological replicates were used, and 3 technical replicates were performed for each of these. Transcript levels in mutant nam-1 lines are presented as relative to those of the Col-0 samples at dawn (represented by values of 1, with a dotted line to indicate the baseline of wild type expression). Error bars denote ± SEM. A two-way Analysis of Variance (ANOVA) was performed for each gene assessed and found there to be a significant difference both between time of sampling, and genotype for the gene *LHY*, as well as between genotypes for the *TOC1* gene. Bonferroni's multiple comparisons tests were also performed between Col-0 at dawn and all other samples. The results of these comparisons are denoted by asterisks above bars ($p<0.05$ *, $p<0.005$ **, $p<0.0005$ *** and $p<0.00005$ ****).

In agreement with the results of the previous study (Davies, 2013), we found that the *nam-1* mutant had significantly elevated *LHY* transcript levels at dusk relative to the wild type plants (Figure 5.1, A). It is worth noting, as has been discussed in the aforementioned study that as *LHY* is a morning-phased gene, with very low expression levels at dusk, the very large fold-changes observed in *nam-1*'s *LHY* expression may suggest a more drastic change than the biological actuality on account of levels being normalised against the control. This effect is also true of changes in *CCA1*, which like *LHY* has very low expression at dusk, and of *TOC1*, which is evening-phased and expressed at very low levels at dawn.

The *nam-1* mutant did not have significantly different expression of *CCA1* and (Figure 5.1, B), however it did exhibit a significant fold change in TOC1 (Figure 5.1, C) transcript levels at dawn despite only having previously been characterised as being able to bind to *pLHY*. Together these results agree with previous findings that NAM is a negative regulator of *LHY* under normal 12:12LD photocycles (Davies, 2013). We have further characterised the circadian phenotype of the *nam-1* mutant to include significantly elevated *TOC1* expression at dawn.

Having successfully repeated a previously described phenotype of *nam-1*, we proceeded with further phenotypic analysis. Our principal goal in this assessment was the characterisation of its immunity phenotype, such that we might ascertain the role of NAM in plant immunity, particularly in response to infection by *P. syringae pv. tomato* in which the effector HopAO1 is expressed. To this end we began by assessing the propensity of *nam-1* to undergo leaf collapse following infection with *Pst*, as the collapse of leaf tissue is a symptom associated with disease (Popham et al., 1993). Furthermore, since transgenic expression of HopAO1 is known to produce leaf collapse and the development of chlorotic lesions in *A. thaliana* between 3 and 7 days of its induction (Underwood et al., 2007), we could therefore assess whether or not HopAO1 requires NAM in order to produce this symptom. The strain DC3000 is known to induce leaf collapse *in planta* (Wei et al., 2015), while type III secretion system mutants do not (Sohn et al., 2014). Thus, 4-week old *A. thaliana* Col-0 and *nam-1* plants were pressure infiltrated with virulent *Pst* DC3000 or avirulent *Pst hrcC* at OD_{600} 0.2, or a mock infiltration solution as a negative control. Infiltrated leaves (7

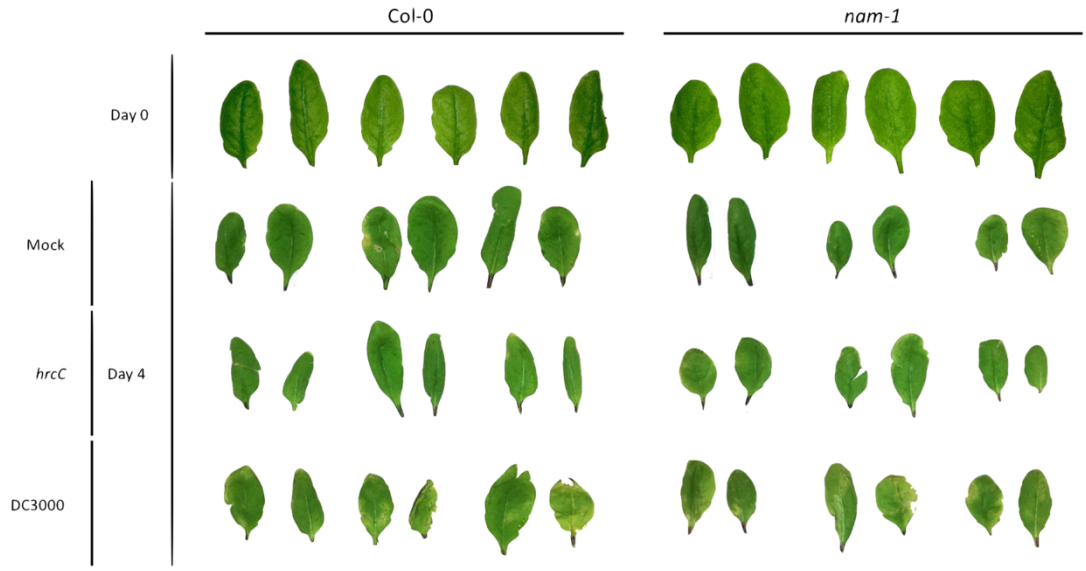

Figure 5.2: The mutant *nam-1* exhibits a similar leaf collapse phenotype to wild type *A. thaliana* following infection by virulent *Pst.* 4-week old *A. thaliana* plants were marked on the stems of rosette leaves 7 and 8 were with a marker pen ahead of treatment. 3 pairs of leaves from 3 individual plants were imaged per condition. Plants were sprayed with virulent *Pst* DC3000 or avirulent *Pst hrcC* at OD_{600} 0.2, or a mock infiltration solution as a negative control (10mM $MgCl_2$) then kept covered for 4 days until leaf collapse, and chlorosis became visible. Leaves 7 and 8 from spray treated plants were then excised and imaged.

and 8) were detached and imaged for visual comparison on the day of infiltration or on the fourth day. Leaves in the *nam-1* line were unaffected by the mock solution and infection by *Pst hrcC*, but began to show evidence of tissue collapse and cell death by the fourth day when infected with DC3000, as can be seen by the inward crumpling of the leaf itself as well as increased yellowing and tissue deterioration (Figure 5.2). The extent of these symptoms was similar to that of the control Col-0. These results suggest that the *nam-1* mutant does not have an altered immunity phenotype.

Next we analysed the contribution of NAM to the resistance of *A. thaliana* against infection of *Pst* through the quantification of bacterial growth. This was achieved by infecting *nam*-1 and Col-0 plants, again using pressure infiltration, with virulent *Pst* DC3000 or avirulent *Pst hrcC* at OD_{600} 0.001, or mock infiltration solution as a negative control. Subsequent growth of bacteria within the leaf was analysed 2 days later by lysing discs of infiltrated leaf tissue and counting bacterial colony forming units (CFUs) that were able to grow from a suspension of the lysate on solid media.

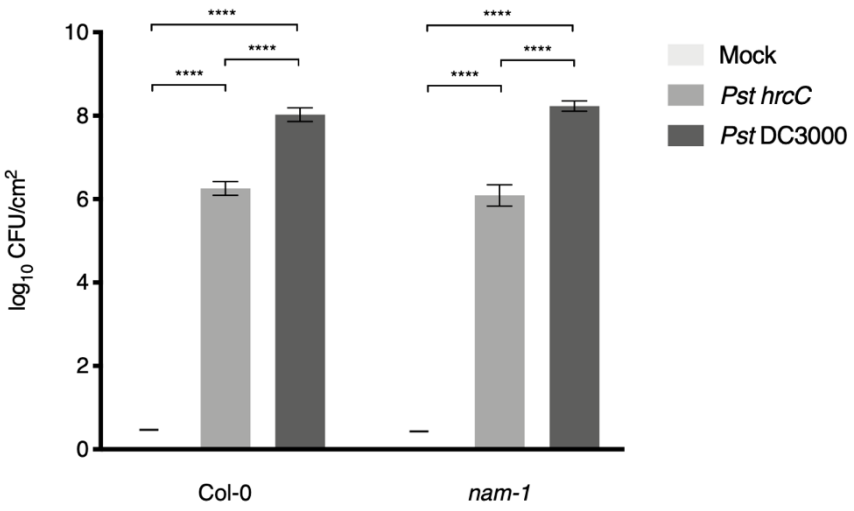

Figure 5.3: The NAM KO mutant *nam-1* is no more or less resistant to infection by virulent and avirulent *Pst* than wild type *A. thaliana*. 4-week-old wild-type Columbia (Col-0) and *nam-1 Arabidopsis* plants were grown at 22°C in 12:12 LD conditions. Leaves 7 and 8 in the rosette were pressure infiltrated with a needleless syringe at dawn with virulent *Pst* DC3000 (dark grey) or avirulent *Pst hrcC* (light grey) at OD_{600} 0.001, or mock infiltration solution as a negative control (10mM $MgCl_2$) (lightest grey, produced no growth in both cases). Bacterial counts were recorded (CFU/cm^2 ± SEM, n = 6) in leaves at 48 hours post infection (hpi). Two-way Analysis of Variance (ANOVA) revealed there to be no significant difference between Col-0 and *nam-1* bacterial growth phenotype. Tukey's multiple comparison test revealed that for both Col-0 and *nam-1* there was a highly significant difference between all treatment types ($p<0.0001$, ****)

It was expected that if NAM was required for effector-mediated susceptibility (ETS) then the knockout mutant would exhibit reduced bacterial growth in the virulent DC3000 infected plants on account of lacking a susceptibility factor. Alternatively, if NAM were to contribute to host resistance, bacterial enumeration in DC3000 treated *nam-1* would be greater, as *Pst* growth would be less inhibited. If NAM contributed specifically to MTI this increase in bacterial growth might also be seen in *nam-1* plants treated with *hrcC*, which can elicit MTI that is not dampened by effector function. It was found that *nam-1* was no more or less resistant to infection by either *hrcC* or DC3000 than the Col-0 plants (Figure 5.3). Both lines of plants exhibited typical amounts of DC3000 and *hrcC* growth (with lower growth of *hrcC* on account of virulence loss without a functioning T3SS), and no growth in the mock-infiltrated control. This suggests that despite its interaction with HopAO1, the NAM mutant does not have an immunity phenotype. This does not necessarily mean that NAM is uninvolved in the immune response, however as this could be due to functional

redundancy between NAM and another protein such as NAC074, which also binds HopAO1, and is phylogenetically close to NAM.

It has been reported that the expression of a senescence marker gene *LSC54* in *A. thaliana* leaves is concurrent with the induction of HR by virulent *P. syringae,* indicating that there may be common steps in the initiation of pathways causing cell death and senescence (Butt et al., 1998). We reasoned that the apparent lack of a role in immunity for NAM in this pathosystem could therefore also be due to the fact that the transcription factor is far more greatly expressed in the senescent leaf (Klepikova et al., 2016), and evidence of its role in immunity might require more than 2 days to become apparent as senescence pathways are initiated.

We hypothesized that NAM may play a role in the later stages of infection when *Pst* switches from a biotrophic to a necrotrophic lifestyle. To rule out the need for extended bacterial incubation to perceive a role for NAM in *Pst* virulence we performed another assessment of bacterial growth, counting colonies 3, 4 and 5 days after infection. In this assay plants were only infected with *Pst* DC3000 but were pre-treated one day in advance of infection with either the MTI elicitor flg22 peptide or H_2O as a negative control. HopAO1 is known to diminish the increased resistance observed in *A. thaliana* following activation of MTI by flg22 treatment prior to infection (Macho et al., 2014), so it was also thought that NAM might be important for this priming of immune responsiveness. Although treating plants of both lines with flg22 prior to infection was found to significantly decrease bacterial growth overall in comparison to those treated with water, the *nam-1* mutant again revealed no significant difference in susceptibility to DC3000 on any of the days assessed when compared with Col-0, regardless of pre-treatment (Figure 5.4). These results indicate that NAM immunity phenotypes are potentially masked due to genetic redundancy.

One pathway involved in effector-triggered immunity (ETI) is the extent of electrolyte leakage produced by infected leaves, which occurs as a result of a loss of cell membrane integrity and is a common definition of cell death (Hatsugai and Katagiri, 2018). To determine whether NAM mutants have an altered extent of ion leakage in response to *Pst* infection we therefore measured ion leakage in the *nam-1* mutant

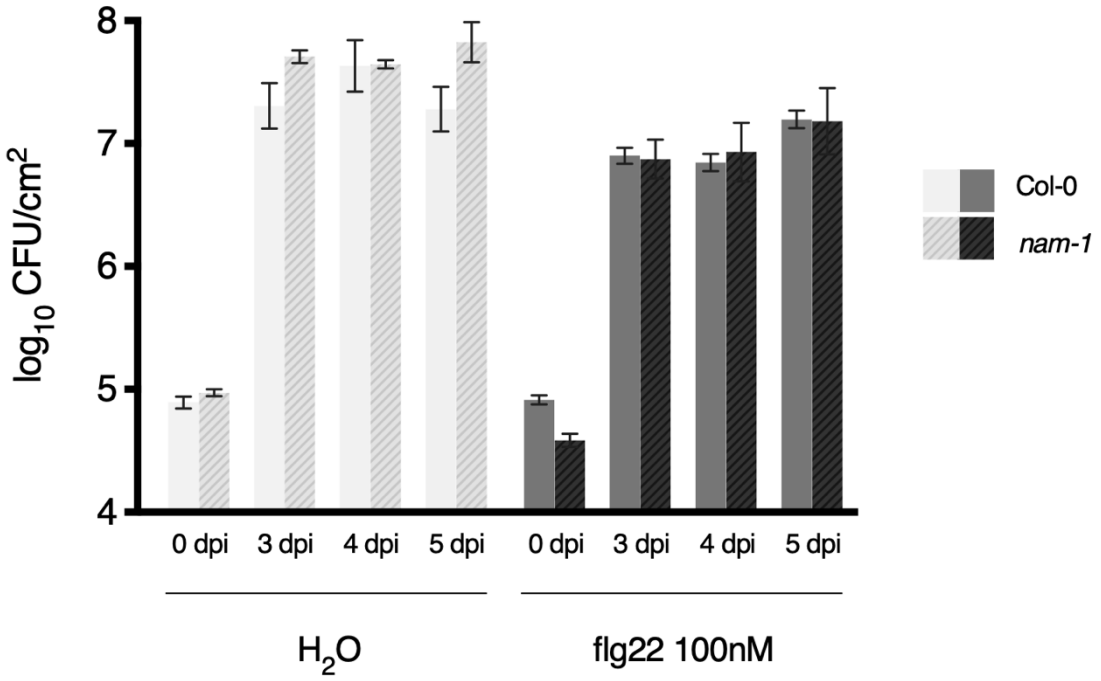

Figure 5.4: The NAM mutant *nam-1* is no more or less resistant during the first 5 days of infection by *Pst* DC3000 after treatment with immune elicitor flg22 than wild type *A. thaliana*. 4-week-old wild-type Columbia (Col-0, solid bars) and *nam-1* (diagonal striped bars) *Arabidopsis* plants were grown at 22°C in 12:12 LD conditions. Leaves 7 and 8 in the rosette were pressure infiltrated with a needleless syringe at dawn with 100nM flg22 (dark grey) or H_2O (light grey, negative control) on the first day. On the second day the same laves were infiltrated again with virulent *Pst* DC3000 at OD_{600} 0.001. Bacterial counts were recorded (CFU/cm^2 ± SEM, $n \geq 4$) in leaves at 0, 3, 4, and 5 days post infection (dpi). Two-way Analyses of Variance (ANOVAs) revealed there to be no significant difference between Col-0 and *nam-1* bacterial growth phenotype on any of the days assessed. A paired t-test showed there to be a significant difference ($p<0.005$) in bacterial growth overall as a result of treatment type (H_2O vs flg22).

compared to Col-0 following infection. 4-week old *nam-1* and Col-0 plants were pressure infiltrated with either mock infiltration media as a negative control, or one of three bacterial suspensions at OD_{600} 0.1: virulent *Pst* DC3000, avirulent *Pst hrcC*, or the ETI-inducing avirulent *Pst* DC3000 (*AvrRpm1*). Discs of leaf tissue were immediately taken from the infiltrated leaves and suspended in sterile water, which was measured hourly for conductivity for the first 8 hours post infection (hpi), then again at 22hpi. There was found to be no significant difference between Col-0 and *nam-1* in the extent of ion leakage following any of the four treatment types (Figure 5.5) providing further evidence that the *nam-1* mutant has an unaltered immunity phenotype, and that NAM alone is not required for ETI, at least when measured by ion leakage.

Finally, with regards to the immunity phenotype of the *nam-1* mutant, we wanted to investigate the ability for both NAM and NAC074 to influence the induction of cell

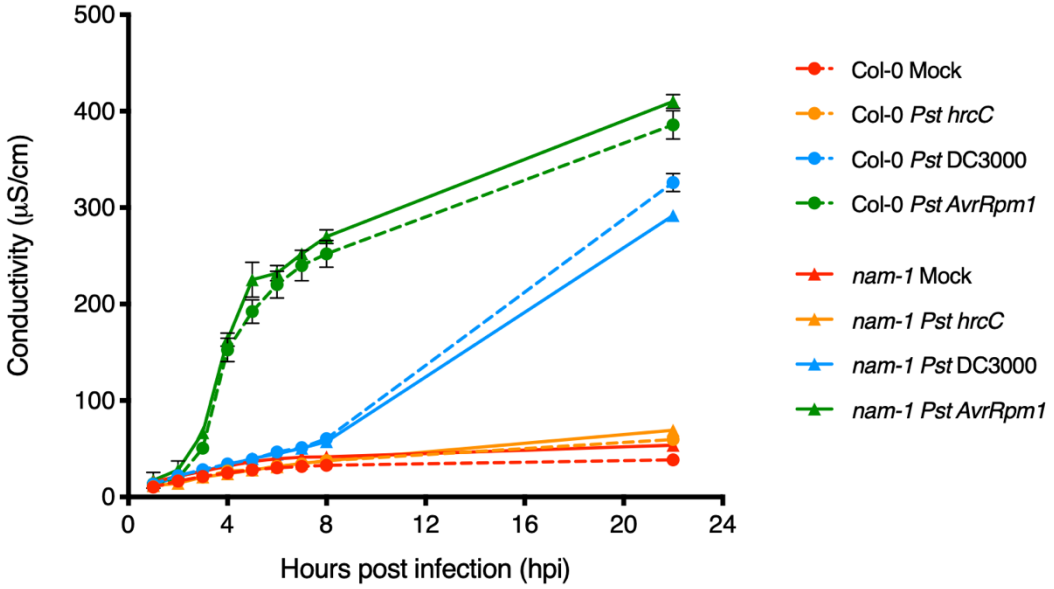

Figure 5.5: The mutant *nam-1* and wild type *A. thaliana* do not exhibit significant differences in the extent of ion leakage following infection with *Pst.* Rosette leaves 7 and 8 in 4 week-old *A. thaliana* plants were pressure infiltrated using a needless syringe with either mock infiltration media (10mM $MgCl_2$), or one of three bacterial suspensions at OD_{600} 0.1: virulent *Pst* DC3000, avirulent *Pst hrcC*, or the HR inducing *Pst* DC3000 (*AvrRpm1*) as a positive control for rapid ion leakage. A pair of leaf discs was taken from each infiltrated plant to represent each biological replicate (n=6). Leaf discs were suspended in sterile water within a 24 well plate and conductance of the solution was measured every hour for the first 8 hours, and again at 22 hours post infection (hpi). Multiple t-tests in the means of measured conductance in response to each treatment type found there to be no significant difference between Col-0 and *nam-1* in the extent of ion leakage in response to any of the treatment types. Error bars denote ± SEM.

death brought on by HopAO1 expression. To do this, *Nicotiana benthamiana* plants were used to transiently express HopAO1 by infiltration with transformed *A. tumefaciens* in a partially overlapping region of leaf tissue transiently expressing either NAM, NAC074, or an empty vector control. We found that HopAO1 produced the first symptoms of HR within 3 days of infiltration (images not shown), and a stronger HR by day 4, with clear tissue necrosis (Figure 5.6). In agreement with previous work by Gao et al. (2018), NAC074 also induced HR, with symptoms that were more severe than those caused by HopAO1. The overlapping leaf region between HopAO1 and NAC074 appeared to experience a more severe HR than that of HopAO1, and less than that of NAC074. This indicates that NAC074 and HopAO1 may both act on the same HR induction pathway, although the fact that each independently induces HR makes it unclear whether NAC074 exacerbates the effect brought on by HopAO1, or

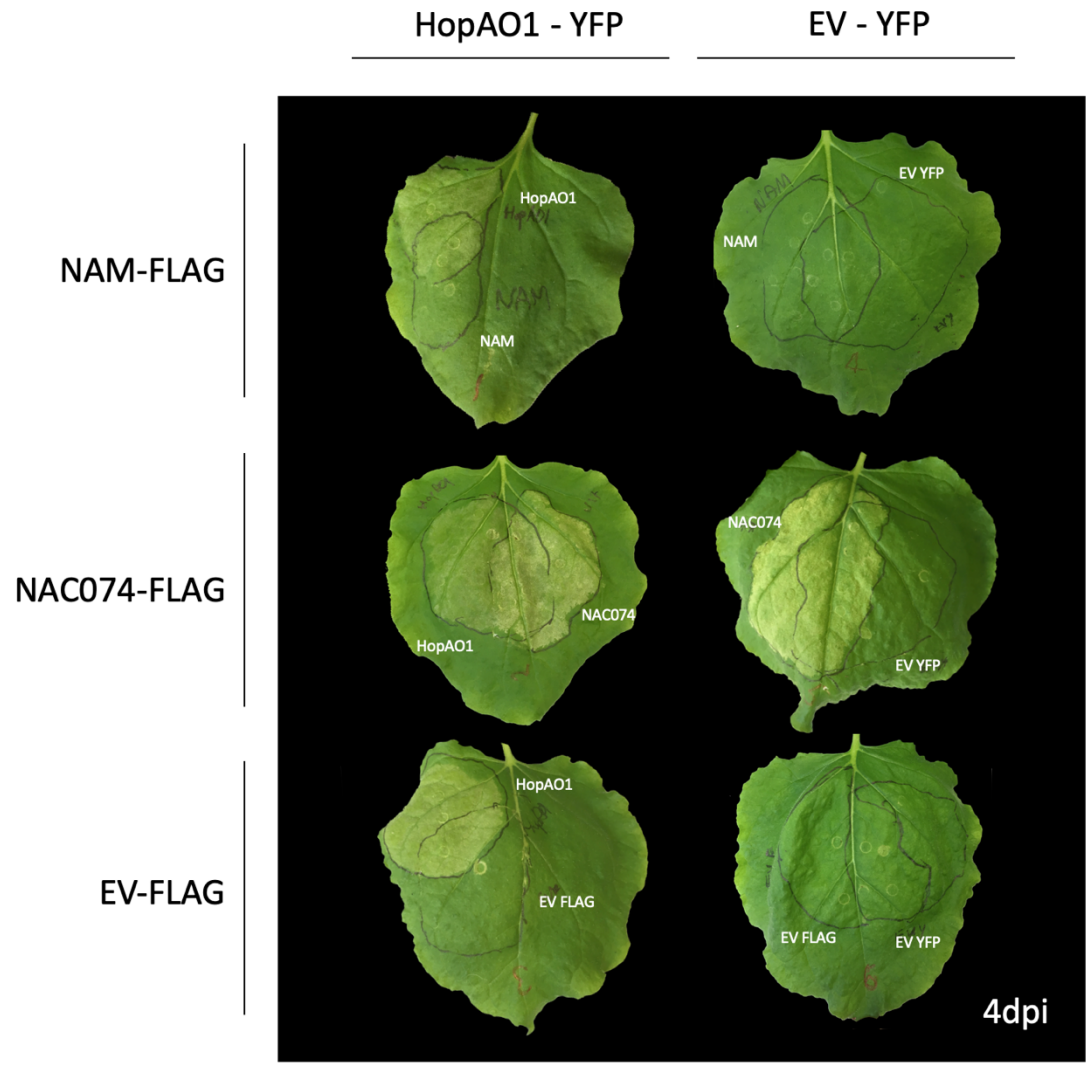

Figure 5.6: Transiently expressed HopAO1 and NAC074, but not NAM induce the hypersensitive cell death response in *N. benthamiana.* 5 week-old *N. benthamiana* plants were pressure infiltrated using a needleless syringe in their largest fully expanded leaves with two different genotypes of *A. tumefaciens* that had been transformed with one of 5 constructs, at an OD_{600} of 0.4. NAM and NAC074 were expressed in the pEG202 N-terminal FLAG-tag vector, while HopAO1 was expressed in the pEG104 N-terminal YFP-tag vector. Empty vectors (EV) for each vector were also used as negative controls. Leaves were infiltrated with two of these constructs such that a bacterial culture expressing one FLAG construct saturated leaf tissue in a circle which was marked with a black marker pen, and that of a YFP construct filled another partially overlapping circle of the same leaf which was similarly marked. Infiltrated leaves were imaged 4 days following infiltration when symptoms of the hypersensitive cell death response had become visually apparent. Each leaf pictured was representative of a minimum of 3 leaves from separate individual plants.

HopAO1 limits the effect caused by NAC074. The latter theory better agrees with the fact that HopAO1 is able to delay the onset of the HR brought on by expression of HopAD1 in *N. benthamiana* (Espinosa et al., 2003). Since HR does eventually develop in this system, perhaps HopAO1 is able to diminish symptoms of HR, but not sufficiently to compensate for the activation of HR by host resistance pathways. NAM

does not induce HR, nor does it limit the extent of HR brought on by expression of HopAO1. If NAM and NAC074 have overlapping functionality, the induction of HR is not one of their shared roles. This also indicates that when NAC074 induces HR, it likely does so via a pathway that is independent of its possibly binding the *LHY* promoter.

Having assessed the immunity phenotype of the *nam-1* mutant, we next sought to characterise the rate at which it undergoes senescence. Given that NAM is a negative regulator of *LHY* expression (Davies, 2013), and *LHY* knockouts have advanced onset of senescence (Song et al., 2018), we hypothesised that NAM knockout mutants would exhibit delayed senescence. It has been shown that extended incubation of detached *A. thaliana* leaves in the dark induces the onset of senescence as evidenced by leaf yellowing, and the method is widely used as a model for age-triggered senescence (Weaver and Amasino, 2001; Song et al., 2014). As a way of analysing the rate at which senescence is able to occur in the absence of NAM, we therefore detached leaf pairs from 4-week old *nam-1* and Col-0 *A. thaliana* plants and incubated them in the dark for 4 days. By imaging these leaf pairs before and after the dark treatment we hoped to view changes in leaf colouration and attribute them to the function of the NAC transcription factor.

We found that the *nam-1* mutants did not appear to have more or less obviously discoloured leaves than Col-0 at 4DD (Figure 5.7). In order to quantify these differences and examine the possibility of the mutant having accelerated senescence relative to the wild type, we also calculated the chlorophyll content of leaves both before dark treatment (0DD), and every day for 4 more days in darkness. Chlorophyll concentrations were quantified by submerging detached leaves in a 95% acetone/ethanol solution (v/v = 2:1, 5% ddH_2O) for 12 hours in a foil wrapped tube (to prevent deterioration of chlorophyll by the light), and then measuring absorbance of the solution. Values were calculated relative to the fresh weight of leaf pairs to account for any differences in the amount of tissue collected between samples. When chlorophyll content was assessed in this way, there was revealed to be a significant increase in the levels of both Chlorophyll A and Chlorophyll B in the *nam-1* mutant before dark incubation, amounting to approximately 0.5mg/g of fresh weight of

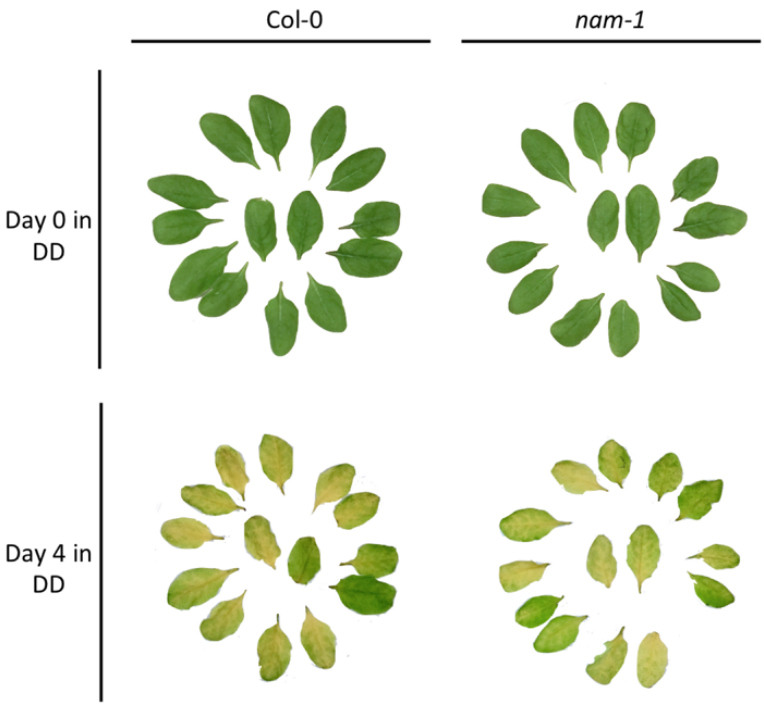

Figure 5.7: *nam-1* and wild type *A. thaliana* plants exhibit a visually similar extent of leaf yellowing as a result of dark-induced senescence. Rosette leaves 7 and 8 were detached from 4-week old *nam-1* and Col-0 *A. thaliana* plants, arranged in pairs in a plastic petri dish, and imaged immediately following excision at the start of the assay when leaves had not yet been kept in constant darkness (DD). Leaves were then incubated in the dishes, which were wrapped in aluminium foil to ensure total darkness, for 4 days in order to induce senescence. Leaf pairs were then imaged again for comparison.

Chlorophyll A, and 0.25mg/g of Chlorophyll B (Figure 5.8, A). After 1, 2, and 3 days being incubated in the dark, levels of chlorophyll in the *nam-1* mutant were not significantly different to those of Col-0 (Figure 5.8, B-D), however by the 4th day in darkness levels of both chlorophylls in *nam-1* were significantly lower than the wild type, amounting to approximately 0.3mg/g difference in chlorophyll A, and 0.1mg/ml of chlorophyll B.

Furthermore, while *nam-1* chlorophyll levels appeared to gradually diminish every day in total darkness, chlorophyll degradation in Col-0 was much slower. The mean total chlorophyll A+B in *nam-1* underwent a 71% decrease by 4DD (from 1.81mg/g to 0.53mg/g), whereas Col-0 only lost 7% of total chlorophyll A and B by 4DD (from 1.02mg/g to 0.96mg/g). While Song et al. (2014) reported that dark induced Col-0 leaves underwent about a 25% loss of chlorophyll content after 4 days, which is a greater loss than we find in the current study, the comparative loss of chlorophyll in

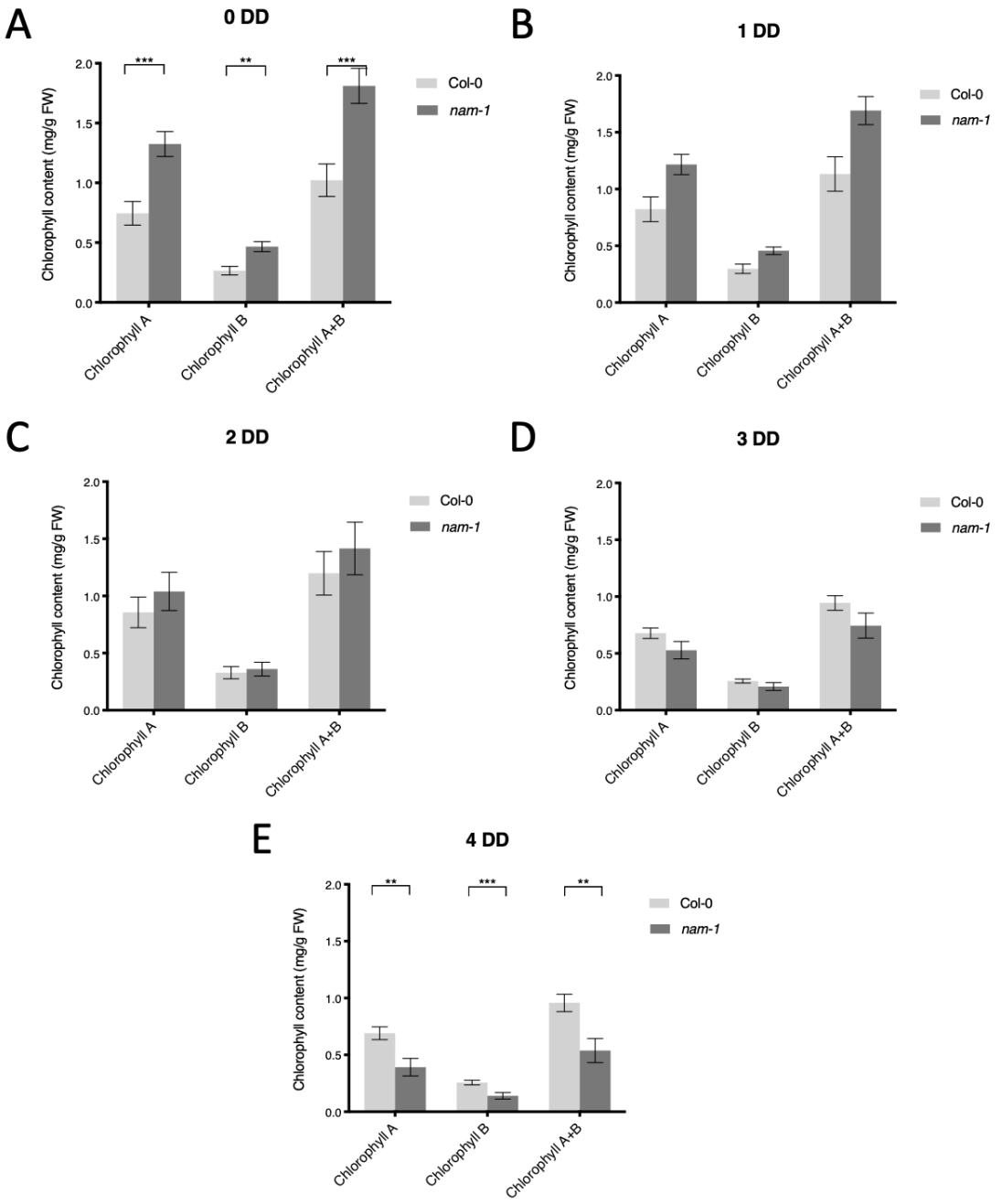

Figure 5.8: The mutant *nam-1* exhibits elevated concentrations of chlorophyll in leaf tissue, as well as an accelerated rate of chlorophyll degradation when senescence is dark-induced. Rosette leaves 7 and 8 were excised from 4-week old wild type Col-0 and *nam-1* mutant *A. thaliana* plants that had been kept in constant darkness (DD) for 0 (A), 1 (B), 2 (C), 3 (D) or 4 (E) days. Each leaf pair represented one biological replicate ($n \geq 4$). Detached leaf pairs were weighed, incubated in 95% acetone/ethanol (v/v = 2:1, 5% ddH_2O) for 12 hours, then concentrations of chlorophyll A and chlorophyll B per gram of fresh weight were quantified by measuring absorbance of the solution at 645 and 663 nm. Multiple paired t-tests were performed comparing Col-0 and nam-1 on each day for significant differences in chlorophyll content (where $p<0.05$, **, $p<0.005$, **). Error bars denote ± SEM.

the *nam-1* mutant is still very stark compared to this published figure for the wild type line.

These results of the chlorophyll quantification assay suggest that *nam-1* may undergo a more rapid rate of dark-induced senescence than wild type *A. thaliana* plants, indicating a possible role for NAM in accelerating the onset of senescence. Considering the previously described accelerated senescence phenotype observed in *LHY* mutants this points to NAM repressing *LHY* expression in order to induce senescence (Song et al., 2018). The results presented in Figure 5.8 do not, however, fully corroborate with the degree of leaf yellowing observed in Figure 5.7, which suggest that chlorophyll degradation is comparable between the mutant and the wild type line at the 4-day mark. It may therefore be the case that NAM's influence on chlorophyll degradation corresponds to only a minimal visually detectable change overall on the rate of dark induced leaf senescence.

As the final part of our phenotypic analysis of the *nam-1* mutant, we investigated whether or not NAM was likely to be required for any fundamental developmental processes by comparing the rosette fresh weight and leaf morphology of adult *nam-1* and Col-0 plants. There was found to be a small but significant decrease in rosette fresh weight of *nam-1* mutants in comparison to Col-0, amounting to approximately 29.5mg, however this was only mildly significant, with a p value of 0.0312 (Figure 5.9, A). With regards to leaf morphology, rosette leaves 1-12 were compared amongst several representative individual plants of each line. For the most part, leaf shape at all stages did not appear to vary between the wild type and the mutant. It is notable however, that in very occasional instances, the *nam-1* mutant would produce leaves (stage 7 and later) that were asymmetrical in shape, with one half of the leaf exhibiting sloping edges that were more spatulate than round as in the wild type. While this was less common at the 4-week old stage, it became more frequent in leaves developing during the flowering stage, particularly around the bolting stem itself. This implies that NAM may have some role in development that becomes more prominent during late stages of *A. thaliana* growth, in agreement with its increased levels of expression during senescence (Klepikova et al., 2016).

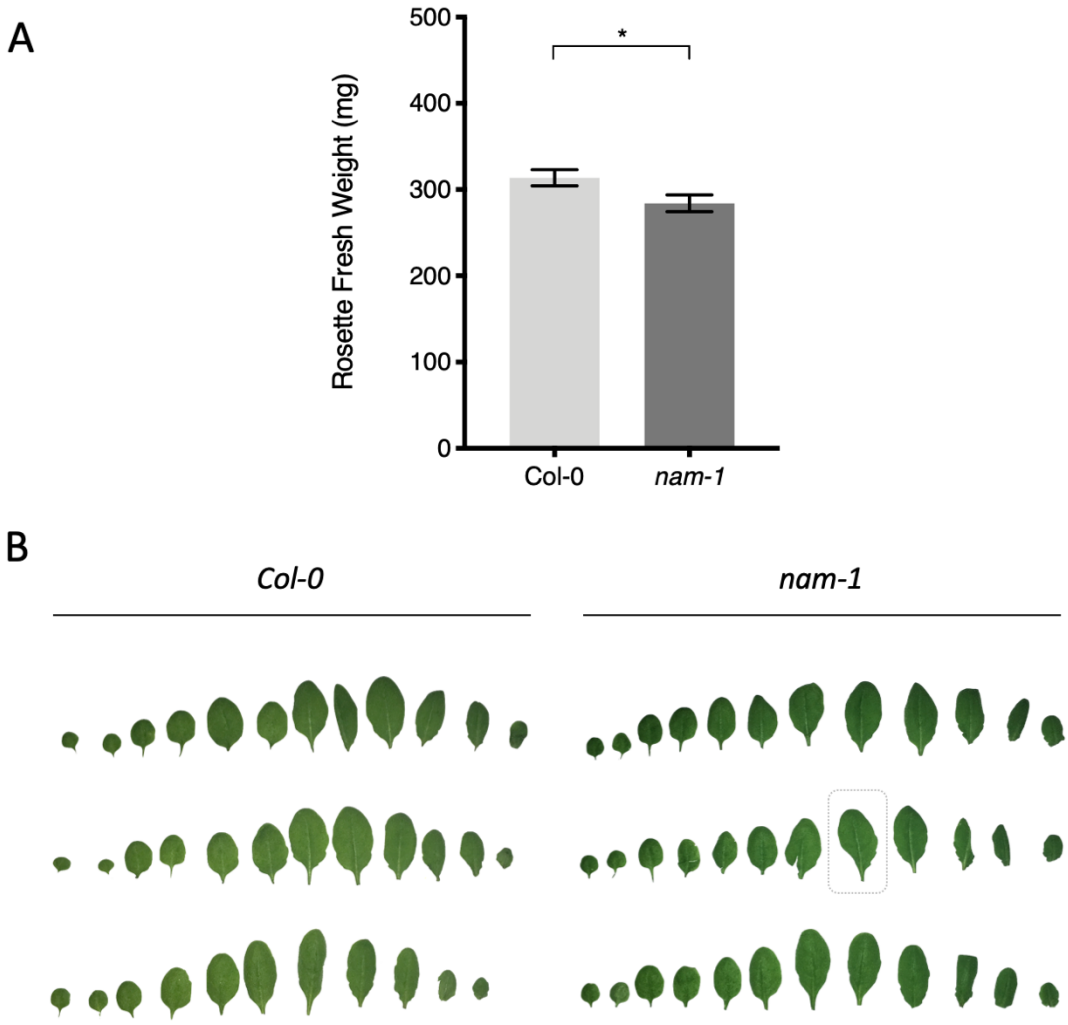

Figure 5.9: *nam-1* and wild type *A. thaliana* plants exhibit only minor differences in adult rosette fresh weight or leaf morphology. A) 5-weekold *nam-1* and Col-0 *A. thaliana* plants were cut at the base of the leaf rosette to separate them from roots and soil, then whole rosettes were weighed (n≥45). An unpaired t-test found there to be a small, but mildly significant difference in fresh weight between the mutant and wild type (p=0.0312, *). Error bars denote ± SEM. B) Rosette leaves 1-12 were excised from 3 representative 4-week old individual *nam-1* and Col-0 *A. thaliana* plants and imaged to demonstrate any differences in leaf size and shape. The dotted box highlights occasional instances of leaf shape asymmetry observed in *nam-1* mutant plants.

Together these results agree with and extend previous characterisation of the *nam-1* mutant by Davies (2013), revealing a negative regulatory role for not only *LHY,* but for another core clock gene, *TOC1*. We find that functional disruption of NAM alone does not produce significant differences in susceptibility or resistance to infection by *P. syringae pv. tomato*. This may indicate that NAM possesses functional redundancy with other members of the NAC TF family. The *nam-1* mutant experiences accelerated rates of chlorophyll degradation, and subtle changes in leaf morphology and rosette

weight, particularly at later stages of growth, which also suggests NAM may have a role in late stage developmental regulation.

5.2.2 Investigating the importance of HopAO1's subcellular localisation on its induction of transcriptomic changes in A. thaliana

We have established at this point that in the host nucleus HopAO1 binds to the NAC transcription factor NAM, a proven negative regulator of *LHY* expression as well as another clock gene, *TOC1*. Furthermore, HopAO1 enhances the binding of NAM to *pLHY*. HopAO1 also produces a distinct disrupted circadian phenotype when transfected into protoplasts. We therefore hypothesised that HopAO1 has a novel function in the host nucleus disrupting the circadian clock, by enhancing the repression of *LHY* through its interaction with NAM which leads to knock-on effects on the expression levels of other clock genes within the clock's transcriptional-translational feedback loop. In order to test the impact that HopAO1 localisation in the host cell has on its ability to induce transcriptional changes we generated three transgenic *A. thaliana* lines expressing a HopAO1-GFP fusion protein under an estradiol inducible promoter (Figure 5.10). The fusion protein possessed a different N-terminal tag in each of the three lines. This was either a nuclear localisation sequence (NLS), a nuclear exclusion sequence (NES), or a 3HA-FLAG tag which would not confer limitations

Figure 5.10: Transgenic *A. thaliana* plants were generated expressing *Pst* effector HopAO1 under the control of a β-estradiol inducible promoter, with varying N-terminal localisation tags. The transgene conferred a fusion protein of HopAO1 that possessed an N-terminal tag, either an NLS, NES, or 3HA-FLAG sequence that would cause HopAO1 to be localized to the nucleus, to be localized outside of the nucleus, or to not have predetermined localisation, respectively, as well as a C-terminal GFP tag that would allow confocal confirmation of localisation tag efficacy. HopAO1 would only be expressed following the perception of β-estradiol by the XVE estradiol receptor, and subsequent stimulation of an estradiol inducible promoter system (containing 8 copies of the LexA operator upstream of a -46 35S minimal promoter). The FAST-R seed selection cassette allowed for selection of successful transgene uptake by stereomicroscopic selection of only red fluorescing seeds. The construct was assembled by Golden Gate assembly in the level 2 pAGM4723 vector backbone (see section 2.6.2 for details). Transgenic plants were created by stable Agrobacterium-mediated transformation of *LHY::LUC* plants in the Col-0 ecotype background.

on HopAO1 localisation as a control. These constructs were created using the Golden Gate assembly method, and introduced to plants by stable *Agrobacterium*-mediated transformation of *LHY::LUC* plants in the Col-0 ecotype background. The original T0 transformants of these plants were selected for successful uptake of the construct by stereomicroscopy (enabled by the FAST-R cassette, which makes seeds fluoresce red), and used to produce another generation of transformants (T1). Seeds produced by the T1 plants were again selected by stereomicroscopy, and then the resultant seed stocks from two individual plants of each construct were tested for equal HopAO1 expression levels by RT-qPCR. This was because we wanted to ensure any transcriptomic differences between lines could be attributed to localisation of HopAO1 and would not be due to differences in overall *HopAO1* expression.

A minimum of 3 10-day old estradiol induced seedlings for each individual seed stock being tested was used to represent a single biological replicate. Each biological replicate was used to extract RNA and subsequently synthesize cDNA which could be used for RT-qPCR, from which three technical replicates were generated. cDNA samples were tested against two different pairs of primers specific for *HopAO1* as a further check of reliably comparable expression levels. We did not find a significant difference in the expression levels of *HopAO1* between any of the lines tested or for either *HopAO1* primer pair, indicating that transcriptomic changes could confidently be compared between them (Figure 5.11). Line number #1 was therefore chosen for all three lines, as although none were significantly different from each other, these stocks appeared to produce particularly even *HopAO1* expression levels.

Before proceeding with transcriptomic analysis, we also needed to verify that the localisation tags placed at the N-terminus of the HopAO1 fusion proteins were correctly targeting the effector to the intended subcellular locations within plant host cells. To do this, we induced expression of the construct by estradiol infiltration in leaves 7 or 8 of 4-week old *A. thaliana* plants from each transgenic line, then imaged leaf discs taken from these using confocal microscopy.

As intended HopAO1 in the NLS-tagged line localised to the nucleus, in the NES line localised primarily to the cytosol immediately surrounding the nucleus, and partially to the chloroplast, while the uninhibited 3HA-tagged line localised primarily to the

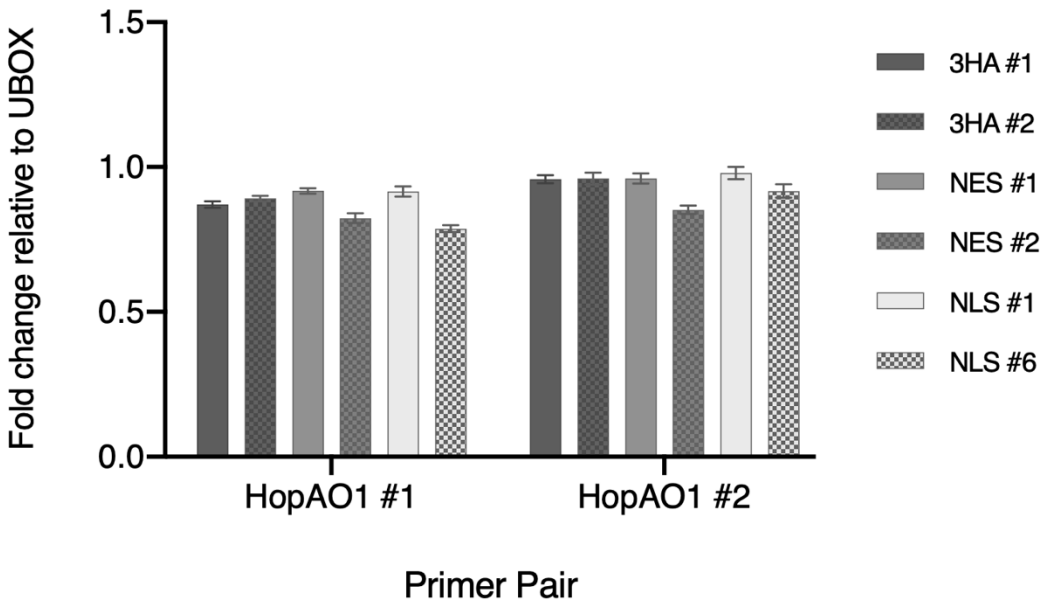

Figure 5.11: Equal expression of *HopAO1* is shown amongst lines of transgenic plants expressing a construct conferring inducible HopAO1-GFP with varying N-terminal tags. A minimum of 3 10-day old seedlings was used to represent one biological replicate, and to generate RNA from three pairs of *A. thaliana* lines, where each pair transgenically expresses one of three golden gate constructs: *est::3HA-HopAO1-GFP, est::NES-HopAO1-GFP*, and *est::NLS-HopAO1-GFP*. 3 biological replicates were used from each line (all of which had first been induced for transgene expression by incubating for 24 hours in 20μM β-estradiol), from which 3 technical replicates were generated. RNA samples were used to quantify HopAO1 expression in each of the lines using 2 sets of primers specific to HopAO1. Fold change in HopAO1 transcript levels were quantified relative to the housekeeping gene UBOX (AT5G15400). Tukey's multiple comparisons test was performed to assess any significant differences in HopAO1 expression between the transgenic lines, however levels of HopAO1 transcript were not significantly different between any of the samples.

nucleus, and partially to the cytosol and chloroplasts (Figure 5.12). This localisation suggests that the N-terminal localisation tags are working correctly, as when its movement is uninhibited HopAO1 has been seen in this and in previous work by Mastorakis (2017) to localise primarily to the nucleus, and partially to the chloroplast and cytosol. Having verified therefore that in these transgenic lines *HopAO1* was expressed correctly in accordance with its given N-terminal localisation tags, as well as evenly regarding transcript levels of the effector, we proceeded with large-scale transcriptomic analysis.

Transgenic plants of the *est::3HA-HopAO1-GFP* line were treated with either estradiol or mock to produce samples which were either induced for the transgene or uninduced as a control for any leaky *HopAO1* expression. They were then further treated with either flg22 or mock to identify which differences in gene expression were specifically

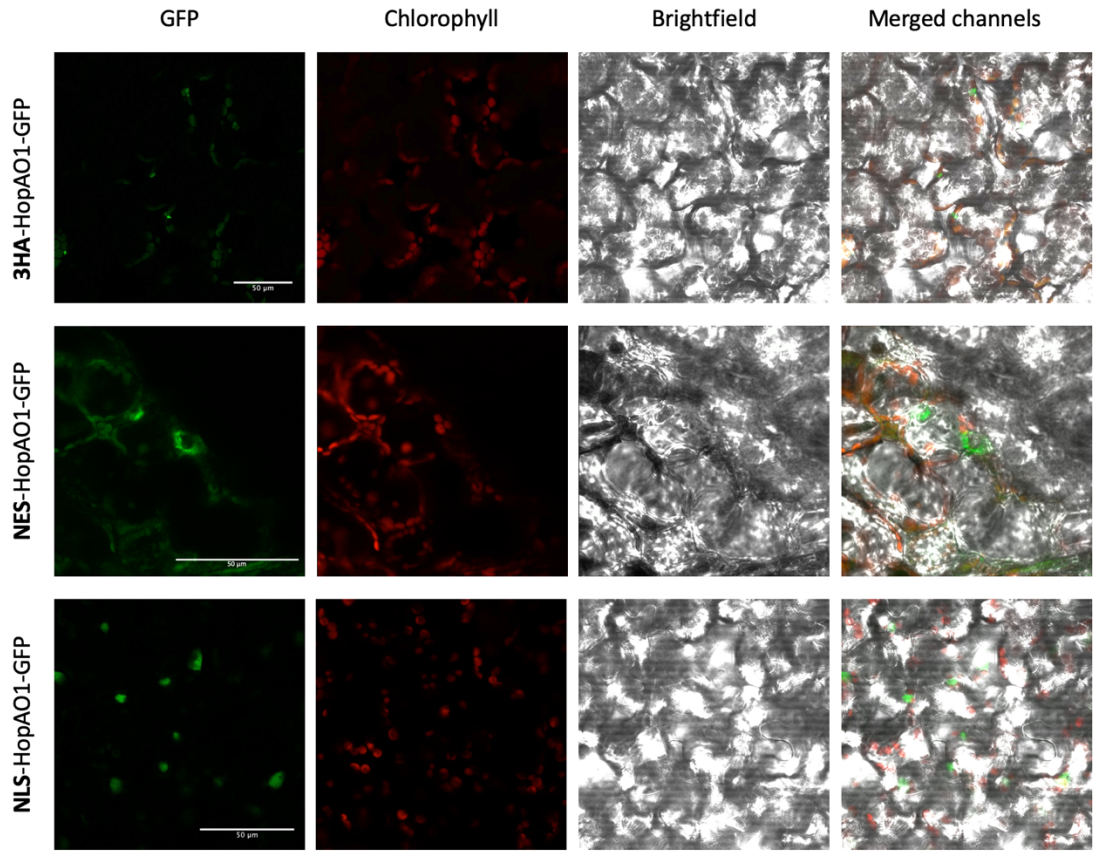

Figure 5.12: Transgenic *A. thaliana* lines expressing HopAO1-GFP show expected differences in sub-cellular localisation in accordance with their N-terminal tags when visualized *in planta* by confocal microscopy. Leaves from 4 week-old *A. thaliana* plants transgenically expressing either *est::3HA-HopAO1-GFP, est::NES-HopAO1-GFP*, and *est::NLS-HopAO1-GFP* (conferring the estradiol inducible HopAO1-GFP fusion protein with a 3xHA, nucleus exclusion signal, or nuclear localisation signal N-terminal tag respectively) were induced by incubation for 24 hours in 20µM β-estradiol, then imaged using confocal microscopy. The 3HA-tagged effector line is a control which represents the effector's native localisation within the host cell. GFP and chlorophyll autofluorescence were detected using lasers at 488nm and 633nm, respectively. Images were processed using both Zeiss 2011 and ImageJ software, and show channels for GFP (green), chlorophyll (red), brightfield (grayscale), as well as a composite of all channels merged into one image. Scale bars represent a length of 50µm. Images shown are representative of a minimum of 6 individual plants imaged across 3 separate days.

due to the action of HopAO1, as opposed to in response to MTI signaling following MAMP (flg22) perception by the host. These plants constituted the first 4 sample groups: 1) 3HA + est + flg22, 2) 3HA + mock +flg22, 3) 3HA + est + mock, and 4) 3HA + mock + mock. The fifth and sixth sample groups were made up of plants of the NLS and NES-tagged lines, respectively, which were treated with both estradiol and flg22; 5) NLS + est + flg22, and 6) NES +est +flg22.

For each sample group a minimum of 3 10-day old seedlings was used for each of 3 biological replicates where samples were harvested, and flash-frozen in liquid nitrogen at dawn (ZT0). RNA was then extracted from the lysed, frozen samples, and contaminating genomic DNA was removed. All subsequent steps in the RNA-Seq assay, starting from library preparation and including bioinformatics analysis were performed by the BGI sequencing group (BGI, Hong Kong) according to their protocols which are described in full in section 2.17.4. The quality of libraries was first assessed, where clean reads were filtered using the SOAPnuke software (Chen et al., 2018) so as to remove reads with adaptors, with more than 10% unknown (N) bases, and with low quality reads (where low quality is defined as the percentage of bases with a quality of less than 15 being greater than 50% within a read). The quality metrics for clean reads can be found in Supplementary Figure S5.1. Next clean reads (of which there were between 20 and 30 million for all samples) were mapped to the TAIR *A. thaliana* reference genome (Berardini et al., 2015) using the HISAT2 program (Kim et al., 2015). The average mapping for all samples was 98.3%, and the high degree of uniformity between the total mapping ratios amongst samples of the same experimental groups is indicative of highly comparable biological replicates (Supplementary Figure S5.2). Finally, Pearson correlation coefficients were calculated between all samples and plotted as a heatmap to reflect the overall gene expression correlation between samples. These coefficients represent the strength of linear association between a pair of samples. Within sample groups (i.e. amongst biological replicates of the same transgenic lines and treatment types) the Pearson coefficients were all found to be equal to or greater than 0.827 (where a value closer to 1 indicates a higher correlation) indicating that biological replicates within all of the groups were sufficiently comparable (Supplementary Figure S5.3).

We found that the genes that were expressed in varying amounts according to each of the treatment types used in the study (Figure 5.13). Induction of MTI pathways following host perception of the bacterial peptide flg22 results in changes to the broad transcriptome of both estradiol-induced and uninduced *est::3HA-HopAO1-GFP* plants (Figure 5.13, C and G). The induction of *est::3HA-HopAO1-GFP* expression with estradiol alters the transcriptome even when MTI has not been induced (Figure 5.13, F). The inhibition of HopAO1's nuclear localisation (i.e. comparing the NES to the 3HA line) produces changes in the transcriptome, however the induction of non-

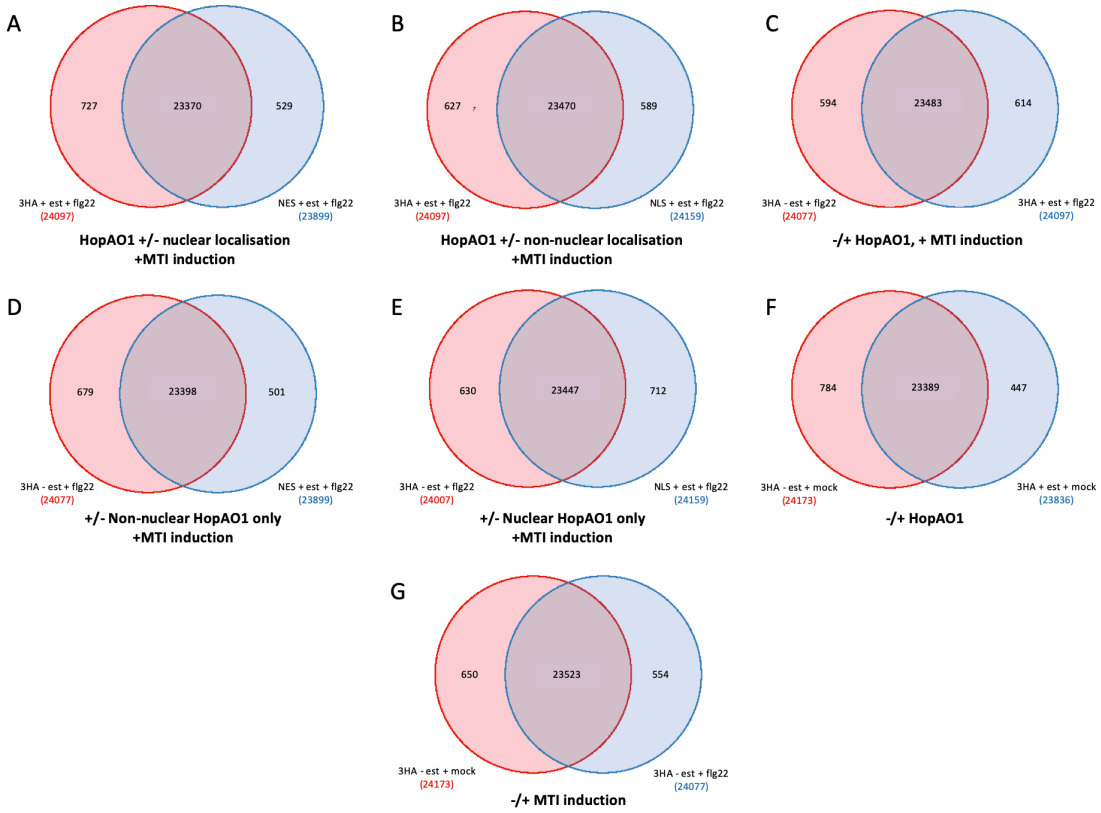

Figure 5.13: Comparison between the lists of genes detected by RNA-Seq analyses in different sample groups. A-G) Number of genes expressed in and between RNA-Seq sample groups is shown in non-proportional Venn diagrams. The broad experimental consequences being compared between each pair of sample groups is written beneath Venn diagrams.

nuclear localised HopAO1 by itself (i.e. comparing NES to no HopAO1 at all) also causes changes (Figure 5.13, A and D). This suggests that HopAO1 can influence transcription as a result of its function outside of the nucleus. HopAO1 is also, however, clearly able to induce transcriptomic changes in the nucleus, as removing non-nuclear function from HopAO1 alters which genes are expressed (comparing 3HA to NLS), as does expression of solely nuclear-localised HopAO1 (comparing NLS to no HopAO1 at all, Figure 5.13, B and E).

Principle component analysis (PCA) was performed next. In this, an orthogonal transformation is used to convert a set of observations of potentially correlated variable (here gene expression levels between biological replicates of differing experimental sample groups) into a set of values of linearly uncorrelated variables called principle components. These principle components are represented in 2 dimensions as a PCA plot. The percentage of variability that each computationally determined principle

component accounts for across all of the samples is included in this PCA plot. The first principle component (PCA1) accounts for the largest degree of variability in genes expressed within the samples, while the second component (PCA2) accounts for the next most substantial contributor of variability.

The PCA plot generated from the RNA-seq data in this study shows that the gene expression of the various transgenic HopAO1 samples is clearly ordinated along two planes (Figure 5.14). One these planes runs very approximately along the x axis according to PCA1, while the other is roughly vertical according to the contribution of PCA2. The points corresponding to each sample within an experimental group (denoted by dots of like colour) are in all cases roughly grouped, suggesting once again that samples of the same treatment types have gene expression profiles that are similar to one another.

Perhaps the most striking observation from this plot is that the variability in gene expression denoted by PCA1 accounts for 85.64% of the total variability in the transcriptome of all samples, and that the only experimental group that appears to largely vary along this axis is that of *est::NLS-HopAO1-GFP* samples treated with flg22 and induced with β-estradiol. This indicates that the expression of solely nuclear-localised HopAO1 produced the largest changes in which transcripts were detected amongst all tested samples. It is important to note that two sample groups for the *est::3HA-HopAO1-GFP* line were included in this study (one with and one without flg22 treatment), and so the variability attributed to this principle component is not due to the loss of non-nuclear HopAO1 function, or else they too would presumably be grouped further along this axis. Rather expression of nuclear HopAO1 without the contribution of the effector's function from elsewhere in the cell is responsible for these broad changes. This also reinforces the notion from Figure 5.13 (Panels A, B, D and E) that the genes expressed in response to flg22 treatment have more overlap with those expressed in response to induction of non-nuclear HopAO1 (NES) than nuclear HopAO1 (NLS). HopAO1 in the nucleus therefore seems more likely to be influencing the transcription of genes not related to MTI. Another consideration when assessing the *est::NLS-HopAO1-GFP* samples' distribution with regard to PCA1 on the x axis is that one of the replicates exhibits notably less variance according to PCA1 than the other two within its group (Figure 5.14), which could give the impression that this

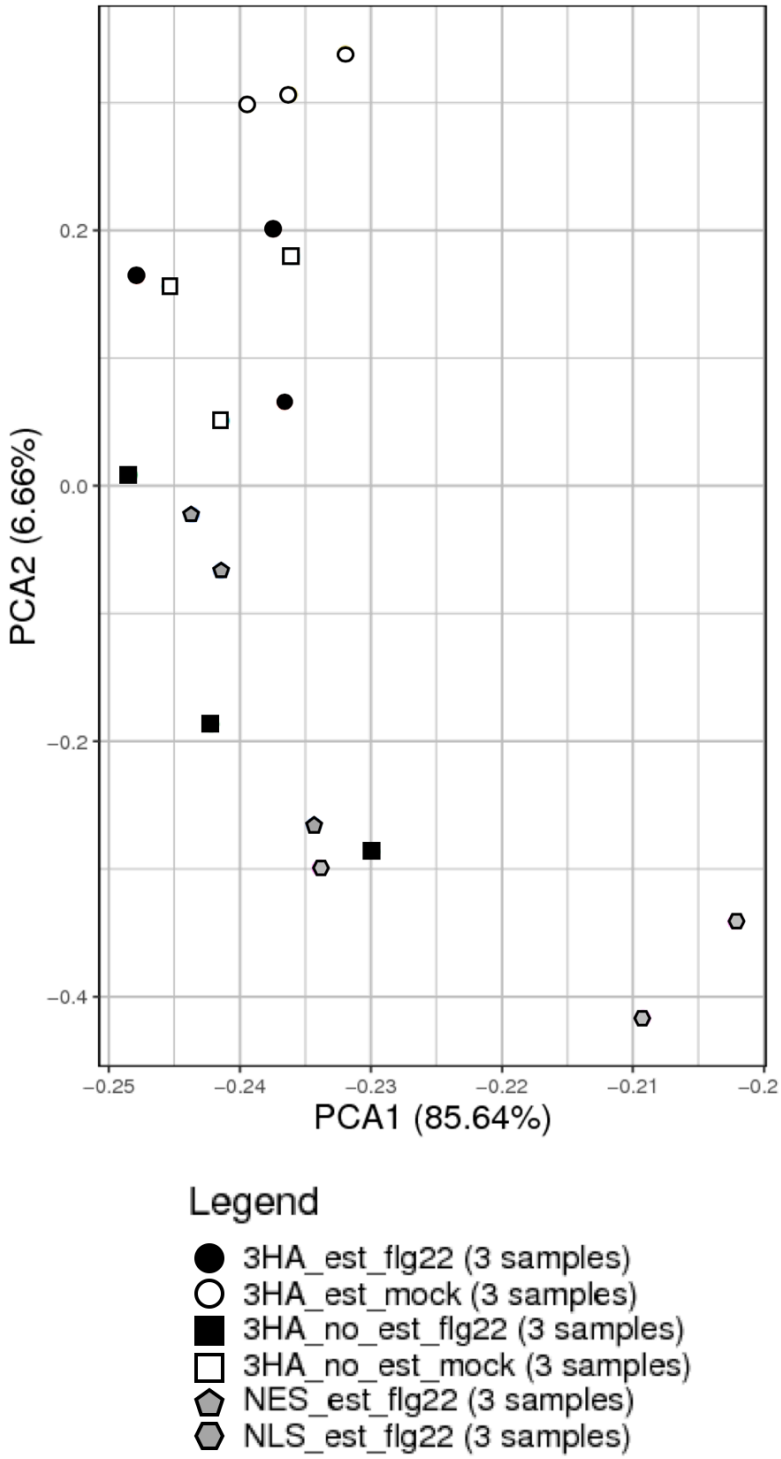

Figure 5.14: Principle Component Analysis (PCA) of RNA-Seq samples. The X axis represents the contributor rate of the first component (PCA1), while the Y axis represents the contributor rate of the second component (PCA2). Points represent each sample, containing within them 3 biological replicates each. Samples belonging to the same experimental group are denoted by points of the same colour (see legend above). PCA percentages correspond to the contribution of each component to total variation within the dataset. Regarding group sample names, "est" refers to induction with estradiol, while "no_est" refers to treatment with mock instead of estradiol. Similarly, "flg22" means samples were treated with flg22, while "mock" denotes they were treated with mock instead of flg22.

sample was mislabeled during the analysis process, and perhaps belonged to one of the uninduced sample groups. Mapping of clean sequence reads to the *Pst* DC3000 genome found that indeed one of the NLS-tagged samples (5A) had fewer reads aligned to HopAO1 than the other two replicates in its group (Supplementary Figure S5.4). This could account for its reduced PCA1-associated variability, as well as its having higher similarity in gene expression profiles to certain replicates from other RNA-seq sample groups according to Pearson coefficient analysis (Supplementary Figure S5.3), however it still exhibited a marked increase in HopAO1 reads compared to all 6 samples in the two uninduced sample groups indicating this was less likely to be as a result of misattributed sample groups, but rather due to slight differences in the extent of HopAO1 transgene induction.

There does not appear to be an obvious explanation for the variance enacted by the second determined principle component (PCA2), as increasing values along this axis do not correlate with specific experimental treatments. The uppermost points on the PCA2 axis are the closely grouped samples of *est::3HA-HopAO1-GFP* when estradiol-induced and treated with mock instead of flg22, while 3 of the 4 flg22 treated sample groups are at the lower end of the axis. This might suggest that treatment with flg22 induces the variability in gene expression brought on by PCA2, however this effect is less distinct, as estradiol-induced and flg22-treated *est::3HA-HopAO1-GFP* samples are also closely grouped toward the uppermost end of the PCA2 axis. The fact that the NES and NLS tagged HopAO1 lines are at the bottommost of the PCA2 axis along with an uninduced 3HA-HopAO1 group could also suggest that this axis of variance is caused by some interplay between the functions of HopAO1 in and outside of the nucleus, which is lost when the effector is limited in its capacity to freely localize within the host cell.

We next looked not at genes that were differentially expressed between sample groups, i.e. not just which genes were expressed at all, but whether transcripts were detected to a greater or lesser extent according to treatment type and transgenic line. Gene expression levels were calculated with RSEM (Li and Dewey, 2011), and differentially expressed genes (DEGs) were detected between sample groups using DESeq2 (Love et al., 2014). We found that treating *est::3HA-HopAO1-GFP* plants with flg22 only (i.e. no induction of effector) caused 1659 genes to be upregulated (Figure 5.15). In

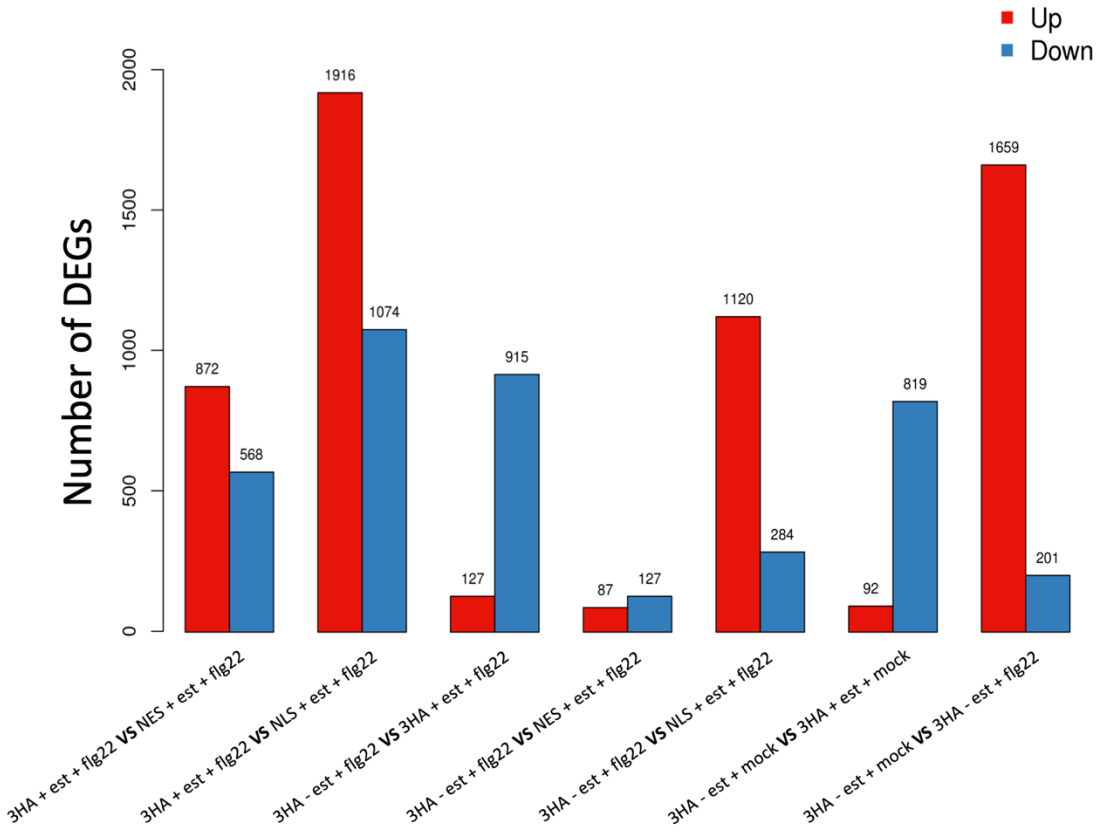

Figure 5.15: Summary of Differentially Expressed Genes (DEGs) between RNA-Seq sample groups. Genes that were differentially expressed between experimental sample groups were compared, and separated into those genes which were activated, versus those that were repressed. The X axis denotes the RNA-seq sample groups being compared, while the Y axis represents the number of DEGs. Red bars represent up-regulated DEGs. Blue bars represent down-regulated DEGs.

agreement with previous work on the induced transcriptional effects of flg22 and peptidoglycan perception in plants (Boudsocq et al., 2010; Denoux et al., 2008; Gust et al., 2007), several genes previously identified as being upregulated in response to flg22 were also identified as being significantly upregulated in our analysis. Among these were the defense-associated genes *MAPK5* (AT4G11330, fold change ~2.36, p = $1.42e^{-27}$), *MAPK3* (AT3G45640, fold change ~1.85, p = $2.86e^{-29}$), *WRKY40* (AT1G80840, fold change ~1.67, p = $5.43e^{-19}$), *BIK1* (AT2G39660, fold change ~1.31, p = $4.28e^{-12}$), *EFR* (AT5G20480, fold change ~1.17, p = $9.79e^{-08}$), *FLS2* (AT5G46330, fold change ~1.17, p = 0.00025), *RIN4* (AT3G25070, fold change ~1.34, p = $6.91e^{-12}$), and *RPM1* (AT3G07040, fold change ~1.16, p = 0.0003). We can conclude that we were successful in inducing MTI by treating our samples with flg22.

The estradiol induction of 3HA-HopAO1 in both mock and flg22-treated plants results in substantial gene repression (819 and 915 downregulated genes respectively), and a

much smaller number of genes being activated (92 and 127), suggesting that HopAO1 is able to inhibit a substantial proportion of the genes upregulated upon flg22 perception during MTI. Interestingly, the induction of non-nuclear localized HopAO1 (NES) when compared to no HopAO1 expression in flg22-treated plants produces relatively few transcriptomic changes, amounting to the downregulation of 127 genes and activation of only 87. It does not produce a similar extent of downregulation of genes to that seen when 3HA-HopAO1 plants are induced. Induction of nuclear HopAO1 compared to no HopAO1 induction in flg22-treated plants further increases the number of activated genes, but also downregulates 284. The number of genes downregulated by either NES or NLS-tagged HopAO1 does not amount to the full 915 genes downregulated by 3HA-tagged HopAO1. This suggests that the inhibition of flg-22 induced gene upregulation achieved by HopAO1 relies both on action by HopAO1 inside and outside the nucleus, but also potentially on HopAO1 in other subcellular compartments (such as in the chloroplast), or indeed on a complex interplay of pathways regulated by HopAO1 presence in multiple sub-cellular compartments at once. HopAO1 clearly has distinct functions according to its localisation. The latter of these theories is corroborated with the fact that loss of non-nuclear or nuclear HopAO1 in flg22-treated plants (i.e. compared to 3HA-HopAO1 induced) results in far greater changes in gene regulation than in comparison to uninduced plants. When nuclear *HopAO1* alone is induced, for instance, it downregulates 284 genes. When nuclear HopAO1 function is lost however, 872 genes are upregulated relative to 3HA-HopAO1 expressing plants.

It is clear that HopAO1 expression results in the differential expression of many genes not triggered by flg22 treatment. A Venn diagram showing the DEGs shared by *A. thaliana* plants treated with flg22 versus those in which 3HA-HopAO1 expression has also been induced has an overlap of 625 genes, but 417 genes are differentially expressed solely in response to expression of HopAO1, and 1235 only when HopAO1 is not present (Figure 5.16, A). This tells us that HopAO1 triggers transcriptional changes in pathways other than those altered by flg22 treatment. These pathways are likely to extend beyond the induction of MTI by the host. Furthermore, while 625 genes differentially expressed in response to flg22 are subject to further regulation when HopAO1 is expressed, only 263 of these are differentially expressed when HopAO1 localisation is limited either to the nucleus, or solely outside the nucleus

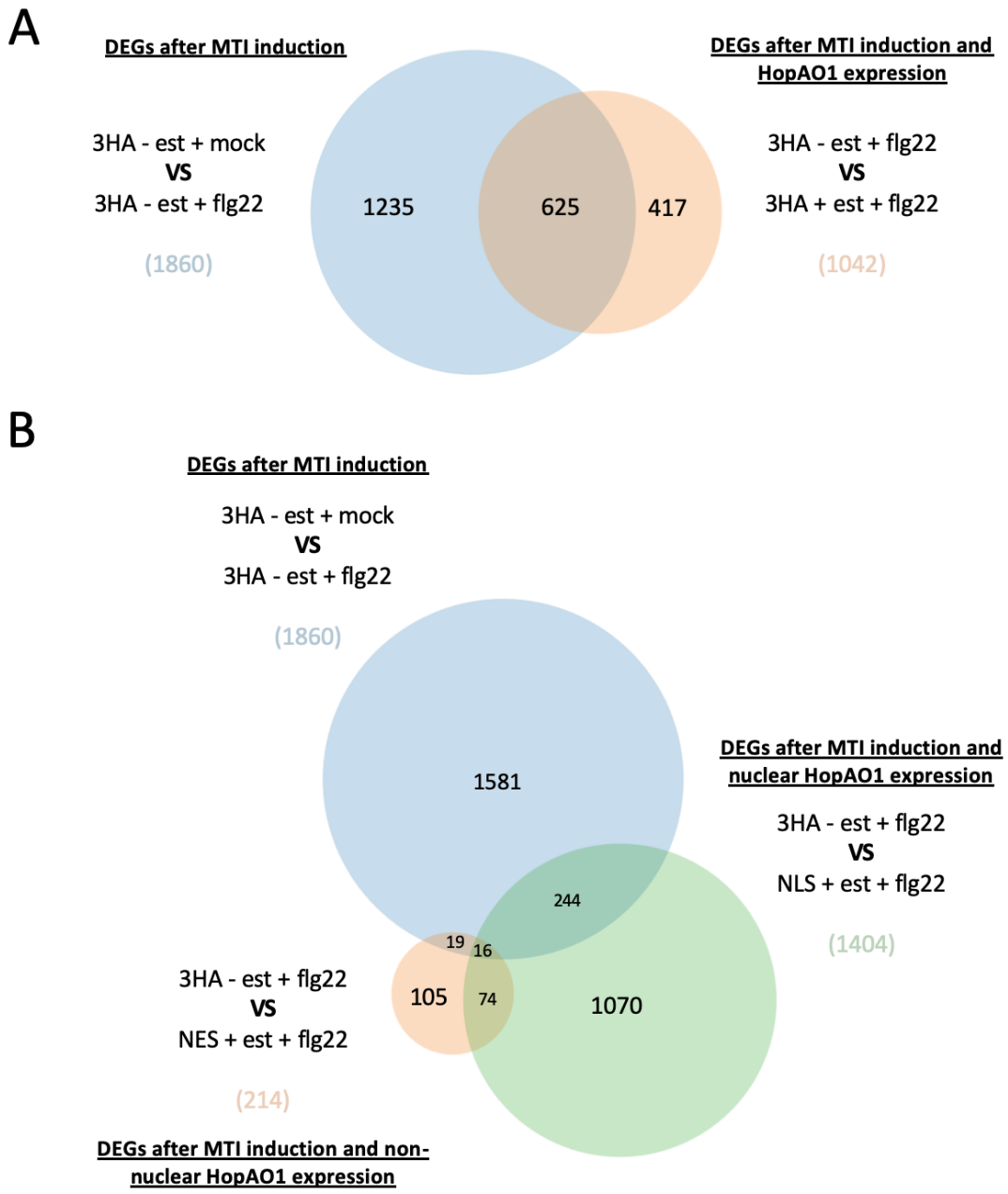

Figure 5.16: Proportional Venn diagrams of DEGs between groups of RNA-Seq samples. Venn diagrams show the number of differentially expressed genes shared amongst RNA-Seq sample comparison groups. A) 2-way comparison of DEGs between "3HA -est +mock vs. 3HA -est +flg22" and "3HA -est +flg22 vs. 3HA +est +flg22". B) 3-way comparison of DEGs between "3HA -est +mock vs. 3HA -est +flg22", "3HA -est +flg22 vs. NLS +est +flg22", and "3HA -est +flg22 vs. NES +est +flg22".

(Figure 5.16, B). This means that HopAO1 needs to localise elsewhere in the cell, or act on pathways from within and without the nucleus simultaneously in order to alter

transcript levels of all 625 genes. HopAO1 must have coordinate function in different areas of the cell. Interestingly, the expression of only nuclear HopAO1 impacts the expression of far more genes than its 3HA-tagged form, and NES-tagged HopAO1 far fewer. This further supports the interplay of HopAO1 functions in different sub-cellular compartments. Only 90 DEGs were identified in both NLS and NES induced samples suggesting that HopAO1's ability to induce transcriptional changes is highly dependent on its localisation within the host cell.

By investigating the identity of the flg22 induced DEGs subject to further regulation by HopAO1 (the overlapping region of 625 DEGs in Figure 5.16, A) it was found that 41% of them were regulated by NLS-HopAO1 only, while only 5.6% were regulated only in response to NES-HopAO1. 2.6% of the 625 could be differentially regulated by HopAO1 wherever it was localised, and the remaining 50.8% were only differentially regulated by 3HA-HopAO1, meaning that their regulation was dependent on the coordinate function of HopAO1 in various subcellular locations. This tells us that nuclear HopAO1 alone accounts for the regulation of a far larger proportion of flg22 induced genes than HopAO1 localised elsewhere, but that a larger number still relies on coordinate function of HopAO1 in multiple subcellular locations.

Finally, we looked at the specific pathways being enriched to a differential extent according to flg22 treatment and HopAO1 localisation. To do this we used the Kyoto Encyclopedia of Genes and Genomes (KEGG) annotation where DEGs were categorised into groups of specific functional pathways according to official classification, and subject to pathway functional enrichment analysis (Figure 5.17).

Figure 5.17: KEGG Pathway functional enrichment of DEGs between groups of RNAseq samples. (Overleaf) The colour of each point indicates the q-value of each pathway (high: light, low: dark, red for upregulated genes, blue for down). A lower q-value indicates more significant pathway enrichment. Point size indicates the number of DEGs in the comparison group. Bigger dots refer to a larger amount of DEGs. "Rich Factor" refers to the value of enrichment factor, which is the quotient of the foreground value (the number of DEGs) and background value (total gene amount). The larger the value, the more significant the enrichment. A) Plant-pathogen interaction. B) MAPK signalling C) Circadian Rhythm.

A

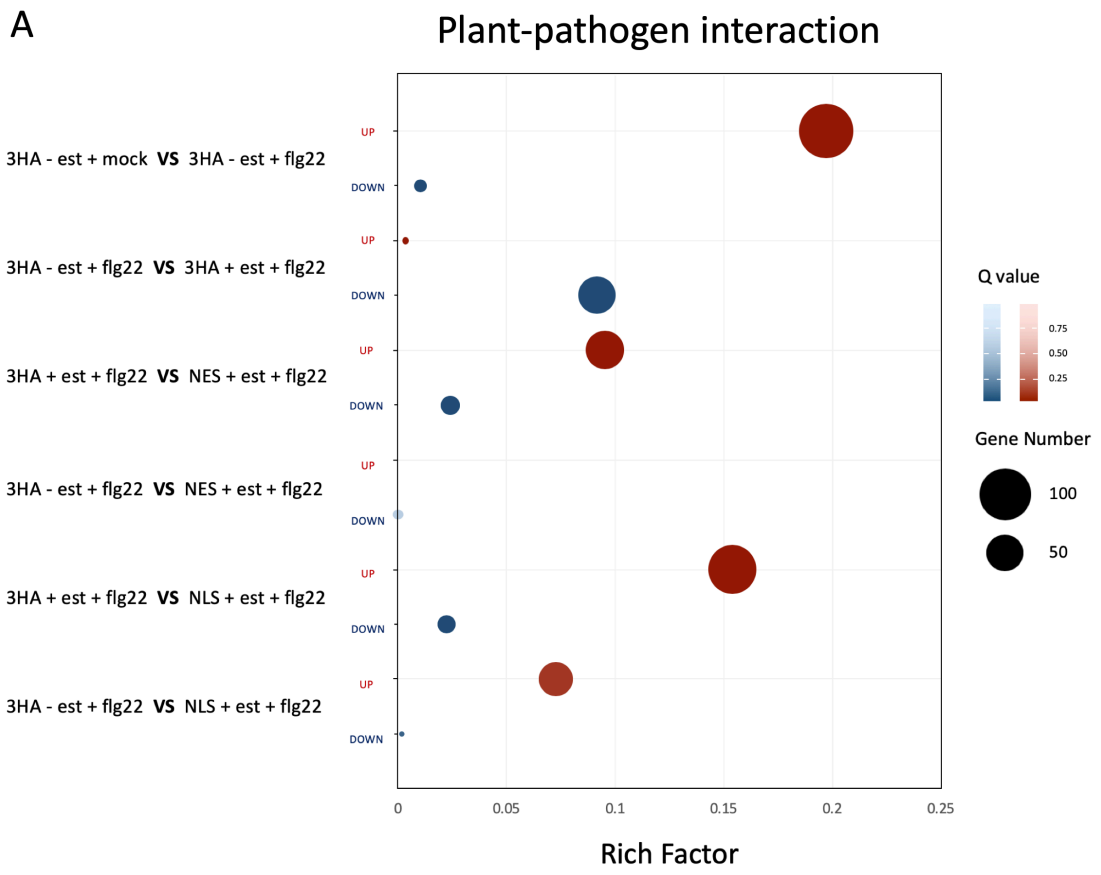
Plant-pathogen interaction
3HA - est + mock VS 3HA - est + flg22
3HA - est + flg22 VS 3HA + est + flg22
3HA + est + flg22 VS NES + est + flg22
3HA - est + flg22 VS NES + est + flg22
3HA + est + flg22 VS NLS + est + flg22
3HA - est + flg22 VS NLS + est + flg22
UP
DOWN
0
0.05
0.1
0.15
0.2
0.25
Rich Factor
Q value
0.75
0.50
0.25
Gene Number
100
50

B

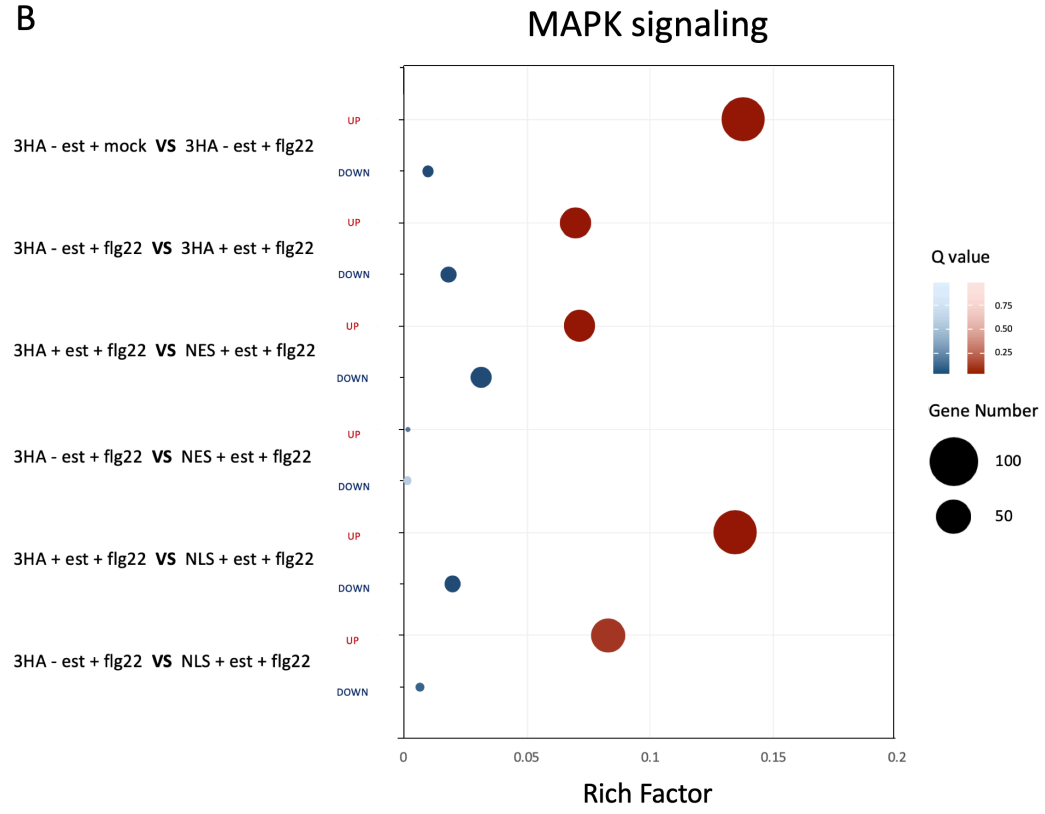
MAPK signaling
3HA - est + mock VS 3HA - est + flg22
3HA - est + flg22 VS 3HA + est + flg22
3HA + est + flg22 VS NES + est + flg22
3HA - est + flg22 VS NES + est + flg22
3HA + est + flg22 VS NLS + est + flg22
3HA - est + flg22 VS NLS + est + flg22
UP
DOWN
0
0.05
0.1
0.15
0.2
Rich Factor
Q value
0.75
0.50
0.25
Gene Number
100
50

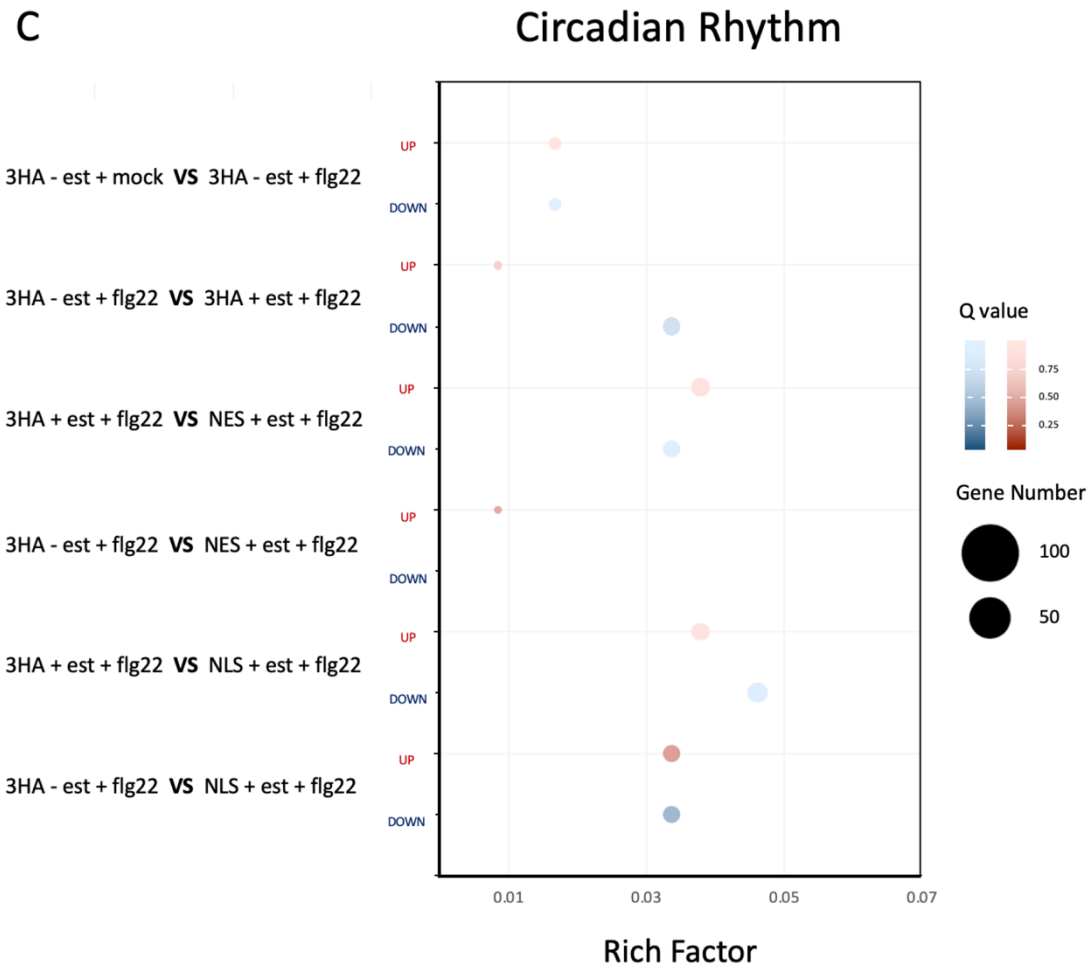

As expected, treatment with only flg22 resulted in significant enrichment for DEGs involved in plant-pathogen interactions (120 total DEGs in this pathway) and MAPK signalling pathways (89 total DEGs), both of which substantiated largely by DEGs being upregulated (Figure 5.17 A and B). Flg22 treatment also resulted in the metabolism and biosynthesis of numerous defence-associated compounds such as zeatin, phenylpropanoids and fatty acids (Supplemental Figure S5.5, A) (Großkinsky et al., 2013; Dixon et al., 2002; Walley et al., 2013). The induction of 3HA-HopAO1 in flg22-treated plants caused further differential expression of genes involved in defence (Figure 5.17, A), with defence DEG's predominantly being downregulated following the effector's expression being induced. Whereas the gene encoding NB-LRR *RPM1* (AT3G07040) is upregulated in response to flg22 treatment, induction of 3HA-HopAO1 results in a significant downregulation of the gene (fold change -1.07, $p = 0.0018$). Other genes in this category for which the same is true include those encoding transmembrane receptor protein SERK4 which has redundant cell death-

triggering function with BAK1 (de Oliveira et al., 2016) and 12 WRKY transcription factors. Importantly, while the induction of 3HA-tagged HopAO1 (i.e. free localisation) resulted in significant downregulation of host genes involved in defence, induction of either NES or NLS-tagged HopAO1 did not, although the loss of HopAO1 being able to localise in or outside of the nucleus produced significant upregulation of genes in this pathway (Figure 5.17 A). This indicates the need for HopAO1 to localise to multiple sub-cellular compartments simultaneously in order to inhibit host immunity, and suggests that HopAO1 existing either in or out of the nucleus alone is likely detrimental to the pathogen.

It is interesting to note that the expression of NLS-HopAO1 versus uninduced plants produced a significant enrichment for genes in the MAPK signalling pathway, but expression of NES-HopAO1 versus uninduced plants did not (Figure 5.17 B). We did not find evidence of HopAO1 inducing differential expression of *MPK3* or *MPK6*, in contrast with previous findings in which it was reported to activate these MAP kinases (Underwood et al., 2007). While HopAO1 expression did lead to the downregulation of several other genes involved in MAPK signalling pathways such as *MEK1* (AT4G26070) and *MAPKKK15* (AT5G55090) which could support a model more in line with that put forward by Espinosa et al. (2003) in which HopAO1 downmodulates MAPK signalling pathways, the overall trend seen by HopAO1 induction favours the upregulation of genes involved in the MAPK pathways, even if those DEG's found here are not the same genes as reported by Underwood et al. (2007). Our results are also at odds with the suggestion that a system in which HopAO1 is stably expressed under an inducible promoter in transgenic *A. thaliana* host plants could account for the differences seen by Underwood et al. (2007) as our study also follows this experimental design.

Pathways that were significantly enriched specifically in response to HopAO1 rather than flg22 alone included the biosynthesis of flavonoids, in which many DEGs were downregulated (Supplemental Figure S5.5, B). Since flavonoids have strong antioxidant capabilities and are capable of inactivating ROS compounds (Vicente and Boscaiu, 2018) this result is intriguing, as HopAO1 has been seen to reduce the production of ROS in the host cell during MTI (Castañeda-Ojeda et al., 2017). Downregulating their biosynthesis is therefore not in line with the disease sympotoms

previously associated with the effector. This suggests that HopAO1 in host cells might result in the repression of flavonoid biosynthesis, but that the effector may act on genes in other pathways to counteract ROS production.

Although the plant circadian rhythm does not appear as a pathway that is significantly enriched overall compared to others following HopAO1 expression (Figure 5.17 C), we did find 10 DEGs when 3HA-HopAO1 was induced that are associated with the clock. Among these were *FKF1* (AT1G68050), which encodes a blue light receptor that together with ZTL mediates day length discrimination (Imaizumi et al., 2003; Zoltowski and Imaizumi, 2014), and *BZS1* (AT4G39070) which is thought to mediate crosstalk between the light input pathway and brassinosteroid signalling (Fan et al., 2012). It is not altogether surprising that the circadian rhythm KEGG pathway is not seen to be enriched among DEGs in this study, however, if we consider that by disrupting relatively few components of the central oscillator, effectors such as HopAO1 could still achieve dysregulation of a large number of genes in clock output pathways that would benefit pathogenic virulence. The samples' individual DEGs within the circadian rhythm pathways are of more interest.

Remarkably, although 3HA-HopAO1 induction was not highly enriched overall for genes involved in the plant circadian rhythm, the loss of nuclear HopAO1 (i.e. comparing 3HA-HopAO1 to NES-HopAO1) did result in notable changes to the clock transcriptome (Figure 5.17, C). When HopAO1 could not localise to the nucleus, the changes to *FKF1* and *BZS1*, along with other unnamed genes in the pathway were reversed. Additionally, there was significant upregulation of *LHY* (AT1G01060, fold change ~1.02, p value = $5.88e^{-05}$), and downregulation of *PRR5* (AT5G24470, fold change ~-1.70, p value = $7.73e^{-06}$) and *PRR7* (AT5G02810, fold change ~1.06, p value = 0.00046), both of which are typically repressed by LHY (Adams et al., 2015). This supports our proposed model in which NAM's binding of *pLHY* is enhanced by HopAO1 in the nucleus in order to negatively regulate its expression. Contrastingly, *CCA1* and *TOC1* were not found to be differentially expressed when HopAO1 nuclear localisation was inhibited by an NES tag. This somewhat agrees with our RT-qPCR results for the *nam-1* mutant in which *LHY* transcripts underwent more drastic and highly significant changes in fold change relative to the other two clock genes. It is not clear why, if this is the case, induced *3HA-HopAO1* lines did not have differential

expression of *LHY*, as in this sample group *LHY* transcripts were lowered, but not significantly so. Perhaps HopAO1's impact on *LHY* is countered by the action of other genes regulated by HopAO1 in the nucleus, but that the effector's regulation of genes involved in the light input pathways is still sufficient to produce disrupted circadian phenotypes.

Perhaps unexpected was the finding that expression of NAM was significantly upregulated in response to flg22 treatment (AT3G12910, fold change ~5.23, p value = $5.40e^{-39}$), as well as in response to HopAO1 in the nucleus (fold change ~1.81, p value = 0.035), but not in response to NES or 3HA-HopAO1 induction. Furthermore, loss of non-nuclear HopAO1 (3HA-HopAO1 vs NLS-HopAO1 induced) produced significant upregulation of NAM (fold change ~2.76, p value = 0.003). This indicates the host upregulates expression of NAM during MTI, and that when HopAO1 is in the nucleus this results in further upregulation, but that when HopAO1 is also present elsewhere in the cell, this triggers downregulation of NAM. Together these results suggest that expression of NAM is likely beneficial to the host during MTI, but that regulation of its expression is contended for in response to HopAO1-responsive pathways both in and out of the nucleus. Perhaps during MTI, NAM is upregulated, and during ETI NAM is downregulated. MTI is known to inhibit certain ETI pathways, thus if NAM was typically downregulated during later stages of infection it might be beneficial to the pathogen to activate *nam* (Hatsugai et al., 2017).

The plant circadian rhythm is not a pathway enriched amongst the DEGs identified in samples expressing NLS-HopAO1 in comparison to 3HA-HopAO1 (Figure 5.17, D), supporting a role for clock disruption by HopAO1 in the nucleus. While loss of non-nuclear HopAO1 (comparing NLS-HopAO1 to 3HA-HopAO1) does impact expression of some clock genes, *LHY*, *PRR5,* and *PRR7* are not amongst them although *FKF1* was. This might indicate that HopAO1 is able to impact the clock from elsewhere in the cell. The loss of nuclear or non-nuclear HopAO1 resulted in the differential expression of 44 and 67 genes associated with plant hormone signalling, respectively, as well as 62 and 93 genes associated with MAPK signalling, and 69 and 102 genes associated with plant-pathogen interaction.

Taken together, we can conclude from this that the expression of HopAO1 in the host triggers transcriptomic changes to a wide variety of pathways, and that these changes are highly dependent on its subcellular localisation in the host. As hypothesised, HopAO1 has the capacity to alter the expression of genes involved in the plant circadian rhythm in a way that is at least partially reliant on its being able to localise in the nucleus, although we suspect that DEGs associated with this pathway might be more significantly enriched following expression of HopAO1 over a longer duration. We find that expression of flg22 induces upregulation of the transcription factor NAM, and that this upregulation is exacerbated by expression of HopAO1 purely in the nucleus, but partially compensated for by HopAO1 when localised elsewhere, suggesting that NAM may be beneficial to the host during MTI, and that HopAO1 differentially contends for regulation of its expression between different cellular compartments. HopAO1 is able to significantly impact the level of expression of approximately one third of genes differentially expressed following flg22-treatment, supporting a role for HopAO1 in suppressing symptoms of MTI. While approximately 46.6% of these DEGs can be attributed to the function of HopAO1 specifically in or outside of the nucleus (41% by only nuclear and 5.6% by non-nuclear), the bulk of the remaining genes are only differentially expressed when HopAO1 is able to localise both to the nucleus and to other sub-cellular compartments, revealing a complex interplay between HopAO1 functions throughout the cell.

5.3 Discussion

5.3.1 The loss of transcription factor NAM function alone results in changes to the clock and the onset of senescence, but not response to infection by Pst.

In this chapter, it was our hope that we would be able to elucidate the potential role played by NAM in the response of *A. thaliana* to infection by the bacterial pathogen *Pst.* While the *nam-1* loss of function mutant has been previously described with regards to its dawn and dusk *LHY* transcript levels both under normal photoperiod and constant light conditions (Davies, 2013), we hoped to expand upon this phenotypic

characterisation to include other circadian genes, as well as evaluate the immunity phenotype of the mutant.

If we first consider the role NAM plays on regulation of the circadian clock, our findings agree with those put forward in the aforementioned study, finding that under typical 12:12LD photoperiods NAM has a negative regulatory effect on *LHY* expression at dusk. We also find the mutant to have increased transcript levels for another core clock gene *TOC1* at dawn. It might have been expected that an increase in LHY at dusk would result in decreased levels of TOC1 at dusk on account of the repressive activity of the *TOC1* gene by the LHY/CCA1 heterodimer (Alabadi et al., 2001). The fact that this was not the case may be an indication that NAM is also able to negatively regulate *TOC1* expression such that loss of NAM causes an increase in dusk TOC1 levels sufficient to overcome the repressive activity of LHY. This would also account for the significant increase in *TOC1* transcripts at dawn in the *nam-1* mutant, when *LHY* and *CCA1* levels were not significantly elevated. Given that TOC1 is also a repressor of *CCA1* and *LHY*, both through its association with the chaperone CHE and its inhibition of *GI*, a suggested activator of *CCA1* (Pruneda-Paz et al., 2009; Martin-Tryon et al., 2006), its increased levels at dawn in the *nam-1* mutant may account for the lack of elevated *LHY* and *CCA1* transcripts at this time.

Although the capacity for NAM to bind to *CCA1* and *TOC1* has not been assessed, it is theoretically possible that it may also physically repress transcription of both these genes. NAM is thought to bind to *pLHY* in a way that is dependent on three specific, proximal 5A motifs (AAAAA) (Davies, 2013). Given that *CCA1* and *LHY* exhibit three near-perfect matches for evolutionarily conserved regions within their upstream promoter sequences, and furthermore *CCA1* has 14 upstream 5A motifs (Spensley et al., 2009), it certainly seems possible that NAM could also repress *CCA1,* although the results of the qPCR assay do not support this. This is however also possible for the evening-phased *TOC1* gene, whose upstream activation sequence is also enriched for 5A motifs, possessing 9 within the 577 base pairs preceding the start of its coding sequence according to data in the NCBI genome browser (O'Leary et al., 2016). The results here presented indicate that NAM has a repressive effect on *LHY*, and directly or indirectly on *TOC1*.

It is perhaps surprising that NAM loss-of-function scarcely produced any changes in the responsiveness of *nam-1* to infection by *Pst*, as in every case the mutant proffered no significant difference in immunological phenotype when compared to Col-0 wild type plants. Particularly given the fact that HopAO1 binds to a number of DELLA homolog proteins, one of which has been experimentally confirmed to interact with NAM (Rosa et al., 2014), as well as to CHE, which directly regulates *LHY* (Zheng et al., 2015), it seemed natural to expect the interaction between NAM and HopAO1 to benefit either the pathogen or the host in some tangible way. The fact that no impact on immune function could be identified at all in the *nam-1* mutant therefore may be an indication that NAM shares genetic redundancy with another host protein, and thus loss of NAM is compensated for. If NAM is a susceptibility factor then this protein with shared function could perhaps be NAC074, a phylogenetically close relative of NAM which was shown to also bind HopAO1 and exhibited enhanced binding to *pLHY* in the effector's presence. If NAM has positive regulatory function of immunity against *Pst* then genetic redundancy could also arise with other close NAC TF homologs which did not interact with HopAO1, such that HopAO1's binding NAM is not detrimental to the host. This would be in line with reports that *LHY* overexpression results in increased susceptibility to *Pst* in an *A. thaliana* Ler ecotype background (Zhang et al., 2013). In order to fully ascertain the role of NAM in plant immunity therefore, we suggest the characterisation of NAC TF polymutants such as NAM and NAC074 double knockouts.

We had thought it was also possible that the *nam-1* mutant might exhibit a phenotype of delayed senescence, in a model by which NAM negatively regulates *LHY* expression. However, the NAM mutant had, if anything, an accelerated rate of senescence. It is not clear how this corroborates with the accelerated senescence reported in *LHY* loss of function mutants, but might be due to differences in the way in which senescence is triggered by age versus by extended dark incubation, as the *LHY* mutant phenotype was recorded in plants that had aged naturally to 6 weeks old, rather than being "forced" at 4 weeks old (Song et al., 2018). Alternatively, it may be that any disruption of the circadian system that puts the TTFL out of sync with its normal oscillations leads to the dysregulation of downstream pathways controlling senescence. If NAM binding by HopAO1 were enhanced to further delay senescence, this may in fact extend the period in which *Pst* could multiply in healthy live host plant

tissue. As a hemibiotroph, *Pst* can survive as a saprotroph would on decaying organic matter, however it thrives in the apoplast of living plant tissue, and so delaying the onset of senescence-induced cell death would no doubt be a viable mechanism of virulence (Xin et al., 2018; Preston, 2000). This agrees with both our findings of the *nam-1* mutant immunity phenotype and our hypothesis of NAM having genetic redundancy. If NAM is a negative regulator of senescence, this would account for the *nam-1* mutant having accelerated chlorophyll degradation. If, however, there is genetic redundancy between NAM and other NAC TFs, the *nam-1* mutant would not be expected to have an altered immunity phenotype because HopAO1 could act on the other NAC TF in NAM's stead. Studying the senescence and immunity phenotypes of the inducible HopAO1 lines would provide insight into this potential mechanism in the future, as we would expect only the NES-HopAO1 line to have relatively reduced bacterial growth, and for the NLS and 3HA- lines to have relatively delayed onset of senescence.

We should consider the fact that NAM may be involved in the regulation of immunity through changes in stomatal aperture. It has been shown that *lhy* single loss-of-function mutants exhibit increased stomatal aperture in response to *P. syringae pv maculicola* (Zhang et al., 2013), thus it may be that NAM alone is capable of negatively regulating immunity, but that we are masking its contribution by infecting plants via pressure infiltration. By spray-infecting *nam-1* mutants we may see differences in bacterial growth relative to the wild type, as we would not be bypassing the stage in which *Pst* enters the inner leaf tissue through the stomata. Another consideration is the fact that in the wild type Col-0 plants, NAM may simply not be sufficiently abundant prior to the onset of senescence, and that this might account for NAM's mutant lack of differences in immune phenotype. If NAM is not present in Col-0 until a later stage of growth, then loss of function would not impact pathogenic resistance in the *nam-1* mutant by comparison.

It seems highly unlikely, however, that NAM has no role at all in plant immunity. The upregulation of NAM in response to flg22 treatment, its differential expression upon induction of non-nuclear localised HopAO1 and its interaction with HopAO1 and the enhanced binding of NAM on the *pLHY* in the presence of the effector collectively present an exceptionally strong argument for NAM being actively involved in the *Pst*-

A. thaliana pathosystem, be it as part of immune signalling cascades and/or as a susceptibility factor. The emergingly complex role NAM seems to exert within the host allows us to foresee mechanisms by which it might act in either of these roles. NAM may by upregulated during MTI and act as a protector of the DELLA proteins, limiting HopAO1's ability to subvert their regulation of hormone signalling pathways by competitively binding to the effector. As a susceptibility factor, NAM might increasingly repress *LHY* in order to delay senescence therefore extending the period in which *Pst* could multiply in the apoplast, as well as induce circadian dysfunction, or increase stomatal aperture. We therefore propose that NAM is highly likely to have a role in plant immunity, which HopAO1 is able to influence, but that this either cannot be seen through assessment of the *nam-1* mutant alone, cannot be seen in plants up to the 4-week old stage, or cannot be seen when plants are infected in a way that bypasses entry through the stomata. We suggest that this is either on account of a) NAM having functional redundancy with other transcription factors within the NAC family, b) its only being important during the infection of plants at a later developmental stage, or c) it being subverted to enhance virulence through stomata dependent mechanisms.

5.3.2 RNA-seq analysis of HopAO1 reveals distinct transcriptomic changes dependent on its localisation, as well as a possible role for the effector targeting the circadian clock

In light of the results presented in Chapters 3 and 4 we hypothesised that the effector HopAO1 had novel uncharacterised function in the nucleus, and that this would include the regulation of genes involved in the plant circadian clock. While the transcriptomic data presented in the current chapter certainly shows this to be the case, we find that the impact of HopAO1 in the host cell produces changes that are far more complex than simply "acting on pathway X in the cytosol" and "acting on pathway Y in the nucleus". Rather, we reveal that the HopAO1-induced transcriptome probably relies on intricate associations between pathways responsive to expression of the effector in multiple cellular compartments at once.

Previous transcriptomic data on plants expressing HopAO1 has provided much insight into the effector's gene regulatory effects in an *A. thaliana* host, particularly regarding DEG's whose expression levels were dependent on its function as a tyrosine phosphatase (Underwood et al., 2007), and in comparison to work by Thilmony et al. (2006) who documented MAMP-regulated changes to the *A. thaliana* transcriptome. This study found stably expressed HopAO1 plants to induce the differential expression of only 20 MAMP-regulated genes. Of these, 4 of the 6 MAMP-activated genes were more strongly activated by HopAO1, and 12 of the 14 MAMP-repressed genes were more strongly repressed. In spite of this apparently non-virulent behaviour on the part of HopAO1, the authors describe a number of other defence-related genes differentially repressed in response to HopAO1 expression that were not associated with MTI. We report in the current study that expression of HopAO1 led to the differential expression of vastly more flg22 responsive genes than this, totalling 625. The discrepancies between our system and that of the previous study may partially account for this difference. Firstly, while both studies made use of stable, inducible transgenic HopAO1 lines, our was induced by treatment with β-estradiol instead of dexamethasone, and so these hormones themselves may have induced changes independently of those caused by the effector fusion protein. Secondly, our RNA samples came from 10-day old seedlings rather than 4-6-week old plants. This substantial difference in developmental stage would no doubt result in large changes in the transcriptome when assessed in this way. Thirdly, the transgenic lines in the previous study were generated in a Col-0 *gl1* background, which carries a mutation in *gl1* conferring reduced trichome development in order to facilitate infiltration of leaves (Bloomer et al., 2012). This mutation could produce further differences in differential gene expression. While some of our findings regarding specific DEGs differ from the work by Underwood et al. (2007), such as the lack of repression of the SA-induced defence marker gene *PR1*, and the activation of *MAPK3* and *MAPK6,* our findings do corroborate in the sense that we too find HopAO1 to have induced differential expression of many genes that lack a published role in MTI. Genes in this category would be deserving of further characterisation in the future as a way identifying novel immune components in *A. thaliana*.

Additionally, we extend the findings of such previous transcriptomics studies through the use of inducible HopAO1 transgenic lines in which the effector is specifically

localised to certain sub-cellular compartments in order to elucidate its impact throughout the host cell. Our finding that the expression of only nuclear HopAO1 impacts the expression of far more genes than the NES-tagged HopAO1 supports the idea of there being complex interplay of HopAO1 functions in different sub-cellular compartments. This may also be the result of HopAO1 being more greatly concentrated in the nucleus. The action of HopAO1 outside of the nucleus seems to temper the changes brought on by HopAO1 in the nucleus. This could indicate that HopAO1 outside of the nucleus suppresses genes by preventing the full activation of MTI, and that when HopAO1 is only present in the nucleus, MTI continues to be fully activated resulting in larger downstream transcriptional changes that would benefit the host. It is fascinating that despite the extensive characterisation of HopAO1 function in the cytosol and at the cell plasma membrane, the effector seems able to enact the biggest changes to the host transcriptome when localised to the nucleus. Indeed, expression of HopAO1 that lacks the ability to localise to the nucleus when compared to flg22-treated plants produced by far the fewest number of DEGs of any comparison within the study. Thus, while HopAO1 has been clearly shown to impact immunity in a substantial way outside of the nucleus, its ability to induce transcriptional changes is highly dependent on its function in the nucleus as well. This confirms our hypothesis that the effector possesses as-of-yet uncharacterised function in the nucleus.

With regards to HopAO1's ability to disrupt the clock we made several important discoveries. KEGG pathway enrichment analysis did not reveal enrichment for DEGs associated with the plant circadian rhythm in all of the HopAO1 induced experimental groups, however we did find that in plants in which MTI is activated by flg22 treatment, induction of 3HA-HopAO1 resulted in the further differential expression of 10 genes within the KEGG group, most notable of which were *FKF1* and *BZS1*. Most interestingly, given the interaction between HopAO1 and NAM which has been heavily in focus throughout this investigation, we found that the loss of nuclear HopAO1 reversed the effects on *FKF1* and *BZS1*, which in 3HA-HopAO1 induced lines were activated and repressed, respectively. Additionally, loss of nuclear HopAO1 caused significant upregulation of *LHY* and downregulation of afternoon phased *PRR5* and *PRR7* which fittingly are both targeted for repression by *LHY*. It is worth noting that transformation of HopAO1 in protoplasts in Chapter 3 produced greatly diminished amplitude of CCA1 and GI protein levels, however the severity of this phenotype increased over 5 days under constant light. The samples used here were

assessed by RNA-seq were generated from seedlings kept in normal 12:12LD photoperiods, and were harvested 24 hours after transgene induction. It may therefore be the case that HopAO1 expression is able to generate more prominent changes in the clock transcriptome over time, as knock-on effects from the disrupted light input pathway gradually dysregulate expression of other genes in the TTFL. Nonetheless, our model in which HopAO1 localises to the nucleus where it enhances the binding of NAM in order to bring about reduced *LHY* expression, and subsequently circadian disfunction is supported by the results of this transcriptomic analysis. This also confirms our previous hypothesis that amongst the novel functions of HopAO1 in the nucleus is the targeting of the circadian clock. Whether or not HopAO1's impact on *LHY* specifically results in a net gain or loss of virulence for the pathogen *Pst* remains to be seen and is an area we propose warrants further study in the future.

5.3.3 Overview

The results presented in this chapter provide substantial evidence for the *Pst* T3SE HopAO1 not only having novel function specifically in the host cell nucleus, but also participating in the induction of vast changes to the *A. thaliana* transcriptome in a way that is highly dependent on its coordinate function in various sub-cellular compartments at once.

We have generated a trio of stable transgenic lines expressing a HopAO1-GFP fusion protein with one of 3 N-terminal tags that localise the effector both in and out of the nucleus and verified both equal expression of the effector by RT-qPCR and localisation by confocal microscopy. These transgenic lines enable not only the transcriptional assessment of localised HopAO1 function in the host as in the present study but would also permit investigation into the impact of HopAO1 localisation on its contribution to *Pst* virulence if used for the characterisation of immunity phenotypes. RNA-seq analysis of these transgenic lines has revealed that HopAO1 expression causes significant changes in the expression levels of core clock genes, some of which are dependent on the effector being localised in the nucleus. We also find HopAO1 is able to significantly downregulate the expression of several genes

associated with plant pathogen interaction providing further evidence for HopAO1 inhibiting MTI, as well as significantly upregulate expression of many genes in the MAPK signalling pathway which offers clarification where contrasting findings had previously been reported (Underwood et al., 2007; Espinosa et al., 2003).

We have performed an extensive phenotypic analysis of the *nam-1* mutant, finding loss of NAM function alone to substantially impact the expression of core clock genes, as well as advance the rate of chlorophyll degradation during dark-induced senescence. The gene was significantly upregulated in response to both MTI elicitation and induction of HopAO1. Whether NAM is a positive regulator of defence or a susceptibility factor is yet to be determined, but spray infection assays of the *nam-1* mutant as well as analysis of the senescence and immunity phenotypes of the transgenic HopAO1 lines would likely elucidate NAM's role. We also propose that NAM is likely to share genetic redundancy with other NAC transcription factors.

The results of this chapter lead us to conclude that HopAO1 exerts substantial transcriptomic changes in *A. thaliana*, which are highly dependent on its sub-cellular localisation, and include disruption of the circadian clock in agreement with results presented in previous chapters. We suggest that the effector's dysregulation of the core clock gene *LHY* is a result of its interaction with the NAC transcription factor NAM, and that NAM likely has a role in plant immunity.

Chapter 6: Summary of conclusions and future work

6.1 Research aims

When this project began there existed in the literature a distinct lack of knowledge concerning the mechanistic links between the plant circadian clock and the immune system, particularly concerning the ways in which bacterial infection might result in altered rhythmicity in host tissue. We hypothesised that bacteria were able to manipulate the plant clock in order to enhance their own virulence through the use of type III secreted effector proteins. The research presented in this project therefore aimed to clarify the ability of the bacterial plant pathogen *Pseudomonas syringae pv. tomato* (*Pst*) to employ these effectors and interfere with the circadian clock in *Arabidopsis thaliana*, as well as characterise the mechanisms by which this occurs.

6.2 The Pst Type III secreted effector (T3SE) HopAO1 acts through a NAC transcription factor to repress LHY expression and is one of several T3SEs capable of producing altered circadian phenotypes.

In Chapter 3 we investigated the importance of a functioning type III secretion system (T3SS) in the altering of circadian rhythmicity during infection of *A. thaliana* by *Pst*. We found that in this pathosystem the plant induced significant changes in the amplitude of expression for the core clock genes *CCA1* and *TOC1* following the induction of MAMP-triggered immunity (MTI) by the avirulent T3SS mutant *hrcC*, and that these changes were buffered during infection by the virulent *Pst* DC3000. Inferring from this that the delivery of effectors through the T3SS was important for *Pst*'s ability to induce altered expression of circadian genes, we performed a screen of 23 *Pst* effector proteins for the ability to disrupt circadian gene expression profiles in *A. thaliana* protoplasts. This screen uncovered 6 effectors that were able to elicit significant and consistent alterations to the clock, all reducing clock gene amplitude. While the effectors assayed varied considerably in their sub-cellular localisation and previously characterised function, we found that none of the effectors produced an

increase in the amplitude of *CCA1* or *GI* expression, indicating that the *Pst* T3SE repertoire makes a concerted effort to diminish circadian output of the host. Of the 6 effectors with clock impacting function, we chose to further explore the mechanism of action employed by one in particular- a tyrosine phosphatase, HopAO1.

In Chapter 4, we verified a report in work by Mastorakis (2017) that HopAO1 has dual localisation in the nucleus and in the cytosol where it was shown to dephosphorylate transmembrane pattern-recognition receptors (PRRs) in order to prevent the activation of downstream immune signalling cascades (Macho et al., 2014). We therefore hypothesised that HopAO1 had additional functions in the nucleus, including the ability to disrupt the circadian clock. A yeast 2-hybrid screen enabled us to identify a number of transcription factors that can interact with HopAO1. Among those detected were a suite of functionally close transcription factors with partially overlapping roles in hormone homeostasis, senescence and the clock. These included various homologs of the DELLA proteins, the circadian regulator and *TOC1* chaperone CHE, and the NAC family transcription factor NAM. NAM had been shown in the past to directly associate with the promoter of the core clock gene *LHY* and repress *LHY* transcription (Davies, 2013). In light of this, we postulated a model in which HopAO1 might target NAM to achieve mis-regulation of clock gene expression. We tested this model first by assessing the ability of HopAO1 to influence NAM's interacting with *pLHY* in a yeast one-hybrid system, and found the effector was able to enhance the strength of the interaction. Thus, we proposed that HopAO1 produces circadian defects by enhancing NAM's repression of *pLHY*. HopAO1 was also able to associate with a phylogenetically close relative of NAM within the NAC TF family, NAC074, leading us to presume that the NAC TFs might possess genetic redundancy in their function.

In Chapter 5 we sought to clarify the downstream mechanism of HopAO1 in the *A. thaliana* nucleus. One way in which we achieved this was by adopting an RNA-seq approach, looking for changes in the effector-induced transcriptome during MAMP-triggered immunity (MTI) that were significantly impacted by HopAO1's subcellular localisation. We generated a trio of stable transgenic lines expressing a HopAO1-GFP fusion protein with one of 3 N-terminal tags that targeted the effector to different sub-cellular compartments including the nucleus. In this way we hoped to uncover evidence for nuclear HopAO1 disrupting the clock as well as the nature of its

interaction with NAM. Furthering previous studies performing transcriptomic analysis of HopAO1 as well as the functional characterisation of HopAO1 in the cytosol/at the plasma membrane (Underwood et al., 2007; Macho et al., 2014; Espinosa et al., 2003), we discovered that HopAO1 expression caused significant changes in the expression levels of core clock genes, some of which were dependent on the effector's nuclear function. Loss of HopAO1 in the nucleus resulted in a significant upregulation of *LHY,* in addition to the downregulation of two other core clock genes under *LHY* regulation, *PRR5* and *PRR9*.

We report that HopAO1 is able to significantly downregulate the expression of several genes associated with plant pathogen interaction providing further evidence for HopAO1 inhibiting MTI, as well as significantly upregulate expression of many genes in the MAPK signalling pathway which offers clarification where contrasting findings had previously been reported (Underwood et al., 2007; Espinosa et al., 2003; Macho et al., 2014). Furthermore, we found that HopAO1 was able to significantly regulate the expression of approximately one third of MTI-regulated genes, providing evidence that HopAO1 suppresses the symptoms of MTI. While approximately 41% of these DEGS were attributed to the function of HopAO1 specifically in the nucleus, a substantial number of the remaining genes were only differentially expressed when HopAO1 was able to localise both to the nucleus and to other sub-cellular compartments. We therefore conclude that transcriptomic changes enacted by HopAO1 in *A. thaliana* are heavily reliant on its function in the nucleus, but the majority of changes made by HopAO1 rely on its coordinate function both in and out of the nucleus. Our analysis of the HopAO1 inducible lines revealed that the transcription factor NAM is upregulated during MTI, but further activated specifically by HopAO1 in the nucleus. This leads us to suggest that NAM is likely to have a role in immunity, and may be upregulated during MTI, but its function during effector-triggered immunity (ETI) is hijacked by nuclear HopAO1 in order to bring about susceptibility to the pathogen instead.

In order to characterise the nature of HopAO1's interaction with NAM, the role of NAM was investigated at length through an extensive phenotypic analysis of the loss of function mutant *nam-1*. We characterised the immune responses, senescence onset, and circadian gene expression profiles of this mutant. It was found that the NAM

mutant had an unaltered immunity phenotype but had significant differences from the wild type with regards to its rate of senescence and clock gene expression patterns. The mutant exhibited an accelerated rate of chlorophyll degradation in response to dark induced senescence, suggesting a role for NAM as a negative regulator of senescence. The mutant also had increased expression of *LHY* at dusk (as had previously been described in Davies, 2013) as well as *CCA1* at dusk, and *TOC1* at dawn. This indicated that NAM is a negative regulator not only of *LHY*, but also potentially of *CCA1* and *TOC1* although ascertaining whether the latter two of these are due to direct repression or downstream disruption of clock gene oscillations in the transcriptional-translational feedback loop (TTFL) requires further study.

The fact that no impact on immune function could be identified for the *nam-1* mutant in spite of it being differentially expressed following MTI or HopAO1 induction serves as indication that NAM may share genetic redundancy with another host protein, and thus loss of NAM is compensated for. Therefore, while it is not impossible that NAM is a positive regulator of immunity, we propose that the most likely model of HopAO1's interaction with NAM and its induction of subsequent circadian defects involves NAM as a susceptibility factor sharing genetic redundancy with another NAC TF. In this way, enhancement of NAM's function by HopAO1 might result in delayed senescence benefitting the pathogen by extending its biotrophic phase of development, increased stomatal aperture through *LHY* repression, or another yet undiscovered mechanism of virulence. Studying the senescence and immunity phenotypes of the inducible HopAO1 lines will no doubt provide insight into this potential mechanism in the future.

6.3 Future work

The data presented in this thesis provides new insight into roles for *P. syringae* type III secreted effectors inducing altered circadian phenotypes in the model organism *A. thaliana*. In particular we have explored the function of the effector HopAO1 which is revealed to produce extensive changes to the plant transcriptome when localised in the nucleus and is proposed to act through NAM to disrupt the clock and enhance

pathogenic virulence. It is hoped that the findings described throughout this work will enable further advances in our understanding of the interconnected pathways of plant immunity and circadian rhythmicity. Some potential experiments that would expand on the results presented here and elucidate the interplay between these two systems, as well as the clock-disrupting mechanism of HopAO1 include the following:

- We identified 6 *Pst* T3SEs with consistent and robust capacity to dysregulate the circadian clock. While functional characterisation of the mechanisms of all 6 these effectors was not possible within the scope of this project, we suggest that the effectors HopX1 and HopF2 in particular would be worthwhile subjects for investigation. We anticipate that HopX1 is likely to induce circadian defects through the degradation of JAZ proteins in the nucleus, and that HopF2 may be of use as a synthetic tool in circadian studies for inducing an increase in period length if its ability to induce a lengthened period is found to be independent of its virulent function.

- The inducible and localised HopAO1 transgenic lines were generated in an *LHY:LUC* background. This was in order to permit the future bioluminescent analysis of *LHY* expression *in planta* as was performed in Chapter 3. It would be useful to determine whether induction of HopAO1 in and out of the nucleus corresponds to detectable changes in LHY abundance as well as to *LHY* transcripts as shown in Chapter 5. We anticipate that a disruption in the *LHY* expression rhythm would be seen in the 3HA and NLS-HopAO1 lines, but not the NES line in accordance with HopAO1's clock disrupting function relying on its nuclear localisation.

- The screen for effectors' clock disrupting functions in protoplasts in Chapter 3 involved measurement of *CCA1* and *GI* expression and found HopAO1 to diminish the amplitude of each. This however did not fully corroborate with the results of the RNAseq assay in which differential expression of these genes was not detected. Measuring the expression rhythms of the *LHY* gene of protoplasts transfected with HopAO1 would no doubt clarify the relationship between the effector's transcriptomic and translatomic phenotypes. We

anticipate that the *LHY* rhythm would be more severely affected by HopAO1 expression than that of *CCA1* and *GI*.

- The verification of the HopAO1 interaction with both NAM and NAC074 through transient expression *in planta* and subsequent Co-immunoprecipitation and/or mass spectrometry would provide suitable evidence that the interaction occurs in plants as well as in yeast and would negate the caveats associated with yeast 2-hybrid determined interactions.

- In order to better understand the interaction between HopAO1 and NAM/NAC074 it would be prudent to assess whether the transcription factors were being dephosphorylated by the effector. To this end, a phosphoproteomics approach could be applied in which the phosphorylation status of NAM/NAC074 could be determined by Mass spectrometry in plants both expressing and not expressing HopAO1, as well as repeating the Y2H and Y1H assays in Chapter 4 using the catalytically inactive form of HopAO1 (Macho et al., 2014). Together these experiments would indicate whether or not the TFs were dephosphorylated by HopAO1, and whether or not this was required in order for the effector to enhance their binding of *pLHY*.

- The circadian regulatory function of NAM could be clarified by assessing the TF's propensity to bind to the promoters of *TOC1* and *CCA1* using a Y2H approach as in Chapter 4. This would determine whether the increased *TOC1* transcripts seen in the *nam-1* mutant in Chapter 5 were due to the relieving of direct or indirect repression by NAM.

- If NAM has a role in immunity by indirectly regulating stomatal aperture though LHY, the immunity phenotype of the *nam-1* mutant would have been masked by infection of plants using pressure infiltration as this bypasses stomatal entry by the pathogen. To determine whether NAM enhances HopAO1-mediated virulence by increased stomatal aperture, we advise the spray infection of *nam-1* mutants with *Pst*, as well as spray infection of the NLS/NES/3HA transgenic HopAO1 lines.

- We suspect that the lack of immunity phenotype in the *nam-1* mutant could also have been due to genetic redundancy between NAM and other NAC TF mutants. It would therefore be prudent to repeat the immunity phenotype assays performed in Chapter 5 on a double loss-of-function mutant of NAM and NAC074 (currently being generated in the Ntoukakis lab), and other NAM/NAC polymutants. We hypothesise that HopAO1 acts through NAM and NAC074 interchangeably, thus reduced bacterial growth would only be visible in a double mutant.

- A full immunity phenotype analysis such as in Chapter 5 of the inducible transgenic HopAO1 lines would provide insight into the contribution of HopAO1 in each sub-cellular compartment/coordinate function from multiple sub-cellular compartments to *Pst* virulence. We suspect that the enhanced bacterial growth reported in response to HopAO1 expression would be reduced in the NES-HopAO1 line if either NAM or nuclear localisation of the effector is required for HopAO1-induced virulence.

- Analysing the rate of senescence onset and chlorophyll degradation in the transgenic HopAO1 lines would elucidate whether or not HopAO1 enhances *Pst* virulence by delaying senescence and extending the pathogen's biotrophic phase, such as in the proposed model with NAM.

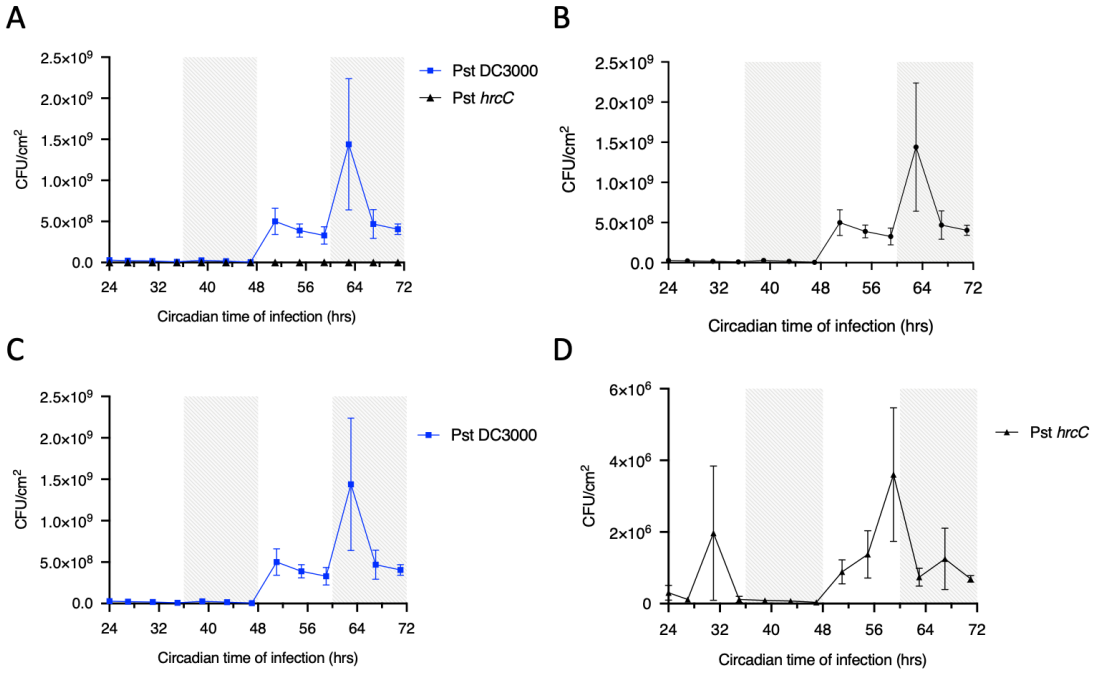

Supplementary Figure S3.1: Temporal variation of *Arabidopsis thaliana* in its susceptibility to infection by both virulent and avirulent *P. syringae pv. tomato,* presented on a linear scale. A) 4-week-old wild-type Columbia (Col-0) *Arabidopsis* plants were grown at 22°C in 12:12 LD conditions, then moved to LL for 24 hours. Leaves were pressure infiltrated at the times indicated with *Pst* DC3000 (blue squares) or *hrcC* (black triangles) at OD_{600} 0.001. Bacterial counts were recorded (CFU/cm^2 ± SEM, n = 4) in leaves at 48 hours post infection (hpi). Two-way Analysis of Variance (ANOVA) revealed a significant effect of time of infection on bacterial growth, as well as on pathogen genotype ($p<0.0001$), but not on the interaction between time of infection and genotype. B) Difference in bacterial titre between *Pst* DC3000 and *hrcC* infected wild-type Columbia (Col-0) *Arabidopsis* at different times of day (± SEM, n = 4). C-D) Bacterial growth counts of DC3000 (C) and *hrcC* (D) infected plants are plotted separately to show trends in bacterial enumeration more clearly, as the difference in the virulence of each genotype means *hrcC* values are masked when plotted alongside DC3000 in panel A. Grey shaded areas indicate subjective night.

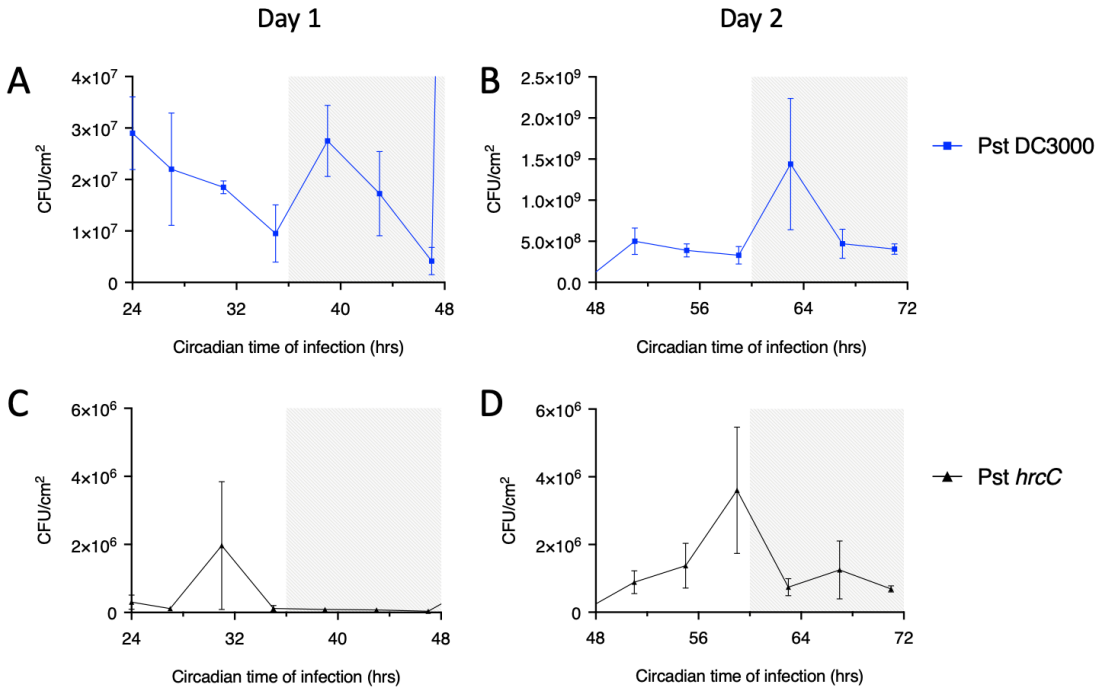

Supplementary Figure S3.2: Temporal variation of *Arabidopsis thaliana* in its susceptibility to infection by both virulent and avirulent *P. syringae pv. tomato* on days 1 and 2 of infection, presented on a linear scale. 4-week-old wild-type Columbia (Col-0) *Arabidopsis* plants were grown at 22°C in 12:12 LD conditions, then moved to LL for 24 hours. Leaves were pressure infiltrated at the times indicated with *Pst* DC3000 (blue squares) or *hrcC* (black triangles) at OD_{600} 0.001. Bacterial counts of DC3000 (A and B) and *hrcC* (C and D) infected plants were recorded (CFU/cm^2 ± SEM, n = 4) in leaves at 48 hours post infection (hpi). Counts are further separated and plotted for each 24-hour period to demonstrate differences on the first (A and C) and second (B and D) day of inoculations. Grey shaded areas indicate subjective night.

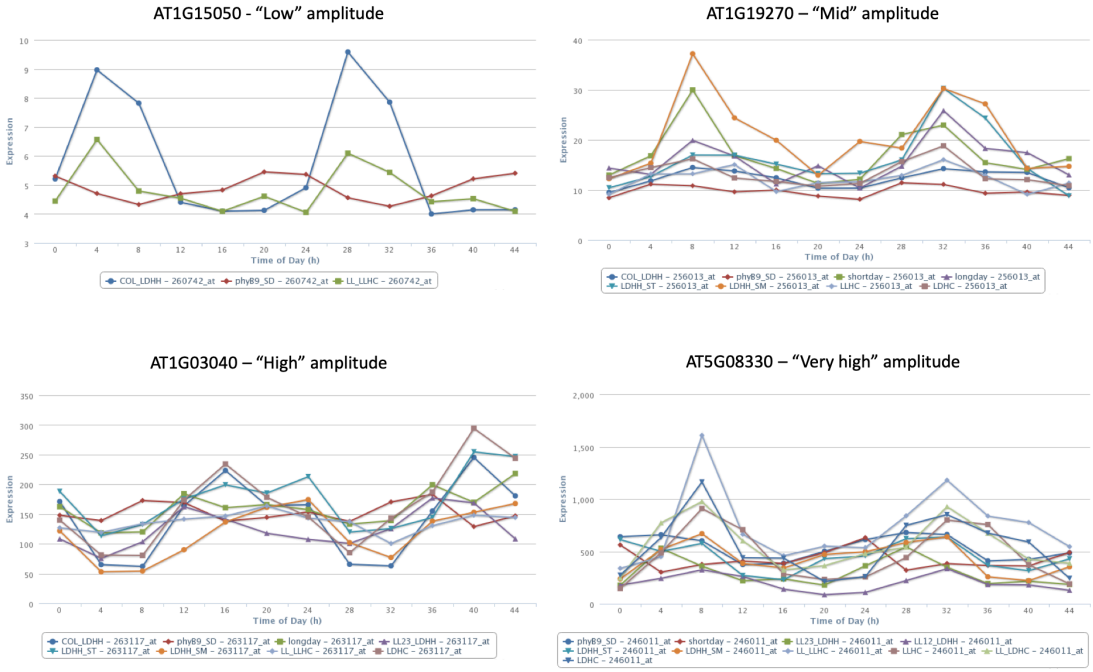

Supplementary Figure S4.1: Descriptions of gene expression amplitude are shown alongside examples of transcription factors found to interact with HopAO1 in the Y2H assay, and represent the descriptive terminology used in Table 4.1. Amplitude of normalized gene expression is termed as being low (peaks < 10), mid (10 ≤ peaks < 50), high (50 ≤ peaks < 500), or very high (500 ≤ peaks) according to data obtained using DIURNAL online tool (Mockler et al., 2007).

Supplementary Figure S4.2: Full sequence alignment of NAM (AT3G12910) versus three other NAC TFs (NAC042, AT2G43000; NAC074, AT4G28530; Unnamed NAC TF, AT3G12977). The alignment was performed using the Clustal Omega Multiple Sequence Alignment software (Madeira et al., 2019). Shown highlighted in yellow are the predicted phosphotyrosine residues exclusive to the NAM sequence, Y_{192}, Y_{212}, Y_{240}, and Y_{252}, highlighted in yellow. Asterisks indicate positions where the sequences have a single, fully conserved residue.

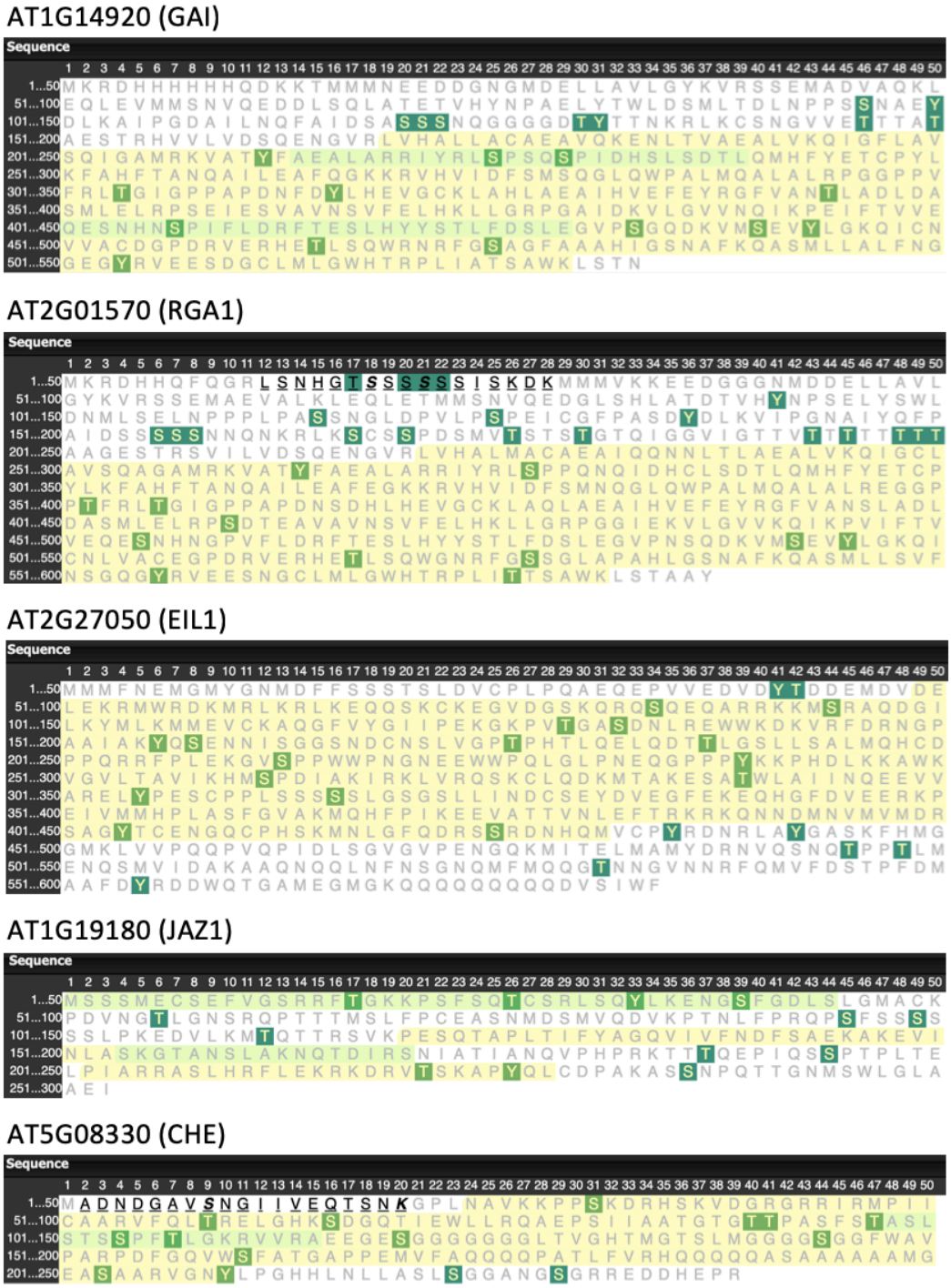

Supplementary Figure S4.3: Binding partners of HopAO1 associated with GA signaling and the clock possess tyrosine residues predicted to be subject to phosphorylation. Protein targets of HopAO1 involved in hormone biosynthesis and/or the circadian clock (GAI, RGA1, EIL1, JAZ1, and CHE) as determined by Y2H were analysed using the phosphorylation site database and predictor (Durek et al., 2010) to identify residues predicted to be phosphorylated. Yellow highlighted regions represent a conserved protein family domain. Green highlighted regions denote phosphorylation hotspots.

Sample Name	Total Raw Reads (Mb)	Total Clean Reads (Mb)	Total Clean Bases (Gb)	Clean Reads Q20 (%)	Clean Reads Q30 (%)	Clean Reads Ratio (%)
3HA_+est_+flg22_1A	25.9	25.83	1.29	99.15	94.47	99.73
3HA_+est_+flg22_1B	25.93	25.86	1.29	99.13	94.23	99.73
3HA_+est_+flg22_1C	25.72	25.63	1.28	99.15	94.37	99.65
3HA_+mock_+flg22_2A	26.06	25.93	1.3	99.09	94.14	99.51
3HA_+mock_+flg22_2B	26.08	26.01	1.3	99.09	94.2	99.72
3HA_+mock_+flg22_2C	26.02	25.93	1.3	99.12	94.42	99.66
3HA_+est_+mock_3A	26.1	26.01	1.3	99.12	94.32	99.64
3HA_+est_+mock_3B	26.1	25.86	1.29	99.05	93.96	99.08
3HA_+est_+mock_3C	25.6	24.96	1.25	99.17	94.43	97.52
3HA_+mock_+mock_4A	25.82	25.75	1.29	99.13	94.44	99.73
3HA_+mock_+mock_4B	26	25.9	1.3	99.12	94.42	99.62
3HA_+mock_+mock_4C	26.05	25.98	1.3	99.11	94.32	99.71
NLS_+est_+flg22_5A	24.83	24.75	1.24	99.06	93.82	99.67
NLS_+est_+flg22_5B	26.05	25.95	1.3	99.09	94.2	99.58
NLS_+est_+flg22_5C	25.98	25.89	1.29	99.07	94.02	99.68
NES_+est_+flg22_6A	26.13	26.07	1.3	99.06	93.97	99.77
NES_+est_+flg22_6B	25.85	25.78	1.29	99.2	94.57	99.72
NES_+est_+flg22_6C	26.06	25.87	1.29	99.05	93.87	99.29

Supplementary Figure S5.1: Clean reads quality metrics for RNA-Seq samples. Total Raw Reads (Mb): The amount of reads before filtering. Total Clean Reads (Mb): The amount of reads after filtering. Total Clean Bases (Gb): The total amount of bases after filtering. Clean Reads Q20 (%): The Q20 value for the clean reads. Clean Reads Q30 (%): The Q30 value for the clean reads. Clean Reads Ratio (%): The ratio of the amount of raw to clean reads.

Sample Name	Total Clean Reads	Total Mapping Ratio	Unique Mapping Ratio
3HA_+est_+flg22_1A	25827737	98.49%	93.26%
3HA_+est_+flg22_1B	25857731	98.58%	93.38%
3HA_+est_+flg22_1C	25630783	98.62%	93.03%
3HA_+mock_+flg22_2A	25930086	98.20%	92.83%
3HA_+mock_+flg22_2B	26005007	98.42%	93.08%
3HA_+mock_+flg22_2C	25932428	98.29%	93.13%
3HA_+est_+mock_3A	26006903	98.45%	93.42%
3HA_+est_+mock_3B	25861912	98.36%	93.11%
3HA_+est_+mock_3C	24963167	98.51%	92.90%
3HA_+mock_+mock_4A	25748891	98.31%	92.93%
3HA_+mock_+mock_4B	25904260	98.22%	92.92%
3HA_+mock_+mock_4C	25975052	98.20%	92.96%
NLS_+est_+flg22_5A	24751125	98.18%	92.88%
NLS_+est_+flg22_5B	25945073	97.58%	92.60%
NLS_+est_+flg22_5C	25894912	97.46%	92.28%
NES_+est_+flg22_6A	26070198	98.44%	93.25%
NES_+est_+flg22_6B	25779833	98.66%	93.30%
NES_+est_+flg22_6C	25872212	98.34%	92.92%

Supplementary Figure S5.2: Summary of genome mapping for RNA-Seq samples. Total Clean Reads: The number of clean reads. Total Mapping Ratio: The percentage of reads successfully mapped to the TAIR *A. thaliana* genome using HISAT2 (Kim et al., 2015)h. Average Mapping for all samples was 98.30%. Uniformity of total mapping ratio suggests that the samples are comparable. Unique Mapping Ratio: The percentage of reads that map to only one location of reference.

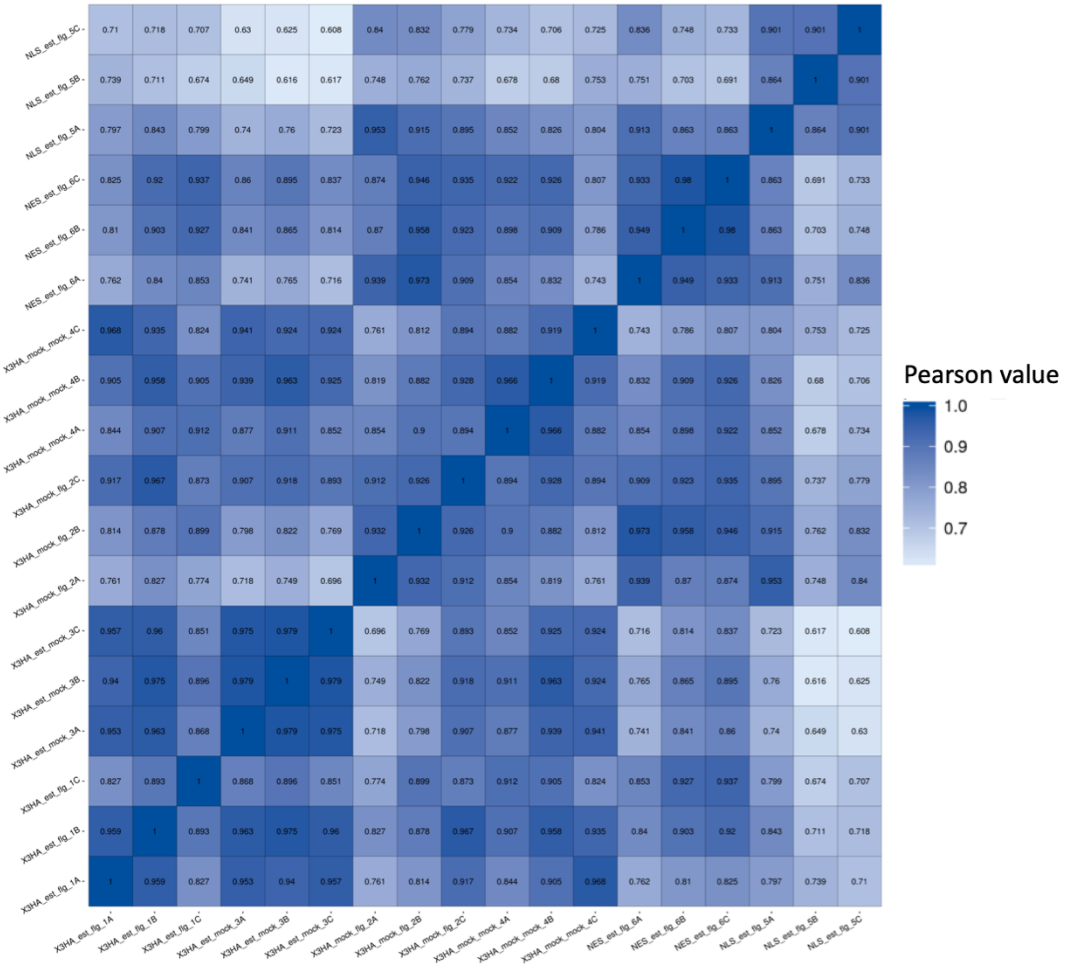

Supplementary Figure S5.3: Heatmap denoting correlation analysis between RNA-Seq samples. In order to reflect the gene expression correlation between samples, the Pearson correlation coefficients for all gene expression levels between each two samples were calculated. These coefficients represent the strength of linear association between a pair of samples and are reflected in the form of a heat map. The X and Y axes represent each sample. The colour of each box on the heatmap represents the correlation coefficient between the two samples lined up across and beneath it (the darker the colour, the higher the correlation, the lighter the colour, the lower the correlation).

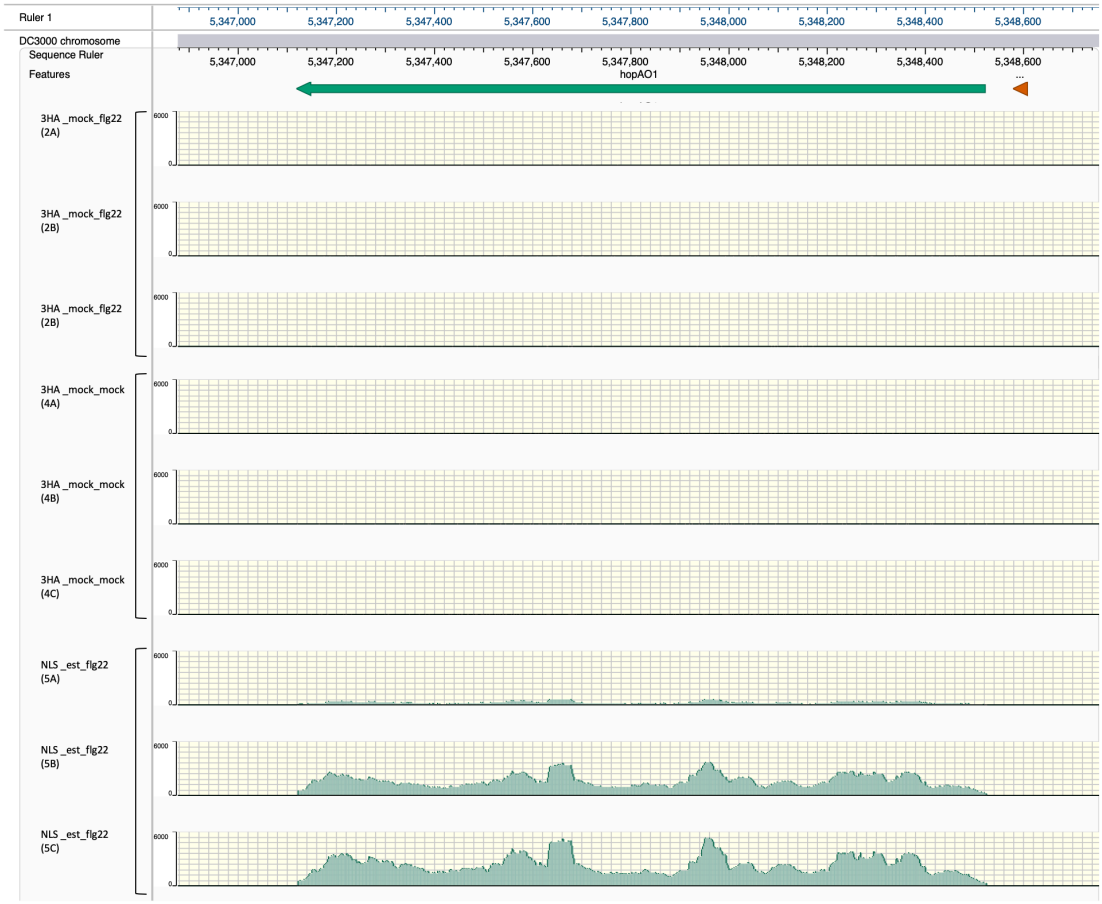

Supplementary Figure S5.4: *Pst* DC3000 HopAO1 alignment between induced NLS-tagged and non-estradiol induced RNA-Seq samples. In order to rule out the possibility that one of the NLS-tagged line samples was incorrectly grouped during PCA analysis clean reads were mapped to the *Pst* DC3000 genome, such that confirmation of HopAO1 expression in the induced NLS line could be confirmed. Genome mapping was performed using Lasergene software (DNAStar Inc., Wisconsine, USA) and clean reads were mapped to the *Pseudomonas syringae pv.* DC3000 genome available on NCBI. Values for clean mapped reads were normalised and stated in Reads Per Kilobase of transcript per Million mapped reads (RPKM).

Supplementary Figure S5.5: Pathway functional enrichment of DEGs between groups of RNAseq samples (Overleaf). The colour of each point indicates the q-value of each pathway (high: white, low: blue). A lower q-value indicates more significant pathway enrichment. Point size indicates the number of DEGs in the comparison group. Bigger dots refer to a larger amount of DEGs. “Rich Factor” refers to the value of enrichment factor, which is the quotient of the foreground value (the number of DEGs) and background value (total gene amount). The larger the value, the more significant the enrichment. A) 3HA -est +mock vs. 3HA -est +flg22. B) 3HA -est +flg22 vs. 3HA +est +flg22. C) 3HA +est +flg22 vs. NES +est +flg22. D) 3HA -est +flg22 vs. NES +est +flg22. E) 3HA +est +flg22 vs. NLS +est +flg22. F) 3HA -est +flg22 vs. NLS +est +flg22.

A

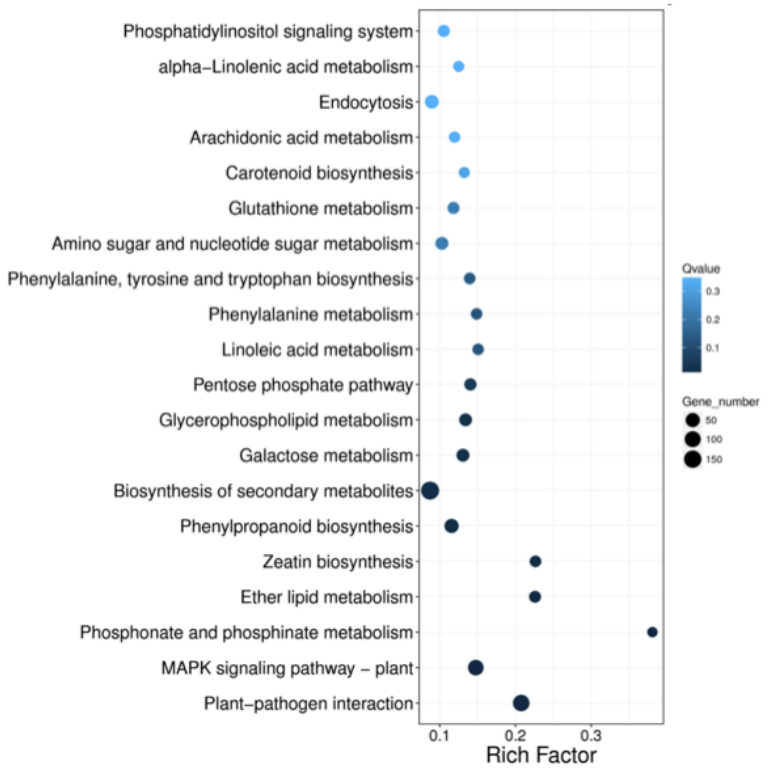

3HA - est + mock **VS** 3HA - est + flg22

B

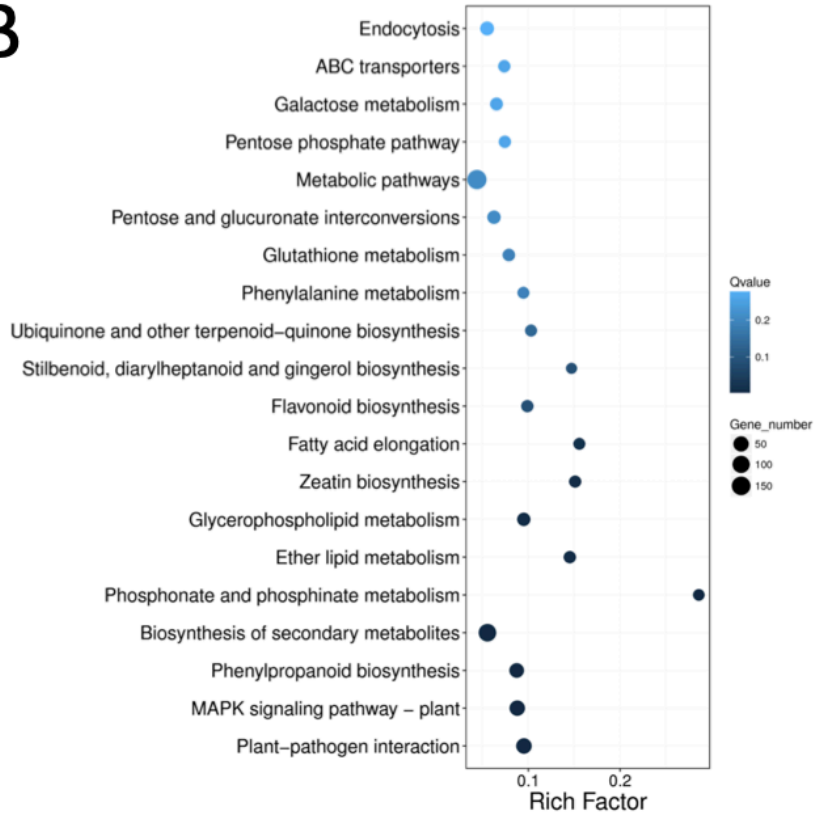

3HA - est + flg22 **VS** 3HA + est + flg22

C

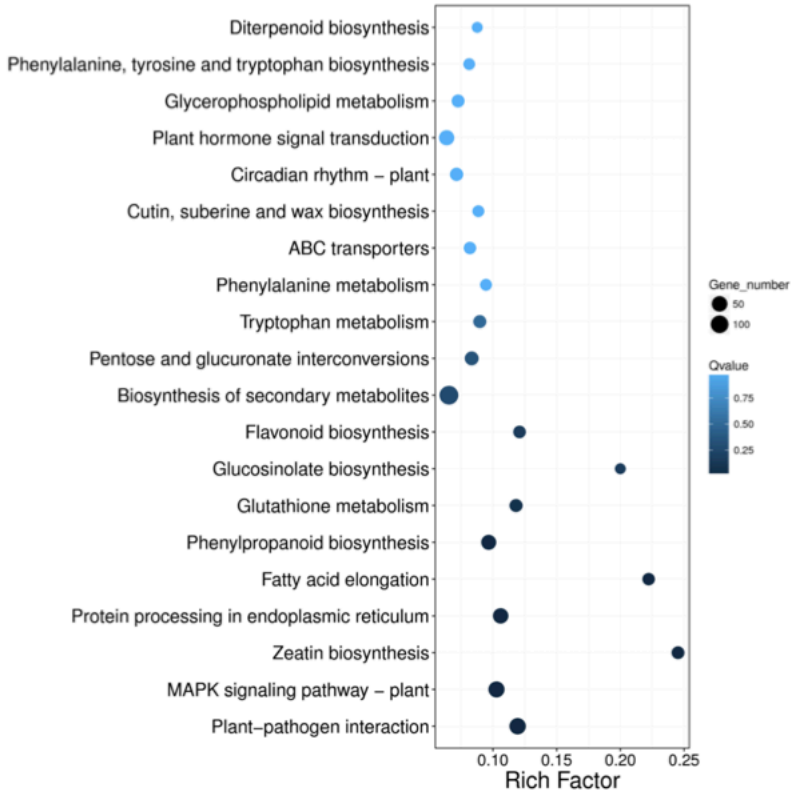

3HA + est + flg22 **VS** NES + est + flg22

D

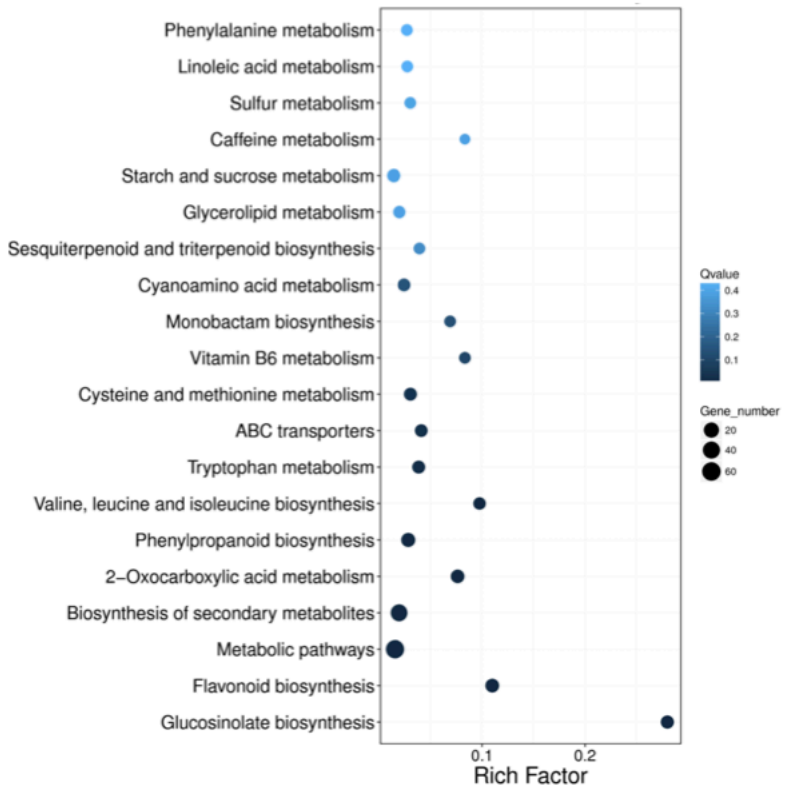

3HA - est + flg22 **VS** NES + est + flg22

E

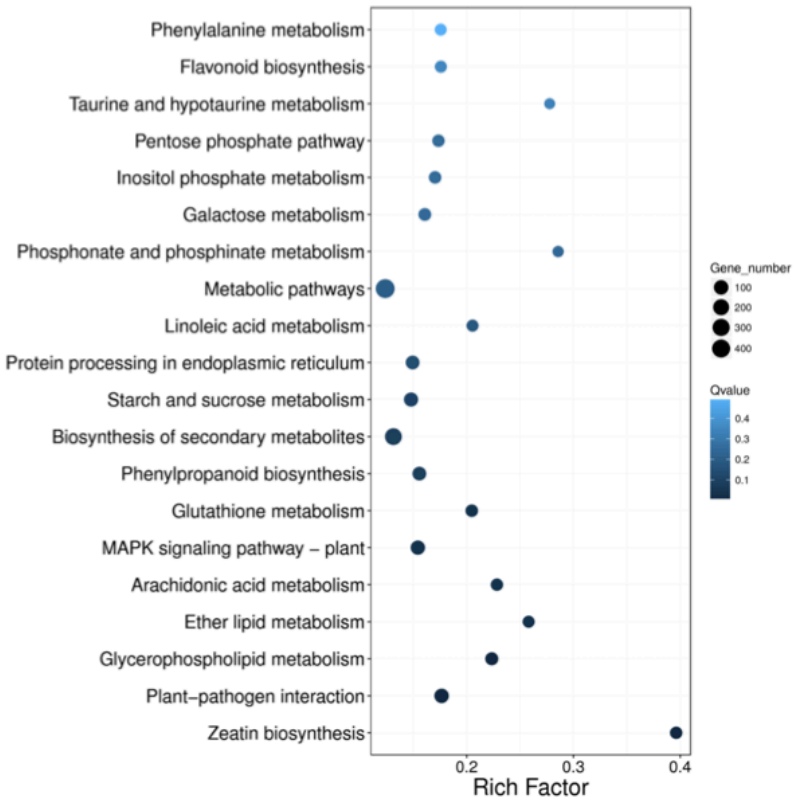

3HA + est + flg22 **VS** NLS + est + flg22

F

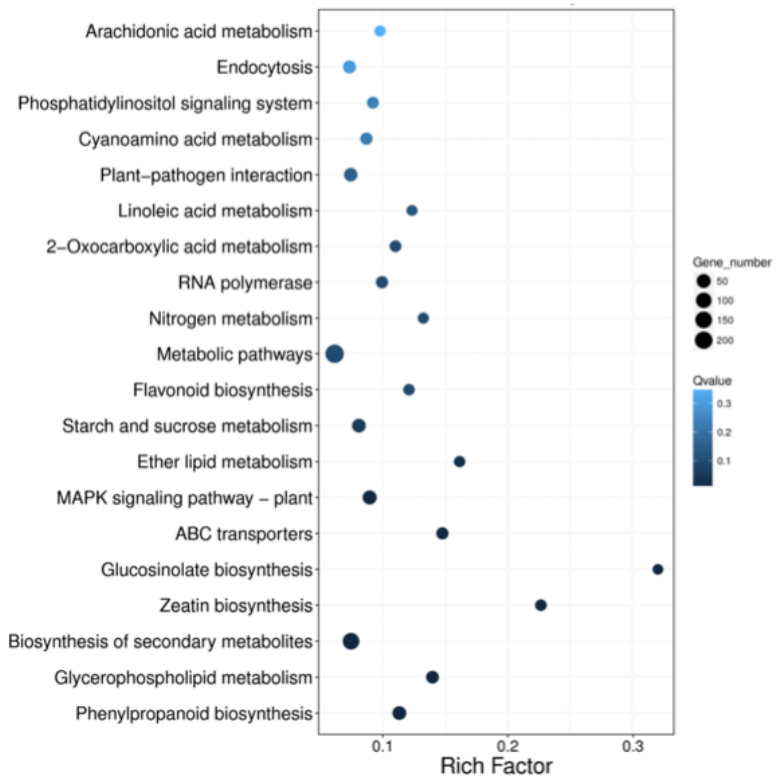

3HA - est + flg22 **VS** NLS + est + flg22

References

Abramovitch, R.B., Kim, Y.-J., Chen, S., Dickman, M.B., and Martin, G.B. (2003). Pseudomonas type III effector AvrPtoB induces plant disease susceptibility by inhibition of host programmed cell death. EMBO J. **22**: 60–69.

Achard, P., Cheng, H., De Grauwe, L., Decat, J., Schoutteten, H., Moritz, T., Van Der Straeten, D., Peng, J., and Harberd, N.P. (2006). Integration of plant responses to environmentally activated phytohormonal signals. Science **311**: 91–4.

Achard, P., Gusti, A., Cheminant, S., Alioua, M., Dhondt, S., Coppens, F., Beemster, G.T.S., and Genschik, P. (2009). Gibberellin Signaling Controls Cell Proliferation Rate in Arabidopsis. Curr. Biol. **19**: 1188–1193.

Achard, P., Renou, J.-P., Berthomé, R., Harberd, N.P., and Genschik, P. (2008). Plant DELLAs Restrain Growth and Promote Survival of Adversity by Reducing the Levels of Reactive Oxygen Species. Curr. Biol. **18**: 656–660.

Adachi, H., Derevnina, L., and Kamoun, S. (2019). NLR singletons, pairs, and networks: evolution, assembly, and regulation of the intracellular immunoreceptor circuitry of plants. Curr. Opin. Plant Biol. **50**: 121–131.

Adams, S., Manfield, I., Stockley, P., and Carré, I.A. (2015). Revised Morning Loops of the Arabidopsis Circadian Clock Based on Analyses of Direct Regulatory Interactions. PLoS One **10**: e0143943.

Alabadi, D., Oyama, T., Yanovsky, M.J., Harmon, F.G., Más, P., and Kay, S.A. (2001). Reciprocal Regulation Between TOC1 and LHY/CCA1 Within the Arabidopsis Circadian Clock. Science (80-.). **293**: 880–883.

Alfano, J.R., Charkowski, A.O., Deng, W.-L., Badel, J.L., Petnicki-Ocwieja, T., van Dijk, K., and Collmer, A. (2000). The Pseudomonas syringae Hrp pathogenicity island has a tripartite mosaic structure composed of a cluster of type III secretion genes bounded by exchangeable effector and conserved effector loci that contribute to parasitic fitness and pathogenicity in plants. Proc. Natl. Acad. Sci. **97**: 4856–4861.

Andersen, E.J., Ali, S., Byamukama, E., Yen, Y., and Nepal, M.P. (2018). Disease Resistance Mechanisms in Plants. Genes (Basel). **9**: 339–369.

Anderson, J.C., Pascuzzi, P.E., Xiao, F., Sessa, G., and Martin, G.B. (2006). Host-

Mediated Phosphorylation of Type III Effector AvrPto Promotes Pseudomonas Virulence and Avirulence in Tomato. Plant Cell **18**: 502–514.

Andreani, T.S., Itoh, T.Q., Yildirim, E., Hwangbo, D.-S., and Allada, R. (2015). Genetics of Circadian Rhythms. Sleep Med. Clin. **10**: 413.

Arana, M.V., Marín-de la Rosa, N., Maloof, J.N., Blázquez, M.A., and Alabadí, D. (2011). Circadian oscillation of gibberellin signaling in Arabidopsis. Proc. Natl. Acad. Sci. U. S. A. **108**: 9292–7.

Arnaud, D. and Hwang, I. (2015). A Sophisticated Network of Signaling Pathways Regulates Stomatal Defenses to Bacterial Pathogens. Mol. Plant **8**: 566–581.

Arnon, D.I. (1949). Copper enzymes in isolated chloroplasts. Polyphenoloxidase in beta vulgaris. Plant Physiol. **24**: 1–15.

Asai, S., Furzer, O.J., Cevik, V., Kim, D.S., Ishaque, N., Goritschnig, S., Staskawicz, B.J., Shirasu, K., and Jones, J.D.G. (2018). A downy mildew effector evades recognition by polymorphism of expression and subcellular localization. Nat. Commun. **9**: 5192.

Asai, T., Tena, G., Plotnikova, J., Willmann, M.R., Chiu, W.-L., Gomez-Gomez, L., Boller, T., Ausubel, F.M., and Sheen, J. (2002). MAP kinase signalling cascade in Arabidopsis innate immunity. Nature **415**: 977–983.

Ausubel, F.M. (2005). Are innate immune signaling pathways in plants and animals conserved? Nat. Immunol. **6**: 973–979.

Barysz, H.M. and Malmström, J. (2018). Development of Large-scale Cross-linking Mass Spectrometry. Mol. Cell. Proteomics **17**: 1055–1066.

Beckers, G.J.M., Jaskiewicz, M., Liu, Y., Underwood, W.R., He, S.Y., Zhang, S., and Conrath, U. (2009). Mitogen-Activated Protein Kinases 3 and 6 Are Required for Full Priming of Stress Responses in *Arabidopsis thaliana*. Plant Cell **21**: 944–953.

Berardini, T.Z., Reiser, L., Li, D., Mezheritsky, Y., Muller, R., Strait, E., and Huala, E. (2015). The arabidopsis information resource: Making and mining the "gold standard" annotated reference plant genome. genesis **53**: 474–485.

Bertani, G. (1951). Studies on lysogenesis. I. The mode of phage liberation by lysogenic Escherichia coli. J. Bacteriol. **62**: 293–300.

Bhardwaj, V., Meier, S., Petersen, L.N., Ingle, R.A., and Roden, L.C. (2011). Defence Responses of Arabidopsis thaliana to Infection by Pseudomonas syringae Are Regulated by the Circadian Clock. PLoS One **6**: e26968.

Van der Biezen, E.A. and Jones, J.D. (1998). Plant disease-resistance proteins and the gene-for-gene concept. Trends Biochem. Sci. **23**: 454–6.

Bigeard, J. et al. (2015). Signaling mechanisms in pattern-triggered immunity (PTI). Mol. Plant **8**: 521–39.

Block, A. and Alfano, J.R. (2011). Plant targets for Pseudomonas syringae type III effectors: virulence targets or guarded decoys? Curr. Opin. Microbiol. **14**: 39–46.

Block, A., Toruño, T.Y., Elowsky, C.G., Zhang, C., Steinbrenner, J., Beynon, J., and Alfano, J.R. (2014). The *Pseudomonas syringae* type III effector HopD1 suppresses effector-triggered immunity, localizes to the endoplasmic reticulum, and targets the Arabidopsis transcription factor NTL9. New Phytol. **201**: 1358–1370.

Bloomer, R.H., Juenger, T.E., and Symonds, V. V. (2012). Natural variation in GL1 and its effects on trichome density in Arabidopsis thaliana. Mol. Ecol. **21**: 3501–3515.

Böhm, H., Albert, I., Fan, L., Reinhard, A., and Nürnberger, T. (2014). Immune receptor complexes at the plant cell surface. Curr. Opin. Plant Biol. **20**: 47–54.

Boudsocq, M., Willmann, M.R., McCormack, M., Lee, H., Shan, L., He, P., Bush, J., Cheng, S.-H., and Sheen, J. (2010). Differential innate immune signalling via Ca2+ sensor protein kinases. Nature **464**: 418–422.

Boyes, D.C., Nam, J., and Dangl, J.L. (1998). The Arabidopsis thaliana RPM1 disease resistance gene product is a peripheral plasma membrane protein that is degraded coincident with the hypersensitive response. Proc. Natl. Acad. Sci. **95**: 15849–15854.

Bradley, D.J., Kjellbom, P., and Lamb, C.J. (1992). Elicitor- and wound-induced oxidative cross-linking of a proline-rich plant cell wall protein: a novel, rapid defense response. Cell **70**: 21–30.

Bretz, J.R., Mock, N.M., Charity, J.C., Zeyad, S., Baker, C.J., and Hutcheson, S.W. (2003). A translocated protein tyrosine phosphatase of Pseudomonas syringae pv. tomato DC3000 modulates plant defence response to infection. Mol. Microbiol. **49**: 389–400.

Briggs, W.R. and Christie, J.M. (2002). Phototropins 1 and 2: versatile plant blue-light receptors. Trends Plant Sci. **7**: 204–10.

De Bruyne, L., Höfte, M., and De Vleesschauwer, D. (2014). Connecting Growth and Defense: The Emerging Roles of Brassinosteroids and Gibberellins in Plant

Innate Immunity. Mol. Plant **7**: 943–959.

Budde, I.P. and Ullrich, M.S. (2000). Interactions of *Pseudomonas syringae* pv. *glycinea* with Host and Nonhost Plants in Relation to Temperature and Phytotoxin Synthesis. Mol. Plant-Microbe Interact. **13**: 951–961.

Butt, A., Mousley, C., Morris, K., Beynon, J., Can, C., Holub, E., Greenberg, J.T., and Buchanan-Wollaston, V. (1998). Differential expression of a senescence-enhanced metallothionein gene inArabidopsisin response to isolates ofPeronospora parasiticaandPseudomonas syringae. Plant J. **16**: 209–221.

Büttner, D. et al. (2016). Behind the lines-actions of bacterial type III effector proteins in plant cells. FEMS Microbiol. Rev. **103**: 60–69.

Caarls, L., Pieterse, C.M.J., and Van Wees, S.C.M. (2015). How salicylic acid takes transcriptional control over jasmonic acid signaling. Front. Plant Sci. **6**: 170.

Canonne, J. and Rivas, S. (2012). Bacterial effectors target the plant cell nucleus to subvert host transcription. Plant Signal. Behav. **7**: 217–21.

Castañeda-Ojeda, M.P., Moreno-Pérez, A., Ramos, C., and López-Solanilla, E. (2017). Suppression of Plant Immune Responses by the Pseudomonas savastanoi pv. savastanoi NCPPB 3335 Type III Effector Tyrosine Phosphatases HopAO1 and HopAO2. Front. Plant Sci. **8**: 680.

Chatr-aryamontri, A., Ceol, A., Palazzi, L.M., Nardelli, G., Schneider, M.V., Castagnoli, L., and Cesareni, G. (2007). MINT: the Molecular INTeraction database. Nucleic Acids Res. **35**: D572-4.

Chen, Y. et al. (2018). SOAPnuke: a MapReduce acceleration-supported software for integrated quality control and preprocessing of high-throughput sequencing data. Gigascience **7**: 1–6.

Chen, Z.A. and Rappsilber, J. (2018). Protein Dynamics in Solution by Quantitative Crosslinking/Mass Spectrometry. Trends Biochem. Sci. **43**: 908–920.

Chinchilla, D., Bauer, Z., Regenass, M., Boller, T., and Felix, G. (2006). The Arabidopsis receptor kinase FLS2 binds flg22 and determines the specificity of flagellin perception. Plant Cell **18**: 465–476.

Chinchilla, D., Zipfel, C., Robatzek, S., Kemmerling, B., Nürnberger, T., Jones, J.D.G., Felix, G., and Boller, T. (2007). A flagellin-induced complex of the receptor FLS2 and BAK1 initiates plant defence. Nature **448**: 497–500.

Choi, I.Y., Hong, S.H., Cho, S.E., Zhao, T.T., and Shin, H.D. (2018). First Report of Powdery Mildew Caused by *Golovinomyces orontii* on Common Poppy in

Korea. Plant Dis. **102**: 244–244.

Collier, S.M. and Moffett, P. (2009). NB-LRRs work a "bait and switch" on pathogens. Trends Plant Sci. **14**: 521–529.

Cornelis, G.R. (2006). The type III secretion injectisome. Nat. Rev. Microbiol. **4**: 811–825.

Couto, D. and Zipfel, C. (2016). Regulation of pattern recognition receptor signalling in plants. Nat. Rev. Immunol. **16**: 537–552.

Covington, M.F., Maloof, J.N., Straume, M., Kay, S.A., and Harmer, S.L. (2008). Global transcriptome analysis reveals circadian regulation of key pathways in plant growth and development. Genome Biol. **9**: R130.

Crabill, E., Joe, A., Block, A., van Rooyen, J.M., Alfano, J.R., Boller, T., and Jones, J. (2010). Plant immunity directly or indirectly restricts the injection of type III effectors by the Pseudomonas syringae type III secretion system. Plant Physiol. **154**: 233–44.

Cunnac, S., Chakravarthy, S., Kvitko, B.H., Russell, A.B., Martin, G.B., and Collmer, A. (2011). Genetic disassembly and combinatorial reassembly identify a minimal functional repertoire of type III effectors in Pseudomonas syringae. Proc. Natl. Acad. Sci. **108**: 2975–2980.

Dangl, J.L., Horvath, D.M., and Staskawicz, B.J. (2013). Pivoting the Plant Immune System from Dissection to Deployment. Science **341**: 746–51.

Daniel, X., Sugano, S., and Tobin, E.M. (2004). CK2 phosphorylation of CCA1 is necessary for its circadian oscillator function in Arabidopsis. Proc. Natl. Acad. Sci. U. S. A. **101**: 3292–7.

Davies, S.E.W. (2013). Transcription Factor Interactions at the Promoter of the Arabidopsis Circadian Clock Gene LHY.

DebRoy, S., Thilmony, R., Kwack, Y.-B., Nomura, K., and He, S.Y. (2004). A family of conserved bacterial effectors inhibits salicylic acid-mediated basal immunity and promotes disease necrosis in plants. Proc. Natl. Acad. Sci. **101**: 9927–9932.

Delga, A., Le Roux, C., and Deslandes, L. (2015). Plant immune receptor decoy: pathogens in their own trap. Oncotarget **6**: 15748–9.

Denoux, C., Galletti, R., Mammarella, N., Gopalan, S., Werck, D., De Lorenzo, G., Ferrari, S., Ausubel, F.M., and Dewdney, J. (2008). Activation of Defense Response Pathways by OGs and Flg22 Elicitors in Arabidopsis Seedlings. Mol.

Plant **1**: 423–445.

Desclos-Theveniau, M., Arnaud, D., Huang, T.-Y., Lin, G.J.-C., Chen, W.-Y., Lin, Y.-C., and Zimmerli, L. (2012). The Arabidopsis Lectin Receptor Kinase LecRK-V.5 Represses Stomatal Immunity Induced by Pseudomonas syringae pv. tomato DC3000. PLoS Pathog. **8**: e1002513.

Deslandes, L., Olivier, J., Peeters, N., Feng, D.X., Khounlotham, M., Boucher, C., Somssich, I., Genin, S., and Marco, Y. (2003). Physical interaction between RRS1-R, a protein conferring resistance to bacterial wilt, and PopP2, a type III effector targeted to the plant nucleus. Proc. Natl. Acad. Sci. **100**: 8024–8029.

Dill, A. and Sun, T. (2001). Synergistic derepression of gibberellin signaling by removing RGA and GAI function in Arabidopsis thaliana. Genetics **159**: 777–85.

Dixon, R.A., Achnine, L., Kota, P., Liu, C.-J., Reddy, M.S.S., and Wang, L. (2002). The phenylpropanoid pathway and plant defence-a genomics perspective. Mol. Plant Pathol. **3**: 371–390.

Dodd, A.N., Salathia, N., Hall, A., Kévei, E., Tóth, R., Nagy, F., Hibberd, J.M., Millar, A.J., and Webb, A. a R. (2005). Plant circadian clocks increase photosynthesis, growth, survival, and competitive advantage. Science **309**: 630–633.

Dodds, P.N. and Rathjen, J.P. (2010). Plant immunity: towards an integrated view of plant–pathogen interactions. Nat. Rev. Genet. **11**: 539–548.

Dreze, M., Monachello, D., Lurin, C., Cusick, M.E., Hill, D.E., Vidal, M., and Braun, P. (2010). High-quality binary interactome mapping. Methods Enzymol. **470**: 281–315.

Dubiella, U., Seybold, H., Durian, G., Komander, E., Lassig, R., Witte, C.-P., Schulze, W.X., and Romeis, T. (2013). Calcium-dependent protein kinase/NADPH oxidase activation circuit is required for rapid defense signal propagation. Proc. Natl. Acad. Sci. **110**: 8744–8749.

Durek, P., Schmidt, R., Heazlewood, J.L., Jones, A., MacLean, D., Nagel, A., Kersten, B., and Schulze, W.X. (2010). PhosPhAt: the Arabidopsis thaliana phosphorylation site database. An update. Nucleic Acids Res. **38**: D828–D834.

Eisen, M.B., Spellman, P.T., Brown, P.O., and Botstein, D. (1998). Cluster analysis and display of genome-wide expression patterns. Proc. Natl. Acad. Sci. **95**: 14863–14868.

Elphinstone, J.G., Allen, C., Prior, P., and Hayward, A.C. (2005). The current

bacterial wilt situation: a global overview.: 9–28.

Engler, C., Youles, M., Gruetzner, R., Ehnert, T.-M., Werner, S., Jones, J.D.G., Patron, N.J., and Marillonnet, S. (2014). A Golden Gate Modular Cloning Toolbox for Plants. ACS Synth. Biol. **3**: 839–843.

Espinosa, A., Guo, M., Tam, V.C., Fu, Z.Q., and Alfano, J.R. (2003). The Pseudomonas syringae type III-secreted protein HopPtoD2 possesses protein tyrosine phosphatase activity and suppresses programmed cell death in plants. Mol. Microbiol. **49**: 377–387.

Eulgem, T. (2005). Regulation of the Arabidopsis defense transcriptome. Trends Plant Sci. **10**: 71–78.

Fan, X.-Y., Sun, Y., Cao, D.-M., Bai, M.-Y., Luo, X.-M., Yang, H.-J., Wei, C.-Q., Zhu, S.-W., Sun, Y., Chong, K., and Wang, Z.-Y. (2012). BZS1, a B-box protein, promotes photomorphogenesis downstream of both brassinosteroid and light signaling pathways. Mol. Plant **5**: 591–600.

Fankhauser, C. and Staiger, D. (2002). Photoreceptors in Arabidopsis thaliana : light perception, signal transduction and entrainment of the endogenous clock. Planta **216**: 1–16.

Farmer, E., Farmer, E., Mousavi, S., and Lenglet, A. (2013). Leaf numbering for experiments on long distance signalling in Arabidopsis. Protoc. Exch.

Fones, H. and Gurr, S. (2015). The impact of Septoria tritici Blotch disease on wheat: An EU perspective. Fungal Genet. Biol. **79**: 3–7.

Fu, Z.Q. and Dong, X. (2013). Systemic acquired resistance: turning local infection into global defense. Annu. Rev. Plant Biol. **64**: 839–63.

Fu, Z.Q., Guo, M., Jeong, B., Tian, F., Elthon, T.E., Cerny, R.L., Staiger, D., and Alfano, J.R. (2007). A type III effector ADP-ribosylates RNA-binding proteins and quells plant immunity. Nature **447**: 284–288.

Fujiwara, S., Wang, L., Han, L., Suh, S.-S., Salomé, P.A., McClung, C.R., and Somers, D.E. (2008). Post-translational Regulation of the *Arabidopsis* Circadian Clock through Selective Proteolysis and Phosphorylation of Pseudo-response Regulator Proteins. J. Biol. Chem. **283**: 23073–23083.

Gao, X., Chen, X., Lin, W., Chen, S., Lu, D., Niu, Y., Li, L., Cheng, C., McCormack, M., Sheen, J., Shan, L., and He, P. (2013). Bifurcation of Arabidopsis NLR Immune Signaling via Ca2+-Dependent Protein Kinases. PLoS Pathog. **9**: e1003127.

Gao, Z. et al. (2018). KIRA1 and ORESARA1 terminate flower receptivity by promoting cell death in the stigma of Arabidopsis. Nat. Plants **4**: 365–375.

Gimenez-Ibanez, S., Boter, M., Fernández-Barbero, G., Chini, A., Rathjen, J.P., and Solano, R. (2014). The Bacterial Effector HopX1 Targets JAZ Transcriptional Repressors to Activate Jasmonate Signaling and Promote Infection in Arabidopsis. PLoS Biol. **12**: e1001792.

Gimenez-Ibanez, S., Hann, D.R., Chang, J.H., Segonzac, C., Boller, T., and Rathjen, J.P. (2018). Differential Suppression of Nicotiana benthamiana Innate Immune Responses by Transiently Expressed Pseudomonas syringae Type III Effectors. Front. Plant Sci. **9**: 688.

Gimenez-Ibanez, S., Hann, D.R., Ntoukakis, V., Petutschnig, E., Lipka, V., and Rathjen, J.P. (2009). AvrPtoB Targets the LysM Receptor Kinase CERK1 to Promote Bacterial Virulence on Plants. Curr. Biol. **19**: 423–429.

Giraud, E., Ng, S., Carrie, C., Duncan, O., Low, J., Lee, C.P., Van Aken, O., Millar, A.H., Murcha, M., and Whelan, J. (2010). TCP transcription factors link the regulation of genes encoding mitochondrial proteins with the circadian clock in Arabidopsis thaliana. Plant Cell **22**: 3921–34.

Glazebrook, J. (2005). Contrasting Mechanisms of Defense Against Biotrophic and Necrotrophic Pathogens. Annu. Rev. Phytopathol. **43**: 205–227.

Göhre, V., Spallek, T., Häweker, H., Mersmann, S., Mentzel, T., Boller, T., de Torres, M., Mansfield, J.W., and Robatzek, S. (2008). Plant Pattern-Recognition Receptor FLS2 Is Directed for Degradation by the Bacterial Ubiquitin Ligase AvrPtoB. Curr. Biol. **18**: 1824–1832.

Gómez-Gómez, L. and Boller, T. (2000). FLS2: An LRR receptor-like kinase involved in the perception of the bacterial elicitor flagellin in Arabidopsis. Mol. Cell **5**: 1003–1011.

Goodspeed, D., Chehab, E.W., Min-Venditti, A., Braam, J., and Covington, M.F. (2012). Arabidopsis synchronizes jasmonate-mediated defense with insect circadian behavior. Proc. Natl. Acad. Sci. U. S. A. **109**: 4674–7.

Gottig, N. et al. (2010). Mechanisms of infection used by Xanthomonas axonopodis pv. citri in citrus canker disease. Curr. Res. Technol. Educ. Top. Appl. Microbiol. Microb. Biotechnol. **1**: 196–204.

Govrin, E.M. and Levine, A. (2000). The hypersensitive response facilitates plant infection by the necrotrophic pathogen Botrytis cinerea. Curr. Biol. **10**: 751–757.

Green, R.M., Tingay, S., Wang, Z.-Y., and Tobin, E.M. (2002). Circadian rhythms confer a higher level of fitness to Arabidopsis plants. Plant Physiol. **129**: 576–84.

Greenham, K. and McClung, C.R. (2015). Integrating circadian dynamics with physiological processes in plants. Nat. Rev. Genet. **16**: 598–610.

Großkinsky, D.K., Edelsbrunner, K., Pfeifhofer, H., van der Graaff, E., and Roitsch, T. (2013). Cis- and trans-zeatin differentially modulate plant immunity. Plant Signal. Behav. **8**: e24798.

Grundy, J., Stoker, C., and Carré, I.A. (2015). Circadian regulation of abiotic stress tolerance in plants. Front. Plant Sci. **6**: 648.

Guillaume, H., Thonart, P., and Ongena, M. (2012). PAMPs, MAMPs, DAMPs and others: an update on the diversity of plant immunity elicitors. Biotechnol. Agron. Soc. Environ. **16**: 257–268.

Guo, M., Kim, P., Li, G., Elowsky, C.G., and Alfano, J.R. (2016). A Bacterial Effector Co-opts Calmodulin to Target the Plant Microtubule Network. Cell Host Microbe **19**: 67–78.

Gust, A.A., Biswas, R., Lenz, H.D., Rauhut, T., Ranf, S., Kemmerling, B., Götz, F., Glawischnig, E., Lee, J., Felix, G., and Nürnberger, T. (2007). Bacteria-derived peptidoglycans constitute pathogen-associated molecular patterns triggering innate immunity in Arabidopsis. J. Biol. Chem. **282**: 32338–48.

Hake, K. and Romeis, T. (2019). Protein kinase-mediated signalling in priming: Immune signal initiation, propagation, and establishment of long-term pathogen resistance in plants. Plant. Cell Environ. **42**: 904–917.

Haney, C. (2014). Innate Immunity in Plants and Animals. Biochem. (Lond). **36**: 1–5.

Hann, D.R., Domínguez-Ferreras, A., Motyka, V., Dobrev, P.I., Schornack, S., Jehle, A., Felix, G., Chinchilla, D., Rathjen, J.P., and Boller, T. (2014). The *Pseudomonas* type III effector HopQ1 activates cytokinin signaling and interferes with plant innate immunity. New Phytol. **201**: 585–598.

Hansen, L.L. and van Ooijen, G. (2016). Rapid Analysis of Circadian Phenotypes in Arabidopsis Protoplasts Transfected with a Luminescent Clock Reporter. J. Vis. Exp.: e54586–e54586.

Hanson, M.R. and Köhler, R.H. (2001). GFP imaging: methodology and application to investigate cellular compartmentation in plants. J. Exp. Bot. **52**: 529–39.

Harmer, S.L. (2009). The Circadian System in Higher Plants. Annu. Rev. Plant Biol.

60: 357–377.

Harper, S.M. et al. (2003). Structural basis of a phototropin light switch. Science **301**: 1541–4.

Hatsugai, N., Igarashi, D., Mase, K., Lu, Y., Tsuda, Y., Chakravarthy, S., Wei, H., Foley, J.W., Collmer, A., Glazebrook, J., and Katagiri, F. (2017). A plant effector-triggered immunity signaling sector is inhibited by pattern-triggered immunity. EMBO J. **36**: 2758–2769.

Hatsugai, N. and Katagiri, F. (2018). Quantification of Plant Cell Death by Electrolyte Leakage Assay. BIO-PROTOCOL **8**.

Hauck, P., Thilmony, R., and He, S.Y. (2003). A Pseudomonas syringae type III effector suppresses cell wall-based extracellular defense in susceptible Arabidopsis plants. Proc. Natl. Acad. Sci. U. S. A. **100**: 8577–82.

He, P., Shan, L., Lin, N.-C., Martin, G.B., Kemmerling, B., Nürnberger, T., and Sheen, J. (2006). Specific Bacterial Suppressors of MAMP Signaling Upstream of MAPKKK in Arabidopsis Innate Immunity. Cell **125**: 563–575.

Herrero, E. et al. (2012). EARLY FLOWERING4 Recruitment of EARLY FLOWERING3 in the Nucleus Sustains the Arabidopsis Circadian Clock. Plant Cell **24**: 428–43.

Heuer, H., Yin, Y.-N., Xue, Q.-Y., Smalla, K., and Guo, J.-H. (2007). Repeat Domain Diversity of avrBs3-Like Genes in Ralstonia solanacearum Strains and Association with Host Preferences in the Field. Appl. Environ. Microbiol. **73**: 4379–4384.

Hevia, M.A., Canessa, P., Müller-Esparza, H., and Larrondo, L.F. (2015). A circadian oscillator in the fungus *Botrytis cinerea* regulates virulence when infecting *Arabidopsis thaliana*. Proc. Natl. Acad. Sci. **112**: 8744–8749.

Hoffman, E.A., Frey, B.L., Smith, L.M., and Auble, D.T. (2015). Formaldehyde crosslinking: a tool for the study of chromatin complexes. J. Biol. Chem. **290**: 26404–11.

de Hoon, M.J.L., Imoto, S., Nolan, J., and Miyano, S. (2004). Open source clustering software. Bioinformatics **20**: 1453–1454.

Van der Hoorn, R.A.L. and Kamoun, S. (2008). From Guard to Decoy: a new model for perception of plant pathogen effectors. The Plant cellb **20**: 2009–17.

Van der Hoorn, R.A.L., De Wit, P.J.G.M., and Joosten, M.H.A.J. (2002). Balancing selection favors guarding resistance proteins. Trends Plant Sci. **7**: 67–

71.

Horsefield, S. et al. (2019). NAD+ cleavage activity by animal and plant TIR domains in cell death pathways. Science (80-.). **365**: 793–799.

Horvath, D.M., Stall, R.E., Jones, J.B., Pauly, M.H., Vallad, G.E., Dahlbeck, D., Staskawicz, B.J., and Scott, J.W. (2012). Transgenic resistance confers effective field level control of bacterial spot disease in tomato. PLoS One **7**: e42036.

Hou, S., Yang, Y., Wu, D., and Zhang, C. (2011). Plant immunity: evolutionary insights from PBS1, Pto, and RIN4. Plant Signal. Behav. **6**: 794–9.

Hou, X., Lee, L.Y.C., Xia, K., Yan, Y., and Yu, H. (2010). DELLAs Modulate Jasmonate Signaling via Competitive Binding to JAZs. Dev. Cell **19**: 884–894.

Hsu, P.Y., Devisetty, U.K., and Harmer, S.L. (2013). Accurate timekeeping is controlled by a cycling activator in *Arabidopsis*. Elife **2**: e00473.

Hsu, P.Y. and Harmer, S.L. (2014). Wheels within wheels: the plant circadian system. Trends Plant Sci. **19**: 240–249.

Huang, H. and Nusinow, D.A. (2016). Into the Evening: Complex Interactions in the Arabidopsis Circadian Clock. Trends Genet. **32**: 674–686.

Huang, W.-Y., Wu, Y.-C., Pu, H.-Y., Wang, Y., Jang, G.-J., and Wu, S.-H. (2017). Plant dual-specificity tyrosine phosphorylation-regulated kinase optimizes light-regulated growth and development in *Arabidopsis*. Plant. Cell Environ.

Huang, W., Pérez-García, P., Pokhilko, A., Millar, A.J., Antoshechkin, I., Riechmann, J.L., and Mas, P. (2012). Mapping the Core of the Arabidopsis Circadian Clock Defines the Network Structure of the Oscillator. Science (80-.). **336**.

Hubbard, C.J., Brock, M.T., van Diepen, L.T., Maignien, L., Ewers, B.E., and Weinig, C. (2018). The plant circadian clock influences rhizosphere community structure and function. ISME J. **12**: 400–410.

Hubbard, K.. and Dodd, A.N. (2016). Rhythms of Life: The Plant Circadian Clock. Plant Cell **28**.

Hussain, A. and Peng, J. (2003). DELLA Proteins and GA Signalling in Arabidopsis. J. Plant Growth Regul. **22**: 134–140.

Imaizumi, T., Tran, H.G., Swartz, T.E., Briggs, W.R., and Kay, S.A. (2003). FKF1 is essential for photoperiodic-specific light signalling in Arabidopsis. Nature **426**: 302–306.

Ingle, R.A., Stoker, C., Stone, W., Adams, N., Smith, R., Grant, M., Carré, I., Roden, L.C., and Denby, K.J. (2015). Jasmonate signalling drives time-of-day differences in susceptibility of Arabidopsis to the fungal pathogen Botrytis cinerea. Plant J. **84**: 937–48.

Jia, Y., McAdams, S.A., Bryan, G.T., Hershey, H.P., and Valent, B. (2000). Direct interaction of resistance gene and avirulence gene products confers rice blast resistance. EMBO J. **19**: 4004–4014.

Jiang, Y., Han, B., Zhang, H., Mariappan, K.G., Bigeard, J., Colcombet, J., and Hirt, H. (2019). MAP 4K4 associates with BIK 1 to regulate plant innate immunity. EMBO Rep.

Johansson, O.N., Nilsson, A.K., Gustavsson, M.B., Backhaus, T., Andersson, M.X., and Ellerström, M. (2015). A quick and robust method for quantification of the hypersensitive response in plants. PeerJ **3**: e1469.

Jones, J.D.G. and Dangl, J.L. (2006). The plant immune system. Nature **444**: 323-329fhor.

Kadota, Y., Sklenar, J., Derbyshire, P., Stransfeld, L., Asai, S., Ntoukakis, V., Jones, J.D., Shirasu, K., Menke, F., Jones, A., and Zipfel, C. (2014). Direct regulation of the NADPH oxidase RBOHD by the PRR-associated kinase BIK1 during plant immunity. Mol. Cell **54**: 43–55.

Kamioka, M., Takao, S., Suzuki, T., Taki, K., Higashiyama, T., Kinoshita, T., and Nakamichi, N. (2016). Direct Repression of Evening Genes by CIRCADIAN CLOCK-ASSOCIATED1 in the Arabidopsis Circadian Clock. Plant Cell Online **28**.

Kamiunten, H., Nakao, T., and Oshida, S. (2000). Pseudomonas syringae pv. cerasicola, pv. nov., the Causal Agent of Bacterial Gall of Cherry Tree. J. Gen. Plant Pathol. **66**: 219–224.

Kang, Y., Jelenska, J., Cecchini, N.M., Li, Y., Lee, M.W., Kovar, D.R., and Greenberg, J.T. (2014). HopW1 from Pseudomonas syringae Disrupts the Actin Cytoskeleton to Promote Virulence in Arabidopsis. PLoS Pathog. **10**: e1004232.

Keller, H., Boyer, L., and Abad, P. (2016). Disease susceptibility in the Zig-Zag model of host-microbe interactions: only a consequence of immune suppression? Mol. Plant Pathol. **17**: 475–479.

Kennedy, E.P. and Beattie, G.A. (1982). Osmotic regulation and the biosynthesis of membrane-derived oligosaccharides in Escherichia coli. Proc. Natl. Acad. Sci. U.

S. A. **79**: 1092–5.

Keskin, O. and Nussinov, R. (2007). Similar Binding Sites and Different Partners: Implications to Shared Proteins in Cellular Pathways. Structure **15**: 341–354.

Kiba, T., Henriques, R., Sakakibara, H., and Chua, N.-H. (2007). Targeted Degradation of PSEUDO-RESPONSE REGULATOR5 by an SCFZTL Complex Regulates Clock Function and Photomorphogenesis in Arabidopsis thaliana. Plant Cell Online **19**.

Kim, D., Langmead, B., and Salzberg, S.L. (2015). HISAT: a fast spliced aligner with low memory requirements. Nat. Methods **12**: 357–360.

Kim, H.J., Park, J.-H., Kim, J., Kim, J.J., Hong, S., Kim, J., Kim, J.H., Woo, H.R., Hyeon, C., Lim, P.O., Nam, H.G., and Hwang, D. (2018). Time-evolving genetic networks reveal a NAC troika that negatively regulates leaf senescence in Arabidopsis. Proc. Natl. Acad. Sci. U. S. A. **115**: E4930–E4939.

Kim, J. and Somers, D.E. (2010). Rapid Assessment of Gene Function in the Circadian Clock Using Artificial MicroRNA in Arabidopsis Mesophyll Protoplasts. Plant Physiol. **154**: 611–621.

Kim, J.S., Jung, H.J., Lee, H.J., Kim, K.A., Goh, C.-H., Woo, Y., Oh, S.H., Han, Y.S., and Kang, H. (2008). Glycine-rich RNA-binding protein 7 affects abiotic stress responses by regulating stomata opening and closing in Arabidopsis thaliana. Plant J. **55**: 455–66.

Kim, S.H., Son, G.H., Bhattacharjee, S., Kim, H.J., Nam, J.C., Nguyen, P.D.T., Hong, J.C., and Gassmann, W. (2014). The Arabidopsis immune adaptor SRFR1 interacts with TCP transcription factors that redundantly contribute to effector-triggered immunity. Plant J. **78**: 978–989.

Kim, W.-Y., Fujiwara, S., Suh, S.-S., Kim, J., Kim, Y., Han, L., David, K., Putterill, J., Nam, H.G., and Somers, D.E. (2007). ZEITLUPE is a circadian photoreceptor stabilized by GIGANTEA in blue light. Nature **449**: 356–360.

King, E.O., Ward, M.K., and Raney, D.E. (1954). Two simple media for the demonstration of pyocyanin and fluorescin. J. Lab. Clin. Med. **44**: 301–7.

Kinkema, M., Fan, W., and Dong, X. (2000). Nuclear localization of NPR1 is required for activation of PR gene expression. Plant Cell **12**: 2339–2350.

Klepikova, A. V., Kasianov, A.S., Gerasimov, E.S., Logacheva, M.D., and Penin, A.A. (2016). A high resolution map of the *Arabidopsis thaliana* developmental transcriptome based on RNA-seq profiling. Plant J. **88**: 1058–1070.

Koegl, M. and Uetz, P. (2008). Improving yeast two-hybrid screening systems. Briefings Funct. Genomics Proteomics **6**: 302–312.

Kubota, A., Shim, J.S., and Imaizumi, T. (2015). Natural variation in transcriptional rhythms modulates photoperiodic responses. Trends Plant Sci. **20**: 259–261.

Kumar, D. (2014). Salicylic acid signaling in disease resistance. Plant Sci. **228**: 127–134.

Kunze, G., Zipfel, C., Robatzek, S., Niehaus, K., Boller, T., and Felix, G. (2004). The N Terminus of Bacterial Elongation Factor Tu Elicits Innate Immunity in Arabidopsis Plants. Plant Cell **16**: 3496–3507.

Lamb, C. and Dixon, R.A. (1997). The oxidative burst in plant disease resistance. Annu. Rev. Plant Physiol. Plant Mol. Biol. **48**: 251–275.

Langmead, B. and Salzberg, S.L. (2012). Fast gapped-read alignment with Bowtie 2. Nat. Methods **9**: 357–359.

Lau, O.S., Huang, X., Charron, J.-B., Lee, J.-H., Li, G., and Deng, X.W. (2011). Interaction of Arabidopsis DET1 with CCA1 and LHY in mediating transcriptional repression in the plant circadian clock. Mol. Cell **43**: 703–12.

Le Roux, C. et al. (2015). A Receptor Pair with an Integrated Decoy Converts Pathogen Disabling of Transcription Factors to Immunity. Cell **161**: 1074–1088.

Lebeis, S.L., Paredes, S.H., Lundberg, D.S., Breakfield, N., Gehring, J., McDonald, M., Malfatti, S., Glavina del Rio, T., Jones, C.D., Tringe, S.G., and Dangl, J.L. (2015). PLANT MICROBIOME. Salicylic acid modulates colonization of the root microbiome by specific bacterial taxa. Science **349**: 860–4.

Lee, A.H.-Y., Middleton, M.A., Guttman, D.S., and Desveaux, D. (2013). Phytopathogen type III effectors as probes of biological systems. Microb. Biotechnol. **6**: 230–40.

Lee, H.-J., Park, Y.-J., Seo, P.J., Kim, J.-H., Sim, H.-J., Kim, S.-G., and Park, C.-M. (2015). Systemic Immunity Requires SnRK2.8-Mediated Nuclear Import of NPR1 in Arabidopsis. Plant Cell **27**: 3425–38.

Lee, S., Choi, H., Suh, S., Doo, I.S., Oh, K.Y., Choi, E.J., Schroeder Taylor, A.T., Low, P.S., and Lee, Y. (1999). Oligogalacturonic acid and chitosan reduce stomatal aperture by inducing the evolution of reactive oxygen species from guard cells of tomato and Commelina communis. Plant Physiol. **121**: 147–152.

Levine, A., Tenhaken, R., Dixon, R., and Lamb, C. (1994). H2O2 from the oxidative

burst orchestrates the plant hypersensitive disease resistance response. Cell **79**: 583–593.

Li, B. and Dewey, C.N. (2011). RSEM: accurate transcript quantification from RNA-Seq data with or without a reference genome. BMC Bioinformatics **12**: 323.

Li, B., Meng, X., Shan, L., and He, P. (2016). Transcriptional Regulation of Pattern-Triggered Immunity in Plants. Cell Host Microbe **19**: 641–50.

Li, G., Froehlich, J.E., Elowsky, C., Msanne, J., Ostosh, A.C., Zhang, C., Awada, T., and Alfano, J.R. (2014). Distinct Pseudomonas type-III effectors use a cleavable transit peptide to target chloroplasts. Plant J. **77**: 310–21.

Li, Z., Bonaldi, K., Uribe, F., and Pruneda-Paz, J.L. (2018). A Localized Pseudomonas syringae Infection Triggers Systemic Clock Responses in Arabidopsis. Curr. Biol. **0**.

Lindeberg, M., Cunnac, S., and Collmer, A. (2012). Pseudomonas syringae type III effector repertoires: last words in endless arguments. Trends Microbiol. **20**: 199–208.

Lindemann, J. (1984). Use of an Apparent Infection Threshold Population of *Pseudomonas syringae* to Predict Incidence and Severity of Brown Spot of Bean. Phytopathology **74**: 1334.

Liu, T.L., Newton, L., Liu, M.-J., Shiu, S.-H., and Farré, E.M. (2016). A G-Box-Like Motif Is Necessary for Transcriptional Regulation by Circadian Pseudo-Response Regulators in Arabidopsis. Plant Physiol. **170**: 528–39.

Locascio, A., Blázquez, M.A., and Alabadí, D. (2013). Genomic Analysis of DELLA Protein Activity. Plant Cell Physiol. **54**: 1229–1237.

López-Solanilla, E., Bronstein, P.A., Schneider, A.R., and Collmer, A. (2004). HopPtoN is a Pseudomonas syringae Hrp (type III secretion system) cysteine protease effector that suppresses pathogen-induced necrosis associated with both compatible and incompatible plant interactions. Mol. Microbiol. **54**: 353–365.

Love, M.I., Huber, W., and Anders, S. (2014). Moderated estimation of fold change and dispersion for RNA-seq data with DESeq2. Genome Biol. **15**: 550.

Lozano-Durán, R., Bourdais, G., He, S.Y., and Robatzek, S. (2014). The bacterial effector HopM1 suppresses PAMP-triggered oxidative burst and stomatal immunity. New Phytol. **202**: 259–269.

Lu, D., Wu, S., Gao, X., Zhang, Y., Shan, L., and He, P. (2010). A receptor-like cytoplasmic kinase, BIK1, associates with a flagellin receptor complex to initiate

plant innate immunity. Proc. Natl. Acad. Sci. **107**: 496–501.

Lu, H., McClung, C.R., and Zhang, C. (2017). Tick Tock: Circadian Regulation of Plant Innate Immunity. Annu. Rev. Phytopathol. **55**: annurev-phyto-080516-035451.

Lu, S.X., Webb, C.J., Knowles, S.M., Kim, S.H.J., Wang, Z., and Tobin, E.M. (2012). CCA1 and ELF3 Interact in the Control of Hypocotyl Length and Flowering Time in Arabidopsis. Plant Physiol. **158**: 1079–1088.

Luna, E., Pastor, V., Robert, J., Flors, V., Mauch-Mani, B., and Ton, J. (2011). Callose Deposition: A Multifaceted Plant Defense Response. Mol. Plant-Microbe Interact. **24**: 183–193.

Macho, A.P. et al. (2014). A Bacterial Tyrosine Phosphatase Inhibits Plant Pattern Recognition Receptor Activation. Science (80-.). **343**.

Macho, A.P. and Zipfel, C. (2015). Targeting of plant pattern recognition receptor-triggered immunity by bacterial type-III secretion system effectors. Curr. Opin. Microbiol. **23**: 14–22.

Mackey, D., Belkhadir, Y., Alonso, J.M., Ecker, J.R., and Dangl, J.L. (2003). Arabidopsis RIN4 is a target of the type III virulence effector AvrRpt2 and modulates RPS2-mediated resistance. Cell **112**: 379–89.

Mackey, D., Holt, B.F., Wiig, A., and Dangl, J.L. (2002). RIN4 interacts with Pseudomonas syringae type III effector molecules and is required for RPM1-mediated resistance in Arabidopsis. Cell **108**: 743–54.

Madeira, F., Park, Y. mi, Lee, J., Buso, N., Gur, T., Madhusoodanan, N., Basutkar, P., Tivey, A.R.N., Potter, S.C., Finn, R.D., and Lopez, R. (2019). The EMBL-EBI search and sequence analysis tools APIs in 2019. Nucleic Acids Res. **47**: W636–W641.

Mansfield, J. et al. (2012). Top 10 plant pathogenic bacteria in molecular plant pathology. Mol. Plant Pathol. **13**: 614–629.

Marín-de la Rosa, N. et al. (2015). Genome Wide Binding Site Analysis Reveals Transcriptional Coactivation of Cytokinin-Responsive Genes by DELLA Proteins. PLOS Genet. **11**: e1005337.

Marino, D., Dunand, C., Puppo, A., and Pauly, N. (2012). A burst of plant NADPH oxidases. Trends Plant Sci. **17**: 9–15.

Martin-Tryon, E.L., Kreps, J.A., and Harmer, S.L. (2006). GIGANTEA Acts in Blue Light Signaling and Has Biochemically Separable Roles in Circadian Clock

and Flowering Time Regulation. PLANT Physiol. **143**: 473–486.

McDonald, B.A. and Stukenbrock, E.H. (2016). Rapid emergence of pathogens in agro-ecosystems: global threats to agricultural sustainability and food security. Philos. Trans. R. Soc. Lond. B. Biol. Sci. **371**.

McHale, L., Tan, X., Koehl, P., and Michelmore, R.W. (2006). Plant NBS-LRR proteins: adaptable guards. Genome Biol. **7**: 212.

Melotto, M., Underwood, W., Koczan, J., Nomura, K., and He, S.Y. (2006). Plant Stomata Function in Innate Immunity against Bacterial Invasion. Cell **126**: 969–980.

Melotto, M., Zhang, L., Oblessuc, P.R., and He, S.Y. (2017). Stomatal Defense a Decade Later. Plant Physiol. **174**: 561–571.

Mi, H., Dong, Q., Muruganujan, A., Gaudet, P., Lewis, S., and Thomas, P.D. (2010). PANTHER version 7: improved phylogenetic trees, orthologs and collaboration with the Gene Ontology Consortium. Nucleic Acids Res. **38**: D204–D210.

Michael, T.P. et al. (2008). Network Discovery Pipeline Elucidates Conserved Time-of-Day–Specific cis-Regulatory Modules. PLoS Genet. **4**: e14.

Michael, T.P. and McClung, C.R. (2002). Phase-specific circadian clock regulatory elements in Arabidopsis. Plant Physiol. **130**: 627–38.

Michelmore, R.W. and Meyers, B.C. (1998). Clusters of Resistance Genes in Plants Evolve by Divergent Selection and a Birth-and-Death Process. Genome Res. **8**: 1113–1130.

Millar, A.J. (2016). The Intracellular Dynamics of Circadian Clocks Reach for the Light of Ecology and Evolution. Annu. Rev. Plant Biol. **67**: 595–618.

Mockler, T.C., Michael, T.P., Priest, H.D., Shen, R., Sullivan, C.M., Givan, S.A., McEntee, C., Kay, S.A., and Chory, J. (2007). The Diurnal Project: Diurnal and Circadian Expression Profiling, Model-based Pattern Matching, and Promoter Analysis. Cold Spring Harb. Symp. Quant. Biol. **72**: 353–363.

Murashige, T. and Skoog, F. (1962). A Revised Medium for Rapid Growth and Bio Assays with Tobacco Tissue Cultures. Physiol. Plant. **15**: 473–497.

Navarro, L., Bari, R., Achard, P., Lisón, P., Nemri, A., Harberd, N.P., and Jones, J.D.G. (2008). DELLAs Control Plant Immune Responses by Modulating the Balance of Jasmonic Acid and Salicylic Acid Signaling. Curr. Biol. **18**: 650–655.

Nicaise, V., Joe, A., Jeong, B.R., Korneli, C., Boutrot, F., Westedt, I., Staiger, D.,

Alfano, J.R., and Zipfel, C. (2013). Pseudomonas HopU1 modulates plant immune receptor levels by blocking the interaction of their mRNAs with GRP7. EMBO J. **32**: 701–712.

Nimchuk, Z.L., Fisher, E.J., Desveaux, D., Chang, J.H., and Dangl, J.L. (2007). The HopX (AvrPphE) Family of *Pseudomonas syringae* Type III Effectors Require a Catalytic Triad and a Novel N-Terminal Domain for Function. Mol. Plant-Microbe Interact. **20**: 346–357.

Nohales, M.A. and Kay, S.A. (2016). Molecular mechanisms at the core of the plant circadian oscillator. Nat. Struct. Mol. Biol. **23**: 1061–1069.

Nomura, K., DebRoy, S., Lee, Y.H., Pumplin, N., Jones, J., and He, S.Y. (2006). A Bacterial Virulence Protein Suppresses Host Innate Immunity to Cause Plant Disease. Science (80-.). **313**.

O'Brien, H.E., Thakur, S., and Guttman, D.S. (2011). Evolution of Plant Pathogenesis in Pseudomonas syringae : A Genomics Perspective . Annu. Rev. Phytopathol. **49**: 269–289.

O'Leary, N.A. et al. (2016). Reference sequence (RefSeq) database at NCBI: current status, taxonomic expansion, and functional annotation. Nucleic Acids Res. **44**: D733–D745.

Oakenfull, R.J. and Davis, S.J. (2017). Shining a light on the Arabidopsis circadian clock. Plant. Cell Environ.

Oerke, E.C. (2006). Crop losses to pests. J. Agric. Sci. **144**: 31–43.

Ohara, T., Fukuda, H., and Tokuda, I.T. (2015). Phase response of the Arabidopsis thaliana circadian clock to light pulses of different wavelengths. J. Biol. Rhythms **30**: 95–103.

Okabe, N. (1933). Bacterial diseases of plants occurring in Formosa II. J. Soc. Trop. Agric. **5**: 26–36.

de Oliveira, M.V. V et al. (2016). Specific control of Arabidopsis BAK1/SERK4-regulated cell death by protein glycosylation. Nat. plants **2**: 15218.

Olivier, D., Maina, M., Andrew, O.E., Peter, M.M., and Careen, I.C. (2018). Application of molecular and biotechnological techniques in plant disease management: A review. African J. Biotechnol. **17**: 938–948.

Pauwels, L. and Goossens, A. (2011). The JAZ proteins: a crucial interface in the jasmonate signaling cascade. Plant Cell **23**: 3089–100.

Perales, M. and Más, P. (2007). A functional link between rhythmic changes in

chromatin structure and the Arabidopsis biological clock. Plant Cell **19**: 2111–23.

Petersen, M. et al. (2000). Arabidopsis MAP Kinase 4 Negatively Regulates Systemic Acquired Resistance. Cell **103**: 1111–1120.

Piquerez, S.J.M., Balmuth, A.L., Sklenář, J., Jones, A.M.E., Rathjen, J.P., and Ntoukakis, V. (2014). Identification of post-translational modifications of plant protein complexes. J. Vis. Exp.: e51095.

Popham, P.L., Pike, S.M., Novacky, A., and Pallardy, S.G. (1993). Water Relation Alterations Observed during Hypersensitive Reaction Induced by Bacteria. Plant Physiol. **103**: 1243–1247.

Preston, G.M. (2000). Pseudomonas syringae pv. tomato: the right pathogen, of the right plant, at the right time. Mol. Plant Pathol. **1**: 263–275.

Prior, P. (Philippe), Allen, C. (Caitilyn), Elphinstone, J.G., and International Bacterial Wilt Symposium (2nd : 1997 : Gosier, G. Bacterial wilt disease : molecular and ecological aspects.

Pritchard, L. and Birch, P.R.J. (2014). The zigzag model of plant–microbe interactions: is it time to move on? Mol. Plant Pathol. **15**: 865–870.

Pruneda-Paz, J.L., Breton, G., Nagel, D.H., Kang, S.E., Bonaldi, K., Doherty, C.J., Ravelo, S., Galli, M., Ecker, J.R., and Kay, S.A. (2014). A genome-scale resource for the functional characterization of Arabidopsis transcription factors. Cell Rep. **8**: 622–32.

Pruneda-Paz, J.L., Breton, G., Para, A., and Kay, S.A. (2009). A Functional Genomics Approach Reveals CHE as a Component of the Arabidopsis Circadian Clock. Science (80-.). **323**.

Qin, Q., Wang, W., Guo, X., Yue, J., Huang, Y., Xu, X., Li, J., and Hou, S. (2014). Arabidopsis DELLA protein degradation is controlled by a type-one protein phosphatase, TOPP4. PLoS Genet. **10**: e1004464.

Reinhardt, J.A., Baltrus, D.A., Nishimura, M.T., Jeck, W.R., Jones, C.D., and Dangl, J.L. (2009). De novo assembly using low-coverage short read sequence data from the rice pathogen Pseudomonas syringae pv. oryzae. Genome Res. **19**: 294–305.

Rodríguez-Herva, J.J. et al. (2012). A bacterial cysteine protease effector protein interferes with photosynthesis to suppress plant innate immune responses. Cell. Microbiol. **14**: 669–681.

Roine, E., Wei, W., Yuan, J., Nurmiaho-Lassila, E.L., Kalkkinen, N., Romantschuk, M., and He, S.Y. (1997). Hrp pilus: an hrp-dependent bacterial surface appendage produced by Pseudomonas syringae pv. tomato DC3000. Proc. Natl. Acad. Sci. U. S. A. **94**: 3459–64.

Ronald, P.C., Salmeron, J.M., Carland, F.M., and Staskawicz, B.J. (1992). The cloned avirulence gene avrPto induces disease resistance in tomato cultivars containing the Pto resistance gene. J. Bacteriol. **174**: 1604–11.

Rosa, N.M. la, Sotillo, B., Miskolczi, P., Gibbs, D.J., Vicente, J., Carbonero, P., Oñate-Sánchez, L., Holdsworth, M.J., Bhalerao, R., Alabadí, D., and Blázquez, M.A. (2014). Large-Scale Identification of Gibberellin-Related Transcription Factors Defines Group VII ETHYLENE RESPONSE FACTORS as Functional DELLA Partners. Plant Physiol. **166**: 1022–1032.

Saldanha, A.J. (2004). Java Treeview--extensible visualization of microarray data. Bioinformatics **20**: 3246–3248.

Sarris, P.F. et al. (2015). A Plant Immune Receptor Detects Pathogen Effectors that Target WRKY Transcription Factors. Cell **161**: 1089–1100.

Sarris, P.F., Gao, S., Karademiris, K., Jin, H., Kalantidis, K., and Panopoulos, N.J. (2011). Phytobacterial type III effectors HopX1, HopAB1 and HopF2 enhance sense-post-transcriptional gene silencing independently of plant R gene-effector recognition. Mol. Plant. Microbe. Interact. **24**: 907–17.

Satoh, K., Sasajima, H., Nyoumura, K., Yokosawa, H., and Sawada, H. (2001). Assembly of the 26S Proteasome Is Regulated by Phosphorylation of the p45/Rpt6 ATPase Subunit †. Biochemistry **40**: 314–319.

Sauerbrunn, N. and Schlaich, N.L. (2004). PCC1 : a merging point for pathogen defence and circadian signalling in Arabidopsis. Planta **218**: 552–561.

Savary, S., Willocquet, L., Pethybridge, S.J., Esker, P., McRoberts, N., and Nelson, A. (2019). The global burden of pathogens and pests on major food crops. Nat. Ecol. Evol. **3**: 430–439.

Schaffer, R., Ramsay, N., Samach, A., Corden, S., Putterill, J., Carré, I.A., and Coupland, G. (1998). The late elongated hypocotyl Mutation of Arabidopsis Disrupts Circadian Rhythms and the Photoperiodic Control of Flowering. Cell **93**: 1219–1229.

Schiessl, S. et al. (2015). Diverse regulatory factors associate with flowering time and yield responses in winter-type Brassica napus. BMC Genomics **16**: 737.

Schornack, S., Meyer, A., Römer, P., Jordan, T., and Lahaye, T. (2006). Gene-for-gene-mediated recognition of nuclear-targeted AvrBs3-like bacterial effector proteins. J. Plant Physiol. **163**: 256–272.

Schulze, B., Mentzel, T., Jehle, A.K., Mueller, K., Beeler, S., Boller, T., Felix, G., and Chinchilla, D. (2010). Rapid Heteromerization and Phosphorylation of Ligand-activated Plant Transmembrane Receptors and Their Associated Kinase BAK1. J. Biol. Chem. **285**: 9444–9451.

Scofield, S.R., Tobias, C.M., Rathjen, J.P., Chang, J.H., Lavelle, D.T., Michelmore, R.W., and Staskawicz, B.J. (1996). Molecular Basis of Gene-for-Gene Specificity in Bacterial Speck Disease of Tomato. Science (80-.). **274**: 2063–2065.

Seo, P.J. and Mas, P. (2014). Multiple layers of posttranslational regulation refine circadian clock activity in Arabidopsis. Plant Cell **26**: 79–87.

Seybold, H., Boudsocq, M., and Romeis, T. (2017). CDPK Activation in PRR Signaling. In, pp. 173–183.

Shan, L., He, P., Li, J., Heese, A., Peck, S.C., Nürnberger, T., Martin, G.B., and Sheen, J. (2008). Bacterial Effectors Target the Common Signaling Partner BAK1 to Disrupt Multiple MAMP Receptor-Signaling Complexes and Impede Plant Immunity. Cell Host Microbe **4**: 17–27.

Shi, H., Wei, Y., and He, C. (2016). Melatonin-induced CBF/DREB1s are essential for diurnal change of disease resistance and CCA1 expression in Arabidopsis. Plant Physiol. Biochem. **100**: 150–155.

Shimada, T.L., Shimada, T., and Hara-Nishimura, I. (2010). A rapid and non-destructive screenable marker, FAST, for identifying transformed seeds of *Arabidopsis thaliana*. Plant J. **61**: 519–528.

Shimono, M., Lu, Y.-J., Porter, K., Kvitko, B.H., Henty-Ridilla, J.L., Creason, A., He, S.Y., Chang, J.H., Staiger, C.J., and Day, B. (2016). The Pseudomonas syringae type-III effector HopG1 induces actin remodeling to promote symptom development and susceptibility during infection. Plant Physiol. **171**: pp.01593.2016.

Shin, J., Heidrich, K., Sanchez-Villarreal, A., Parker, J.E., and Davis, S.J. (2012). TIME FOR COFFEE Represses Accumulation of the MYC2 Transcription Factor to Provide Time-of-Day Regulation of Jasmonate Signaling in Arabidopsis. Plant Cell **24**: 2470–2482.

Silverstone, A.L., Jung, H.S., Dill, A., Kawaide, H., Kamiya, Y., and Sun, T.P. (2001). Repressing a repressor: gibberellin-induced rapid reduction of the RGA protein in Arabidopsis. Plant Cell **13**: 1555–66.

Smith, J.M. and Heese, A. (2014). Rapid bioassay to measure early reactive oxygen species production in Arabidopsis leave tissue in response to living Pseudomonas syringae. Plant Methods **10**: 6.

Società italiana di patologia vegetale., P., Pepori, A.L., Migliorini, D., Botella, L., and Luchi, N. (1997). Journal of plant pathology : an international journal of the Italian Phytopathological Society.

Sohn, K.H., Segonzac, C., Rallapalli, G., Sarris, P.F., Woo, J.Y., Williams, S.J., Newman, T.E., Paek, K.H., Kobe, B., and Jones, J.D.G. (2014). The Nuclear Immune Receptor RPS4 Is Required for RRS1SLH1-Dependent Constitutive Defense Activation in Arabidopsis thaliana. PLoS Genet. **10**: e1004655.

Somers, D.E., Devlin, P.F., and Kay, S.A. (1998). Phytochromes and Cryptochromes in the Entrainment of the Arabidopsis Circadian Clock. Science (80-.). **282**.

Song, Y., Jiang, Y., Kuai, B., and Li, L. (2018). CIRCADIAN CLOCK-ASSOCIATED 1 Inhibits Leaf Senescence in Arabidopsis. Front. Plant Sci. **9**: 280.

Song, Y., Yang, C., Gao, S., Zhang, W., Li, L., and Kuai, B. (2014). Age-triggered and dark-induced leaf senescence require the bHLH transcription factors PIF3, 4, and 5. Mol. Plant **7**: 1776–87.

Song, Y.H., Ito, S., and Imaizumi, T. (2010). Similarities in the circadian clock and photoperiodism in plants. Curr. Opin. Plant Biol. **13**: 594–603.

Spensley, M., Kim, J.-Y., Picot, E., Reid, J., Ott, S., Helliwell, C., and Carré, I.A. (2009). Evolutionarily conserved regulatory motifs in the promoter of the Arabidopsis clock gene LATE ELONGATED HYPOCOTYL. Plant Cell **21**: 2606–23.

Spoel, S.H. and Dong, X. (2012). How do plants achieve immunity? Defence without specialized immune cells. Nat. Rev. Immunol. **12**: 89–100.

Staley, C. et al. (2017). Diurnal cycling of rhizosphere bacterial communities is associated with shifts in carbon metabolism. Microbiome **5**: 65.

Strawn, M.A., Marr, S.K., Inoue, K., Inada, N., Zubieta, C., and Wildermuth, M.C. (2007). *Arabidopsis* Isochorismate Synthase Functional in Pathogen-induced Salicylate Biosynthesis Exhibits Properties Consistent with a Role in

Diverse Stress Responses. J. Biol. Chem. **282**: 5919–5933.

Suffert, F., Sache, I., and Lannou, C. (2011). Early stages of septoria tritici blotch epidemics of winter wheat: build-up, overseasoning, and release of primary inoculum. Plant Pathol. **60**: 166–177.

Sugano, S., Andronis, C., Green, R.M., Wang, Z.-Y., and Tobin, E.M. (1998). Protein kinase CK2 interacts with and phosphorylates the Arabidopsis circadian clock-associated 1 protein. Proc. Natl. Acad. Sci. **95**: 11020–11025.

Sugano, S., Andronis, C., Ong, M.S., Green, R.M., and Tobin, E.M. (1999). The protein kinase CK2 is involved in regulation of circadian rhythms in Arabidopsis. Proc. Natl. Acad. Sci. U. S. A. **96**: 12362–6.

Sun, T. and Gubler, F. (2004). MOLECULAR MECHANISM OF GIBBERELLIN SIGNALING IN PLANTS. Annu. Rev. Plant Biol. **55**: 197–223.

Swiderski, M.R., Birker, D., and Jones, J.D.G. (2009). The TIR Domain of TIR-NB-LRR Resistance Proteins Is a Signaling Domain Involved in Cell Death Induction. Mol. Plant-Microbe Interact. **22**: 157–165.

Takatsuji, H. (2014). Development of disease-resistant rice using regulatory components of induced disease resistance. Front. Plant Sci. **5**: 630.

Tasset, C., Bernoux, M., Jauneau, A., Pouzet, C., Brière, C., Kieffer-Jacquinod, S., Rivas, S., Marco, Y., and Deslandes, L. (2010). Autoacetylation of the Ralstonia solanacearum Effector PopP2 Targets a Lysine Residue Essential for RRS1-R-Mediated Immunity in Arabidopsis. PLoS Pathog. **6**: e1001202.

Tena, G., Boudsocq, M., and Sheen, J. (2011). Protein kinase signaling networks in plant innate immunity. Curr. Opin. Plant Biol. **14**: 519–529.

Thilmony, R., Underwood, W., and He, S.Y. (2006). Genome-wide transcriptional analysis of the *Arabidopsis thaliana* interaction with the plant pathogen *Pseudomonas syringae* pv. *tomato* DC3000 and the human pathogen *Escherichia coli* O157:H7. Plant J. **46**: 34–53.

Torres, M.A., Jones, J.D.G., and Dangl, J.L. (2005). Pathogen-induced, NADPH oxidase–derived reactive oxygen intermediates suppress spread of cell death in Arabidopsis thaliana. Nat. Genet. **37**: 1130–1134.

Ugolini, S. and Bruschi, C. V (1996). The red/white colony color assay in the yeast Saccharomyces cerevisiae: epistatic growth advantage of white ade8-18, ade2 cells over red ade2 cells. Curr. Genet. **30**: 485–92.

Uknes, S., Mauch-Mani, B., Moyer, M., Potter, S., Williams, S., Dincher, S.,

Chandler, D., Slusarenko, A., Ward, E., and Ryals, J. (1992). Acquired resistance in Arabidopsis. Plant Cell **4**: 645–656.

Underwood, W., Zhang, S., and He, S.Y. (2007). The Pseudomonas syringae type III effector tyrosine phosphatase HopAO1 suppresses innate immunity in Arabidopsis thaliana. Plant J. **52**: 658–672.

Üstün, S., Sheikh, A., Gimenez-Ibanez, S., Jones, A.M.E., Ntoukakis, V., and Börnke, F. (2016). The proteasome acts as a hub for plant immunity and is targeted by Pseudomonas type-III effectors. Plant Physiol. **172**: pp.00808.2016.

Vellicce, G.R., Ricci, J.C.D., Hernández, L., and Castagnaro, A.P. (2006). Enhanced Resistance to Botrytis cinerea Mediated by the Transgenic Expression of the Chitinase Gene ch5B in Strawberry. Transgenic Res. **15**: 57–68.

Vicente, O. and Boscaiu, M. (2018). Flavonoids: Antioxidant compounds for plant defence... and for a healthy human diet. Not. Bot. Horti Agrobot. Cluj-Napoca **46**: 14–21.

Walley, J.W., Kliebenstein, D.J., Bostock, R.M., and Dehesh, K. (2013). Fatty acids and early detection of pathogens. Curr. Opin. Plant Biol. **16**: 520–526.

Wan, L., Essuman, K., Anderson, R.G., Sasaki, Y., Monteiro, F., Chung, E.-H., Osborne Nishimura, E., DiAntonio, A., Milbrandt, J., Dangl, J.L., and Nishimura, M.T. (2019). TIR domains of plant immune receptors are NAD+-cleaving enzymes that promote cell death. Science **365**: 799–803.

Wang, G.-Y., Shi, J.-L., Ng, G., Battle, S.L., Zhang, C., and Lu, H. (2011a). Circadian clock-regulated phosphate transporter PHT4;1 plays an important role in Arabidopsis defense. Mol. Plant **4**: 516–26.

Wang, J., Hu, M., Wang, J., Qi, J., Han, Z., Wang, G., Qi, Y., Wang, H.-W., Zhou, J.-M., and Chai, J. (2019a). Reconstitution and structure of a plant NLR resistosome conferring immunity. Science **364**: eaav5870.

Wang, J., Wang, J., Hu, M., Wu, S., Qi, J., Wang, G., Han, Z., Qi, Y., Gao, N., Wang, H.-W., Zhou, J.-M., and Chai, J. (2019b). Ligand-triggered allosteric ADP release primes a plant NLR complex. Science (80-.). **364**: eaav5868.

Wang, W., Barnaby, J.Y., Tada, Y., Li, H., Tör, M., Caldelari, D., Lee, D., Fu, X.-D., and Dong, X. (2011b). Timing of plant immune responses by a central circadian regulator. Nature **470**: 110–114.

Wang, Y., Li, J., Hou, S., Wang, X., Li, Y., Ren, D., Chen, S., Tang, X., and Zhou, J.-M. (2010). A Pseudomonas syringae ADP-ribosyltransferase inhibits

Arabidopsis mitogen-activated protein kinase kinases. Plant Cell **22**: 2033–44.

Wang, Y., Wu, J.-F., Nakamichi, N., Sakakibara, H., Nam, H.-G., and Wu, S.-H. (2011c). LIGHT-REGULATED WD1 and PSEUDO-RESPONSE REGULATOR9 form a positive feedback regulatory loop in the Arabidopsis circadian clock. Plant Cell **23**: 486–98.

Wang, Y.H., Donaldson, L., Gehring, C., and Irving, H.R. (2011d). Plant natriuretic peptides: control of synthesis and systemic effects. Plant Signal. Behav. **6**: 1606–8.

Wang, Z.-X., Yamanouchi, U., Katayose, Y., Sasaki, T., and Yano, M. (2001). Expression of the Pib rice-blast-resistance gene family is up-regulated by environmental conditions favouring infection and by chemical signals that trigger secondary plant defences. Plant Mol. Biol. **47**: 653–661.

Wang, Z. and Schey, K.L. (2011). Aquaporin-0 Interacts with the FERM Domain of Ezrin/Radixin/Moesin Proteins in the Ocular Lens. Invest. Ophthalmol. Vis. Sci. **52**: 5079.

Wang, Z.Y., Tobin, E.M., Straume, M., McClung, C.., Hangarter, R.., Meeks-Wagner, D.., Sakaki, Y., Vitaterna, M.., Kornhauser, J.., Lowrey, P.., and al., et (1998). Constitutive expression of the CIRCADIAN CLOCK ASSOCIATED 1 (CCA1) gene disrupts circadian rhythms and suppresses its own expression. Cell **93**: 1207–17.

Weaver, L.M. and Amasino, R.M. (2001). Senescence is induced in individually darkened Arabidopsis leaves, but inhibited in whole darkened plants. Plant Physiol. **127**: 876–86.

Webber, J.F., Parkinson, N.M., Rose, J., Stanford, H., Cook, R.T.A., and Elphinstone, J.G. (2008). Isolation and identification of Pseudomonas syringae pv. aesculi causing bleeding canker of horse chestnut in the UK. Plant Pathol. **57**: 368–368.

Wei, H.-L., Chakravarthy, S., Mathieu, J., Helmann, T.C., Stodghill, P., Swingle, B., Martin, G.B., and Collmer, A. (2015). Pseudomonas syringae pv. tomato DC3000 Type III Secretion Effector Polymutants Reveal an Interplay between HopAD1 and AvrPtoB. Cell Host Microbe **17**: 752–62.

Wei, H.-L., Zhang, W., and Collmer, A. (2018). Modular Study of the Type III Effector Repertoire in Pseudomonas syringae pv. tomato DC3000 Reveals a Matrix of Effector Interplay in Pathogenesis. Cell Rep. **23**: 1630–1638.

Williams, S.J. et al. (2014). Structural Basis for Assembly and Function of a Heterodimeric Plant Immune Receptor. Science (80-.). **344**: 299–303.

Wilton, M., Subramaniam, R., Elmore, J., Felsensteiner, C., Coaker, G., and Desveaux, D. (2010). The type III effector HopF2 Pto targets Arabidopsis RIN4 protein to promote Pseudomonas syringae virulence. Proc. Natl. Acad. Sci. **107**: 2349–2354.

Winter, D., Vinegar, B., Nahal, H., Ammar, R., Wilson, G. V., and Provart, N.J. (2007). An "Electronic Fluorescent Pictograph" Browser for Exploring and Analyzing Large-Scale Biological Data Sets. PLoS One **2**: e718.

Wu, J.-F., Tsai, H.-L., Joanito, I., Wu, Y.-C., Chang, C.-W., Li, Y.-H., Wang, Y., Hong, J.C., Chu, J.-W., Hsu, C.-P., and Wu, S.-H. (2016). LWD-TCP complex activates the morning gene CCA1 in Arabidopsis. Nat. Commun. **7**: 13181.

Wu, J.-F., Wang, Y., and Wu, S.-H. (2008). Two New Clock Proteins, LWD1 and LWD2, Regulate Arabidopsis Photoperiodic Flowering. PLANT Physiol. **148**: 948–959.

Xiang, T., Zong, N., Zhang, J., Chen, J., Chen, M., and Zhou, J.-M. (2011). BAK1 Is Not a Target of the *Pseudomonas syringae* Effector AvrPto. Mol. Plant-Microbe Interact. **24**: 100–107.

Xiang, T., Zong, N., Zou, Y., Wu, Y., Zhang, J., Xing, W., Li, Y., Tang, X., Zhu, L., Chai, J., and Zhou, J.-M. (2008). Pseudomonas syringae Effector AvrPto Blocks Innate Immunity by Targeting Receptor Kinases. Curr. Biol. **18**: 74–80.

Xin, X.-F., Kvitko, B., and He, S.Y. (2018). Pseudomonas syringae: what it takes to be a pathogen. Nat. Rev. Microbiol. **16**: 316–328.

Xin, X.-F., Nomura, K., Aung, K., Velásquez, A.C., Yao, J., Boutrot, F., Chang, J.H., Zipfel, C., and He, S.Y. (2016). Bacteria establish an aqueous living space in plants crucial for virulence. Nature **539**: 524–529.

Xu, Y.-J., Lei, Y., Li, R., Zhang, L.-L., Zhao, Z.-X., Zhao, J.-H., Fan, J., Li, Y., Yang, H., Shang, J., Xiao, S., and Wang, W.-M. (2017). XAP5 CIRCADIAN TIMEKEEPER Positively Regulates RESISTANCE TO POWDERY MILDEW8.1-Mediated Immunity in Arabidopsis. Front. Plant Sci. **8**: 2044.

Yuan, J. and He, S.Y. (1996). The Pseudomonas syringae Hrp regulation and secretion system controls the production and secretion of multiple extracellular proteins. J. Bacteriol. **178**: 6399–402.

Yuliar, Nion, Y.A., and Toyota, K. (2015). Recent trends in control methods for

bacterial wilt diseases caused by Ralstonia solanacearum. Microbes Environ. **30**: 1–11.

Zerbino, D.R. et al. (2018). Ensembl 2018. Nucleic Acids Res. **46**: D754–D761.

Zhang, C. et al. (2013). Crosstalk between the Circadian Clock and Innate Immunity in Arabidopsis. PLoS Pathog. **9**: e1003370.

Zhang, C. et al. (2019). LUX ARRHYTHMO mediates crosstalk between the circadian clock and defense in Arabidopsis. Nat. Commun. **10**: 1–14.

Zhang, H., Tang, X., Munske, G.R., Tolic, N., Anderson, G.A., and Bruce, J.E. (2009). Identification of Protein-Protein Interactions and Topologies in Living Cells with Chemical Cross-linking and Mass Spectrometry. Mol. Cell. Proteomics **8**: 409.

Zhang, L., Zhang, F., Melotto, M., Yao, J., and He, S.Y. (2017). Jasmonate signaling and manipulation by pathogens and insects. J. Exp. Bot.: erw478.

Zhang, W., He, S.Y., and Assmann, S.M. (2008). The plant innate immunity response in stomatal guard cells invokes G-protein-dependent ion channel regulation. Plant J. **56**: 984–996.

Zhang, X., Henriques, R., Lin, S.-S., Niu, Q.-W., and Chua, N.-H. (2006). Agrobacterium-mediated transformation of Arabidopsis thaliana using the floral dip method. Nat. Protoc. **1**: 641–646.

Zhang, Y., Liu, Z., Wang, X., Wang, J., Fan, K., Li, Z., and Lin, W. (2018). DELLA proteins negatively regulate dark-induced senescence and chlorophyll degradation in Arabidopsis through interaction with the transcription factor WRKY6. Plant Cell Rep. **37**: 981–992.

Zhang, Z., Wu, Y., Gao, M., Zhang, J., Kong, Q., Liu, Y., Ba, H., Zhou, J., and Zhang, Y. (2012). Disruption of PAMP-Induced MAP Kinase Cascade by a Pseudomonas syringae Effector Activates Plant Immunity Mediated by the NB-LRR Protein SUMM2. Cell Host Microbe **11**: 253–263.

Zhao, Y., Thilmony, R., Bender, C.L., Schaller, A., He, S.Y., and Howe, G.A. (2003). Virulence systems of *Pseudomonas syringae* pv. *tomato* promote bacterial speck disease in tomato by targeting the jasmonate signaling pathway. Plant J. **36**: 485–499.

Zheng, X.-Y., Zhou, M., Yoo, H., Pruneda-Paz, J.L., Spivey, N.W., Kay, S.A., and Dong, X. (2015). Spatial and temporal regulation of biosynthesis of the plant immune signal salicylic acid. Proc. Natl. Acad. Sci. U. S. A. **112**: 9166–73.

Zhou, M., Wang, W., Karapetyan, S., Mwimba, M., Marqués, J., Buchler, N.E., and Dong, X. (2015). Redox rhythm reinforces the circadian clock to gate immune response. Nature **523**: 472–476.

Zipfel, C., Kunze, G., Chinchilla, D., Caniard, A., Jones, J.D.G., Boller, T., and Felix, G. (2006). Perception of the Bacterial PAMP EF-Tu by the Receptor EFR Restricts Agrobacterium-Mediated Transformation. Cell **125**: 749–760.

Zipfel, C., Robatzek, S., Navarro, L., Oakeley, E.J., Jones, J.D.G., Felix, G., and Boller, T. (2004). Bacterial disease resistance in Arabidopsis through flagellin perception. Nature **428**: 764–767.

Zoltowski, B.D. and Imaizumi, T. (2014). Structure and Function of the ZTL/FKF1/LKP2 Group Proteins in Arabidopsis. Enzym. **35**: 213–39.

Zuo, J., Niu, Q.W., and Chua, N.H. (2000). Technical advance: An estrogen receptor-based transactivator XVE mediates highly inducible gene expression in transgenic plants. Plant J. **24**: 265–73.